Improving Environmental Sustainability of Regional Railway Services

Kapetanović, M.

DOI
10.4233/uuid:a8225d35-bb57-4d76-a288-8f96d215f246

Publication date
2023

Document Version
Final published version

Citation (APA)
Kapetanović, M. (2023). *Improving Environmental Sustainability of Regional Railway Services*. [Dissertation (TU Delft), Delft University of Technology]. https://doi.org/10.4233/uuid:a8225d35-bb57-4d76-a288-8f96d215f246

Improving Environmental Sustainability of Regional Railway Services

Marko Kapetanović

This thesis has been funded by Arriva Personenvervoer Nederland B.V. as part of the PhD project "Improving Sustainability of Regional Railway Services" of Delft University of Technology.

Cover image by Arriva Personenvervoer Nederland B.V.

Improving Environmental Sustainability of Regional Railway Services

Dissertation

for the purpose of obtaining the degree of doctor
at Delft University of Technology,
by the authority of the Rector Magnificus Prof. dr. ir. T.H.J.J. van der Hagen,
chair of the Board of Doctorates,
to be defended publicly on
Wednesday 28 June 2023 at 12:30 o'clock
by

Marko KAPETANOVIĆ
Master of Science in Transport and Traffic Engineering,
University of Belgrade, Serbia
born in Loznica, Serbia

This dissertation has been approved by the:
Promotor: Prof.dr. R.M.P. Goverde
Copromotor: Dr.ir. N. van Oort

Composition of the doctoral committee:

Rector Magnificus	Chairman
Prof.dr. R.M.P. Goverde	Delft University of Technology, promotor
Dr.ir. N. van Oort	Delft University of Technology, copromotor

Independent members:

Prof.dr.ir. P. Bauer	Delft University of Technology
Prof.dr.ir. L.A. Tavasszy	Delft University of Technology
Prof.dr. N. Bojović	University of Belgrade, Serbia
Prof.dr. F. Corman	Eidgenössische Technische Hochschule Zürich, Switzerland
Prof.dr.ir. B. van Arem	Delft University of Technology, reserve member

Other members:

Dr.ir. A.A. Núñez Vicencio	Delft University of Technology

TRAIL Thesis Series no. T2023/6, the Netherlands Research School TRAIL

TRAIL
P.O. Box 5017
2600 GA Delft
The Netherlands
E-mail: info@rsTRAIL.nl

ISBN: 978-90-5584-325-1

Printed in the Netherlands

Dedicated to my parents

Preface

The beauty of transportation science lies in its multidisciplinarity. This feature has strongly attracted me since my undergraduate and master studies in Belgrade, where I learned of and tackled a wide range of problems from the railway transportation domain. My PhD research has given me the privilege and pleasure to address one of the burning issues facing humanity - global warming, and to contribute to its resolution in the field I love - railways.

The work presented in this thesis was carried out as part of the PhD project funded by Arriva Personenvervoer Nederland B.V., the largest regional railway undertaking in the Netherlands. The goal of the project was to identify and assess potential solutions in reducing the overall greenhouse gas emissions from regional railway services, and to provide the railway undertaking with a decision support tool in the strategic planning of future rolling stock and operation. Considered solutions were focused primarily on alternative propulsion systems and energy carriers, in the context of the non-electrified regional railway network in provinces Friesland and Groningen.

An old African proverb, *"It takes a village to raise a child"*, can be literally applied in the context of a PhD research. Here, I would like to take the opportunity to thank many people who have directly and indirectly helped me to finalize this dissertation. First and foremost, I would like to express my sincere gratitude to my supervisory team, Niels, Alfredo and Rob, for all your guidance, support and knowledge. Without you, this journey would not be possible. Niels, special thanks for showing me and helping me adopt the strong enthusiasm in disseminating our research both with academic community and practitioners, and interest in research valorisation. *"Practice what you preach"* is the motto you deeply infused into me, which I will carry throughout my future career. Alfredo, thank you for your strong devotion to my development in every step throughout this journey. Special thanks for your detailed comments and constructive criticism which contributed to the high quality of our research and a steep learning curve I experienced. Rob, your rigorous eye helped in keeping the mathematics in my research perfectly clear and precise. I appreciate your constructive feedback and the opportunity to assist in teaching activities in the master course during the last three years.

I would furthermore like to thank the amazing team from Arriva who have been involved in the project: Anne, Froukje, Yvonne, Gerrit, Pim, Bart, Willem, Jieskje, Marten, André, Daniël, and Pieter. I appreciate your help in providing the data, and your constructive feedback during and after each part of the research. Fruitful discussions during our monthly meetings ensured that our work encompassed and reflected the real-world challenges we were tackling. I truly believe that with this project, together, we have set the bar high and paved the road for a greener railway transport sector. I would also like to thank Floris and the team from Stadler for providing the

rolling stock data needed for the application of models and the overall assessment of energy use and emissions in the Northern lines.

I would like to thank all my colleagues at the Transport & Planning department for motivating, open and inclusive environment. I had the pleasure and privilege to be part of the two amazing labs. Thanks to all my colleagues from the Smart Public Transport Lab and the Digital Rail Traffic Lab for collaborative and positive atmosphere during and outside office hours. Special thanks to my officemates for making the room 4.17 such a joyful and inspiring place to be. Nikola, Milan and Pavle, thank you for making my landing in Delft smooth, for all the moments together, and our discussions that often resulted with a new research idea.

I am deeply grateful to my parents, Vidoje and Milanka, for unconditional love and support to my sister and me. You have been giving yourselves unreservedly, devoting your lives so we could become educated and above all honourable people. Each of my achievements in life is as much yours as it is mine! And Mirjana, thank you for being there for me my whole life. I am blessed to have you as my sister. Furthermore, I would like to thank my uncle Obrad and my aunt Živka, for all your love, care and wisdom you shared all these years. I would also like to express my gratitude to family De Jong. Ko, Ilonka, Patrick, Gaby, thank you for all your love and kindness.

I owe a special debt of gratitude to my life companion Lisa. We made it! Thank you for your everlasting and unconditional support, understanding, patience and love throughout these years. I am fortunate to have you in my life and looking forward to many happy and colourful years ahead. And Emma, my daughter, thank you for bringing a smile to my face every day. You are daddy's inexhaustible inspiration and greatest motivation on this life journey.

Rotterdam, the Netherlands, April 2023

Marko Kapetanović

Contents

1 Introduction ... 1
  1.1 Context and background ... 1
  1.2 Aspects, contributions and challenges ... 3
    1.2.1 Alternative traction options for regional trains ... 3
    1.2.2 Approaches in assessing the energy use and greenhouse gas emissions ... 5
    1.2.3 Modelling alternative propulsion systems ... 8
    1.2.4 Energy management and control strategies for alternative propulsion systems ... 9
    1.2.5 Design of alternative propulsion systems ... 10
  1.3 Research objective and research questions ... 12
  1.4 Thesis contributions ... 13
    1.4.1 Scientific contributions ... 13
    1.4.2 Societal relevance ... 14
  1.5 Collaborations in the thesis ... 15
  1.6 Thesis outline ... 15
2 Reducing fuel consumption and related emissions through optimal sizing of energy storage systems for diesel-electric trains ... 17
  2.1 Introduction ... 17
    2.1.1 Related work ... 19
    2.1.2 Chapter contribution ... 22
  2.2 Modelling of standard and hybrid DMU ... 23
    2.2.1 Vehicle ... 25
    2.2.2 Axle gear ... 26
    2.3.3 Electric motor ... 26
    2.2.4 Internal combustion engine – electric generator set ... 26
    2.2.5 Energy storage system ... 27
  2.3 Optimal ESS sizing and control ... 29

2.3.1 Optimal ESS sizing methodology 29
2.3.2 Optimal energy management strategy 30
2.3.3 Bi-level optimization methodology 33
2.4 Case study of regional railway services in the Northern Netherlands 35
2.4.1 Track parameters 35
2.4.2 Vehicle parameters 37
2.4.3 Results 40
2.5 Discussion 47
2.6 Conclusions 48
3 Analysis of hybrid and plug-in hybrid alternative propulsion systems for regional diesel-electric multiple unit trains 51
3.1 Introduction 51
3.2 Configuration of standard, hybrid and plug-in hybrid propulsion systems 53
3.3 Modelling and control of alternative propulsion systems 55
3.3.1 Simulation model 55
3.3.2 Energy management strategy 61
3.4 Case study of the Dutch Northern regional railway lines 65
3.4.1 Benchmark railway vehicle 65
3.4.2 Benchmark railway line selection 67
3.4.3 Comparative assessment results 69
3.5 Discussion 71
3.6 Conclusions 72
4 Analysis of hydrogen-powered propulsion system alternatives for diesel-electric regional trains 75
4.1 Introduction 75
4.2 Literature review 76
4.3 Hydrogen-powered propulsion systems modelling and control 80
4.3.1 Propulsion system configurations 80
4.3.2 Simulation model 83
4.3.3 Energy management and control strategy 88
4.4 Design and analysis of alternative propulsion systems 91
4.4.1 Benchmark vehicle selection 91
4.4.2 Benchmark route selection 92
4.4.3 Technology selection 93
4.4.4 Powertrain components sizing for alternative system configurations 95
4.4.5 Comparative assessment 98
4.5 Conclusions 103

5 Energy use and greenhouse gas emissions of traction alternatives for regional railways 105
5.1 Introduction 105
5.2 Literature review 107
5.3 Methodology 109
5.3.1 Framework for the assessment of overall energy use and greenhouse gas emissions 109
5.3.2 Alternative propulsion systems 111
5.3.3 Energy carriers 115
5.4 Case study of the Dutch Northern lines 118
5.4.1 Rolling stock fleet 118
5.4.2 Regional railway network and passenger services 119
5.4.3 Overview of scenarios and external factors 122
5.4.4 Comparative assessment results 123
5.5 Conclusions 131
6 Conclusions 133
6.1 Main findings 133
6.2 Recommendations for practice 136
6.3 Future research 137
Appendix A Simulation results for standard, hybrid and plug-in hybrid regional railway vehicles 139
Appendix B Well-to-Wheel analysis input data and main results 143
Bibliography 181
Summary 197
Samenvatting 201
About the author 205
TRAIL Thesis Series 209

Chapter 1

Introduction

1.1 Context and background

Global warming, caused by greenhouse gas (GHG) emissions from anthropogenic sources, led to an increase of 1.07°C in Earth's average surface temperature between 1850 and 2019 (IPCC, 2021). The effects such as rising sea level and extreme weather conditions became increasingly visible in the last decades. Global concerns for potential consequences led to several international treaties, such as the Kyoto Protocol (UN, 1998) and the follow-up Paris Agreement (UN, 2015), resulting in recommendations and defined targets to reduce the emissions. The transport sector is identified as one of the most significant contributors to GHG emissions and therefore targets have been defined for transport systems at all levels. In the European Union (EU), the transport sector accounts for one quarter of the total GHG emissions, and requires a 90% reduction of its emissions to reach climate neutrality by 2050 (EC, 2019). Modal shift from road and aviation to railways is promoted as one of the main instruments in achieving this goal.

In 2015, the rail sector accounted for 2.9% of the carbon dioxide (CO_2) emissions from transport (26.64 million tCO_2), and for 2.1% (269 PJ) of transport-related energy demand in the EU, with passenger rail activity (in passenger-km) increased by 8.9% between 2005 and 2015 (IEA and UIC, 2017). For European railways, emission reduction targets were set in 2008 by the International Union of Railways (UIC) and the Community of European Railway and Infrastructure Companies (CER). A short-term target was to decrease specific average CO_2 emissions by 2020 by 30% compared to the 1990 base year level, with medium and long-term targets for further reduction by 50% in 2030, and carbon-neutral train operation by 2050 (UIC and CER, 2012). Besides CO_2 as prevalent GHG in transport-related emissions, other most represented GHGs include methane (CH_4), nitrous oxide (N_2O), sulphur hexafluoride (SF_6), hydrofluorocarbons (HFC) and perfluorocarbons (PFC) (EC, 2017). In quantifying the amount and the composition of emitted GHGs, in order to make different types of GHGs comparable, a so called CO_2 equivalence factor (CO_2e) is defined for each of them (IPCC, 2007). This factor expresses the global warming potential (GWP) of one unit of a GHG compared with one unit of CO_2. For instance, N_2O has a CO_2e factor of 298, i.e. one ton of N_2O has the same global warming effect as 298 tons of CO_2 (JRC, 2020a).

In addition to GHG emissions, local pollutants such as nitrogen oxides (NO_x) and particle matter (PM) gained increasing attention in the railway community over recent years. This is mainly due to the introduction of the EU Non-Road Mobile Machinery (NRMM) Directive in 2016 to diesel rail vehicles and the application of the Stage IIIB emission limits. Addressing the limits of local pollutants raises significant challenges such as new considerations of vehicle design and manufacturing, reliability of new equipment in terms of produced emissions, and new assessments of life cycle costs (Beatrice et al., 2013). However, the focus of this thesis is on GHG emissions, and not on the local pollutants, as they are primarily conditioned by the implemented internal combustion engine (ICE) technology, which is mainly under the sphere of influence of external stakeholders such as equipment manufacturers. Beatrice et al. (2016) analysed a number of emerging ICE technologies and exhaust after-treatment systems (ATS) for on-road heavy-duty ICEs that are transferable to the rail sector. The results indicate the great potential of waste heat recovery in improving ICE fuel efficiency. Moreover, combining different ATSs, such as exhaust gas recirculation (EGR), diesel particulate filter (DPF), and selective catalytic reduction (SCR) technologies, can contribute in meeting the most stringent local pollutants emission requirements imposed for the rail sector (Konstandopoulos et al., 2015).

With GHG emissions from transport activities being directly related to energy consumption, a special focus is put on the environmental requirement of reducing total energy usage. Another important incentive in this regard is the reduction of energy costs (DiDomenico and Dick, 2015). All previous aspects led to a number of initiatives and measures taken by the European railway companies in order to improve their energy efficiency and reduce their carbon footprint. In addition to GHG emission regulations, companies are also imposing voluntary emission reduction targets, not only because of corporate responsibility, but also in an attempt to improve their market share, company image, and value.

Synergetic electrification of railway lines (Buzzoni and Pede, 2012; Deur et al., 2015) and an increase of renewable sources in electricity production (Shakya and Shrestha, 2011) are recognized as two of the most effective measures in improving energy efficiency and reducing GHG emissions. The share of electrified versus non-electrified railway lines has increased from less than 30% in 1975 to up to more than 60% in 2008 in the EU. However, this share remained relatively constant over the years 2008-2015 (IEA and UIC, 2017). Non-electrified lines in Europe are mainly part of regional railway networks, where high capital investments (Al-Tony and Lashine, 2000; Cambridge Systematics Inc., 2012) and low transport demand (low utilization) compared to the main corridors make their complete electrification often not economically viable. In addition, the planning and construction phase takes several years or even decades (Klebsch et al., 2019). The emergence of new traction options for railways such as alternative fuels (Dincer and Zamfirescu, 2016) and propulsion systems (Meinert et al., 2015a, 2015b) are potentially suitable alternatives.

The Netherlands have one of the highest rail electrification rates in the EU with over 75% of the railway network electrified (EC, 2018), and with the traction electricity claimed to be completely produced from wind power (EcoWatch, 2017). In 2018, electricity accounted for 85% of total energy demand in the Dutch railway sector (IEA, 2020), while the remaining 15% is attributed mainly to diesel trains operating on non-electrified regional lines, with an estimated share in total diesel consumption of 55-60% for passengers transport (CE Delft, 2020). Considering the scale and high utilization of the Dutch railway network, this share results in GHG emissions measured in millions of kilograms per year. This imposes a significant challenge to railway undertakings (RUs) and policy makers in identifying alternative solutions. This thesis focusses on the Dutch Northern lines (in Dutch, *Noordelijke lijnen*), a common name for the seven non-electrified railway lines that constitute the regional railway network in the provinces of Friesland and Groningen. Passenger services on the network are provided by Arriva, the largest regional RU in the Netherlands. As part of the new 15-years concession that started in December 2020, the RU committed to significantly reduce the overall GHG emissions on the network (Arriva, 2019).

As identified by Scheepmaker et al. (2017), the reduction of energy consumption (and thus related GHG emissions) from railway operation can be achieved in several ways: more energy-efficient rolling stock, minimizing energy consumption of auxiliary systems during stabling periods, optimization of the rolling stock deployment based on capacity and demand, energy-efficient timetabling and energy-efficient train control. This thesis focuses on the first two options. In particular, the first option is considered through the assessment of potential energy savings and GHG emissions reduction from the implementation of advanced (hybrid) propulsion systems in regional diesel-electric multiple unit (DEMU) vehicles, as a predominant vehicle category in regional railway networks. Furthermore, similar to the car-free zones in urban areas, an increasing number of railways are introducing zero-emission train operation in station areas with high passenger concentration. Thus, the second option is implicitly considered by imposing this particular requirement to the selection and/or design of alterative propulsion systems. In addition to the energy efficiency improvement from the advanced vehicle powertrains, alternative fuels aim to reduce overall carbon footprint, including both emissions from direct combustion and those related to their production and distribution, with a number of alternatives to fossil diesel emerged in the transport sector, including first and second generation biofuels, hydrogen, synthetic or e-fuels, etc. (Andersson and Börjesson, 2021).

The transition from conventional DEMUs to alternative systems is a complex and context-specific dynamic decision-making process that requires involvement of multiple stakeholders and consideration on numerous aspects. It requires in-depth analyses that include identification of available technology, design, modelling, and assessment of potential alternatives, with respect to the particular case-related constraints imposed by infrastructure, technical and operational characteristics and requirements (e.g., track geometry, speed, and axle load limitations, implemented onboard power control of different power sources, maintaining existing timetables, noise-free and emission-free operation in stations, etc.). This thesis aims to support the railway undertaking in this decision-making process by providing a comprehensive comparative model-based assessment of different solutions in terms of overall energy consumption and produced GHG emissions.

1.2 Aspects, contributions and challenges

1.2.1 Alternative traction options for regional trains

Vehicle hybridization, achieved by adding an energy storage system (ESS), enables the storing of braking energy and support to the ICE, resulting in a significant reduction in fuel consumption and related emissions (Bai and Liu, 2021). Various ESS technologies have emerged in the transport sector over the last decades, with detailed characteristics of different ESS technologies provided in reviews by Bagotsky et al. (2015) and Ghaviha et al. (2017). Batteries, double-layer capacitors (DLCs), and flywheels are being the most represented solutions depending on the particular application and requirements (Vazquez et al., 2010). Due to their high energy-to-weight ratio, no memory effect, low self-discharge rates, rapid technology development, and commercial availability, lithium-ion batteries (LBs) are the most represented battery and ESS technology in railway applications (Meinert et al., 2015a). DLCs provide high power density and low energy density, making them suitable for peak power shaving and maximizing recuperation of braking energy. They are often coupled with LBs in a hybrid energy storage system (HESS), that combines individual benefits offered by the two technologies (Dittus et al., 2011; G. Zhang et al., 2019). Flywheels offer fast charging and discharging rates; however, they are featured with various safety issues (González-Gil et al., 2013), high weight and self-discharging rates.

While ESS in hybrid systems relies exclusively on internal charging using the energy from regenerative braking and an ICE, in plug-in hybrid systems it can be additionally charged from an external power source. This additional charge could potentially further improve ICE's efficiency and reduce overall emissions. Hybrid and plug-in hybrid propulsion systems are increasingly being developed and used in road transport with the aim to improve vehicle fuel economy (Fuhs, 2008; Lipman, 2020) and reduce emissions (Doucette and McCulloch, 2011; Requia et al., 2017). A number of hybrid electric vehicles (HEVs) and plug-in hybrid electric vehicles (PHEVs) became commercially available over the last two decades (Orecchini et al., 2014; Orecchini and Santiangeli, 2010), which is likewise reflected in the extensive research efforts on their development as reported in the literature (Williamson, 2013; Tran, 2020).

Regarding hybrid railway vehicles, several European research projects (e.g. ULEV-TAP 2 (EC, 2005), DfTRG/0078/2007 (Hillmansen et al., 2009, 2008), CleanER-D (Marsilla, 2013)) demonstrated significant benefits reflected in fuel savings up to ~40%, depending on the technology and operational characteristics. Despite identified potential benefits, hybridization of railway powertrains is still in the early development stages. Due to a comparably smaller market for railway vehicles, only a small number of hybrid DEMUs exist (Engel and Soefker, 2001; Research and Technology Centre of Deutsche Bahn AG, 2001; Fujii et al., 2004; Shiraki et al., 2010; Railway Gazette International, 2015; Klebsch et al., 2018), mainly as prototypes.

Plug-in hybrid systems offer further exploitation of the benefits offered by the ESS using an external electric power source for their charging during stabling periods. However, practical implementation of a plug-in hybrid concept in the railway sector is limited to shunting locomotives thus far (Alstom, 2016, 2015; INSIDEEVs, 2015; Railcolor News, 2018), with no reported applications nor literature concerning commercial passenger transport. Utilization of fast charging facilities in stations is considered mainly for battery-electric trains, as a complement to partially electrified regional railway lines (Hirose et al., 2012; Kono et al., 2014; Masatsuki, 2011, 2010; Shiraki et al., 2015), or in tram networks (Mwambeleko and Kulworawanichpong, 2017) which represent other use cases than the main subject of this thesis.

While hybrid and plug-in hybrid systems still rely on the ICE as the prime mover, several emission-free alternatives are being developed in recent years. Battery-electric multiple unit (BEMU) and fuel cell multiple unit (FCMU) vehicles are identified as potentially suitable long-term solutions (Klebsch et al., 2019). BEMUs (RailTech, 2019; RailwayTechnology, 2020; Siemens, n.d., n.d.; Railway Gazette International, 2022) allow for catenary-free operation with the traction power provided from an onboard ESS, typically large LB system. In this case, the ESS can be charged during stabling periods and/or during train operation on partially electrified tracks. FCMUs (IRJ, 2019; Alstom, 2020; FuelCellWorks, 2020; 2022) employ hydrogen fuel cell (FC) technology for onboard power generation. FCs offer numerous advantages compared to ICEs, summoned primarily in high efficiency, quiet and emission-free operations at the point of use, with water vapour and heat as the only products (Sun et al., 2021). However, their main drawback is the slow dynamic response, which requires vehicle hybridization with an ESS that would cover power fluctuations and allow for the recuperation of braking energy (Siddiqui and Dincer, 2019). Although BEMUs and FCMUs allow for (locally) emission-free trains operation, their readiness to operate on existing networks is subjected to a number of local requirements and constraints (Mueller et al., 2020). A "zero-one" transition to these vehicles is hindered by numerous aspects related primarily to the vehicle range, techno-economic maturity and availability, and supporting infrastructure requirements (Klebsch et al., 2020). Existing limitations stipulate further development and exploitation of ICEs and DEMUs, while constantly improving their energy efficiency and environmental performance by implementing novel technological solutions in order to meet increasingly stringent emission reduction requirements. Furthermore, considering the service life of conventional DEMUs, typically spanning over 30 years, it could be advantageous to convert existing vehicles to their low or zero-emission counterparts instead of replacing them with new commercially available alternatives. A prominent recent example for the regional train is UK's HydroFLEX, in operation since 2019 (Calvert et al., 2021; Gallucci, 2019).

Although MAN produces hydrogen ICEs for busses (Knorr et al., 1998; MAN, 2020), no commercial railway vehicles are powered by a hydrogen ICE. However, another major ICE manufacturer Deutz recently announced the introduction of hydrogen ICEs in 2024, aimed at railway applications (Deutz, 2021). Hydrogen combustion in ICE does not produce GHG emissions; however, local pollutants such as NO_x are emitted due to high-temperature hydrogen and lubricant oil combustion with air. Their main advantage is that they are based on well-established technology, as they mostly represent modifications of existing ICEs running on compressed natural gas (Akal et al., 2020), and have a service life three times longer than the FCs (Marin et al., 2010). Based on the previous experience with other technologies that found their place in railway applications as a result of spillovers from other modes of transport such as busses and passenger cars, together with the relatively low price compared to the emerging technology as FCs, hydrogen ICEs could be considered as a carbon-neutral bridging solution towards totally-emission free railway transport.

1.2.2 Approaches in assessing the energy use and greenhouse gas emissions

Various approaches are used in assessing the energy use and GHG emissions in the transport sector, differing in the scope, background methodology and assumptions. Life Cycle Assessment (LCA) as the most thorough method includes the entire life cycle of a product, process or activity, i.e., the extraction and processing of raw materials, construction/manufacture, operation, maintenance, and end-of-life processes including recycling and/or disposal (Kapetanović et al., 2019), as shown in Figure 1.1. Traditionally product oriented, LCA provides a set of environmental impact indicators such as global warming potential, ozone depletion, human toxicity, acidification, etc. (Curran, 2012). With local specifications typically not considered and assumed uniform conditions, assessing GHG emissions in such analysis could lead to biased conclusions as they highly depend on the context and case-specific energy sources (Nocera and Cavallaro, 2016). While in some cases that require railway infrastructure construction with related processes resulting in a great environmental impact (Banar and Özdemir, 2015; Stripple and Uppenberg, 2010), a number of LCA studies showed that GHG emissions resulting from train production, maintenance, recycling and/or disposal usually have minor contribution when compared to the operation phase (Andrade and D'Agosto, 2016; Chan et al., 2013; Del Pero et al., 2015; Shinde et al., 2018), mainly due to a long service life of railway vehicles. Regarding hybridized DEMU vehicles, an LCA study by Meynerts et al. (2018) on hybridized diesel railcar with and without additional recharging stations showed that the operation phase accounts for the biggest part of the environmental impact released over the railcar's lifetime, with negligible impact from the production phase, mainly attributed to the battery production. The authors suggest that further progress could be made through the increase in efficiency of using recuperated breaking energy as well as the use of renewable energy for battery recharging.

A Well-to-Wheel (WTW) approach is a sub-class of LCA methods, focusing on the vehicle operation phase and the life cycle of an energy carrier (e.g., diesel, electricity), commonly referred as fuel cycle (Figure 1.1). A WTW analysis is sub-divided into Well-to-Tank (WTT) phase, related to the production and distribution pathway of an energy carrier, and Tank-to-Wheel (TTW) phase, linked to the energy expended and tailpipe emissions emitted directly from the vehicle during its drive cycle. In this way, a clear distinction is made between the energy use and GHG emissions related to the primary energy source and those associated to the vehicle powertrain technology (Nocera and Cavallaro, 2016). In contrast to the LCA approach where stages such as vehicle production, disposal and recycling are influenced by the activities of external parties, e.g. vehicle manufacturers, the WTW system boundary reflects the sphere of influence in which transport operators can actively reduce energy use and GHG emissions, for instance by employing novel propulsion systems and/or alternative transport fuels (Dreier et al., 2018). Moreover, European standards such as EN16258 (CEN, 2012) stipulate the WTW system boundary on calculation and declaration of energy use and GHG emissions from transport services, while explicitly excluding other stages in the vehicle life cycle. Therefore, this thesis limits its analyses to the WTW system boundary.

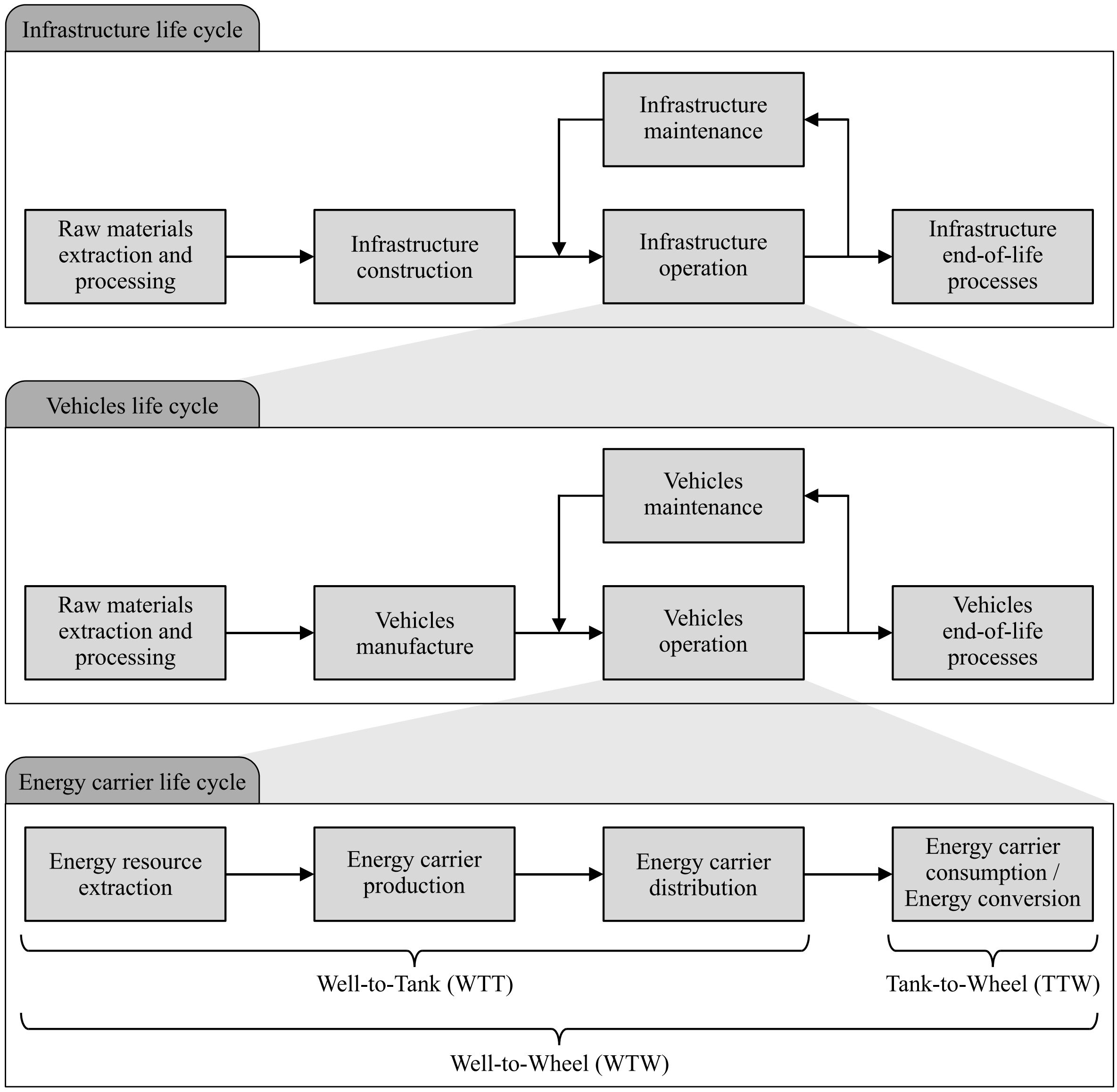

Figure 1.1: System boundary for infrastructure, vehicles and energy carrier life cycle.

While extensive research on WTW energy demand and GHG emissions linked to the alternative powertrain configurations and transport fuels has been carried out for automotive (Küng et al., 2018; Yazdanie et al., 2016, 2014), bus (Dreier et al., 2018; Mao et al., 2020; Pourahmadiyan et al., 2021; Soukhov and Mohamed, 2022) and heavy duty road transport (Gustafsson et al., 2021; Kuttler and Pichlmaier, 2021; Mojtaba Lajevardi et al., 2019), only a few studies have considered the railway sector. Hoffrichter et al. (2012) evaluated WTW energy efficiencies and CO_2 emissions for electric, diesel and hydrogen (both, ICE and FC) traction for railway vehicles using existing estimations in the literature and assumptions for each energy pathway component. They found that gaseous hydrogen has a WTW efficiency of 25% if produced from methane and used in a FC, similar to diesel and electric traction in the UK and the US. They suggest that a CO_2 emissions reduction of about 19% could be achieved when hydrogen gas is used in an FC compared to diesel traction, and a 3% reduction compared to US electricity. The case of diesel traction demonstrated that a high WTW efficiency does not automatically lead to lower emissions. Esters and Marinov (2014) compared different resistance-based methods for calculating emissions of UK rolling stock based on their type (conventional, high-speed and freight) and mode of operation (diesel, electric and bi-mode). The results indicated that diesel trains emit less emissions than electric trains due to domination of a high-carbon primary source for electricity production in the UK. Despite time efficiency, high-speed trains release high emissions due to energy consumption increasing with the square of speed. The authors also identify redundancy of bi-mode trains in the future, having in mind the electrification trends and recommend biodiesel as an alternative fuel as emissions fall significantly with content of biodiesel in fuel blends. Gangwar and Sharma (2014) quantified the WTW emissions from diesel and electric locomotives in India. The study showed that the accumulated carbon footprint of running electric locomotives was higher, as a consequence of using coal as a primary source in electricity production, and suggests that there should be a judicious mix of both tractions to achieve a balance in environmental efficiency, sustainability and equity. Washing and Pulugurtha (2015) estimated WTW efficiencies of electric and hydrogen light rail in Charlotte, North Carolina (US). The inefficiencies of the fuel cell system and hydrogen production process are apparent in the hydrogen train's WTW efficiency value of 16.6–19.6%, assuming hydrogen obtained from steam-methane reforming, while the electric train uses substantially less feedstock energy with a WTW efficiency value of 25.3%. The study confirmed the great influence of the main source of electricity production on the electric train's efficiency by observing other regions, i.e., 24.6% in Cleveland, Ohio (with domination of coal) and 50.3% in Portland, Oregon (with domination of hydroelectric power).

As can be noted, railway-related WTW studies focus mainly on conventional (non-hybrid) powertrain topologies, and biodiesel and/or hydrogen as the only alternatives to diesel fuel. Despite demonstrated significant fuel savings from hybridization of diesel trains (Cipek et al., 2019; Meinert et al., 2015a, 2015b), and the range of alternative fuels that emerged in the transport sector (Dincer et al., 2016; Dincer and Zamfirescu, 2016), no scientific study on the comparative assessment of WTW energy use and GHG emissions from synergetic implementation of such solutions has been found. While a WTW analysis is straightforward in ex-post evaluations for transport that took place already with fuel consumption known, ex-ante assessments for potential future solutions in terms of alternative propulsion systems and energy carriers require application of detailed models in order to obtain reliable estimates of direct (TTW) energy usage. In assessing direct energy consumption, existing literature mainly presents meta-analyses, or implementation of high-level mathematical and simulation models which are unsuitable for hybrid configurations, as the latter include a high complexity reflected in the existence of multiple power sources. Moreover, analysis of real-world cases requires consideration of numerous factors that influence vehicle performance, which are often omitted, e.g., track geometry, passenger load, ambient conditions, etc.

1.2.3 Modelling alternative propulsion systems

Widely used models that can support the assessment of environmental impact in railway operations, such as ARTEMIS (Boulter and McCrae, 2007), EcoTransit (Knörr et al., 2018), or EcoPasssenger (Knörr and Hüttermann, 2016), calculate the fuel consumption and emissions based on mechanical energy using mostly one-lumped efficiency and fixed fuel consumption and emission factors. These models provide predictions for conventional railway vehicles. The case of hybrid vehicles requires more detailed models that include individual components of the powertrain and their interactions. Hybrid vehicle models based on physical relations between the components of the system can be divided into two categories: forward-looking and backward-looking models (Gao et al., 2007; Guzzella and Sciarretta, 2013; Horrein et al., 2012). Forward-looking simulation models follow the physical power flow in the powertrain, starting from the engine, and then to the transmitted and reflected torque to the wheels. They offer realistic control-oriented modelling by capturing driver input/speed control; however, they are usually very complex and characterized by slow execution time and high computer memory requirements. Backward-looking simulation models consider the reverse power flow by computing the tractive contribution required at the wheels and the order of evaluating the system components backward through the system towards the engine, offering a reliable evaluation of vehicle energy consumption based on the drive cycle and detailed vehicle-specific data available beforehand. They typically feature fast execution times compared to the forward-looking models (Fiori et al., 2016; Gao et al., 2007; Wang and Rakha, 2017). Depending on the aim of the study, data availability, and the purpose of the simulation model, the adequate type should be selected. Regarding the hybrid DEMU railway vehicles, a forward simulation approach is usually used in assessing the potential fuel savings for different driving strategies and styles (Schmid et al., 2017), while backward simulations are performed using mostly typical speed profiles and duty cycles, c.f. Lanneluc et al. (2017), Leska et al. (2017, 2014), Leska and Aschemann (2015), Poline et al. (2019).

In addition to the previous physical models, the energetic macroscopic representation (EMR) is an effective graphical modelling approach in the systemic description of complex propulsion systems (Joud et al., 2020). A study by Kréhi Serge Agbli et al. (2016) demonstrated the effectiveness of using EMR in reverse engineering of railway vehicles to describe power flows behaviour and deriving models for the key propulsion system components, disregarding in-depth knowledge of the train energetic devices and sub-systems. It can be particularly useful in case of lack of detailed vehicle-specific parameters due to, e.g. confidentiality aspects or sub-systems provided by subcontractors, by fitting the energetic behaviour of the vehicle with the available test data (Krehi Serge Agbli et al., 2016). In addition, the approach can be successfully applied to perform model-based development of suitable energy management strategies (Mayet et al., 2012).

Furthermore, (sub)models of electrochemical power sources, such as FCs, batteries, and DLCs, can be generally divided into electrochemical models and equivalent electrical circuit models (Zhang et al., 2017). Different dimensions of electrochemical models use electrochemical equations in modelling and describing the distributed electrochemistry reactions in the electrodes and electrolytes. Piraino and Fragiacomo (2020) provided a comprehensive model that incorporates each powertrain component, such as energy sources, power electronics and drivetrain. Although these physics-based models can provide the information on the full dynamic behaviour of the system, they require detailed information and numerous parameters on the physical system, which are often difficult to obtain, and employ a set of partial differential equations, which make them too complex for fast simulation purposes (Ghaviha et al., 2019). On the other hand, different orders of equivalent electrical circuit models use different electrical components such as capacitors and resistors to obtain a response similar to the behaviour of the physical system (see Krastev and Tricoli, 2022). They provide high enough accuracy for power management applications, while avoiding unnecessary complexities of the electrochemical models (Fotouhi et al., 2016).

1.2.4 Energy management and control strategies for alternative propulsion systems

Since the energy management and control strategy (EMCS) is the main driver of the fuel economy for hybrid vehicles, most of the railway literature focuses on this aspect, i.e., its development for a particular predefined powertrain configuration. EMCSs can be generally classified into optimization-based and rule-based strategies, where the former are further divided according to the optimization horizon in global optimization, instantaneous optimization, and real-time optimization (Xu et al., 2015a). Dynamic programming (DP) is a powerful method for solving global optimization problems. Assuming an ideal case, i.e. perfect information on the future duty cycle, DP is used in obtaining a fuel-optimal (combined) driving and energy management strategy by Leska and Aschemann (2015). Using a simplified version of the EMR model from Kréhi Serge Agbli et al. (2016), a DP-based optimization of EMCS for a regional train hybridized with lithium-ion battery is proposed by Sorrentino et al. (2020). The comparative assessment for three different degrees of hybridization (battery size) and two realistic mission profiles for a regional railway route indicated potential fuel savings reaching a significant level up to 18%. Ogawa et al. (2007) proposed an optimal EMCS based on DP for a FC/DLC railway vehicle, further used in deriving an optimal required capacity for a DLC. Although DP allows for deriving a globally optimal ECMS, it is mainly employed for off-line controller optimization, with several drawbacks hindering its real-time applications. These include its requirements for perfect information on the future duty cycle, the extensive calculation time, frequent switches in power distribution, and the inability to deal with variables that include counters due to its non-causal nature, i.e., propagation backward in time. Therefore, these algorithms are often used as a benchmark in developing other causal controls. Such an algorithm based on a sensitivity analysis and the bisection method for a diesel train equipped with a lithium-ion battery is presented by Leska et al. (2014), showing promising benefits in performance and especially computational cost compared to the DP method. The same algorithm is used by Leska et al. (2017), with the analysis extended to DLC as alternative ESS technology. DP is also used as a benchmark in finding optimal dispatch (power distribution between ICEs) strategies by Lu et al. (2011, 2010), with fuel savings up to 7% compared to typical operation. Tao et al. (2021) combined DP and state machine control in obtaining optimal power distribution between the FC and DLC for a tram vehicle, demonstrating significant benefits in terms of fuel economy, efficiency and durability. Regarding regional railway vehicles, Peng et al. (2020b) used DP in deriving a scalable, causal, adaptive EMCS for an FC/LB powertrain, achieving only 0.01-0.09% increase in fuel consumption compared to the optimal case.

The equivalent consumption minimization strategy (ECMS) and Pontryagin's minimum principle (PMP) method are suitable for instantaneous optimization problems. Torreglosa et al. (2011a) presented an ECMS for an FC/battery hybrid tram, with the results showing significant benefits reflected in fuel savings compared to other causal controls, while at the same time maintaining the battery state-of-charge (SoC). A similar approach is proposed by W. Zhang et al. (2017) in a case of an FC/LB/DLC tram. This method is also used as the basis in the development of dynamic power factor control for a FC/LB locomotive (Hong et al., 2018). H. Zhang et al. (2019) proposed a firefly algorithm to optimize the parameters in ECMS for an FC/LB/DLC tram. Liu et al. (2020) employed PMP in defining the optimal energy management and the optimal braking energy recovery strategy for an FC/DLC tram. Peng et al. (2020a) used the same method as a benchmark in deriving a causal real-time control for a regional railway vehicle. The effectiveness of these methods depends on how the future driving conditions and critical parameters, namely the equivalent coefficient in ECMS and the initial value of the co-state in PMP, are estimated (Zhang et al., 2017). Additionally, whether a certain control can be used online is decided by computation costs and storage memory requirements (Li et al., 2019), posing additional challenges in practical applications of such causal controllers. In general, with the future driving conditions properly estimated, the previous two methods can be applied to real-time optimization problems.

Compared to the previous optimization-based methods, rule-based (RB) algorithms use event-triggered Boolean rules in determining the power ratio between different power sources in the system. These rules can be derived from optimization algorithms, heuristics or fuzzy rules based on experts' knowledge (Lanneluc et al., 2017). RB algorithms have been used by Dittus et al. (2011) and García-Garre and Gabaldón (2019) in defining real-time EMCSs for hybrid diesel trains. Garcia et al. (2010) proposed an adaptive RB control for a tram by considering eight states in distributing requested power between the FC and a nickel-metal hydride cell battery. A similar control based on a state machine for a hybrid FC/LB tram is proposed by Han et al. (2016). A two-mode multisource coordination EMCS based on self-convergence droop control for a FC/LB/DLC tram is presented by Han et al. (2018). A power-voltage equilibrium strategy based on droop control for an FC/LB/DLC hybrid tram was proposed by G. Zhang et al. (2019). Peng et al. (2018) used fuzzy logic in developing a sub-optimal control for an FC/LB/DLC tram by incorporating operational uncertainties, performance degradation and SoC balancing. A fuzzy logic controller for an FC/LB tram based on LB SoC, and FC and traction load was proposed by Torreglosa et al. (2011b). Although RB strategies typically cannot offer a proof of optimality, low computation cost and storage memory requirements make them especially suitable for the development of causal real-time controllers, offering at the same time promising benefits in terms of energy consumption reduction (Zhang et al., 2020).

1.2.5 Design of alternative propulsion systems

Vehicles hybridization can be considered a multi-objective design optimization problem, with multiple parameters distributed over multiple levels (topology, technology, size, and control). When this optimization problem is solved sequentially (level by level), it is by definition sub-optimal due to coupled dynamic parameters and non-linear effects (Silvas et al., 2016). While topology and technology choices in the DEMU hybridization process are mainly conditioned to the available fleet and main hybridization requirements, thus making these decisions relatively easy, optimal sizing and control of the ESS are complex tasks, which are in most cases treated separately. Taking into account that oversizing of the ESS might unnecessarily increase total ESS mass and volume, as well as total costs, whereas an undersized ESS might lead to considerable energy waste, a detailed analysis is needed to determine an optimal design, while the sizing method depends upon its main function (González-Gil et al., 2013). In particular, a different approach is required if the main intended function of the ESS is, for instance, supporting auxiliaries during stabling periods, maximizing utilization of braking energy, or converting a DEMU to a catenary-free BEMU. The need for co-design, i.e. integrating the two design optimization levels, has been addressed in hybridization-related literature in general (Fathy et al., 2001), confirming the importance of co-optimization in achieving the best configurations. Although strong interdependence between the optimal ESS sizing and control levels has been widely recognized and established, most of the studies on hybridized DEMU railway vehicles focus only on the optimal control, assuming ESS size given beforehand, or roughly estimated before determining the optimal EMCS. As a rare example, simultaneous optimization of hybrid ESS (LB and DLC) size and energy management strategy for a DEMU is presented by Poline et al. (2019). The authors used the frequency management approach based on a low-pass filter coupled with DP as the optimal control method. The existence of multiple ESS technologies, and the solution approach that considers approximations of mixed-integer and discontinuous variables, in this case, raised significant challenges in terms of computation time and errors.

Transition to hydrogen-based propulsion systems, especially FC-based, is a more complex task than only hybridization of diesel-electric powertrains, as it requires additional considerations of a FC stack and hydrogen storage size, as well as physical limitations linked to this technology such as a slow dynamic response. Several studies reported on a conversion analysis of existing railway vehicles to their hydrogen FC counterparts. For instance, Washing and Pulugurtha (2016) presented a simulation-based analysis of energy use and emissions for a pure FC and a hybrid FC/LB alternative powertrain for a Siemens light rail vehicle operating in North Carolina. Analyses that employ similar simplified vehicle models are reported for locomotives by Miller et al. (2007) and Peng et al. (2014). Concerning the design of hydrogen-based regional vehicles, a conceptual design of FCMUs, both non-hybrid and hybrid with an LB, is presented by Hoffrichter et al. (2016). The authors investigated the feasibility of converting a standard DEMU from Stadler, by incorporating constraints related to the available weight and volume of the components, as well as the range requirements for the FCMUs. In terms of selection and sizing of powertrain components, the vehicle design is based on a simulated round trip and corresponding energy demand of a standard DEMU, with no detailed models that would capture the dynamics of electrochemical power sources (FC and LB), nor active EMCS implemented. A similar study for the British class 150 regional train is presented by Din and Hillmansen (2018). In contrast to the previous conceptual designs that focus more on the practical implementability of a particular technology, while neglecting detailed powertrain and EMCS modelling, some papers employed optimization algorithms that consider the relationship between the EMCS in place and the optimal size of the powertrain components based on selected main criteria and constraints, while focusing mainly on locomotive applications. Such method based on the Krill herd optimization algorithm is presented by Guo et al. (2020) for a hybrid FC/LB locomotive. A Particle Swarm Optimization algorithm combined with several rule-based power controls for a hybrid FC/LB locomotive was presented by Sarma and Ganguly (2020; 2018).

A literature review by Kapetanović et al. (2022) showed that an extensive research has been reported on different aspect of hydrogen propulsion systems deployment in the railway sector, focusing mainly on ECMS development for a particular predefined powertrain configuration. However, several limitations and scientific lacks were identified among the prior research. Existing studies focus exclusively on FCs technology, with no reported detailed analyses on hydrogen ICEs, and with only a scarce number of comparative analyses between alternative powertrain configurations and ESS technologies. Regarding the type of analysed vehicles (market segment), urban railway vehicles (trams) are a predominant category in the literature, followed by locomotives, with a limited number of papers focusing on regional multiple unit railway vehicles. Although the main principles in powertrain design apply to different applications, freight locomotives and trams are characterized with different technical characteristics, stopping patterns, and lower operational speeds, resulting in different energy and power demand, duty cycles, and related design parameters. For instance, Fragiacomo and Piraino (2019) analysed the use of hydrogen-hybrid powertrains including FCs, LBs and/or DLCs in four different contexts in Southern Italian railways, including detailed powertrain modelling, EMCS, and validation using real-world measurements, with the results indicating a significant impact of case related characteristics on both powertrain design and performance. One of the main challenges in realizing a comprehensive comparative design and reliable performance assessment is addressing the issues related to detailed data availability and high complexity of the models.

To improve the environmental sustainability of regional railway services, one needs to obtain reliable estimates of potential benefits linked to the alternative solutions. This thesis aims to develop methods and models for assessing the environmental impacts from different options, while considering present context and elaborated aspects, knowledge gaps and challenges. In doing so, it addresses the research objective and accompanying research questions, which are provided in the next section.

1.3 Research objective and research questions

The main objective of this dissertation is *to identify and assess potential solutions in reducing overall (Well-to-Wheel) energy use and greenhouse gas emissions from the operation of regional trains, focussing primarily on alternative propulsion systems and energy carriers*. Given the range of available propulsion system technologies, energy carriers, and their production pathways, it is essential to understand the overall energy demand and GHG emissions associated with each alternative. This information enables a consistent and credible comparative analysis, which is crucial in policy decision-making and planning of energy efficient and low- or zero-emission regional railway transport. As for the geographical context the present research focuses on the Dutch regional railway network in the Northern provinces Friesland and Groningen in particular (Figure 1.2). Findings are, however, applicable to similar settings in other regional railway lines and networks. In order to structure this thesis, the following key research questions are considered:

1. How to model the dynamic behaviour of alternative propulsion systems and estimate corresponding energy consumption? (Chapters 2-4)

2. How to determine the optimal size of the energy storage system for a hybridized diesel-electric railway vehicle? (Chapter 2)

3. What are the potential energy savings from the implementation of hybrid and plug-in hybrid propulsion system concepts in diesel-electric trains? (Chapter 3)

4. How to develop a conceptual design of hydrogen-powered propulsion systems for the conversion of diesel-electric trains? (Chapter 4)

5. How to estimate Well-to-Wheel energy demand and greenhouse gas emissions from the implementation of alternative propulsion systems and energy carriers? (Chapter 5)

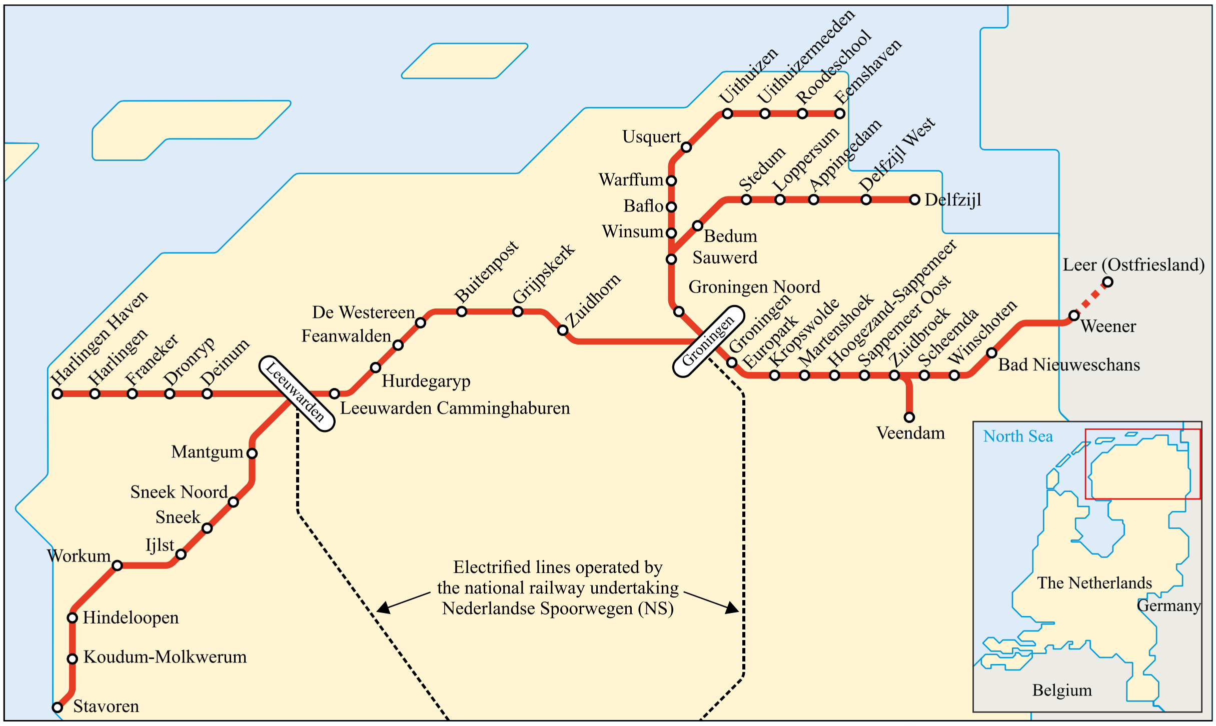

Figure 1.2: Simplified schematic representation of the regional railway network in the Northern Netherlands.

1.4 Thesis contributions

This section provides a summary of the main thesis contributions, separated into scientific contributions (Section 1.4.1), and societal relevance (Section 1.4.2).

1.4.1 Scientific contributions

The scientific contributions as a result of addressing the previously defined research questions, can be grouped into the following five topics:

- *A backward-looking quasi-static simulation model of alternative propulsion systems.*
  A simulation model of various alternative propulsion systems (Chapters 2-4) is successively developed in MATLAB®/Simulink© using the OPEUS Simulink library and simulation tool (Pröhl, 2017a) – a result of the built up knowledge from several European projects, i.e., MERLIN (CORDIS, 2021), Cleaner-D (CleanER-D, 2020) and OPEUS (Shift2Rail, 2021). The existing library is extended with additional modules such as hydrogen fuel cells, and newly developed energy management and control strategies for each powertrain topology. The developed model allows for realistic systems performance evaluation, while requiring only main technology parameters typically published by manufacturers and avoiding issues related to the detailed data unavailability and/or confidentiality.

- *A methodology for determining the optimal size of the energy storage system.*
  A bi-level multi-objective optimization approach is developed for determining the optimal size for the battery-based energy storage system by integrating the sizing and

control optimization levels, while at the same time incorporating emission-free and noise-free operation in stations in the problem formulation (Chapter 2).

- *Propulsion system design and comparative analysis of hybrid and plug-in hybrid concepts.*
  A method to support the conversion of a conventional regional vehicle to its hybrid and plug-in hybrid counterparts is presented in Chapter 3, including two energy storage system technologies and newly developed causal and easy-to-implement real-time power controls, allowing for an estimation of achievable fuel savings.

- *A method to support the design of alternative hydrogen-powered propulsion systems.*
  A conversion of a regional diesel-electric railway vehicle to its hydrogen-powered counterpart (Chapter 4) is proposed considering both an internal combustion engine and a fuel cell system as the prime mover, and various energy storage systems based on lithium-ion battery and/or double-layer capacitor technologies, with explicitly incorporated constraints and requirements related to the power and energy demand, vehicle range, weight and volumetric space.

- *Analysis of Well-to-Wheel energy demand and greenhouse gas emissions from the implementation of alternative propulsion systems and energy carriers.*
  A comprehensive comparative analysis (Chapter 5) is presented including the implementation of various propulsion systems combined with prominent low or zero-emission energy carriers, while including both commercially-mature and novel technologies and energy carrier production pathways. The analysis adopts a bottom-up consumption-based approach, with direct fuel and/or electricity consumption estimated using a detailed simulation model able to capture relevant factors influencing direct energy use, and thus resulting emissions.

1.4.2 Societal relevance

This thesis brings the following contributions to society:

- *A decision support system in planning future investments in rolling stock.*
  The models and methods presented in this thesis can serve as an effective decision support system in planning investments in rolling stock, primarily by considering implementation of alternative propulsion systems and energy carriers. A high level of generality allows for their application to various railway market segments and geographical contexts.

- *Estimations of primary energy use and GHG emissions for a large set of alternatives.*
  Using energy carrier pathways and emission factors relevant for European and the Dutch context, this thesis provides the railway undertaking and policy makers with essential information in planning future rolling stock and infrastructure investments. This thesis provides detailed values for primary energy use and GHG emissions which can also be very useful in future research, especially in comparable cases when detailed vehicle, infrastructure and/or operational parameters are unavailable.

1.5 Collaborations in the thesis

A collection of four scientific articles written with co-authors form the core of this thesis. Most of the work in this thesis has been done independently by the author. The author has been responsible for performing a literature review, formulating research questions, developing and implementing the models, analysing and visualizing the results, and writing the chapters and corresponding articles. In addition to the supervisors, one of the papers has been written with a visiting PhD student from the Sapienza University of Rome, with his contribution to the paper given below. In the thesis, chapters are based on the following articles:

- Chapter 2: Kapetanović, M., Núñez, A., van Oort, N., Goverde, R.M.P. (2021). Reducing fuel consumption and related emissions through optimal sizing of energy storage systems for diesel-electric trains. *Applied Energy*, 294, 117018.

- Chapter 3: Kapetanović, M., Vajihi, M., Goverde, R.M.P. (2021). Analysis of Hybrid and Plug-In Hybrid Alternative Propulsion Systems for Regional Diesel-Electric Multiple Unit Trains. *Energies*, 14, 5920. The second co-author contributed to the conceptualization of the research and writing of the article.

- Chapter 4: Kapetanović, M., Núñez, A., van Oort, N., Goverde, R.M.P. (2022). Analysis of hydrogen-powered propulsion system alternatives for diesel-electric regional trains. *Journal of Rail Transport Planning & Management*, 23, 100338.

- Chapter 5: Kapetanović, M., Núñez, A., van Oort, N., Goverde, R.M.P. (2023). Energy use and greenhouse gas emissions of traction alternatives for regional railways. (*Under review*).

1.6 Thesis outline

This section provides the description of the thesis outline, visually represented in Figure 1.3. Generally, chapters are structured according to the main scope of the analysis into vehicle-based modelling and control, and network-scale Well-to-Wheel analysis. The focus of Chapter 2 is the optimal sizing of a lithium-ion battery energy storage system, based on a detailed simulation model and integrated sizing and control optimization levels. The simulation model is further extended in Chapter 3 with a plug-in hybrid propulsion system, and a new real-time energy management and control strategy based on a finite state machine, while also incorporating a double-layer capacitor as the alternative energy storage system technology. The vehicle simulation model and power controller are further extended and applied to hydrogen-powered propulsion system configurations in Chapter 4. Chapter 5 summons all considered alternative propulsion systems and energy carriers, and provides a Well-to-Wheel analysis of energy demand and greenhouse gas emissions by considering all rolling stock and lines in the network. Finally, the conclusions and recommendations for future research are provided in Chapter 6.

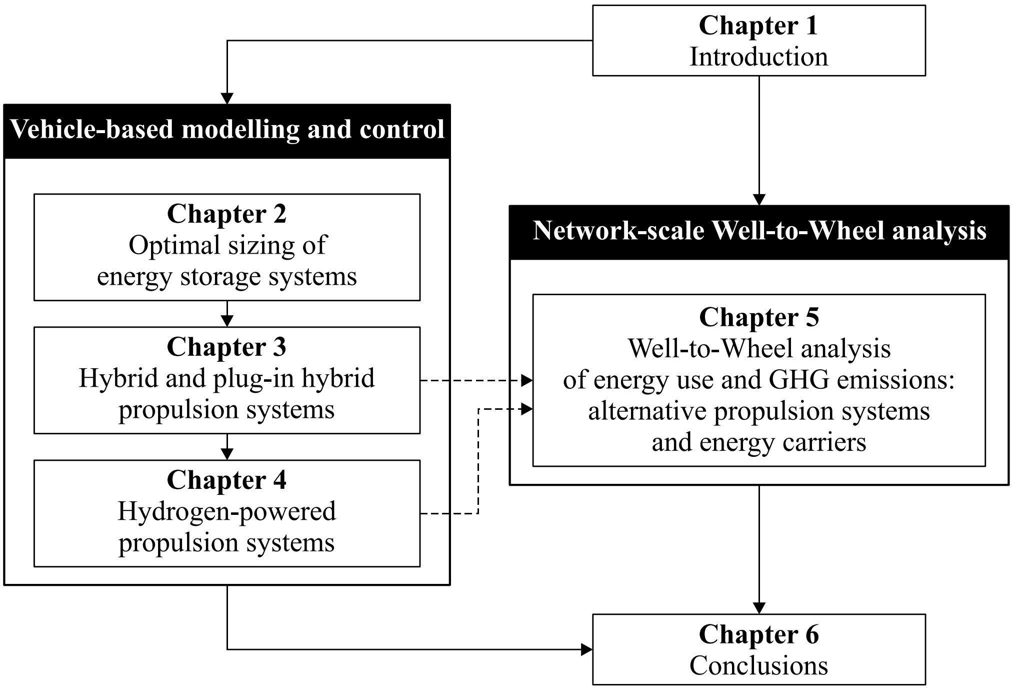

Figure 1.3: Overview of thesis structure.

Chapter 2

Reducing fuel consumption and related emissions through optimal sizing of energy storage systems for diesel-electric trains

Apart from minor updates, this chapter has been published as:

Kapetanović, M., Núñez, A., van Oort, N., Goverde, R.M.P. (2021). Reducing fuel consumption and related emissions through optimal sizing of energy storage systems for diesel-electric trains. *Applied Energy*, 294, 117018.

2.1 Introduction

Air pollution is of great concern in politics, the scientific community, industry, and society in general. The global warming effect caused by greenhouse gasses (GHGs) and especially carbon dioxide (CO_2) emissions from anthropogenic sources led to various international treaties, such as the Kyoto Protocol (UN, 1998) and the follow-up Paris Agreement (UN, 2015), resulting in recommendations and defined targets to reduce the emissions. Particularly, the transport sector is one of the most significant contributors to GHG emissions and therefore targets have been defined for transportation systems at all levels. In the case of the railway sector, targets were set in 2008 by the International Union of Railways (UIC) and the Community of European Railway and Infrastructure Companies (CER). A short-term target was to decrease specific average CO_2 emissions by 2020 by 30% compared to the 1990 base year level. Medium and long-term targets are further decreased by 50% in 2030, and carbon-free train operation by 2050 (UIC and CER, 2012). Additionally, local pollutants such as nitrogen oxides (NO_x) and particle matter (PM) gained increasing attention in the railway community over recent years. This is mainly due to the introduction of the EU Non-Road Mobile Machinery (NRMM) Directive in 2016 to diesel rail vehicles and the application of the Stage IIIB emission limits. Addressing the limits of local pollutants raises significant challenges such as new considerations of vehicle design and manufacturing, reliability of new equipment in terms of produced emissions, and new assessments of life cycle costs, including explicitly the effects of emissions (Beatrice et al., 2013).

Emerging automotive powertrain technologies for electric vehicles (EVs) are considered as a viable solution in reducing environmental footprints from the predominant road transport sector (Ding et al., 2020). Continuous advancements on propulsion systems for EVs offer flexible design, improved vehicle performance and safety (Ding et al., 2021). For the railway sector, synergetic electrification of railway lines (Buzzoni and Pede, 2012; Deur et al., 2015) and an increase of renewable sources in electricity production (Shakya and Shrestha, 2011) is recognized as one of the most effective measures in improving energy efficiency and reducing GHG emissions. The share of electrified versus non-electrified railway lines has increased from less than 30% in 1975 to up to more than 60% in 2008 in the EU-28 countries. However, this share remained relatively constant over the years 2008-2015 (IEA and UIC, 2017). High capital investments (Al-Tony and Lashine, 2000; Cambridge Systematics Inc., 2012) with the significant environmental impact of the electrification process (Jones et al., 2017) and the emergence of new traction options for railways such as alternative fuels (Dincer and Zamfirescu, 2016) and hybrid propulsion systems (Meinert et al., 2015a, 2015b), indicate that non-electrified railways will continue to play an essential role in passengers transport. Hence, there is a constant need to improve their performance in terms of energy efficiency, fuel consumption, and emissions. This especially concerns regional railway networks that are often characterized by non-electrified lines due to high investments required for electrification and a low transport demand (low utilization) compared to the main corridors.

Several emission-free alternatives to diesel multiple units (DMUs), as predominant vehicles employed in non-electrified regional transport, are being developed in recent years. Battery-electric multiple units (BEMUs) and fuel cell multiple units (FCMUs) are identified as suitable long-term solutions (Klebsch et al., 2019). However, existing limitations related to the range, flexibility, supporting infrastructure requirements, as well as techno-economic immaturity of these technologies (Klebsch et al., 2020), stipulate further development and exploitation of internal combustion engines (ICEs). Beatrice et al. (2016) analysed a number of emerging ICE technologies and exhaust after-treatment systems (ATSs) for on-road heavy-duty ICEs that are transferable to the rail sector. The results indicate the great potential of waste heat recovery in improving ICE fuel efficiency. Moreover, combining different ATSs, such as exhaust gas recirculation (EGR), diesel particulate filter (DPF), and selective catalytic reduction (SCR) technologies, can contribute in meeting the most stringent emission requirements imposed for the rail sector (Konstandopoulos et al., 2015).

Since previous technologies relate mainly to the introduction of new rolling stock, and having in mind the long cycle life of DMUs reaching up to 30 years, transport companies are seeking suitable transition solutions towards emission-free operation, mainly through improving energy efficiency. As identified by Scheepmaker et al. (2017), the reduction of energy consumption from railway operation can be achieved in several ways: more energy-efficient rolling stock, minimizing energy consumption of auxiliary systems during stabling periods, optimization of the rolling stock deployment based on capacity and demand, energy-efficient timetabling and energy-efficient train control. This chapter focuses on the first two options, in particular on the assessment of potential fuel savings and emissions reduction from hybridization of existing DMU vehicles that would enable the utilization of regenerated energy, as well as (partial or temporal) electrification of auxiliary systems. Several hybrid railway vehicles from major manufacturers (e.g. Siemens (Railway Gazette International, 2015), Hitachi (Fujii et al., 2004; Shiraki et al., 2010), Alstom (Engel and Soefker, 2001; Research and Technology Centre of Deutsche Bahn AG, 2001)) being tested or already in service, as well as European research projects (e.g. ULEV-TAP 2 (EC, 2005), CleanER-D (Marsilla, 2013), DfTRG/0078/2007 (Hillmansen et al., 2009, 2008)), have demonstrated significant benefits reflected in fuel savings up to ~40%, depending on the technology and operational characteristics.

Focusing on a case study of regional railway services provided by Arriva on the Northern lines in the Netherlands, this chapter proposes an integrated optimization of energy storage system (ESS) size and energy management strategy (EMS), considering conventional DMU vehicles from the Dutch network converted to their hybrid counterpart. The primary requirement for the hybridization defined by the railway undertaking (RU) is achieving emission-free and noise-free operation within railway stations by switching off diesel engines and powering auxiliary systems solely by ESS. This especially concerns terminal stations, characterized by extended stabling periods. Expected benefits are reflected in total fuel consumption reduction by utilizing brake energy, an increase of overall ICE efficiency by avoiding low load engine operation, and support for the ICE during high-power demand (acceleration) phases.

2.1.1 Related work

The reduction of fuel consumption and related emissions of DMUs can be achieved by their hybridization, i.e., by adding an on-board ESS. In this section, we review the literature on rail vehicle hybridization, focusing primarily on passenger diesel-driven vehicles. We will not consider freight locomotives as they represent a different use case, nor catenary-fed vehicles (e.g., trams, electric multiple-units – EMUs) since they are not per definition hybrid vehicles (United Nations. Economic Commission for Europe, 2011). For a comprehensive overview of different measures for energy consumption reduction in the case of urban rail transportation, readers are referred to González-Gil et al. (2014). An overview focusing on strategies and ESS technologies for optimal regenerative braking usage in urban rail transportation systems are provided by González-Gil et al. (2013). We analyse the literature covering the main hybridization aspects, starting from the modelling approaches for hybrid propulsion systems and further investigating different design levels.

Reliable mathematical and simulation models are required to assess potential benefits from hybridization in terms of fuel savings and emissions reduction. Widely used models that can support the assessment of environmental impact in railway operations, such as ARTEMIS (Boulter and McCrae, 2007), EcoTransit (Knörr et al., 2018), or EcoPasssenger (Knörr and Hüttermann, 2016), calculate the fuel consumption and emissions based on mechanical energy using mostly one-lumped efficiency and fixed fuel consumption and emission factors. These models provide predictions for conventional railway vehicles. The case of hybrid vehicles requires more detailed models that include individual components of the powertrain and their interactions. Hybrid vehicle models based on physical relations between the components of the system can be divided into two categories: forward and backward models (Gao et al., 2007; Guzzella and Sciarretta, 2013; Horrein et al., 2012). Forward simulation models follow the physical power flow in the powertrain, starting from the engine, and then to the transmitted and reflected torque to the wheels. They offer realistic control-oriented modelling by capturing driver input/speed control; however, they are usually very complex and characterized by slow execution time and high computer memory. Backward simulation models consider the reverse power flow by computing the tractive contribution required at the wheels and the order of evaluating the system components backward through the system towards the engine, offering a reliable evaluation of vehicle energy consumption based on drive cycle and detailed vehicle-specific data available beforehand. They are also characterized by fast execution times compared to the forward models (Fiori et al., 2016; Gao et al., 2007; Wang and Rakha, 2017). Depending on the aim of the study, data availability, and the purpose of the simulation model, the adequate type should be selected. Regarding the hybrid DMU railway vehicles, a forward simulation approach is usually used in assessing the potential fuel savings for different driving strategies and styles (Schmid et al., 2017), while backward simulations are performed using mostly typical speed profiles and duty cycles (c.f., Lanneluc et al., 2017; Leska et al., 2017, 2014; Leska and Aschemann, 2015; Poline et al., 2019). In addition to the previous physical models, the energetic macroscopic representation (EMR) is an effective graphical modelling approach in the systemic description of complex propulsion systems (Joud et al., 2020). A recent study by Kréhi Serge Agbli et al. (2016) demonstrated the effectiveness of using EMR in reverse engineering of railway vehicles to describe power flows behaviour and derive models for the key propulsion system components, disregarding in-depth knowledge of the train energetic devices and sub-systems. It can be particularly useful in case of lack of detailed vehicle-specific parameters due to, e.g. confidentiality aspects or sub-systems provided by subcontractors, by fitting the energetic behaviour of the vehicle with the available test data (Krehi Serge Agbli et al., 2016). Furthermore, the approach can be successfully exploited to perform model-based development of suitable energy management strategies (Mayet et al., 2012).

Vehicles hybridization can be considered a multi-objective design optimization problem, with multiple parameters distributed over multiple levels (topology, technology, size, and control). When this optimization problem is solved sequentially (level by level), it is by definition sub-optimal due to coupled dynamic parameters and non-linear effects (Silvas et al., 2016). In the case of DMU vehicles, topology level refers to the system architecture in terms of the type of the propulsion system, i.e., diesel-electric (DE), diesel-hydrodynamic (DHD), or diesel-hydromechanical (DHM) (Spiryagin et al., 2014), which directly influences the way the ESS can be integrated into the system. Comparative assessment of the three propulsion systems in terms of integrating different ESS technologies, both mechanical and electrical (see Meinert et al., 2015a), indicated that DE systems lead to fewer additional physical components for ESS integration. Compared to the DHD and DHM, the DE system enables relatively simple hybridization by adding a proper ESS directly into the electric power transmission system (Sun et al., 2013). Since the electric transmission is the only system currently in use on the Northern lines, we limit the analysis to only this particular case in this chapter.

The selection of suitable ESS technology is the next step in the DMU hybridization process. Different ESS technologies have emerged in the transport sector for brake energy harvesting (Vazquez et al., 2010). For railway applications, three technologies are being found to be especially suited: batteries, double-layer capacitors (DLCs), and flywheels (Ghaviha et al., 2017b). Due to their high energy density (energy per unit of mass), rapid technology development and increasing availability on the market, lithium-ion batteries are the most represented ESS technology in hybrid DMU-related literature (Meinert et al., 2015a). Compared to lithium-ion batteries, DLCs are characterized by both low energy density and high power density. This makes DLCs suitable in applications aimed at high peak power shaving and maximizing the utilization of regenerative braking energy. Although flywheels offer a number of advantages reflected in fast charging and discharging processes and long life cycle, several drawbacks hinder their extensive use in railway applications, related primarily to safety issues, relatively high weight, and high self-discharge rates (González-Gil et al., 2013). In particular cases, combining the advantages of different technologies, typically lithium-ion battery and DLC, in a single hybrid ESS, can bring additional benefits compared to a single-technology ESS (Dittus et al., 2011; Poline et al., 2019). Considering the main hybridization requirement in our case – emissions-free and noise-free operation within station areas, characterized by low power demand and high energy required, which sums up over time, lithium-ion batteries are considered by the RU as the most suitable ESS technology.

While topology and ESS technology choices in the DMU hybridization process are mainly conditioned to the available DMU fleet and main hybridization requirements, thus making these decisions relatively easy, optimal sizing and control of the ESS are complex tasks, which are in most cases treated separately. Taking into account that oversizing of the ESS might unnecessarily increase total ESS mass and volume, as well as total costs, whereas an undersized ESS might lead to considerable energy waste, a detailed analysis is needed to determine an optimal design, while the sizing method depends upon its main function (González-Gil et al., 2013). In particular, a different approach is required if the main intended function of the ESS is, for instance, supporting auxiliaries during stabling periods, maximizing utilization of braking energy, or converting a DMU to a catenary-free EMU. The need for co-design, i.e. integrating the two design optimization levels, has been addressed in hybridization-related literature in general (Fathy et al., 2001), confirming the importance of co-optimization in achieving the best configurations. A recent study by Sorrentino et al. (2019) proposed an advanced co-optimization method for fuel cell hybrid vehicles. The two aspects addressed by this co-optimization method are the design of the powertrain affecting the sizing of the system components, and the control of such systems affecting the performance of the system, leading to a trade-off between performance and system sizing. Determination of the component sizing for the fuel cell-battery hybrid energy system for a locomotive application is presented by Sarma and Ganguly (2018), with the influence of the EMS on the primary design problem addressed by incorporating the two rule-based controls in the optimization framework using particle swarm optimization. Furthermore, adopting the previous approach in the work of Sarma and Ganguly (2020), the authors provide a set of alternative solutions with different component sizes, from which a planner can select a solution according to its capital and operational expenditure budgets. Although strong interdependence between the optimal ESS sizing and control levels has been widely recognized and established, most of the studies on hybrid DMU railway vehicles focus only on the optimal control, assuming ESS size given beforehand, or roughly estimated before determining the optimal EMS. As a rare example, simultaneous optimization of hybrid ESS (lithium-ion battery and DLC) size and energy management strategy for a DE railway vehicle is presented by Poline et al. (2019). The authors used the frequency management approach based on a low-pass filter coupled with dynamic programming as the optimal control method. The existence of multiple ESS technologies, and the solution approach that considers approximations of mixed-integer and discontinuous variables, in this case, raised significant challenges in terms of computation time and errors.

Optimal control strategies aim at minimizing the fuel and/or energy consumption by managing the power flows of different energy sources in place (e.g., ICE and ESS), in particular by determining the optimal moments for charging/discharging the ESS. The control strategies can be classified into three general groups (Pisu and Rizzoni, 2007): dynamic programming (DP), rule-based (RB) approaches, and methods based on the equivalent fuel consumption minimization (EFCM). Additionally, from the computational complexity and practical applicability perspective, they can be grouped in off-line and on-line approaches. DP is a widely used global optimization method for off-line controller optimization in DMU vehicles. Assuming an ideal case, i.e. perfect information on the future duty cycle, DP is used in obtaining fuel-optimal (combined) driving and energy management strategy by Leska and Aschemann (2015). Using a simplified version of the EMR model from Kréhi Serge Agbli et al. (2016), a DP-based optimization of EMS for a regional train hybridized with lithium-ion battery is proposed by Sorrentino et al. (2020). The comparative assessment for three different degrees of hybridization (battery size) and two realistic mission profiles for a regional railway route indicated potential fuel savings reaching a significant level up to 18%. Control strategies based on DP typically serve as a benchmark for evaluating other (real-time) algorithms. Such an algorithm based on a sensitivity analysis and bisection method for a DMU equipped with a lithium-ion battery is presented by Leska et al. (2014), showing promising benefits in performance and especially computational cost compared to the DP method. The same algorithm is used by Leska et al. (2017), with the analysis extended to DLC as alternative ESS technology. DP is also used as a benchmark in finding optimal dispatch (power distribution between ICEs) strategies by Lu et al. (2011, 2010), with fuel savings up to 7% compared to typical operation. In RB algorithms, event-triggered Boolean rules are derived from, for instance, heuristics or fuzzy rules based on experts' knowledge (Lanneluc et al., 2017). Due to their easy implementation and low computational times, these algorithms have been widely used in on-line ESS control applications (Dittus et al., 2011; García-Garre and Gabaldón, 2019). However, unlike DP-based control, they cannot guarantee optimality. EFCM method is based on the conversion of electrical power into equivalent fuel consumption. Compared to RB approaches, it offers an explicit formulation of the optimization problem to minimize the instantaneous equivalent fuel consumption using equivalence factors. It is mostly combined with the optimization approaches such as DP and predictive control in defining causal controllers, where the supporting optimization techniques are used for defining the control reference values. EFCM as an on-line causal control is implemented by Schmid et al. (2017) in Siemens LMS Imagine.Lab Amesim simulation software used for the performance assessment of hybrid DMUs with DE and DHM propulsion system, hybridized with lithium-ion battery, DLC, or flywheel as ESS.

Although the scientific literature on DMUs hybridization provides established models and comprehensive analyses of different hybrid system configurations and operational conditions, literature regarding the optimal sizing of ESS is rather scarce. The literature focuses primarily on the optimal control of the ESS with its size and configuration given beforehand or roughly estimated based on some main criteria, such as maximization of expected recuperated energy or electrification of auxiliaries, while neglecting the influence of the control strategy in place on the optimal size of the ESS. Studies in the automotive industry summarized in a review by Silvas et al. (2016) have shown that by integrating these optimization levels, fuel-consumption benefits are obtained, which go beyond the results achieved with solely optimal control for a given topology. Additionally, practical and/or detailed implementations on real-life cases will face additional challenges reflected in consideration of numerous operational constraints and requirements, as well as in detailed data availability.

2.1.2 Chapter contribution

In this chapter, we propose a method to support the conversion decision of standard DMU vehicles to their hybrid counterpart by incorporating an optimally sized lithium-ion battery-based ESS, while taking into account the trade-off between lower fuel consumption and hybridization cost. Using a detailed DMU powertrain simulation model, we then conduct the comparative assessment of fuel consumption and produced emissions of conventional and hybrid DMU vehicles. The presented research is part of a bigger project realized in collaboration with Arriva, the largest regional RU in the Netherlands. The results of this research will be used by the RU in the planning of future rolling stock and operations.

Based on the knowledge gaps presented in Section 2.1.1, the following are defined as the contribution of this chapter:

1. A bi-level multi-objective optimization approach for determining the optimal size for the battery-based ESS by integrating the ESS sizing and control optimization levels, while at the same time incorporating emission-free and noise-free operation in stations in the problem formulation.

2. Two different power flow controls: (i) a non-causal optimal control based on dynamic programming that yields the absolute largest potential in fuel consumption reduction and global optimum for the primary optimization problem, and (ii) a causal sub-optimal rule-based control for emission-free and noise-free operation in stations and prolonged battery life by preventing frequent switches in charging/discharging cycles.
3. Application of the proposed method in a case study of two-coach DMU vehicles operating on a regional non-electrified railway network in the Netherlands, demonstrating potential benefits in terms of fuel savings and hybridization costs.

The chapter is organized as follows. Section 2.2 presents the modelling of a hybrid DMU vehicle. The mathematical formulation of a bi-level optimization problem is given in Section 2.3. The application of the proposed methodology in a Dutch case study is provided in Section 2.4, followed by the discussion in Section 2.5. Section 2.6 concludes this chapter with final remarks and future research directions.

2.2 Modelling of standard and hybrid DMU

The powertrain of standard diesel-electric multiple units consists of an internal combustion engine (ICE) directly connected to an AC electric generator (G), which is further connected via the rectifier and inverter to an AC electric motor (EM) located on the driveshaft. In the case of braking, the EM acts as the generator. The ICE supplies the mechanical auxiliaries (e.g., hydraulic pump), while the electrical auxiliaries are connected to the existing DC link via a DC/AC inverter. The braking energy is, in this case, dissipated through the resistor, which is connected to the DC link via a DC/DC converter. Hybridization of diesel-electric multiple unit can be achieved by adding the appropriate ESS on the DC link, as shown in Figure 2.1.

Compared to road transport, or even to railway freight transport, railway passenger transport is characterized by fixed routes with predetermined stops and timetables, which also enable forecasts of typical driving behaviour, speed profiles and duty cycles. Since the main aim of this chapter is the analysis of the powertrain dynamics under typical operation conditions, rather than to assess the impact of different driving styles and traffic conditions, a backward quasi-static simulation approach (Leska et al., 2017; Pröhl, 2017b) is adopted, following the system architecture shown in Figure 2.1. The simulation model is developed with the MATLAB®/Simulink© tool and OPEUS Simulink library (Pröhl, 2017a). In Figure 2.2, the simulation structure following the system architecture from Figure 2.1 is depicted, where the individual blocks represent the components of the model for the hybrid system. Corresponding to the backward simulation approach, the inputs of the simulation model are the DMU vehicle velocity and track geometry profiles, and the outputs are total fuel consumption with related emissions and ESS state-of-charge (SoC). The arrows indicate the numerical evaluation order of the model components, opposed to the direction of the physical power flow.

The following sub-sections provide the description of the components of the simulation model in Figure 2.2, following the order of their numerical evaluation. For simplicity, the converters are assumed to have high constant efficiency; thus, their dynamics are not captured with this model. It is also assumed that electrical auxiliaries are characterized by a constant power demand P_{elaux} [W]. According to the control strategy implemented in the control unit, the total requested power for tracking the duty cycle is distributed between the ICE and the ESS (see Sections 2.3.2 and 2.4.3). A rheostat is used for converting the excess braking energy into heat, and it is used to keep the balance of energy in the model.

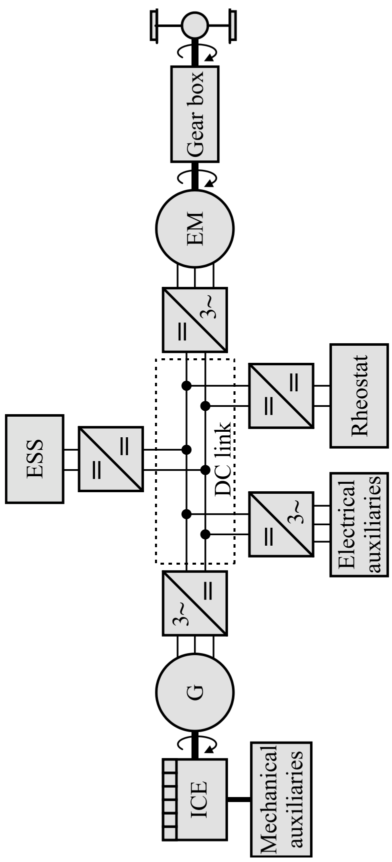

Figure 2.1: Simplified schematic representation of hybrid system architecture for diesel-electric multiple unit.

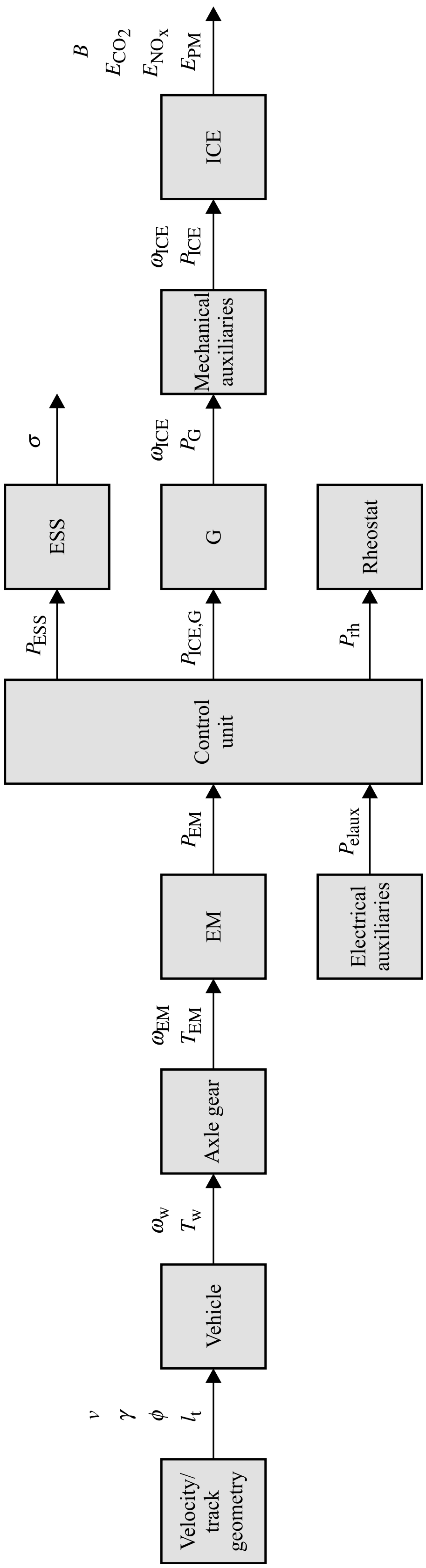

Figure 2.2: Structure of the backward-looking simulation model for the hybrid diesel-electric multiple unit propulsion system.

2.2.1 Vehicle

For the longitudinal vehicle dynamics, the tractive or braking effort at the wheel F_{w} [N] can be expressed as

$$F_{\mathrm{w}}\big(v(t)\big) = m_{\mathrm{v}} \cdot a(t) + R_{\mathrm{v}}\big(v(t)\big) + R_{\mathrm{g}}\Big(\gamma\big(s(t)\big)\Big) + R_{\mathrm{c}}\Big(\phi\big(s(t)\big)\Big) + R_{\mathrm{t}}\Big(l_{\mathrm{t}}\big(s(t)\big), v(t)\Big) \quad (2.1)$$

with

$$R_{\mathrm{v}}\big(v(t)\big) = r_0 + r_1 \cdot v + r_2 \cdot v^2$$

$$R_{\mathrm{g}}\Big(\gamma\big(s(t)\big)\Big) = m_{\mathrm{v}} \cdot g \cdot sin(\gamma)$$

$$R_{\mathrm{c}}\Big(\phi\big(s(t)\big)\Big) = \begin{cases} m_{\mathrm{v}} \cdot 0.03 & \text{if } \phi < 272 \text{ m} \\ m_{\mathrm{v}} \cdot \dfrac{6.5}{\phi - 55} & \text{if } 272 \text{ m} \leq \phi < 2000 \text{ m} \\ 0 & \text{if } \phi \geq 2000 \text{ m} \end{cases}$$

$$R_{\mathrm{t}}\Big(l_{\mathrm{t}}\big(s(t)\big), v(t)\Big) = 5 \cdot \frac{l_{\mathrm{t}}}{S_{\mathrm{t}}/S_{\mathrm{v}} - 1} \cdot (0.036 \cdot v)^2,$$

where t [s] is the time; v [m/s] is the vehicle velocity; s [m] is the distance travelled pre-calculated as $s = \int_0^t v(\tau)d\tau$; a [m/s^2] is the acceleration pre-calculated as the derivative of vehicle velocity to time, i.e., $a = dv/dt$; m_{v} [kg] denotes the total mass of the vehicle which takes into account the rotary inertia of the powertrain and the passengers weight, i.e. $m_{\mathrm{v}} = (1 + \lambda) \cdot m_{\mathrm{tare}} + m_{\mathrm{pax}}$, with λ denoting the dimensionless rotating mass factor, m_{tare} [kg] the vehicle tare weight, and m_{pax} [kg] the total weight of passengers; R_{v} [N] represents the vehicle resistances during motion, including roll resistance and air resistance, modelled as a quadratic function of the vehicle velocity using the Davis equation (Brünger and Dahlhaus, 2014; Davis, 1926), where non-negative coefficients r_0 [N], r_1 [N/(m/s)] and r_2 $\left[\text{N/(m/s)}^2\right]$ are tuned based on the characteristics of the vehicle; R_{g} [N] is the grade resistance, with $g = 9.81$ [m/s^2] representing the gravitational acceleration, and γ [rad] the angle of the slope (Luan et al., 2018); R_{c} [N] denotes the curve resistance which depends on the radius of the curve ϕ [m], calculated using the approach of Hamburger Hochbahn AG (Vučić, 1987) adopted by a number of European railways, and with these resistances set to zero for curves with radius higher than 2000 meters; and R_{t} [N] is the tunnel resistance which depends on the vehicle cross-sectional surface S_{v} [m^2], tunnel length l_{t} [m] and tunnel cross-sectional surface S_{t} [m^2] (Dinić, 1986; Profillidis, 2000), and with its value equal to zero for the tracks outside the tunnels.

Depending on the wheel diameter d_{w} [m] and the train speed v, the torque at the wheel T_{w} [Nm] and the rotational speed of the wheel ω_{w} [rad/s] can be calculated as (Leska et al., 2017)

$$T_{\mathrm{w}} = F_{\mathrm{w}} \cdot \frac{d_{\mathrm{w}}}{2} \quad (2.2)$$

$$\omega_{\mathrm{w}} = 2 \cdot \frac{v}{d_{\mathrm{w}}}. \quad (2.3)$$

2.2.2 Axle gear

The axle gear transmits the power from the shaft to the wheels. With the constant gear ratio i_{ag}, the torque T_{EM} [Nm] and the rotational speed ω_{EM} [rad/s] at the mechanical input of the axle gear can be computed by (Leska et al., 2017)

$$T_{\text{EM}} = \begin{cases} \dfrac{T_{\text{w}}}{i_{\text{ag}} \cdot \eta_{\text{ag}}} & \text{if } T_{\text{w}} \geq 0 \\ \dfrac{T_{\text{w}} \cdot \eta_{\text{ag}}}{i_{\text{ag}}} & \text{if } T_{\text{w}} < 0 \end{cases} \tag{2.4}$$

$$\omega_{\text{EM}} = \omega_{\text{w}} \cdot i_{\text{ag}}\,, \tag{2.5}$$

where η_{ag} represents the efficiency of the gearbox, assumed to be constant.

2.3.3 Electric motor

The electric motor (EM) drive represents an induction machine, used either as a traction motor to move the train or as electro-dynamic brakes (generator mode), enabling the recuperation of the braking energy. Depending on the direction of the power flow (motor or generator operation mode), the electric power of the electric motor P_{EM} [W] can be computed by (Leska et al., 2017)

$$P_{\text{EM}} = \begin{cases} \dfrac{T_{\text{EM}} \cdot \omega_{\text{EM}}}{\eta_{\text{EM}}} & \text{if } T_{\text{EM}} \geq 0 \\ T_{\text{EM}} \cdot \omega_{\text{EM}} \cdot \eta_{\text{EM}} & \text{if } T_{\text{EM}} < 0, \end{cases} \tag{2.6}$$

where the efficiency $\eta_{\text{EM}} = f_{\text{EM}}(T_{\text{EM}}, \omega_{\text{EM}})$ is determined by a linear 2D-interpolation in the efficiency map of the EM.

2.2.4 Internal combustion engine – electric generator set

The ICE, which is directly connected to the electric generator (G), is the primary traction source of the system architecture. The main output of the simulation model is the fuel consumption of the ICE, predicted by a measured static map. In the simulation model, the optimal ICE rotational speed ω_{ICE} [rad/s] is pre-calculated using the Nelder-Mead simplex method (Leska et al., 2012) for different possible levels of requested power and considering the generator's efficiency, mechanical auxiliaries power, and ICE specific fuel consumption. Physical separation of ICE-G set from the EM by a DC link enables the optimal working speed of the ICE for the requested power, irrespectively of the EM speed. With the given requested power $P_{\text{ICE,G}}$ [W], which represents the electrical output power of the generator, the mechanical input power of the generator P_{G} [W] is computed by

$$P_{\text{G}} = T_{\text{G}} \cdot \omega_{\text{ICE}} = \frac{P_{\text{ICE,G}}}{\eta_{\text{G}}}, \tag{2.7}$$

with the efficiency $\eta_{\text{G}} = f_{\text{G}}(T_{\text{G}}, \omega_{\text{G}})$ determined by a linear 2D-interpolation in the efficiency map of the generator. Note that in the case of a standard DMU vehicle, the output power of the generator is equal to the total requested power for traction and powering electrical auxiliaries, i.e. $P_{\text{ICE,G}}(t) = P_{\text{EM}}(t) + P_{\text{elaux}}$, while in the case of a hybrid DMU it depends on the power split ratio between the two power sources, i.e. ICE-G set and ESS (see below). The mechanical auxiliaries power in this study is assumed to be directly proportional to the ICE output power. With p_{maux} representing a constant ratio of the ICE output power used for the mechanical auxiliaries, the total demanded power from the ICE P_{ICE} [W] is calculated by

$$P_{\mathrm{ICE}}(t) = \frac{P_{\mathrm{G}}(t)}{(1 - p_{\mathrm{maux}})}. \tag{2.8}$$

With the obtained simulation inputs, the angular velocity ω_{ICE}, and the requested ICE power P_{ICE}, the specific fuel consumption $\psi = f_{\mathrm{f}}(P_{\mathrm{ICE}}, \omega_{\mathrm{ICE}})$ [kg/Ws] is computed using a 2D-interpolation of the static engine map. The total fuel consumption B [l], from time instant 0 to t, for the ICE becomes (Leska et al., 2017):

$$B(t) = \int_0^t \frac{P_{\mathrm{ICE}}(t) \cdot \psi(\tau)}{\rho} d\tau, \tag{2.9}$$

where ρ [kg/l] denotes the density of the fuel. In addition to the total fuel consumption, the produced emissions are included as additional performance indicators. The CO_2 emissions E_{CO2} [kg] depend on the amount and the type of fuel consumed and are calculated as (Pröhl, 2017a)

$$E_{\mathrm{CO2}}(t) = B(t) \cdot \varepsilon_{\mathrm{CO2}}, \tag{2.10}$$

where $\varepsilon_{\mathrm{CO2}}$ [kg/l] represents the CO_2 emission factor for the fuel in use. The NO_x and PM emissions depend on the physical and operational characteristics of the engine (i.e., engine technology, angular velocity ω_{ICE}, and the requested power P_{ICE}). These are calculated similarly to the total fuel consumption by computing the emissions rate $\varepsilon_{\mathrm{NOx}} = f_{\mathrm{NOx}}(P_{\mathrm{ICE}}, \omega_{\mathrm{ICE}})$ [kg/s] and $\varepsilon_{\mathrm{PM}} = f_{\mathrm{PM}}(P_{\mathrm{ICE}}, \omega_{\mathrm{ICE}})$ [kg/s] using a 2D-interpolation of the static engine maps (Pröhl, 2017a)

$$E_{\mathrm{NOx}}(t) = \int_0^t \varepsilon_{\mathrm{NOx}}(\tau) d\tau \tag{2.11}$$

$$E_{\mathrm{PM}}(t) = \int_0^t \varepsilon_{\mathrm{PM}}(\tau) d\tau. \tag{2.12}$$

2.2.5 Energy storage system

Lithium-ion battery is considered as the ESS in this study. The simplified model of the battery is implemented for the equivalent electrical circuit shown in Figure 2.3. It consists of a SoC-controlled voltage source (open circuit voltage) U_{OC} [V] in series with a constant internal resistance R_{ESS} [Ω], which represents ohmic losses and depends on the direction of the ESS current I_{ESS} [A] (i.e., whether the battery is being charged or discharged). The ESS terminal voltage is denoted as U_{ESS} [V].

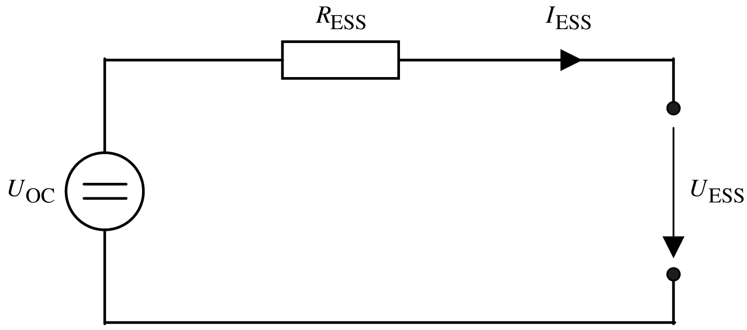

Figure 2.3: Equivalent electrical circuit for the lithium-ion battery-based energy storage system.

With a given ESS SoC $\sigma \in [0,1]$, open circuit voltage U_{OC} and an internal resistance R_{ESS}, the current charging/discharging the ESS is governed by (Prohl and Aschemann, 2019)

$$I_{\mathrm{ESS}}(t) = \frac{U_{\mathrm{OC}}\big(\sigma(t)\big) - \sqrt{U_{\mathrm{OC}}\big(\sigma(t)\big)^2 - 4 \cdot P_{\mathrm{ESS}}(t) \cdot R_{\mathrm{ESS}}\big(I_{\mathrm{ESS}}(t)\big)}}{2 \cdot R_{\mathrm{ESS}}\big(I_{\mathrm{ESS}}(t)\big)}, \tag{2.13}$$

where P_{ESS} [W] represents the power profile at the ESS. Note that the open-circuit voltage U_{OC} depends on the ESS SoC, and that the internal resistance depends on the direction of the power flow. With the ESS nominal capacity $C_{\mathrm{ESS,nom}}$ [As], the derivative of SoC to time is given by

$$\frac{d\sigma}{dt} = \frac{\sqrt{U_{\mathrm{OC}}\big(\sigma(t)\big)^2 - 4 \cdot P_{\mathrm{ESS}}(t) \cdot R_{\mathrm{ESS}}\big(I_{\mathrm{ESS}}(t)\big)} - U_{\mathrm{OC}}\big(\sigma(t)\big)}{2 \cdot R_{\mathrm{ESS}}\big(I_{\mathrm{ESS}}(t)\big) \cdot C_{\mathrm{ESS,nom}}}. \tag{2.14}$$

Based on the ESS current, the terminal voltage U_{ESS} is given by:

$$U_{\mathrm{ESS}}(t) = U_{\mathrm{OC}}\big(\sigma(t)\big) - R_{\mathrm{ESS}}\big(I_{\mathrm{ESS}}(t)\big) \cdot I_{\mathrm{ESS}}(t). \tag{2.15}$$

With the ESS parameters (open-circuit voltage, internal resistance and nominal capacity) provided at the battery cell level, for the battery consisting of n_{par} parallel branches with n_{ser} cells in series per branch their values at the ESS level can be determined by (Leska et al., 2017; Pröhl, 2017b)

$$U_{\mathrm{OC}} = n_{\mathrm{ser}} \cdot U_{\mathrm{OC,cell}} \tag{2.16}$$

$$R_{\mathrm{ESS}} = \frac{n_{\mathrm{ser}}}{n_{\mathrm{par}}} \cdot R_{\mathrm{cell}} \tag{2.17}$$

$$C_{\mathrm{ESS,nom}} = n_{\mathrm{par}} \cdot C_{\mathrm{cell,nom}}, \tag{2.18}$$

where $U_{\mathrm{OC,cell}}$, R_{cell}, and $C_{\mathrm{cell,nom}}$ are the open-circuit voltage, internal resistance, and nominal capacity of one cell, respectively. The maximum charging/discharging power is limited by the maximum current while keeping the limits of the SoC $[\sigma_{\mathrm{min}}, \sigma_{\mathrm{max}}]$ as well as of the battery voltage $[U_{\mathrm{ESS,min}}, U_{\mathrm{ESS,max}}]$, with SoC and voltage assessed using (2.14) and (2.15), respectively. Additionally, to prevent overheating of the battery, the maximum charging and discharging power provided by the manufacturer have to be met. In this study, the maximum continuous power $P_{\mathrm{ESS,cont}}$ of the battery, which depends on the SoC and power direction (i.e., charging or discharging) is defined, thus not allowing short phases where power peaks exceed this threshold.

2.3 Optimal ESS sizing and control

This section presents an integrated ESS sizing and control, formalized as a bi-level multi-objective optimization problem. Using a nested coordination architecture, for each possible ESS size, an optimization of the energy management strategy (EMS) is done by dynamic programming. In this way, the lowest possible fuel consumption for the given ESS configuration (size) is guaranteed and the influence of the EMS choice on the primary optimization problem solution is removed.

2.3.1 Optimal ESS sizing methodology

With the battery-based ESS derived at the cell level, as described in Section 2.2.5, the size of the ESS can be represented with the variable $n_{\mathrm{ESS}} = [n_{\mathrm{par}}\ n_{\mathrm{ser}}]$, where n_{par} denotes the number of battery parallel branches and n_{ser} the number of cells per branch. The weighted sum of fuel consumption and hybridization cost (Ebbesen et al., 2012) is used in defining the objective function $J(n_{\mathrm{ESS}})$ for the primary optimization problem:

$$J(n_{\mathrm{ESS}}) = (1-\alpha) \cdot \frac{J_1(\pi^*, n_{\mathrm{ESS}})}{J_1^{\mathrm{nom}}} + \alpha \cdot \frac{J_2(n_{\mathrm{ESS}})}{J_2^{\mathrm{nom}}}, \tag{2.19}$$

with $\alpha \in [0,1]$ representing the assigned weight, $J_1(\pi^*, n_{\mathrm{ESS}})$ is the lowest possible fuel consumption given the parameters n_{ESS} and the optimal control strategy π^* (see below), and $J_2(n_{\mathrm{ESS}})$ is the total cost of hybridization. The nominal (largest possible) values J_1^{nom} and J_2^{nom} are used to normalize $J_1(\pi^*, n_{\mathrm{ESS}})$ and $J_2(n_{\mathrm{ESS}})$, respectively. Specific lithium-ion battery cost of 200 EUR/kWh is assumed in this study considering research of Cipek et al. (2019), thus resulting in the following hybridization cost function:

$$J_2(n_{\mathrm{ESS}}) = 0.2 \cdot n_{\mathrm{par}} \cdot n_{\mathrm{ser}} \cdot C_{\mathrm{cell,nom}} \cdot U_{\mathrm{cell,max}}. \tag{2.20}$$

The objective is finding n_{ESS} that minimizes the objective function $J(n_{\mathrm{ESS}})$ subject to a number of constraints that guarantee a required level of performance and satisfy the practical limitations. In this case, inequality constraints are set based on the main hybridization requirements given in Section 2.1, and on an additional requirement of the sustenance of the battery SoC. SoC sustenance is achieved by including a constraint on the equality of battery SoC at the beginning and at the end of the duty cycle (see below). This constraint accounts for the vehicle circulation according to the periodic timetable, and at the same time, allows for a fair comparison with the conventional DMU. The resulting constraints are given as follows,

$$n_{\mathrm{par}} \cdot n_{\mathrm{ser}} \cdot P_{\mathrm{cell,cont,dch}}(\sigma_{\mathrm{nom}}) \geq P_{\mathrm{elaux}} \tag{2.21}$$

$$n_{\mathrm{par}} \cdot n_{\mathrm{ser}} \cdot \left(E_{\mathrm{cell,max}}(\sigma_{\mathrm{max}}) - E_{\mathrm{cell,max}}(\sigma_{\mathrm{nom}})\right) \geq E_{\mathrm{elaux,stop,max}} \tag{2.22}$$

$$n_{\mathrm{ser}} \cdot U_{\mathrm{cell,min}} \geq U_{\mathrm{ESS,min}} \tag{2.23}$$

$$n_{\mathrm{ser}} \cdot U_{\mathrm{cell,max}} \leq U_{\mathrm{ESS,max}} \tag{2.24}$$

$$n_{\mathrm{par}} \cdot n_{\mathrm{ser}} \cdot m_{\mathrm{cell}} \leq m_{\mathrm{ESS,max}}, \tag{2.25}$$

where $P_{\mathrm{cell,cont,dch}}$ represents the maximum continuous discharging power of one cell, σ_{nom} is the nominal value for the battery SoC, $E_{\mathrm{cell,max}}$ is the maximum energy of one cell, $E_{\mathrm{elaux,stop,max}}$ is the maximum energy required for supplying electrical auxiliaries during stops, corresponding to the maximum dwell/turnaround time, $U_{\mathrm{cell,min}}$ and $U_{\mathrm{cell,max}}$ are the voltage limits of one cell, m_{cell} is the mass of one cell, and $m_{\mathrm{ESS,max}}$ is the maximum allowed mass for the ESS. Constraints (2.21) and (2.22) ensure that the ESS can provide enough power and energy for supplying electrical auxiliaries during stops when the ICE is switched off. Constraints (2.23) and (2.24) are related to the ESS voltage limits conditioned by, for instance, DC link operating voltage, converter characteristics, etc. Finally, constraint (2.25) imposes the maximum allowed ESS mass, constrained by vehicle axle load limits, required traction performance, etc. The parameters $n_{\mathrm{ESS}}^* = \left[n_{\mathrm{par}}^* \ n_{\mathrm{ser}}^*\right]$ represent the solution of the optimization problem, determined by minimizing the cost function:

$$n_{\mathrm{ESS}}^* = \arg\left(\min_{n_{\mathrm{ESS}}}\{J(n_{\mathrm{ESS}})\}\right). \tag{2.26}$$

Deriving ESS parameters at the cell level enables straightforward discretization of the search space, compared to the case of continuous decision variables where the choice of the discretization approach influences the quality of the solution. Due to a relatively low number of feasible solutions, the present approach also allows for the employment of an exhaustive (brute force) search algorithm instead of meta-heuristic approaches commonly used in case of continuous decision variables, thus guaranteeing to find a global optimum for the given optimization problem in a reasonable amount of time.

2.3.2 Optimal energy management strategy

The optimal energy management strategy aims at minimizing the total fuel consumption B (and related CO_2 emissions E_{CO2}) of the ICE by adjusting the power flows at the DC link, in particular by separating the total demanded power at the DC link between the ICE-G set and the ESS, while at the same time ensuring the sustenance of the ESS SoC, represented by

$$\sigma(T) = \sigma(0) = \sigma_{\mathrm{nom}}, \tag{2.27}$$

where T [s] denotes the total duration of the trip and the final time instant. The total demanded power at the DC link P_{DC} represents the sum of the required traction power P_{EM} and electrical auxiliaries power P_{elaux}:

$$P_{\mathrm{DC}}(t) = P_{\mathrm{EM}}(t) + P_{\mathrm{elaux}}. \tag{2.28}$$

In order to determine the optimal operating strategy, a control variable $x(t) \in [-1,1]$ is introduced, representing the split of the total requested power $P_{\mathrm{DC}}(t)$ between the ICE (via G) and the ESS. Based on the instantaneous values of the control variable x, the total requested power P_{DC}, and the vehicle velocity v given as the main simulation input, the power flow from the ICE-G set and ESS is given by the following equations:

$$P_{\mathrm{ICE,G}}(v, P_{\mathrm{DC}}, x) = \begin{cases} (1-x)\cdot P_{\mathrm{max,1}} + \left(P_{\mathrm{DC}} - P_{\mathrm{max,1}}\right) & \text{if } v > 0, P_{\mathrm{DC}} > 0, x \in [0,1] \\ -x \cdot P_{\mathrm{max,2}} + P_{\mathrm{DC}} & \text{if } v > 0, P_{\mathrm{DC}} > 0, x \in [-1,0) \\ 0 & \text{if } v = 0 \ \vee \ P_{\mathrm{DC}} \le 0 \end{cases} \tag{2.29}$$

$$P_{\mathrm{ESS}}(v, P_{\mathrm{DC}}, x) = \begin{cases} x \cdot P_{\max,1} & \text{if } v > 0, P_{\mathrm{DC}} > 0, x \in [0,1] \\ x \cdot P_{\max,2} & \text{if } v > 0, P_{\mathrm{DC}} > 0, x \in [-1,0) \\ P_{\max,3} & \text{if } v > 0, P_{\mathrm{DC}} \leq 0 \\ P_{\mathrm{DC}} & \text{if } v = 0, \end{cases} \tag{2.30}$$

where $P_{\max,1} = \min\{P_{\mathrm{DC}}, P_{\mathrm{ESS,max,dch}}\}$, $P_{\max,2} = \min\{(\mathrm{P}_{\mathrm{ICE,G,max}} - P_{\mathrm{DC}}), -P_{\mathrm{ESS,max,ch}}\}$ and $P_{\max,3} = \max\{P_{\mathrm{DC}}, P_{\mathrm{ESS,max,ch}}\}$, with $P_{\mathrm{ESS,max,dch}}$ and $P_{\mathrm{ESS,max,ch}}$ denoting the maximum ESS discharging and recuperation (charging) power, respectively. In the case of $x = 1$ and $P_{\mathrm{DC}} \leq P_{\mathrm{ESS,max,dch}}$, the ESS provides the total requested power P_{DC} ("pure electrical mode"), while for $x = 0$ the total power demand P_{DC} is provided solely by ICE ("pure ICE mode"). The so-called "power boost mode," where the total requested power is provided by ICE and ESS together, represents the case of $0 < x < 1$ or the case of $x = 1$ and $P_{\mathrm{DC}} > P_{\mathrm{ESS,max,dch}}$. In "load level increase mode" with negative values of x, the ICE provides more than the requested power P_{DC}, where the excess power is used for recharging the ESS. Note that during stops ($v = 0$), the ICE is switched off and the ESS provides the total requested power, while in case of negative values of total requested power ($P_{\mathrm{DC}} \leq 0$), the ICE operates with no load at idling speed and the ESS is being recharged ("recuperation mode").

In order to obtain a fuel-optimal operating strategy, the DP approach according to Bellman (2003) is used, following the methodology presented by Leska et al. (2017) and Sundström et al. (2010), and with respect to the current system architecture and operation characteristics. First, the continuous optimization problem had to be converted into a multi-stage decision process through discretization, allowing for a numerical solution. Time, as an identifier of the optimization horizon, is discretized into $t \in \{t_k | k = 0, \dots, K\}$ with K regular time intervals and discretization interval (step length) equal to $\Delta t = (t_K - t_0)/K = T/K$. The state variable is discretized into $\sigma \in \{\sigma_i | i = 1, \dots, I\}$ for each discrete time with I equally distributed values for the ESS SoC over the interval $[\sigma_{\min}, \sigma_{\max}]$, and with $\sigma_1 = \sigma_{\min}$ and $\sigma_I = \sigma_{\max}$. In this way, the discretized state-time space is defined with a fixed grid, see Figure 2.4.

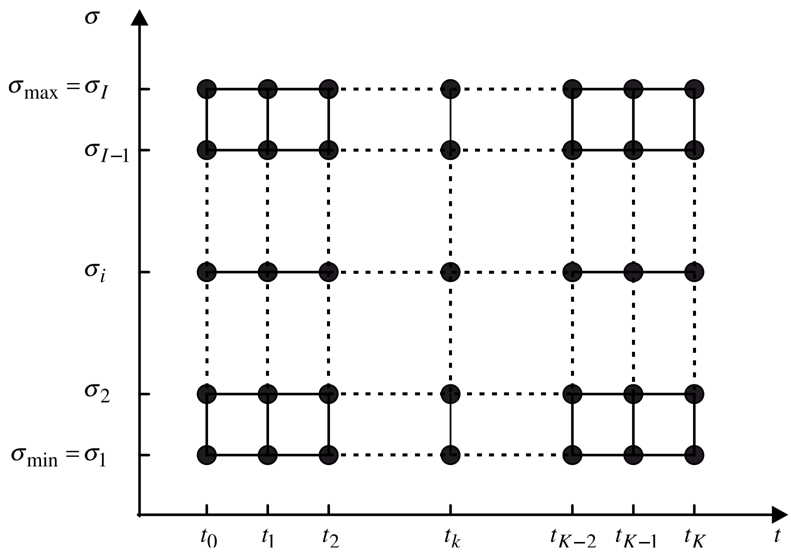

Figure 2.4: Discretized state-time space for the application of dynamic programming algorithm.

The control variable $x(\sigma(t_k), t_k) \in X = \{x_j | j = 1, \dots, M\}$, applied to each state in the given state-time space, is discretized into M equally distributed values for the power split ratio over the interval $[-1,1]$, with $x_1 = -1$ and $x_M = 1$.

With given vehicle and ESS parameters, as well as precalculated velocity $v(t_k)$ and total demanded power $P_{\mathrm{DC}}(t_k)$ for each time step t_k, the dynamics of the system are given by

$$\sigma(t_{k+1}) = f_\sigma(\sigma(t_k), x(\sigma(t_k), t_k); v(t_k), P_{\mathrm{DC}}(t_k)), \quad k = 1, \dots, K-1, \tag{2.31}$$

with $\sigma(t_{k+1})$ representing the resulting state (ESS SoC) one step ahead of $\sigma(t_k)$, obtained by applying the control variable $x(\sigma(t_k), t_k)$ to the state $\sigma(t_k)$, where the transition function f_σ consists of a sequence of equations, i.e., (2.30) and (2.14), describing the given evolution from the initial to the resulting state.

Let $\pi = \{x(\sigma(t_k), t_k) | k = \{0, \dots, K-1\}\}$ denote a control policy. Further, let the total cost-to-go $B_\pi(\sigma(t_0))$ of applying π with initial state $\sigma(t_0) = \sigma_{\mathrm{nom}}$ be

$$B_\pi(\sigma(t_0)) = \sum_{k=0}^{K-1} f_k(\sigma(t_k), x(\sigma(t_k), t_k); v(t_k), P_{\mathrm{DC}}(t_k)) + f_K(\sigma(t_K)), \tag{2.32}$$

with the transition cost function f_k defined as the fuel consumption during one step, when the control variable $x(\sigma(t_k), t_k)$ is applied to the state $\sigma(t_k)$, given by the sequence of equations (2.29), (2.7)-(2.9), and $f_K(\sigma(t_K))$ denoting the terminal cost for the resulting state $\sigma(t_K)$ in the last stage of the horizon, defined in the way that forces constrained final state (2.27), and given by

$$f_K(\sigma(t_K)) = \begin{cases} 0 & \text{if } \sigma(t_K) = \sigma(t_0) = \sigma_{\mathrm{nom}} \\ Inf & \text{otherwise,} \end{cases} \tag{2.33}$$

where *Inf* is a big number representing the penalty. The objective is to find the optimal control policy π^* that minimizes the right-hand side of (2.32), i.e., that leads to the optimal total cost-to-go $B^*(\sigma(t_0))$.

Based on the optimality principle (Bellman, 1952), the DP algorithm evaluates the optimal cost-to-go function $B^*(\sigma(t_k))$ backwards in time at every node of the discretized state-time space $\sigma(t_k) \in \{\sigma_i | i = 1, \dots, I\}$. With the remaining minimum costs starting from the state $\sigma(t_{k+1})$ up to the final stage t_K known, the optimization problem can be rewritten as the recursion from $k = K-1$ down to $k = 0$,

$$B^*(\sigma(t_k)) = \min_{x(\sigma(t_k), t_k) \in X} \{f_k(\sigma(t_k), x(\sigma(t_k), t_k); v(t_k), P_{\mathrm{DC}}(t_k)) + B^*(\sigma(t_{k+1}))\}, \tag{2.34}$$

where $\sigma(t_{k+1})$ is calculated using (2.31). If the resulting state $\sigma(t_{k+1})$ is not equal to one of the I discrete values of the state σ_i, the remaining minimum costs $B^*(\sigma(t_{k+1}))$ are determined by an interpolation between the two closest states.

By backward iteration in time and using (2.34), the optimal control given by an argument that minimizes the right-hand side of (2.34) for all the states in the horizon can be found, with the output of the algorithm given in the form of an optimal control map. With the given optimal control map, by forward simulation starting from the initial state $\sigma(t_0) = \sigma_{\mathrm{nom}}$ and using (2.31), the optimal control sequence and the optimal state trajectory for the entire horizon can be derived. Since the optimal control in the map is only given for the discrete points in the state-time space, it is therefore interpolated when the actual resulting state does not coincide with the discrete points in the state space (Sundström et al., 2010). Note that since all the states in the last time step t_K except one state (i.e., $\sigma(t_K) = \sigma_{\mathrm{nom}}$) have an extremely high cost (i.e., *Inf*), any control sequence which leads to any other final state, results in a high total fuel consumption and is neglected (Ghaviha et al., 2017a). The resulting optimal ESS control is characterized by frequent switches in the power split ratio (Leska et al., 2017). This characteristic of a DP-based control, together with the required computation time, hinders its on-line applicability. However, the obtained results can be regarded as the global optimum. The obtained minimum total cost $B^*(\sigma(t_0))$ represents the lowest possible fuel consumption $J_1(\pi^*, n_{\mathrm{ESS}})$ related to the given ESS size, further implemented in (2.19).

2.3.3 Bi-level optimization methodology

The optimization problem is solved using the following methodology. First, the feasible discrete search space is determined based on the constraints (2.21)-(2.25) that guarantee the required level of performance and satisfy technical and physical limitations. The feasible search space is given by a vector of pairs representing feasible battery configurations in terms of number of parallel branches and number of cells per branch, i.e., by $N_{\mathrm{ESS}}^{\mathrm{fesible}} = [n_{\mathrm{par}}\, n_{\mathrm{ser}}]^S$, with S denoting the number of feasible battery configurations. Using the exhaustive (brute force) search, for each point in the feasible search grid (ESS configuration), the fuel-optimized speed trajectory that comply with the given timetable and track and vehicle parameters (including the maximum tractive effort (see Figure 2.8), and the additional mass of the ESS which influences acceleration/braking characteristics) is generated using the algorithm described by Leska et al. (2013). The algorithm is based on optimizing switching points between cruising and coasting using a bisection method. In this way, the influence of different driving styles on the results is eliminated. Based on the generated speed trajectory, the power profile at the DC link representing the total requested power is computed by evaluating simulation blocks located on the left side of the control unit in the simulation model in Figure 2.2. The optimal control strategy is then determined using DP, and the fuel consumption and hybridization costs are evaluated. This sequence is repeated until all feasible solutions are evaluated. The optimal size of the ESS is then determined by solving the problem in (2.26). The algorithm for the presented bi-level optimization problem based on the nested architecture is illustrated in Figure 2.5.

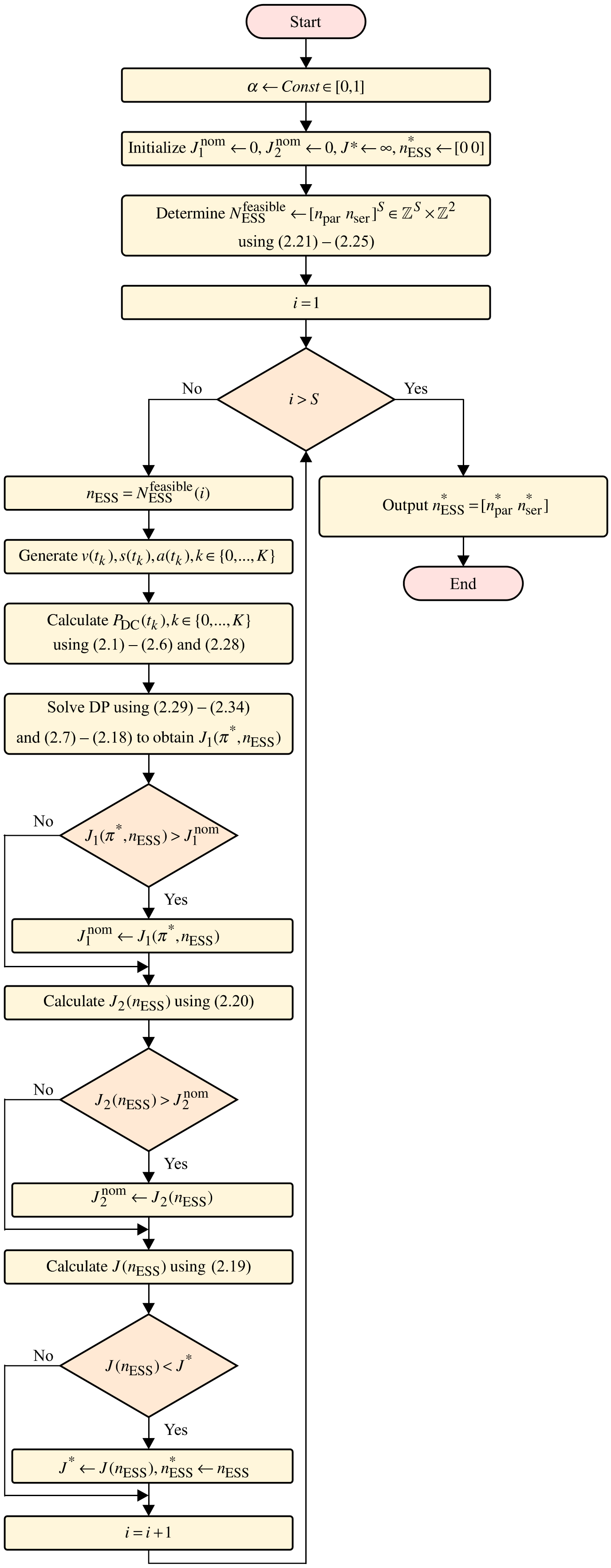

Figure 2.5: Flowchart for the proposed bi-level optimization algorithm based on nested architecture.

2.4 Case study of regional railway services in the Northern Netherlands

The methodology proposed in the previous section is applied to a case study of DMUs from the RU Arriva, operating on the Dutch regional railway network. In the following sub-sections, the input parameters are first defined for the selected railway line and the DMU vehicle, followed by an analysis of different scenarios.

2.4.1 Track parameters

We analyse the railway passenger services provided on the non-electrified regional lines in the Northern part of the Netherlands, in the provinces of Friesland and Groningen. For this study, we selected the train services provided on the 54 km long main railway line, which connects the cities Leeuwarden and Groningen. Two different types of services are being provided by the RU on this line – stopping and express, with the corresponding stops shown in Figure 2.6a. In this study, optimal ESS size and energy management strategy are determined for the vehicles employed on the stopping services with seven intermediate stops.

Due to the difference in line resistances as well as maximum speed limits for the two opposite directions, the vehicle round trip is analysed, which is based on the current periodic timetable and vehicle circulation plan for the given railway line. In order to include relevant factors affecting the vehicle dynamics, track geometry parameters were extracted. Figure 2.6b shows the track height profile compared to the Normal Amsterdam Level (in Dutch, *Normaal Amsterdams Peil, NAP*), and Figure 2.6c the location of the curves with a radius lower than 2000m. There are no tunnels on this part of the network. The maximum allowed speed in both directions is shown in Figure 2.6d. Table 2.1 shows an example of the vehicle round trip with given departure times from each stop. Dwell time of 30 seconds is assumed at intermediate stops. According to the timetable, layover times at the terminal stops are 11 min in Leeuwarden and 12 min in Groningen.

Table 2.1: Departure times for the vehicle round trip on the line Leeuwarden-Groningen.

Stop	**Departure time (hh:mm)**	
	From Leeuwarden to Groningen	**From Groningen to Leeuwarden**
Leeuwarden	hh : 51	hh+2 : 40 (arrival time)
Leeuwarden Camminghaburen	hh : 54	hh+2 : 35
Hurdegaryp	hh+1 : 01	hh+2 : 30
Feanwalden	hh+1 : 05	hh+2 : 25
De Westereen	hh+1 : 08	hh+2 : 20
Buitenpost	hh+1 : 16	hh+2 : 15
Grijskerk	hh+1 : 23	hh+2 : 06
Zuidhorn	hh+1 : 30	hh+2 : 01
Groningen	hh+1 : 39 (arrival time)	hh+1 : 51

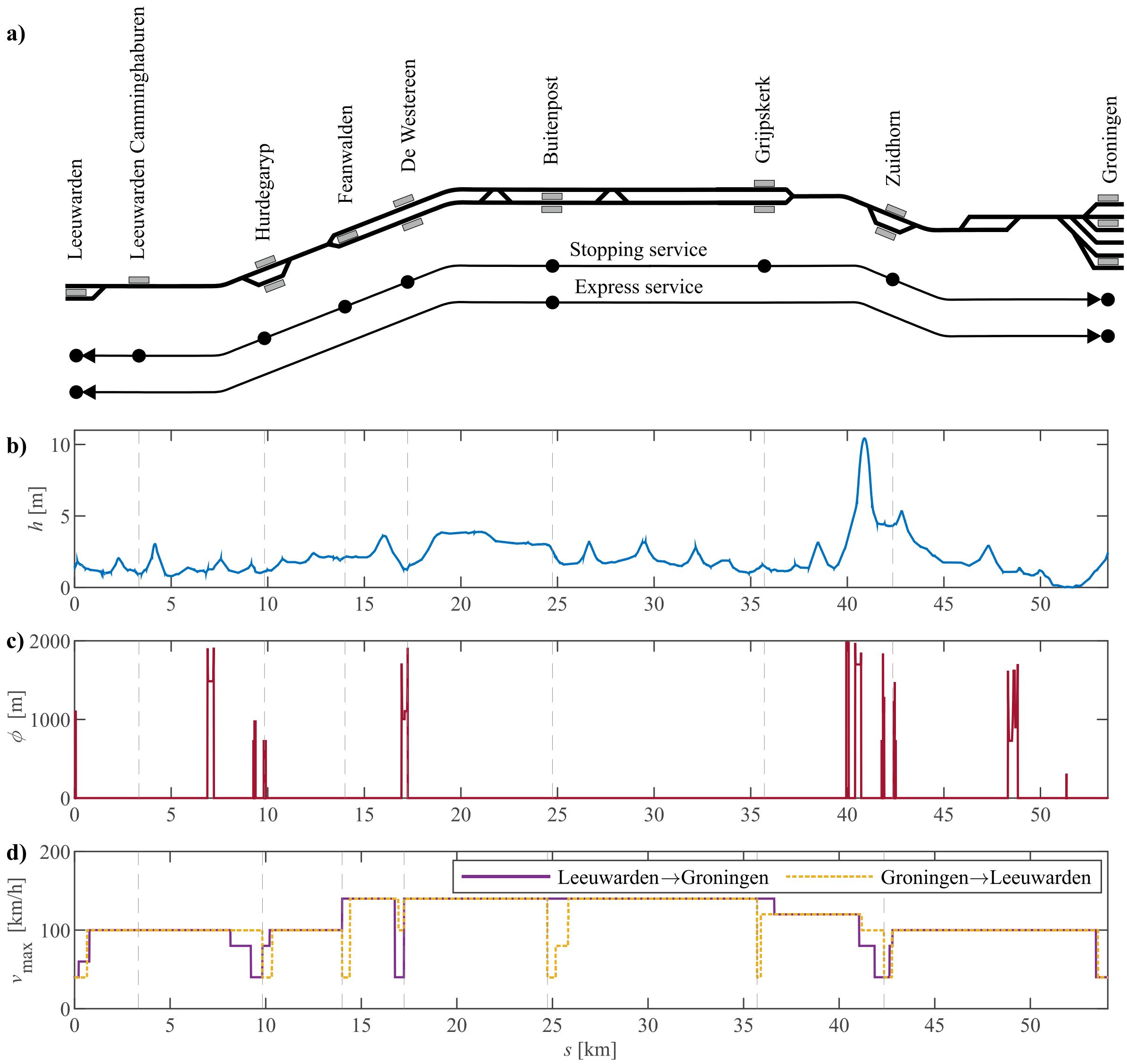

Figure 2.6: Railway line Leeuwarden – Groningen: (a) schematic representation with indicated stops for stopping and express services, (b) track height compared to Normal Amsterdam Level, (c) curves with radius lower than 2000 meters, and (d) maximum allowed speed for the two opposite directions.

2.4.2 Vehicle parameters

The RU Arriva currently provides the services on the network with a fleet of 22 two-coach GTW 2/6 and 29 three-coach GTW 2/8 DMUs from the Swiss manufacturer Stadler. The GTW 2/6 DMU (Figure 2.7) has been selected for the analysis in this chapter. The vehicle parameters provided by the RU are shown in Table 2.2.

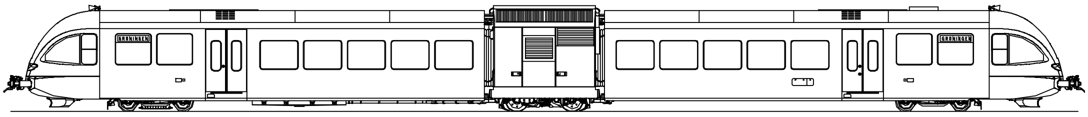

Figure 2.7: Graphical representation of Stadler GTW 2/6 diesel-electric multiple unit (Giro Batalla and Feenstra, 2012).

Table 2.2: Main input parameters for Stadler GTW 2/6 diesel-electric multiple unit.

Parameter	Value	Unit	Description
m_{tare}	70.4	t	Empty mass [a]
λ	0.05	-	Rotating mass factor [b]
m_{v}	77	t	Total mass including passengers [b]
r_0	1001	N	Davis equation coefficient (constant term) [b]
r_1	22.3	N/(km/h)	Davis equation coefficient (linear term) [b]
r_2	0.1	N/(km/h)^2	Davis equation coefficient (quadratic term) [b]
$v_{\max}$	140	km/h	Maximum velocity [c]
$a_{\max}$	1.05	m/s^2	Maximum acceleration [b]
$a_{\min}$	-1	m/s^2	Maximum deceleration [b]
$P_{\text{ICE,max}}$	2 × 390	kW	Diesel engine maximum power [a]
$P_{\text{EM,max}}$	2 × 400	kW	Electrical motor maximum power [a]
d_{w}	0.86	m	Wheel diameter [c]
i_{ag}	1.7218	-	Constant axle gear ratio [d]
η_{ag}	97	%	Gear box efficiency [e]

Source/Note: [a] Giro Batalla and Feenstra (2012); [b] Provided by Arriva; [c] Stadler (2005); [d] Determined from the ratio between the maximum rotational speed of the electrical motor $\omega_{\text{EM,max}} = 1487$ rpm given by Giro Batalla and Feenstra (2012) and the maximum rotational speed of the wheel corresponding to the maximum vehicle speed $v_{\max} = 140$ km/h, as $i_{\text{ag}} = \omega_{\text{EM,max}}/\omega_{\text{w,max}}$; [e] Adopted from Pröhl (2017b).

Since the additional mass of ESS affects both vehicle acceleration and braking performance, it is essential that the velocity profile, which is the main simulation input, complies with the maximum available traction force. The maximum tractive effort curve for GTW 2/6 DMUs is shown in Figure 2.8a, where the negative values are assumed for braking. It consists of a constant maximum tractive effort part for the vehicle velocities $v \leq 27$ km/h, and a constant maximum power hyperbola for $v \geq 27$ km/h. Note that in the case of a conventional DMU, braking power is dissipated at the resistors.

Due to the unavailability of detailed characteristics for GTW's powertrain components (EM, G, and ICE), available sources that provide the data on the powertrain components with similar maximum power/torque are used. The European project CleanER-D (CleanER-D, 2020) reported specifications for the powertrain components in different railway vehicles. Available data include detailed and validated efficiency, fuel consumption and emissions maps. Thus, this source is used in deriving and reconstructing parameters for the DMU analysed in this chapter. The efficiency map of GTW's EM with maximum power $P_{\text{EM,max}} = 400$ kW is derived using the normalized efficiency map $\eta_{\text{EM}} = f_{\text{EM}}^{\text{norm}}(\omega_{\text{EM}}/\omega_{\text{EM,max}}, T_{\text{EM}}/T_{\text{EM,max}})$ provided by Paukert (2011). The resulting efficiency map as a function of torque and angular speed is given in Figure 2.8b.

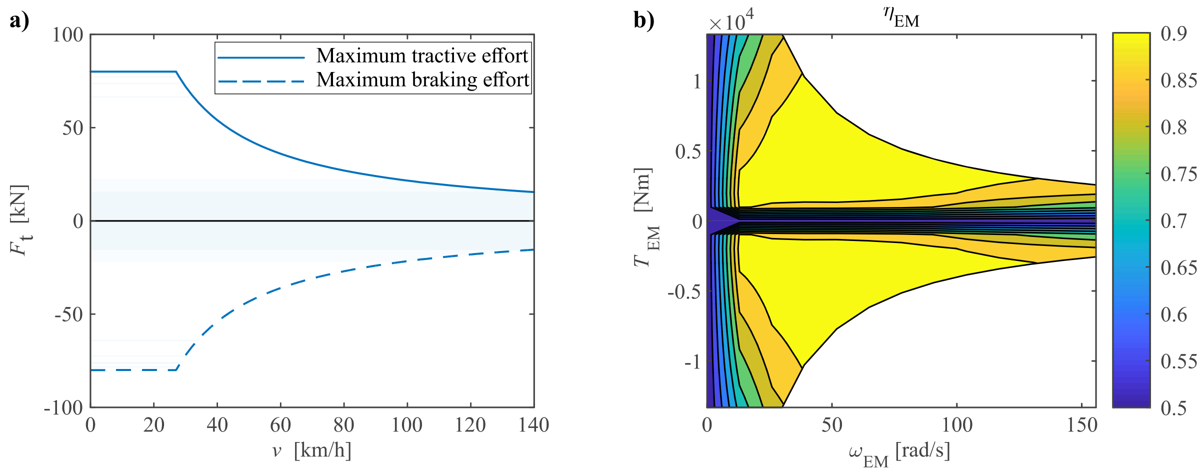

Figure 2.8: (a) Tractive effort vs. speed diagram, and (b) reconstructed electric motor efficiency map for Stadler GTW 2/6 diesel-electric multiple unit.

In order to derive the input parameters for the GTW's ICE-G set, data provided in the same source (Paukert, 2011) are used, wherein the maximum power/torque characteristics, generator's normalized efficiency map $\eta_G = f_G^{norm}(\omega_G/\omega_{G,max}, T_G/T_{G,max})$, ICE specific fuel consumption map $\psi = f_\psi(\omega_{ICE}, P_{ICE})$, as well as NO_x and PM emissions rate maps $\varepsilon_{NOx,PM} = f_{NOx,PM}(\omega_{ICE}, P_{ICE})$ are given for various ICE sizes (with a maximum power of 360, 560 and 1000 kW). The available 360 kW ICE is very similar to the one found in GTW DMU, as both represent adaptations of a heavy-duty truck ICE, complying with Stage IIIA standard. As the maximum power of the ICE found in GTW DMU (390 kW) differs from the ICEs found in the given source, the ICE static maps had to be reconstructed. For this, a scaling methodology based on so-called Willans lines is employed (Pourabdollah, 2012; Pourabdollah et al., 2014, 2013). A second-order polynomial approximates the engine specific fuel consumption for each ICE operating speed, while the ICE torque is scaled linearly with a scaling factor S_{ICE}. The approximation of specific fuel consumption can be written as

$$\psi(\omega_{ICE}, T_{ICE}) = C_0(\omega_{ICE}) \cdot S_{ICE} + C_1(\omega_{ICE}) \cdot T_{ICE} + C_2(\omega_{ICE}) \cdot \frac{T_{ICE}^2}{S_{ICE}}. \tag{2.35}$$

The scaling factor represents the ratio between scaled engine maximum power $P_{ICE,max}$ and the original ICE maximum power $P_{ICE,max0}$. The accuracy of this approach increases as the size of the approximated ICE is closer to the size of the original ICE (Cipek et al., 2019); thus, the ICE with a maximum power of 360 kW is chosen, resulting in the scaling factor

$$S_{ICE} = \frac{P_{ICE,max}}{P_{ICE,max0}} = 1.0833. \tag{2.36}$$

The second-order polynomial approximation coefficients C_0, C_1 and C_2 are first calculated by numerically solving a system of equations for each T_{ICE} vs. ω_{ICE} data point from the original ICE specific fuel consumption map using the least-squares method while setting the scaling factor $S_{ICE} = 1$ in (2.35). Then, by inserting the obtained polynomial coefficients (Figure 2.9a) into (2.35), and by scaling the torque with the scaling factor S_{ICE} given in (2.36), the ICE specific fuel consumption for GTW DMU is reconstructed (Figure 2.9b). The efficiency map for G is obtained in the same way as for EM, while the torque is scaled with the scaling factor S_{ICE}.

Fuel density $\rho = 825$ g/l and CO_2 emission factor $\varepsilon_{CO2} = 3.175$ kg/l for diesel fuel is adopted from Pröhl (2017b). The Willans line technique is also applied in reconstructing the ICE NO_x and PM emissions rate maps for GTW DMU, shown in Figures 2.9c,d. In this chapter, NO_x and PM emissions are included in the analysis as the additional indicators to the primary indicator of total fuel consumption. However, with the available emission rate maps, they can easily be included in the optimization problem as additional terms of the objective functions (2.19), which is left for future research.

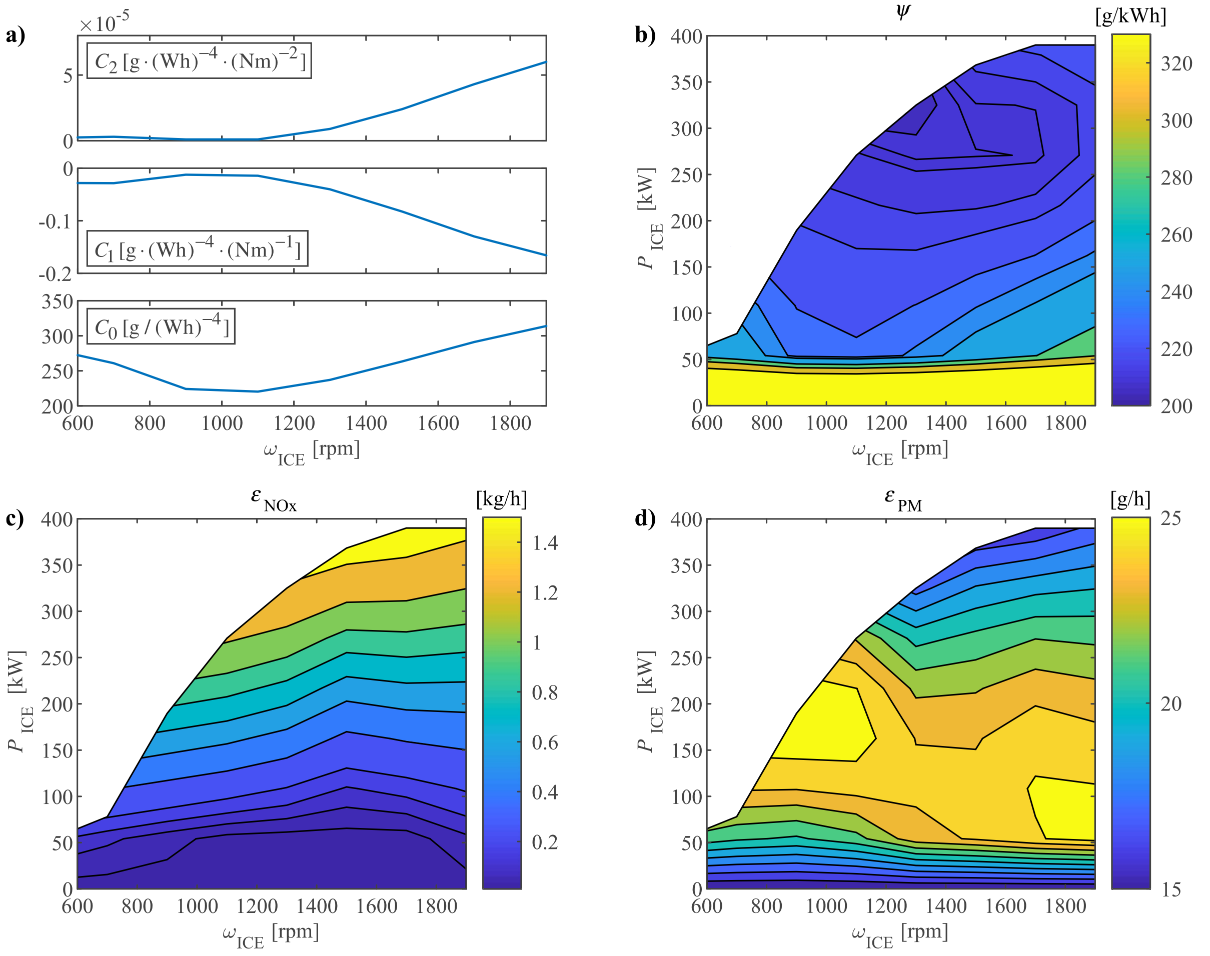

Figure 2.9: (a) Rotational speed-dependent coefficients of the polynomial approximation of specific fuel consumption, (b) specific fuel consumption map, (c) NO_X emissions rate map, and (d) PM emissions rate map of GTW 2/6 internal combustion engine.

The Saft Ion-OnBoard® Regen lithium-ion commercial battery based on sLFP (Super Lithium Iron Phosphate) chemistry (SAFT, n.d.) is considered to define the parameters for the ESS sizing and energy management problem. The parameters are extracted at the cell level by scaling down the values provided for this particular battery by SAFT and UNEW (2017) with respect to the number of its cells. The resulting values are given in Table 2.3, and the resulting cell open-circuit voltage as a function of SoC is shown in Figure 2.10. In order to account for battery aging effects, end-of-life (EoL) values for nominal cell capacity, maximum energy and internal resistance are adopted.

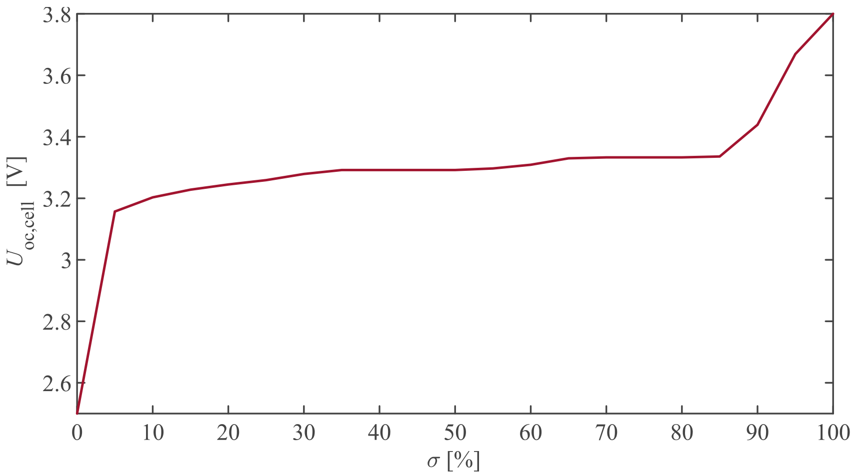

Figure 2.10: The open-circuit voltage of one lithium-ion battery cell as a function of state-of-charge.

Table 2.3: Lithium-ion battery cell parameters.

Parameter	Value	Unit	Description
σ_{max}	90	%	Maximum SoC
σ_{nom}	50	%	Nominal SoC
σ_{min}	10	%	Minimum SoC
$U_{cell,max}$	3.8	V	Maximum cell voltage
$U_{cell,min}$	2.5	V	Minimum cell voltage
$R_{cell,ch}$	0.002700	Ω	Internal cell resistance during charging
$R_{cell,dch}$	0.002716	Ω	Internal cell resistance during discharging
$C_{cell,nom}$	16.8	Ah	Cell nominal capacity
$P_{cell,cont,dch}(\sigma_{max})$	0.626310	kW	Cell maximum continuous discharging power at maximum SoC
$P_{cell,cont,dch}(\sigma_{nom})$	0.569312	kW	Cell maximum continuous discharging power at nominal SoC
$P_{cell,cont,dch}(\sigma_{min})$	0.490697	kW	Cell maximum continuous discharging power at minimum SoC
$P_{cell,cont,ch}(\sigma_{max})$	-0.384697	kW	Cell maximum continuous charging power at maximum SoC
$P_{cell,cont,ch}(\sigma_{nom})$	-0.534478	kW	Cell maximum continuous charging power at nominal SoC
$P_{cell,cont,ch}(\sigma_{min})$	-0.599807	kW	Cell maximum continuous charging power at minimum SoC
$E_{cell,max}(\sigma_{max})$	0.050974	kWh	Cell maximum energy at maximum SoC
$E_{cell,max}(\sigma_{nom})$	0.027133	kWh	Cell maximum energy at nominal SoC
$E_{cell,max}(\sigma_{min})$	0.005254	kWh	Cell maximum energy at minimum SoC
m_{cell}	2.122500	kg	Cell mass

2.4.3 Results

All numerical simulations/calculations are performed in MATLAB®/Simulink© environment, on a PC with Intel® Core™ i7-8650U 1.9 GHz CPU and 8 GB of RAM. A fixed time step $\Delta t = 1\text{s}$ is adopted in all experiments, with the ode3 (Bogacki-Shampine) solver used for numerical integration. The results in terms of resulting fuel consumption and related emissions are compared with the conventional DMU without an ESS. Estimation of the fuel consumption and related emissions of conventional DMU is done by evaluating the model in Figure 2.2, with the total requested power provided by ICE.

Optimal ESS size and resulting fuel consumption and emissions

In order to determine optimal ESS size for the hybridized DMU, the feasible search space representing possible ESS configurations is determined first, such that it satisfies the limitations on requested power from electrical auxiliaries $P_{\text{elaux}} = 45\,\text{kW}$, maximum required energy from ESS for supplying the auxiliaries in terminal stops $E_{\text{elaux,stop,max}} = 9\,\text{kWh}$, corresponding to the layover time of 12 minutes in Groningen, ESS voltage limits $U_{\text{ESS,min}} = 500\,\text{V}$ and $U_{\text{ESS,max}} = 1000\,\text{V}$, and maximum allowed mass for ESS $m_{\text{ESS,max}} = 2.5$ t. Figure 2.11 shows the resulting feasible region of the discrete search space for the ESS sizing problem, bounded by the five inequality constraints (2.21)-(2.25), which contains 228 possible ESS configurations (orange dots in the grid). Lower and upper boundary lines for the number of cells per branch (n_{ser}), reflect the constraints on the ESS voltage. The lower boundary line for the total number of cells, i.e. $n_{\text{ESS}} = n_{\text{par}} \cdot n_{\text{ser}}$, is derived from the constraint on the required energy ESS should be able to provide during stops, while the maximum number of cells is limited by the maximum allowed mass for the ESS. The constraint reflecting the minimum required ESS power is, in this case, already fulfilled with the energy-related requirement and does not restrict the search space.

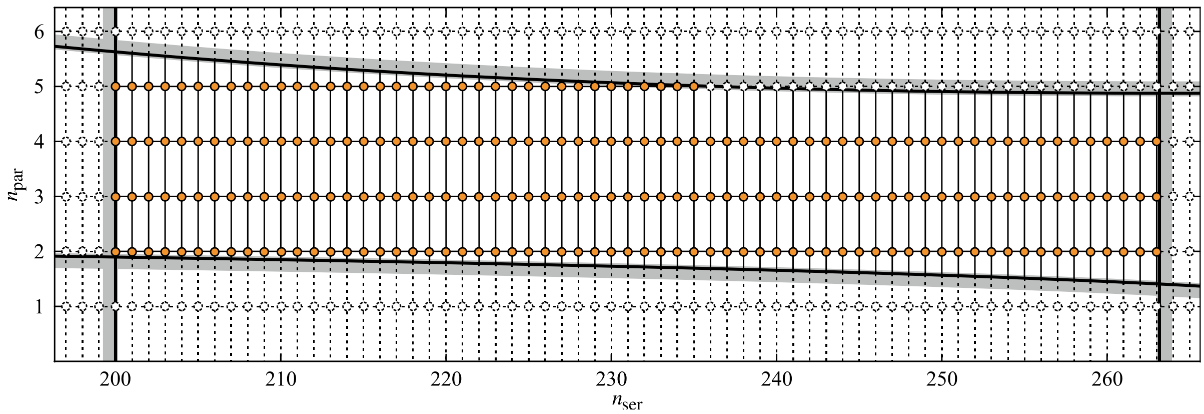

Figure 2.11: The feasible region of the discrete search space for optimal energy storage system sizing problem.

For the application of the DP algorithm, the optimal control problem is discretized into $K = 7200$ regular time steps, with the corresponding time step length equal to 1s, $I = 401$ values for the SoC $\sigma_i, i \in \{1, \dots, 401\}$, equally distributed over the interval $[0.1, 0.9]$, and $M = 201$ values for the power split ratio $x_j, j \in \{1, \dots, 201\}$, equally distributed over the interval $[-1, 1]$. The ESS SoC at the beginning and the end of the round trip is set to $\sigma_{\text{nom}} = 0.5$. The computationally efficient generic DP function (Sundstrom and Guzzella, 2009) is used in determining optimal ESS control, providing a significant reduction of computation time and numerical errors. Optimal control and corresponding fuel consumption were obtained in about 3 min on average per feasible ESS configuration. The weight α in (2.19) is set to 0.2 to reflect a moderate preference towards lower fuel consumption over total hybridization cost. Following the methodology given in Section 2.3, the obtained optimal ESS consists of $n^*_{\text{par}} = 2$ parallel branches with $n^*_{\text{ser}} = 231$ cells in series per branch. The corresponding hybridization costs are 5898.82 EUR. Figure 2.12 shows the simulation results for the hybrid DMU with optimally sized ESS, including the vehicle velocity profile, power split between the ICE and ESS, and the ESS SoC during the trip. As shown, the ESS provides the total requested power during stops with the ICE switched off, thus satisfying the primary hybridization requirement (emissions-free and noise-free operations during stops). At the same time, the request for SoC sustenance is achieved, despite the significant ESS discharge in terminal railway stations.

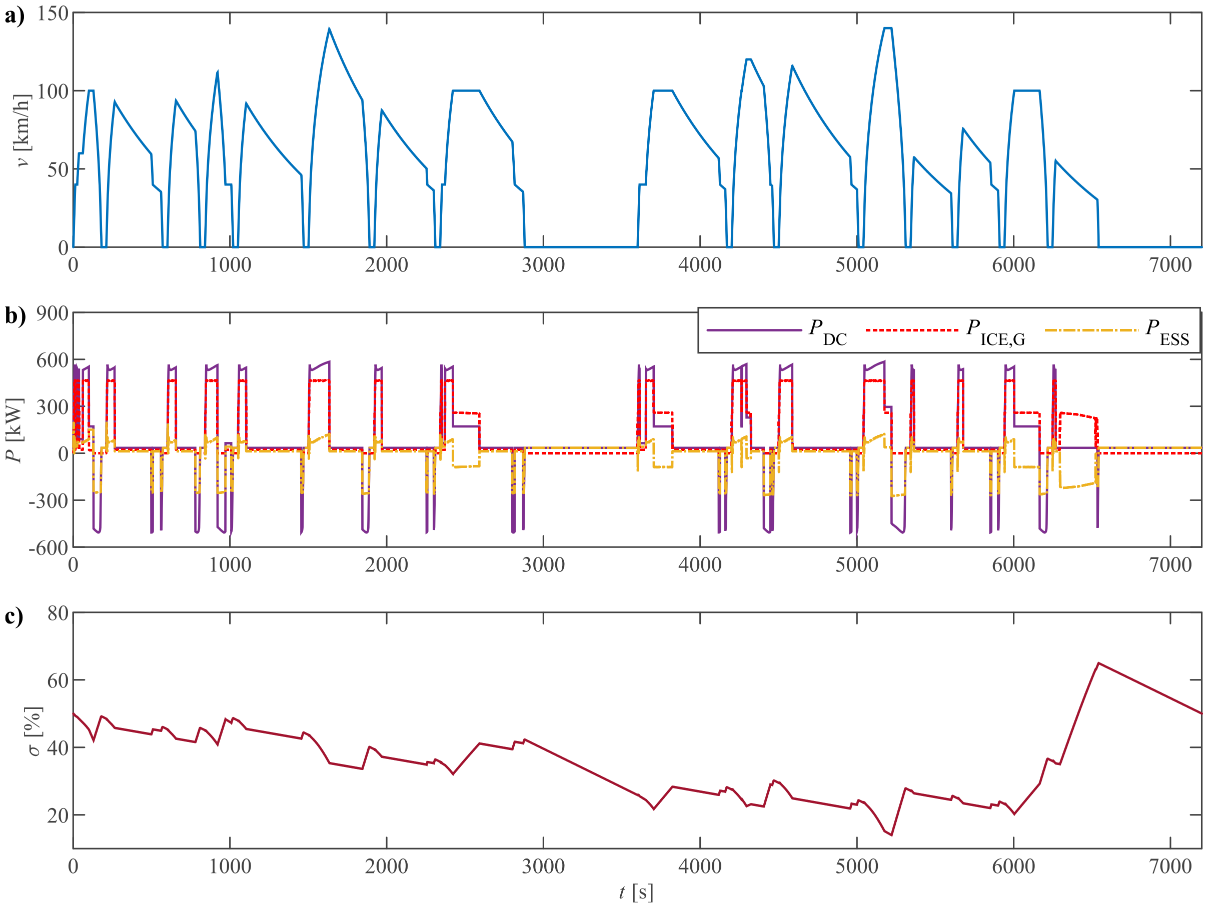

Figure 2.12: Simulation results for hybrid diesel-electric multiple unit with optimally sized energy storage system according to the dynamic programming-based control ($\alpha = 0.2$): (a) vehicle speed profile, (b) total requested power and power provided by internal combustion engine and energy storage system, and (c) energy storage system state-of-charge.

The resulting fuel consumption and related emissions for both conventional and hybrid DMU are given in Table 2.4. Compared to the conventional DMU vehicle, its hybridized counterpart with optimally sized and controlled ESS offers fuel savings and CO_2 emissions reduction of 29.9%. For the additional indicators representing local pollutant emissions, the simulation results show a 6.1% reduction in NO_x emissions and a 22.4% reduction in PM emissions.

Table 2.4: Fuel consumption and produced emissions for conventional and hybrid diesel-electric multiple unit with optimally sized energy storage system.

Indicator	**Unit**	**Conventional DMU**	**Hybrid DMU**	**Savings (%)**
B	liter	116.7103	81.8187	29.9
E_{CO2}	kg	370.5552	259.7744	29.9
E_{NOx}	kg	1.4972	1.4059	6.1
E_{PM}	kg	0.0858	0.0666	22.4

Trade-off between lower fuel consumption and hybridization cost

In order to further investigate the influence of the weight α on the trade-off between better fuel economy and lower hybridization cost, additional analysis was conducted by changing the weight value between 0 and 1, representing the most fuel and cost-efficient solutions, respectively. The results of the analysis are given in Figure 2.13 and Table 2.5. The results indicate that the increase in fuel consumption across α (i.e., between fuel consumption for $\alpha = 0$ and $\alpha = 1$) is 7.5%, giving the fuel savings compared to the conventional DMU vehicle (Table 2.4) ranging from 34.5% down to 29.6%. The total cost of hybridization is, at the same time, reduced by 54.6%.

Compared with the previous case ($\alpha = 0.2$) further reduction of fuel consumption of about 5% would require a significant increase in total hybridization cost of more than 30%. However, by considering the cumulative fuel savings and the vehicle life cycle duration, the investment return period would be relatively short. Results also indicate that the proposed optimization approach excluded the possibility of oversizing the ESS, as would be the case of the only criterion for hybridization being the maximum possible ESS size, conditioned with the mass limitation. In this way, further increase for 25% of total hybridization cost without any improvement of fuel economy is prevented.

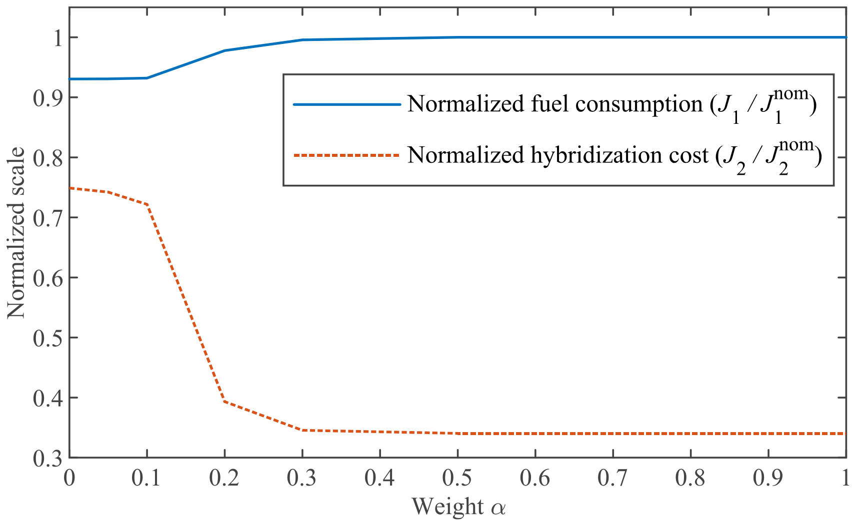

Figure 2.13: The trade-off between lower fuel consumption and lower hybridization cost.

Table 2.5: Optimization results for different values of weight α with implemented dynamic programming-based control.

Indicator	**Unit**	**α**						
		0	**0.05**	**0.1**	**0.2**	**0.3**	**0.5**	**1**
J^*	-	0.9305	0.9213	0.9109	0.8609	0.8006	0.6702	0.3404
J_1	litre	76.4661	76.4852	76.5853	80.3508	81.8187	82.1773	82.1773
J_2	EUR	11235.84	11133.70	10827.26	5898.82	5183.81	5107.20	5107.20
n_{par}^*	cell	4	4	4	2	2	2	2
n_{ser}^*	cell	220	218	212	231	203	200	200

Influence of the control strategy

The influence of the control strategy on the optimal solution is investigated in this section. For this aim, a causal and implementable rule-based strategy is defined. The flowchart of the rules for this controller is presented in Figure 2.14. In order to ensure fulfilment of the main hybridization requirement of emissions-free and noise-free operation during stops, a piecewise lower limit of ESS SoC is introduced, where $\sigma_{\mathrm{min,stop}}$ represents the SoC lower limit during stops, set to a value that satisfies the following condition:

$$n_{\mathrm{par}} \cdot n_{\mathrm{ser}} \cdot P_{\mathrm{cell,cont,dch}}(\sigma_{\mathrm{min,stop}}) \geq P_{\mathrm{elaux}}, \tag{2.37}$$

and $\sigma_{\mathrm{min,run}}$ is the SoC lower limit during motion, set to a value that satisfies the following condition:

$$n_{\mathrm{par}} \cdot n_{\mathrm{ser}} \cdot \left(E_{\mathrm{cell,max}}(\sigma_{\mathrm{min,run}}) - E_{\mathrm{cell,max}}(\sigma_{\mathrm{min,stop}})\right) \geq E_{\mathrm{elaux,stop,max}}. \tag{2.38}$$

Since the condition (2.37) is satisfied for all possible SoC lower limits for all 228 ESS configurations, it is set to $\sigma_{\mathrm{min,stop}} = 10\%$ as in the previous case, while the lover limit during motion is set to $\sigma_{\mathrm{min,run}} = 40\%$. The upper limit remains the same as in the previous case, i.e. $\sigma_{\mathrm{max}} = 90\%$. According to the defined algorithm, during stops ($v = 0$) the ESS provides complete requested power, and the ICE is switched off. If the ESS discharges to $\sigma_{\mathrm{min,stop}}$ before the departure (caused by delayed departure, for instance), the ICE is started and supplies the total demanded power. In case of negative power demand, generally occurring when the vehicle is braking, the braking energy is used for recharging the ESS, and ICE operates with no load. In case of high power demand, in our case set to a value exceeding 60% of the maximum available power from the ICE-G set, the ESS provides maximum available power for supporting the ICE. This typically occurs during vehicle acceleration. For the lower levels of demanded power (i.e., during cruising or coasting phases), the ESS provides support for the ICE limited to the electrical auxiliaries power demand. This operation mode is sustained until $\sigma_{\mathrm{min,run}}$ is reached. Once this occurs, the controller switches to "load level increase" mode, where the ICE provides additional power used for recharging the ESS. In order to prevent frequent switching between ESS charging and discharging, and at the same time from excessive usage of ICE instead of braking power for charging the ESS, a 5% hysteresis for the SoC is considered during this phase of low power demand.

The same approach for determining the ESS optimal size described in Section 2.3 is conducted by using the defined RB control instead of DP. Compared to the DP-based control, simulation time for the entire trip with implemented RB control takes less than 2 seconds on average per feasible ESS configuration. The overall results are given in Table 2.6. The increase in fuel consumption across α, in this case, is 15.2%, while the total cost of hybridization is reduced by 65.8%. Compared to the standard DMU, fuel savings range from 19.2% for the most fuel-efficient solution down to 7% for the most cost-efficient solution. Regarding the ESS size and configuration, achieving the most fuel-efficient solution, in this case, requires significant ESS size and related cost increase compared to the solution obtained with the implemented DP controller. The differences in results from the two control strategies are emphasized in Figure 2.15, where the fuel consumption level for all 228 ESS configurations and related costs is plotted. The fuel consumption is normalized with the results obtained for the standard DMU for overall comparison.

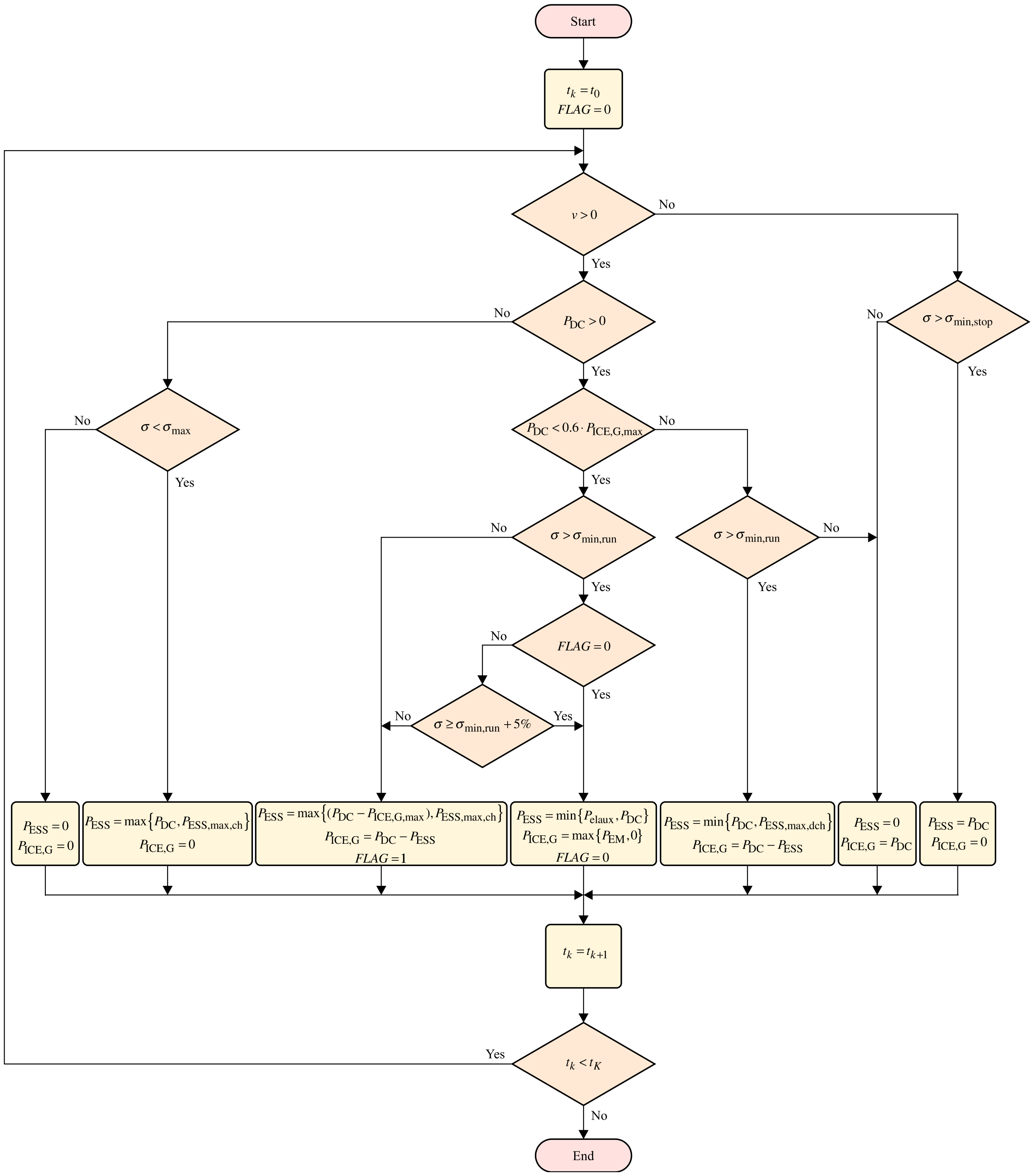

Figure 2.14: Flowchart for the proposed rule-based controller.

Table 2.6: Optimization results for different values of weight α with implemented rule-based control.

Indicator	**Unit**	α						
		0	**0.05**	**0.1**	**0.2**	**0.3**	**0.5**	**1**
J^*	-	0.8530	0.8602	0.8645	0.8530	0.7893	0.6613	0.3404
J_1	litre	94.2559	94.2559	96.5694	108.3127	108.3127	108.5326	108.5326
J_2	EUR	14938.56	14338.56	11695.49	5158.27	5158.27	5107.20	5107.20
n_{par}^*	cell	5	5	4	2	2	2	2
n_{ser}^*	cell	234	234	229	202	202	200	200

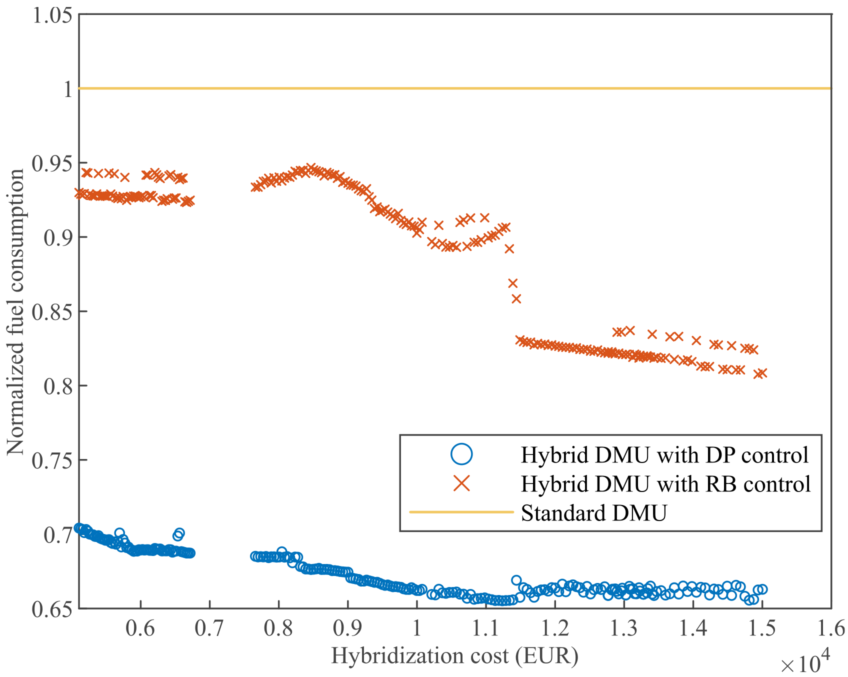

Figure 2.15: Relative fuel savings for hybrid diesel-electric multiple unit as a function of energy storage system size and implemented control, compared to the conventional vehicle.

Figure 2.16 shows the total requested power split and SoC of optimally sized ESS at a weight $\alpha = 0.2$, which contains $n_{\mathrm{par}}^* = 2$ parallel branches with $n_{\mathrm{ser}}^* = 202$ cells per branch. As can be seen, the proposed RB controller ensures fulfilment of the main hybridization requirement imposed by the RU; however, its main drawback is the inability to guarantee the ESS SoC sustenance, caused primarily by its causal nature. The following round trip would start with significantly discharged ESS, considering the given periodic timetable and corresponding vehicle circulation plan. This would result in higher fuel consumption than the given results, thus implying its significant impact and biased input for the primary optimization problem.

Regarding the local pollutants, emissions results are diverse (see Figure 2.17). Depending on the ESS size and configuration, simulation results for DMU with DP controller demonstrated a decrease of NO_x emissions ranging from 3.5% up to 11.8% compared to the standard DMU emissions level, while RB control resulted in an increase of 20.3% up to 34.1%. For PM emissions, both controls demonstrated a reduction compared to the standard DMU ranging between 60.3-61.2% for DP control and between 14.9-21.3% for RB control.

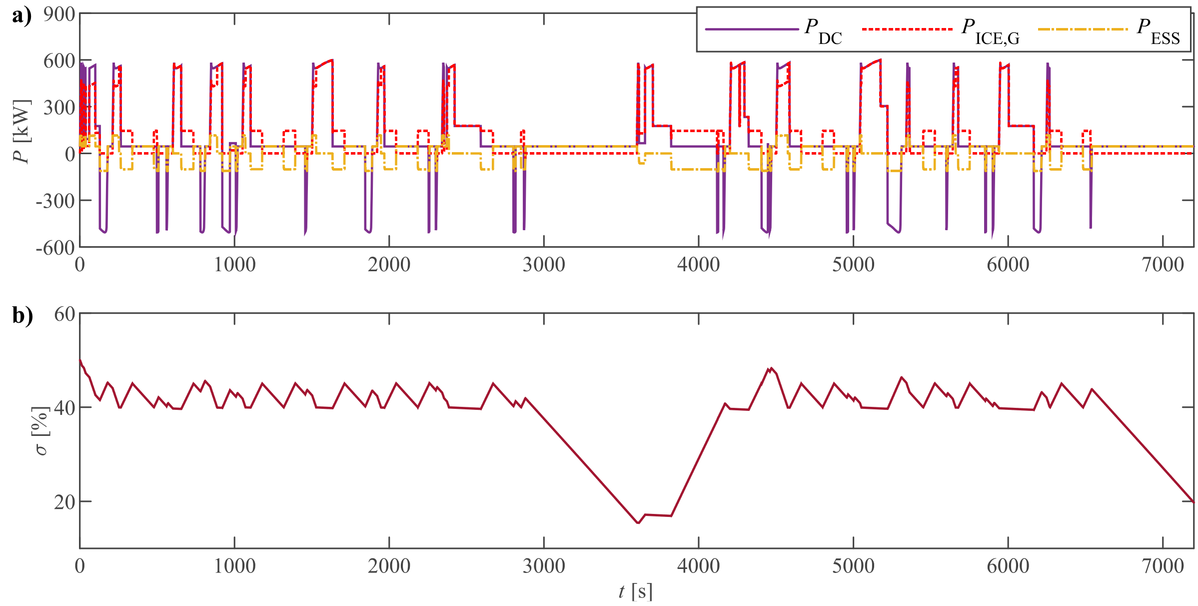

Figure 2.16: Simulation results for hybrid diesel-electric multiple unit with optimally sized energy storage system according to the rule-based control ($\alpha = 0.2$): (a) total requested power and power provided by internal combustion engine and energy storage system, and (b) energy storage system state-of-charge.

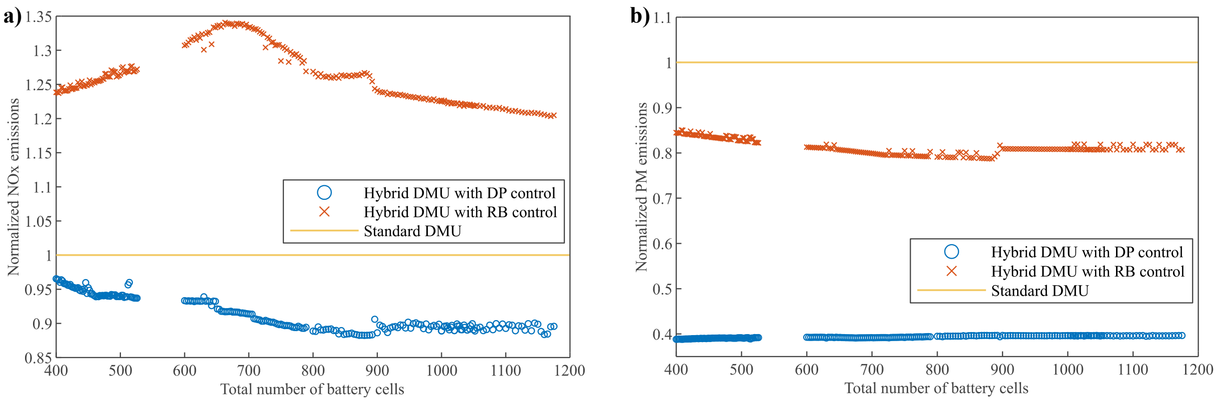

Figure 2.17: Normalized local pollutants emissions for standard and hybrid diesel-electric multiple unit depending on the energy storage system size and implemented control: (a) NO_x emissions, and (b) PM emissions.

2.5 Discussion

The detailed analysis presented in the previous section showed significant potential benefits from hybridization of a DMU vehicle. These benefits are reflected primarily in the reduction of fuel consumption and resulting CO_2 emissions, theoretically reaching almost 35% compared to the conventional DMU. Although the focus of this study was on a specific case study in the Netherlands, the presented methodology can be applied to other regional railway networks and DMU vehicles, regardless of the geographical context. In addition, the proposed optimization algorithm allows for fair generalization and relatively easy adaptation to other railway vehicles and types of services. Moreover, straightforward determination of feasible ESS configurations based on existing technologies allows for a direct implementation of the solution.

Due to its non-causal nature (i.e., assuming perfect information on future driving conditions), frequent switches in ESS control, as well as required computation time (i.e., 3 minutes on average in this case), the DP-based EMS cannot be directly implemented in a real-time controller. However, having in mind the main aim of this study – determining the optimal size of ESS, which represents a strategic decision, the presented approach identifies ESS parameters that yield the absolute largest potential in reducing fuel consumption, regardless of the EMS in place.

The main advantages of the presented RB controller are its straightforward implementation in real-time energy management, at the same time satisfying the main requirement of providing enough power and energy for supplying auxiliaries during stabling periods. Due to implemented hysteresis, it prevents frequent switches in ESS charging/discharging, thus improving its life cycle durability. However, the inability to guarantee ESS SoC sustenance and significantly decreased performance compared to the DP controller make the ESS sizing problem obtained with RB control biased.

This research stresses the importance of synthesizing and practical implementation of real-time energy management that would lead to an optimum or near-optimum performance in terms of energy consumption. In this context, DP-based control can be used either to obtain a reference fuel consumption or to obtain optimal power split trajectories that can later be used in defining implementable real-time control strategies. Heuristic RB controls or combining the EFCM method with DP or optimal control theory (Ambuhl and Guzzella, 2009; Nazari et al., 2019) are promising approaches in this regard. The development of such algorithms, coupled with advanced power management hardware technologies, requires significant effort from the whole industry, and especially from the vehicle manufacturers.

Regarding the local pollutants emissions, results indicate a significant influence of the choice of EMS, with a negative impact on NO_x emissions obtained in case of sub-optimal rule-based control. Even though these emissions are not included in the optimization problem but only as additional indicators, the simulation results with a characteristic mapping of Stage IIIA ICE found in the analysed vehicle show that hybridization as an instrument could not lead to the fulfilment of Stage IIIB emissions limits. Significant specific reduction requirements imposed by the legislation, especially for PM emissions, reaching almost 90% reduction from Stage IIIA to IIIB, together with the fact that the legislation is focusing only on specific load points of ICE (DieselNet, 2020), stipulate the necessity of using advanced exhaust ATSs.

2.6 Conclusions

This chapter presented a method to support the decision in the conversion of standard diesel-electric multiple units to their hybrid counterpart by adding an optimally sized lithium-ion battery-based energy storage system. The proposed bi-level multi-objective optimization approach based on a nested coordination framework includes relevant design aspects, such as the requirement of achieving emissions-free and noise-free operation in stations, the preference between lower fuel consumption and hybridization cost, technical constraints related to battery voltage and maximum allowed mass, and the influence of the energy management strategy. The case study of selected two-coach diesel multiple unit and railway line demonstrated fuel savings and CO_2 emissions reduction ranging between 29.6% and 34.5% with optimal dynamic programming-based control, and from 7% to 19.2% for sub-optimal rule-based control, compared to the conventional vehicle, depending on the ESS size and configuration. At the same time, the implementation of optimal control allowed for preventing ESS oversizing and avoiding additional costs. Additionally, a non-linear dependence between hybridization cost and potential fuel savings was identified. The influence of energy management is even more evident in the case of local pollutants, especially NO_x emissions, where the negative impact compared to a standard vehicle is obtained.

The presented research aimed to provide the basis for further developing a wider-scope tool, coined “CO_2 Barometer”. The aim of the CO_2 Barometer is to enable dynamic monitoring and prediction of overall emissions from regional railway services provided on the Northern lines in the Netherlands, and at the same time to offer a decision support tool for the railway undertaking in the analysis of potential future traction options, by capturing the technical innovation and different technological, operational and policy measures. Future applications of the present research will include other types of rolling stock in the fleet, while considering remaining lines and services on the network. Special focus will be on further testing and validation of the proposed method in real-world operation, within the ongoing rolling stock refurbishment program of Arriva. Further extensions to the current work will include the development of a causal control strategy with respect to the system architecture in place that would be able to provide results that converge to the global optimum. Additionally, analysis of other energy storage and propulsion systems based on supercapacitors and hydrogen fuel cells, as well as the environmental impact of using alternative fuels such as hydrotreated vegetable oil will be conducted, while extending the research scope to Well-to-Wheel and life cycle perspective.

Chapter 3

Analysis of hybrid and plug-in hybrid alternative propulsion systems for regional diesel-electric multiple unit trains

Apart from minor updates, this chapter has been published as:

Kapetanović, M., Vajihi, M., Goverde, R.M.P. (2021). Analysis of Hybrid and Plug-In Hybrid Alternative Propulsion Systems for Regional Diesel-Electric Multiple Unit Trains. *Energies*, 14, 5920.

3.1 Introduction

The transport sector is facing numerous challenges in meeting the greenhouse gas (GHG) emissions reduction targets defined in various international treaties (UN, 2015, 1998), improving energy efficiency and reducing the operational costs (DiDomenico and Dick, 2015). Achieving carbon-neutral railways operation by 2050 (UIC and CER, 2012) is being mainly sought through the synergetic electrification of railway lines and production of traction electricity from renewables. While this instrument is economically viable for the highly utilized main corridors, regional railway lines, which is the main subject in this thesis, require identification of alternative options for the predominant diesel traction. Replacing the typically employed diesel multiple units (DMUs) with battery-electric multiple unit (BEMU) (RailTech, 2019; RailwayTechnology, 2020; Siemens, n.d., n.d.) and/or fuel-cell multiple unit (FCMU) vehicles (Alstom, 2020; FuelCellWorks, 2020; IRJ, 2019) offers a potentially carbon-neutral final solution for catenary-free operation. However, a “zero-one” transition such as this is hindered by numerous aspects related primarily to the vehicle range, technology maturity and availability, relatively high hydrogen and accompanying infrastructure costs, as well as the long life cycle of the existing diesel-driven rolling stock. Thus, this dynamic transition process requires further exploitation of DMUs, while constantly improving their energy and environmental performance by implementing novel technological solutions in order to meet increasingly stringent emission reduction requirements.

Vehicle hybridization, achieved by adding an energy storage system (ESS), enables the storing of braking energy and support to the internal combustion engine (ICE), resulting in a significant reduction in fuel consumption and related emissions (Bai and Liu, 2021). Hybrid and plug-in hybrid propulsion systems are increasingly being developed and used in road transport with the aim to improve vehicle fuel economy (Fuhs, 2008) and reduce emissions (Doucette and McCulloch, 2011). A number of hybrid electric vehicles (HEV) and plug-in hybrid electric vehicles (PHEV) became commercially available over the last two decades (Orecchini et al., 2014; Orecchini and Santiangeli, 2010), which is likewise reflected in the extensive research efforts on their development as reported in the literature (Williamson, 2013). Despite potentially great benefits from DMU hybridization, as confirmed in several research projects (EC, 2005; Hillmansen et al., 2009, 2008; Marsilla, 2013), hybridization of railway powertrains is still in the early development stages. Due to a comparably smaller market for railway vehicles, only a small number of hybrid DMUs exist (Engel and Soefker, 2001; Fujii et al., 2004; Railway Gazette International, 2015; Research and Technology Centre of Deutsche Bahn AG, 2001; Shiraki et al., 2010), mainly as prototypes. Plug-in hybrid systems offer further exploitation of the benefits offered by the ESS using an external electric power source for their charging during stabling periods. However, practical implementation of a plug-in hybrid concept in the railway sector is limited to shunting locomotives thus far (Alstom, 2016, 2015; INSIDEEVs, 2015; Railcolor News, 2018), with no reported applications nor literature concerning commercial passenger transport. Utilization of fast charging facilities in stations is considered mainly for BEMUs operation, as a complement to partially electrified regional railway lines (Hirose et al., 2012; Kono et al., 2014; Masatsuki, 2011, 2010; Shiraki et al., 2015) or in tram networks (Mwambeleko and Kulworawanichpong, 2017), which represent other use cases than the main subject of the present chapter.

Energy management strategies (EMSs) are the main driver of the fuel economy in hybrid vehicles. Consequently, the reported literature on hybrid DMUs focusses primarily on their development and implementation. Their aim is to minimize energy consumption by managing the power flows from different energy sources in the system. Dynamic programming (DP), as a global optimization method, is widely used in EMS optimization for hybrid railway vehicles (Kapetanović et al., 2021a; Ogawa et al., 2007; Sorrentino et al., 2020). It was also used in deriving a fuel-optimal combined driving and energy management strategy (Leska and Aschemann, 2015). Although DP allows for deriving a globally optimal EMS, it is mainly employed for off-line controller optimization, with several drawbacks hindering its real-time applications. These include its requirements for perfect information on the future duty cycle, the extensive calculation time, frequent switches in power distribution, and the inability to deal with variables that include counters due to its non-causal nature, i.e., propagation backward in time. Therefore, the EMS obtained from the DP is mainly used in defining other causal controllers (Peng et al., 2020b), or as a benchmark in evaluating real-time algorithms (Leska et al., 2017, 2014). The equivalent consumption minimization strategies (ECMSs) (Torreglosa et al., 2011a) and Pontryagin's minimum principle (PMP) optimal control strategies (Liu et al., 2020; Peng et al., 2020a) belong to a group of instantaneous optimization methods that can be used in defining causal controllers. The effectiveness of these methods depends on how the future driving conditions and critical parameters, namely the equivalent coefficient in ECMS and the initial value of the co-state in PMP, are estimated (Zhang et al., 2017). Additionally, whether a certain EMS can be used online is decided by computation cost and storage memory requirement (Li et al., 2019), posing additional challenges in practical applications of such causal controllers. Compared to the previous optimization-based methods, rule-based (RB) algorithms use event-triggered Boolean rules in determining the power ratio between different power sources in the system. These rules can be derived from heuristics or fuzzy rules based on experts' knowledge (Lanneluc et al., 2017). Although RB algorithms cannot guarantee optimality, they were widely used in defining real-time EMSs (Dittus et al., 2011; García-Garre and Gabaldón, 2019), mainly due to their low computation time and easy implementation, while also showing promising benefits in terms of fuel savings and emissions reduction.

The present chapter contributes to a bigger project realized in cooperation with Arriva, the largest regional railway undertaking (RU) in the Netherlands, aiming to specify and assess potential innovations in reducing total GHG emissions on a regional non-electrified network in the provinces of Friesland and Groningen. Additionally, requirements of emission-free and noise-free operation in terminal station areas with longer stabling periods (above 5 min) are imposed for the current DMU fleet, with foreseen operation until 2035. The development of detailed simulation models is required to incorporate numerous factors and case-specific constraints affecting trains' performance, and to capture their technological and operational characteristics. With this in mind, and considering previously discussed aspects and identified knowledge gaps, the main contributions of this chapter are twofold:

1. A method to support a hypothetical conversion of a conventional regional DMU vehicle to its hybrid and plug-in hybrid counterparts, equipped with the prominent ESS technologies and newly developed causal and easy-to-implement real-time power control, allowing for a realistic estimation of fuel savings;
2. A comparative analysis of alternative propulsion systems in a case study of a selected benchmark vehicle and railway line in the Northern Netherlands, providing the railway undertaking with an assessment of potential benefits in terms of reduction of produced GHG emissions and energy costs.

The remainder of the chapter is organized as follows. Section 3.2 presents a description of standard, hybrid, and plug-in hybrid propulsion systems. A detailed simulation model and the real-time power control are presented in Section 3.3. A Dutch case study comprising of different systems, railway services, and charging scenarios is given in Section 3.4, followed by a discussion in Section 3.5. The concluding remarks and future work efforts are outlined in Section 3.6.

3.2 Configuration of standard, hybrid and plug-in hybrid propulsion systems

Various propulsion system configurations can be found in regional DMU vehicles based on their type of power transmission from the ICE to the wheels, i.e., an electrical, hydraulic, or mechanical transmission (Spiryagin et al., 2014). We limit our analysis to electrical transmission, namely to diesel-electric multiple units (DEMUs), as the only traction option present in the northern Netherlands. The power-plant of a standard DEMU (Figure 3.1a) consists of an ICE powering an AC electric generator (G). The diesel generator (ICE-G) set powers an AC electric motor (EM) via the rectifier and inverter. With EM acting as a generator during braking, the regenerated energy is, in this case, dissipated through a braking resistor (rheostat), connected to the DC link via a DC/DC converter. We assume total electrification of mechanical auxiliaries, such as hydraulic pump and compressor, with auxiliary systems connected to the DC link via a DC/AC inverter.

Hybridization of a DEMU can be accomplished with a properly sized and implemented ESS. Numerous ESS technologies have emerged in the transport sector (Vazquez et al., 2010). In order to assess the influence of the ESS technology selection for a hybrid diesel-electric multiple unit (HDEMU), we considered the two alternative ESSs that are especially suited for onboard railway applications: lithium-ion batteries (LBs) and double-layer capacitors (DLCs) (Ghaviha et al., 2017b). Compared to LBs, which are characterized by a high energy density, limited power density, and relatively short lifetime, DLCs feature a high number of duty cycles, low energy density, and a high-power density that allows the ESS to store all the energy coming from regenerative braking in a short time period, and to release it to the EM during acceleration (Meinert et al., 2015b). There are different approaches to ESS implementation into the system, i.e., by a direct connection to the DC link (Cipek et al., 2019; Xu et al., 2015b) or via bidirectional DC/DC converters (García-Garre and Gabaldón, 2019). As the application of the DC/DC converter provides the ability to achieve an active control of each power source and match its voltage to the DC bus voltage (Zhang et al., 2017), we adopted the latter approach (Figure 3.1b).

Typically, PHEVs use an electric vehicle supply equipment (EVSE) port and corresponding connector for charging the ESS. For further conversion to a plug-in hybrid diesel-electric multiple unit (PHDEMU), we considered adding a pantograph (or a contact shoe) connected to the DC link via a line inductor in case of a DC external power grid, or via a transformer and AC/DC converter in case of an AC external power source (Figure 3.1c).

a)

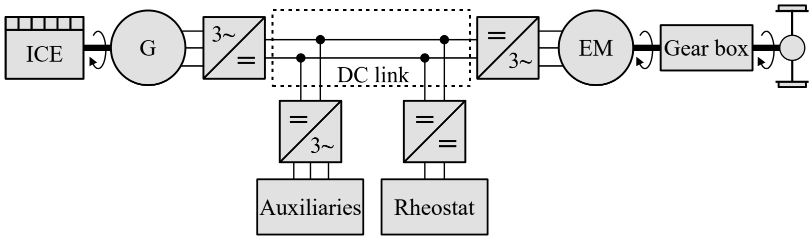

b)

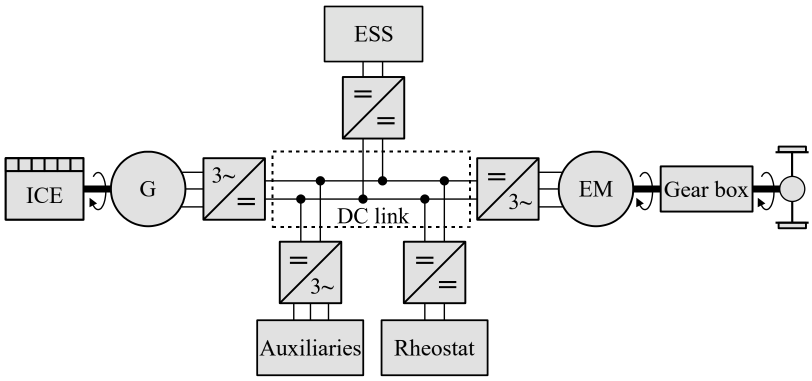

c)

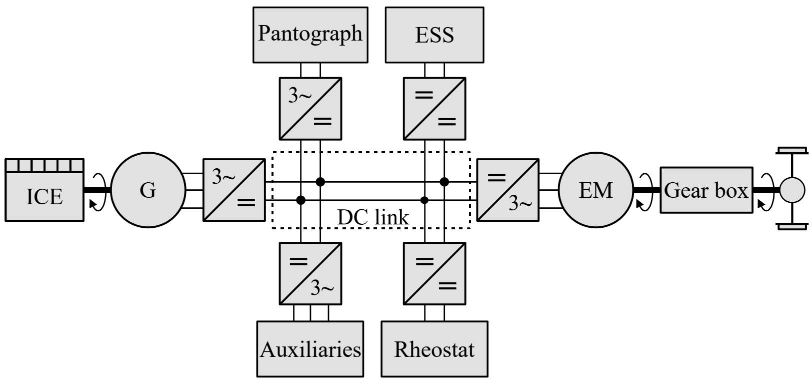

Figure 3.1: Simplified schematic representation of (a) standard, (b) hybrid and (c) plug-in hybrid system architectures for a diesel-electric multiple unit vehicle.

3.3 Modelling and control of alternative propulsion systems

3.3.1 Simulation model

A backward-looking quasi-static simulation approach (Leska et al., 2017; Pröhl, 2017b) was adopted in modelling the dynamics of the previously described system architectures. The simulation model was developed in the MATLAB®/Simulink© environment using the OPEUS Simulink toolbox (Pröhl, 2017a). The model of a hybrid DEMU (Kapetanović et al., 2021a) was extended to include different power sources (i.e., ICE, pantograph, LB, and DLC) and to capture the dynamics of ESSs using typically available parameters published by the manufacturers. The simulation model (Figure 3.2) allowed for the simulation of different configurations by disconnecting components not included in the respective system. According to the backward orientation of the model, the inputs encompass the train velocity and geometry profiles of the track, and the main outputs are cumulative fuel and electricity demand. The arrows designate the numerical evaluation sequence, opposite to the physical power flow. Due to the high efficiencies of the power converters, their dynamics were omitted in the model, with their efficiencies assumed to be ~100%. However, they were considered in the physical system for controlling the power flows and dispatching different system components according to the implemented energy management strategy (see Section 3.3.2). The braking rheostat was used only for assessing the balance of power flows in the system. The description of the low-order models for the system components is provided in the remainder of this section.

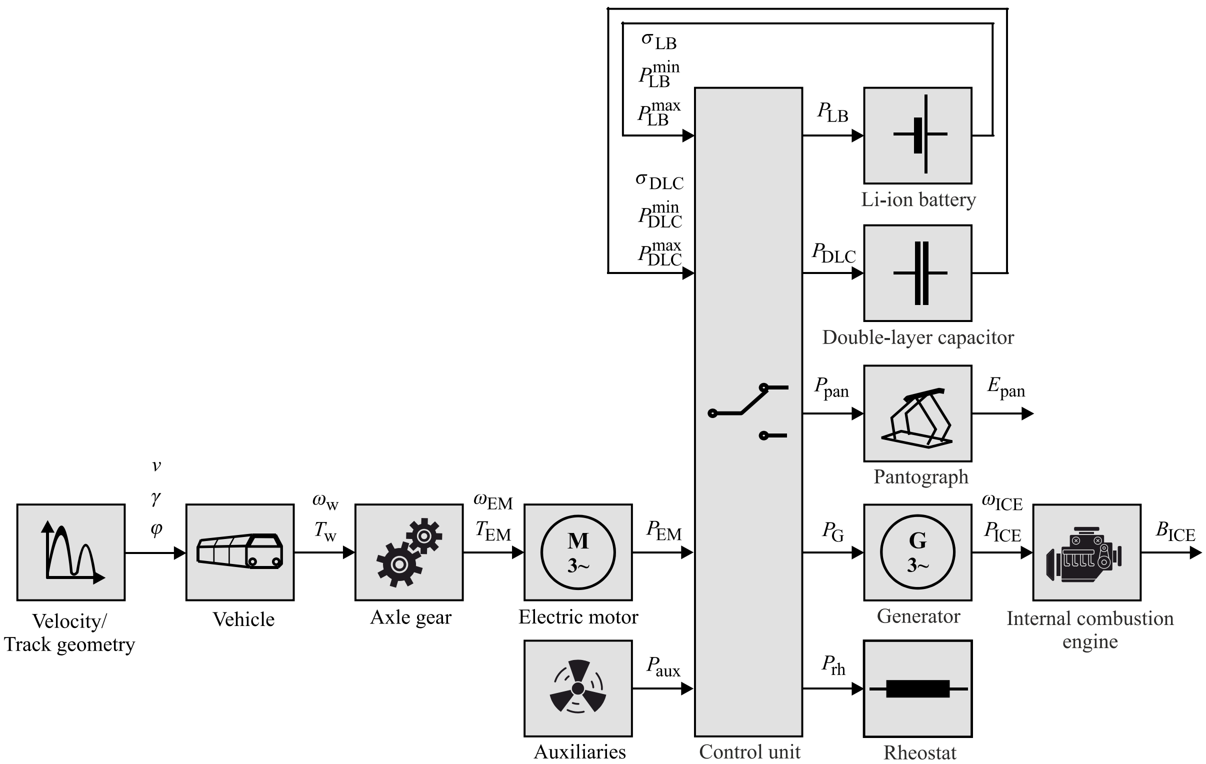

Figure 3.2: Layout of the simulation model for the assessment of the alternative diesel-electric propulsion system configurations.

Vehicle

With the given velocity and track geometry profiles as input signals, the tractive or braking effort at the wheel F_w [N] is determined by

$$F_\mathrm{w}\big(v(t)\big) = m_\mathrm{v} \cdot a(t) + R_\mathrm{v}\big(v(t)\big) + R_\mathrm{g}\Big(\gamma\big(s(t)\big)\Big) + R_\mathrm{c}\Big(\phi\big(s(t)\big)\Big) \tag{3.1}$$

with

$$R_\mathrm{v}\big(v(t)\big) = r_0 + r_1 \cdot v(t) + r_2 \cdot v(t)^2 \tag{3.2}$$

$$R_\mathrm{g}\Big(\gamma\big(s(t)\big)\Big) = m_\mathrm{v} \cdot g \cdot \sin\Big(\gamma\big(s(t)\big)\Big) \tag{3.3}$$

$$R_\mathrm{c}\Big(\phi\big(s(t)\big)\Big) = \begin{cases} m_\mathrm{v} \cdot \dfrac{4.91}{\phi - 30} & \text{if } \phi < 300 \text{ m} \\ m_\mathrm{v} \cdot \dfrac{6.3}{\phi - 55} & \text{if } \phi \geq 300 \text{ m,} \end{cases} \tag{3.4}$$

where t [s] is the time; v [m/s] is the vehicle velocity; $s = \int_0^t v(\tau)d\tau$ [m] is the distance travelled; $a = dv/dt$ [m/s^2] is the acceleration; m_v [kg] is the total mass of the vehicle, i.e. $m_\mathrm{v} = (1+\lambda) \cdot m_\mathrm{tare} + m_\mathrm{pax}$, where λ denotes the factor accounting for rotating masses, m_tare [kg] the vehicle tare weight, and m_pax [kg] the cumulative passengers weight. The vehicle resistance R_v [N] includes roll resistance and air resistance, modelled using the Davis equation (Davis, 1926), with vehicle-specific coefficients r_0 [N], r_1 [N/(m/s)] and r_2 $\left[\text{N/(m/s)}^2\right]$; R_g [N] is the grade resistance, with $g = 9.81$ $\left[\text{m/s}^2\right]$ denoting the gravitational acceleration, and γ [rad] the angle of the slope (Brünger and Dahlhaus, 2014); and the curve resistance R_c [N] is calculated using Roeckl's formula (Huerlimann and Nash, 2003), with ϕ [m] denoting the curve radius. With the given wheel diameter, d_w [m], and the vehicle velocity, v, the torque at the wheel, T_w [Nm], and its rotational speed, ω_w [rad/s], can be calculated by (Kapetanović et al., 2021a; Leska et al., 2017)

$$T_\mathrm{w} = F_\mathrm{w} \cdot \frac{d_\mathrm{w}}{2} \tag{3.5}$$

$$\omega_\mathrm{w} = 2 \cdot \frac{v}{d_\mathrm{w}}. \tag{3.6}$$

Axle gear

The power from the EM shaft to the wheels is transmitted via the axle gear, with the constant gear ratio i_ag and the constant efficiency of the gearbox η_ag. The torque T_EM [Nm] and the rotational speed ω_EM [rad/s] at the mechanical input of the axle gear result from (Kapetanović et al., 2021a; Leska et al., 2017)

$$T_\mathrm{EM} = \begin{cases} \dfrac{T_\mathrm{w}}{i_\mathrm{ag} \cdot \eta_\mathrm{ag}} & \text{if } T_\mathrm{w} \geq 0 \\ \dfrac{T_\mathrm{w} \cdot \eta_\mathrm{ag}}{i_\mathrm{ag}} & \text{if } T_\mathrm{w} < 0 \end{cases} \tag{3.7}$$

$$\omega_{\mathrm{EM}} = \omega_{\mathrm{w}} \cdot i_{\mathrm{ag}}. \tag{3.8}$$

Electric motor

Based on the operation mode (motor or generator), and with the EM efficiency $\eta_{\mathrm{EM}} = f_{\mathrm{EM}}(T_{\mathrm{EM}}, \omega_{\mathrm{EM}})$ determined by a linear 2D-interpolation in the efficiency map, the electric power of the electric motor P_{EM} [W] can be determined by (Kapetanović et al., 2021a; Leska et al., 2017)

$$P_{\mathrm{EM}} = \begin{cases} \dfrac{T_{\mathrm{EM}} \cdot \omega_{\mathrm{EM}}}{\eta_{\mathrm{EM}}} & \text{if } T_{\mathrm{EM}} \geq 0 \\ T_{\mathrm{EM}} \cdot \omega_{\mathrm{EM}} \cdot \eta_{\mathrm{EM}} & \text{if } T_{\mathrm{EM}} < 0. \end{cases} \tag{3.9}$$

Auxiliaries

The total auxiliaries power P_{aux} [W] is modelled as the sum of the constant term $P_{\mathrm{aux,const}}$ [W], representing constant consumers, such as lighting and the heating, ventilation and air conditioning (HVAC) system, and the variable term, which accounts for the cooling power (Pröhl, 2017b), where we introduce the coefficient p_{cool}, representing the proportion of the total traction power required for cooling the main traction components, i.e.:

$$P_{\mathrm{aux}}(t) = P_{\mathrm{aux,const}} + p_{\mathrm{cool}} \cdot |P_{\mathrm{EM}}(t)|. \tag{3.10}$$

Diesel generator set

The diesel generator (ICE-G) set is the prime mover in all the propulsion system configurations considered. Given the requested power from the ICE-G set (electrical output power of the generator) P_{G} [W], the mechanical output power of the ICE P_{ICE} [W] is calculated by:

$$P_{\mathrm{ICE}} = \frac{P_{\mathrm{G}}}{\eta_{\mathrm{G}}}, \tag{3.11}$$

where the efficiency $\eta_{\mathrm{G}} = f_{\mathrm{G}}(T_{\mathrm{G}}, \omega_{\mathrm{ICE}})$ is determined by a linear 2D-interpolation in the efficiency map of the generator. The existence of a DC link between the ICE-G and the EM allows for the independent rotational speed of the EM and ICE-G set, with the optimal ICE-G set rotational speed ω_{ICE} [rad/s] pre-calculated using the Nelder-Mead simplex method (Leska et al., 2012) for different possible levels of requested power, while accounting for the efficiency of the generator and ICE specific fuel consumption. With the specific fuel consumption, $\psi = f_{\mathrm{ICE}}(P_{\mathrm{ICE}}, \omega_{\mathrm{ICE}})$ [kg/Ws], determined by a 2D-interpolation of the static ICE map, and the density of the fuel, ρ [kg/l], the cumulative ICE fuel consumption B_{ICE} [l] follows from (Kapetanović et al., 2021a; Leska et al., 2017)

$$B_{\mathrm{ICE}}(t) = \int_0^t \frac{P_{\mathrm{ICE}}(\tau) \cdot \psi(\tau)}{\rho} d\tau. \tag{3.12}$$

Pantograph

A pantograph is introduced in PHDEMU configurations for connecting to the grid and charging the ESS during stops. With the power received via pantograph P_{pan} [W], the total electrical energy consumed E_{pan} [Ws] at time instant t results from:

$$E_{\text{pan}}(t) = \int_0^t P_{\text{pan}}(\tau)d\tau. \tag{3.13}$$

Lithium-ion battery

The simplified simulation model of a lithium-ion battery (LB) reflects the equivalent electrical circuit presented in Figure 3.3. It comprises a state-of-charge (SoC)-dependent voltage source, U_{OC} [V], and a constant internal resistance, R_{LB} [Ω], which accounts for ohmic losses and depends on the direction of the battery current I_{LB} [A], i.e., charging or discharging phase.

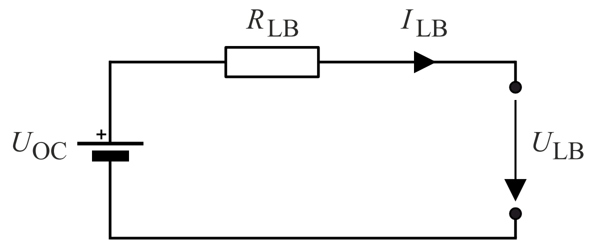

Figure 3.3: Equivalent electrical circuit for the lithium-ion battery-based energy storage system.

Given the power provided from the battery P_{LB} [W], battery SoC $\sigma_{\text{LB}} \in [0,1]$, open circuit voltage U_{OC}, and an internal resistance R_{LB}, the battery current and terminal voltage U_{LB} [V] are defined by (Prohl and Aschemann, 2019):

$$I_{\text{LB}}(t) = \frac{U_{\text{OC}}(\sigma_{\text{LB}}(t)) - \sqrt{U_{\text{OC}}(\sigma_{\text{LB}}(t))^2 - 4 \cdot P_{\text{LB}}(t) \cdot R_{\text{LB}}(I_{\text{LB}}(t))}}{2 \cdot R_{\text{LB}}(I_{\text{LB}}(t))} \tag{3.14}$$

$$U_{\text{LB}}(t) = U_{\text{OC}}(\sigma_{\text{LB}}(t)) - R_{\text{LB}}(I_{\text{LB}}(t)) \cdot I_{\text{LB}}(t). \tag{3.15}$$

With the initial SoC $\sigma_{\text{LB}}(0)$, and nominal battery capacity Q_{LB} [As], the battery SoC at time instant t results from

$$\sigma_{\text{LB}}(t) = \sigma_{\text{LB}}(0) - \frac{1}{Q_{\text{LB}}} \cdot \int_0^t I_{\text{LB}}(\tau)d\tau. \tag{3.16}$$

We limited the maximum (discharging) power $P_{\text{LB}}^{\text{max}}$ [W] and minimum (charging) power $P_{\text{LB}}^{\text{min}}$ [W] by the maximum and minimum current, $I_{\text{LB}}^{\text{max}}$ [A] and $I_{\text{LB}}^{\text{min}}$ [A], respectively, while keeping the limits of the SoC $\sigma \in [\sigma_{\text{LB}}^{\text{min}}, \sigma_{\text{LB}}^{\text{max}}]$, battery voltage $U_{\text{LB}} \in [U_{\text{LB}}^{\text{min}}, U_{\text{LB}}^{\text{max}}]$, and satisfying the limitations defined by the manufacturer, i.e.

$$P_{\mathrm{LB}}^{\max}(t) = \left(U_{\mathrm{OC}}\left(\sigma_{\mathrm{LB}}(t)\right) - R_{\mathrm{LB}}^{\mathrm{dch}} \cdot I_{\mathrm{LB}}^{\max}(t)\right) \cdot I_{\mathrm{LB}}^{\max}(t) \tag{3.17}$$

$$P_{\mathrm{LB}}^{\min}(t) = \left(U_{\mathrm{OC}}\left(\sigma_{\mathrm{LB}}(t)\right) - R_{\mathrm{LB}}^{\mathrm{ch}} \cdot I_{\mathrm{LB}}^{\min}(t)\right) \cdot I_{\mathrm{LB}}^{\min}(t) \tag{3.18}$$

with

$$I_{\mathrm{LB}}^{\max}(t) = \min\left\{\left(\frac{U_{\mathrm{OC}}\left(\sigma_{\mathrm{LB}}(t)\right) - U_{\mathrm{LB}}^{\min}}{R_{\mathrm{LB}}^{\mathrm{dch}}}\right), \left(\frac{\left(\sigma_{\mathrm{LB}}(t) - \sigma_{\mathrm{LB}}^{\min}\right) \cdot Q_{\mathrm{LB}}}{\Delta t}\right), I_{\mathrm{LB}}^{\max,\mathrm{dch}}(t)\right\} \tag{3.19}$$

$$I_{\mathrm{LB}}^{\min}(t) = \max\left\{\left(\frac{U_{\mathrm{OC}}\left(\sigma_{\mathrm{LB}}(t)\right) - U_{\mathrm{LB}}^{\max}}{R_{\mathrm{LB}}^{\mathrm{ch}}}\right), \left(\frac{\left(\sigma_{\mathrm{LB}}(t) - \sigma_{\mathrm{LB}}^{\max}\right) \cdot Q_{\mathrm{LB}}}{\Delta t}\right), I_{\mathrm{LB}}^{\max,\mathrm{ch}}(t)\right\}, \tag{3.20}$$

where Δt [s] is the simulation (integration) time step, and $I_{\mathrm{LB}}^{\max,\mathrm{dch}}$ and $I_{\mathrm{LB}}^{\max,\mathrm{ch}}$ are the maximum discharging and charging current defined by the manufacturer, respectively. Typically, peak (pulse) current values exceeding a defined threshold are allowed for a short amount of time, preventing the damaging of LB. Therefore, we define the last term in (3.19) and (3.20) by:

$$I_{\mathrm{LB}}^{\max,\mathrm{dch}}(t) = \begin{cases} I_{\mathrm{LB}}^{\mathrm{peak},\mathrm{dch}} & \text{if } t_{\mathrm{cnt}}^{\mathrm{dch}}(t) < t_{\mathrm{peak}}^{\mathrm{dch}} \\ I_{\mathrm{LB}}^{\mathrm{cont},\mathrm{dch}} & \text{if } t_{\mathrm{cnt}}^{\mathrm{dch}}(t) \geq t_{\mathrm{peak}}^{\mathrm{dch}} \end{cases} \tag{3.21}$$

$$I_{\mathrm{LB}}^{\max,\mathrm{ch}}(t) = \begin{cases} I_{\mathrm{LB}}^{\mathrm{peak},\mathrm{ch}} & \text{if } t_{\mathrm{cnt}}^{\mathrm{ch}}(t) < t_{\mathrm{peak}}^{\mathrm{ch}} \\ I_{\mathrm{LB}}^{\mathrm{cont},\mathrm{ch}} & \text{if } t_{\mathrm{cnt}}^{\mathrm{ch}}(t) \geq t_{\mathrm{peak}}^{\mathrm{ch}}, \end{cases} \tag{3.22}$$

where $I_{\mathrm{LB}}^{\mathrm{cont},\mathrm{dch}}$ [A] and $I_{\mathrm{LB}}^{\mathrm{cont},\mathrm{ch}}$ [A] are the allowed maximum continuous discharging/charging current values given by the manufacturer; $I_{\mathrm{LB}}^{\mathrm{peak},\mathrm{dch}}$ [A] and $I_{\mathrm{LB}}^{\mathrm{peak},\mathrm{ch}}$ [A] are the peak (pulse) discharging/charging current values provided by the manufacturer, allowed for the limited time period $t_{\mathrm{peak}}^{\mathrm{dch}}$ [s] and $t_{\mathrm{peak}}^{\mathrm{ch}}$ [s]; $t_{\mathrm{cnt}}^{\mathrm{dch}}$ [s] and $t_{\mathrm{cnt}}^{\mathrm{ch}}$ [s] are the introduced discharging/charging counters increased in every time step by the sample time as long as the current value exceeds the allowed maximum continuous values, which are reset in case of a switch between discharging and charging phases. We did not consider the thermal dynamics of the LB, as these characteristics are hardly available, and we assumed that the thermal limitations on the LB were satisfied with the previously defined constraints on the maximum power.

Double-layer capacitor

The DLC can be represented with the equivalent electrical circuit shown in Figure 3.4. It is comprised of an internal resistance R_{DLC} [Ω] in series with a capacitance C_{DLC} [F], both in parallel to a self-discharging resistance R_{dch} [Ω]. Due to the large value of R_{dch} and a duty cycle characterized by short steady-state times, the losses caused by the self-discharging resistance can be neglected (Leska et al., 2017), thus preventing the necessity of additional filtering capacitance for breaking the algebraic loop (Schmid et al., 2017).

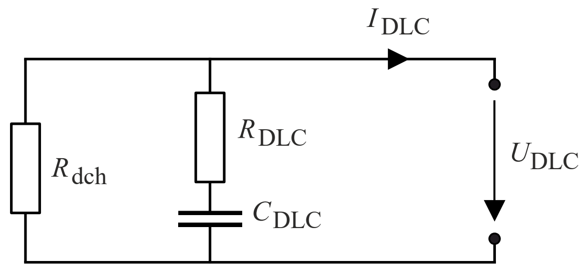

Figure 3.4: Equivalent electrical circuit for the double-layer capacitor-based energy storage system.

Compared to the LB, the DLC has a unique electrostatic energy storage characteristic with its SoC σ_{DLC} being linearly related to its terminal voltage U_{DLC} [V] (Li et al., 2019), which then can be determined by:

$$U_{\text{DLC}}\big(\sigma_{\text{DLC}}(t)\big) = \sigma_{\text{DLC}}(t) \cdot \left(U_{\text{DLC}}^{\max} - U_{\text{DLC}}^{\min}\right) + U_{\text{DLC}}^{\min}, \tag{3.23}$$

where $U_{\text{DLC}}^{\max}$ [V] and $U_{\text{DLC}}^{\min}$ [V] are the maximum and minimum voltage of DLC, respectively. Similar to the LB model, the DLC current I_{DLC} [A] results from:

$$I_{\text{DLC}}(t) = \frac{U_{\text{DLC}}\big(\sigma_{\text{DLC}}(t)\big) - \sqrt{U_{\text{DLC}}\big(\sigma_{\text{DLC}}(t)\big)^2 - 4 \cdot P_{\text{DLC}}(t) \cdot R_{\text{DLC}}}}{2 \cdot R_{\text{DLC}}}. \tag{3.24}$$

With the initial SoC $\sigma_{\text{DLC}}(0)$, and using (3.23) and (3.24) the resulting SoC follows from:

$$\sigma_{\text{DLC}}(t) = \sigma_{\text{DLC}}(0) - \frac{1}{C_{\text{DLC}} \cdot \left(U_{\text{DLC}}^{\max} - U_{\text{DLC}}^{\min}\right)} \cdot \int_0^t I_{\text{DLC}}(\tau) d\tau. \tag{3.25}$$

The maximum and minimum power of the DLC ($P_{\text{DLC}}^{\max}$ [W] and $P_{\text{DLC}}^{\min}$ [W], respectively) are limited by the current of the DLC. Either the maximum (minimum) current is reached in order to keep the voltage constrained $U_{\text{DLC}} \in \left[U_{\text{DLC}}^{\min}, U_{\text{DLC}}^{\max}\right]$, or the maximum (minimum) permitted current for the DLC is reached, i.e.

$$P_{\text{DLC}}^{\max}(t) = U_{\text{DLC}}\big(\sigma_{\text{DLC}}(t)\big) \cdot I_{\text{DLC}}^{\max}(t) \tag{3.26}$$

$$P_{\text{DLC}}^{\min}(t) = U_{\text{DLC}}\big(\sigma_{\text{DLC}}(t)\big) \cdot I_{\text{DLC}}^{\min}(t) \tag{3.27}$$

with

$$I_{\text{DLC}}^{\max}(t) = \min\left\{\frac{\left(U_{\text{DLC}}\big(\sigma_{\text{DLC}}(t)\big) - U_{\text{DLC}}^{\min}\right) \cdot C_{\text{DLC}}}{\Delta t}, I_{\text{DLC}}^{\max,\text{dch}}\right\} \tag{3.28}$$

$$I_{\text{DLC}}^{\min}(t) = \max\left\{\frac{\left(U_{\text{DLC}}\big(\sigma_{\text{DLC}}(t)\big) - U_{\text{DLC}}^{\max}\right) \cdot C_{\text{DLC}}}{\Delta t}, I_{\text{DLC}}^{\max,\text{ch}}\right\}, \tag{3.29}$$

where $I_{\text{DLC}}^{\max,\text{dch}}$ [A] and $I_{\text{DLC}}^{\max,\text{ch}}$ [A] are the maximum discharging and charging current values provided by the manufacturer, respectively.

3.3.2 Energy management strategy

The aim of the EMS implemented in the control unit (see Figure 3.2) is to distribute total demanded power for traction and auxiliaries between different power sources in the system, while satisfying the following requirements, according to the level of priority:

1. Removing emissions and noise in terminal stops by switching off the ICE and supplying auxiliary system from an ESS or electric power grid;
2. Improving fuel economy by maximizing regenerative braking energy and its later use in powering traction and auxiliary systems;
3. Increasing overall ICE-G efficiency by avoiding low load operation;
4. Supporting ICE-G by an ESS during high power demand phases (acceleration).

In order to fulfil these requirements, a real-time control based on a finite state machine (FSM) is proposed for both HDEMU and PHDEMU configurations, which is applicable to any of the two considered ESS technologies, i.e. $\mathrm{ESS} \in \{\mathrm{LB,DLC}\}$. FSM controls can provide effective and implementable management of complex systems, such as hybrid railway vehicles (Han et al., 2017; Yan et al., 2019). They can be easily programmed in microcontrollers (Li et al., 2016), which are then used for dispatching different power sources in the system by controlling their unidirectional or bidirectional converters. The presented EMS thus allows for realistic and achievable estimations of potential fuel savings for the different configurations considered in this chapter.

FSM control for HDEMU vehicle

The FSM control for HDEMU is shown in Figure 3.5. It consists of five states (S1-S5) representing typical operation modes of a propulsion system, and corresponding triggers (T1-T5) covering all theoretically possible transitions between states, irrespective of the degree of hybridization, i.e. relative ICE-G set to ESS power ratio. A line-specific critical track section between the defined critical position, s_{cr} [m], and the position of the terminal stop, s_{ts} [m], was introduced to ensure a maximally charged ESS when reaching the terminal stop. ESS discharge processes were disabled in this section and ESS was being charged from regenerative braking energy and/or ICE-G set. Additionally, a SoC limit $\sigma_{\mathrm{ESS}}^{\mathrm{lim}} \in \left(\sigma_{\mathrm{ESS}}^{\mathrm{min}}, \sigma_{\mathrm{ESS}}^{\mathrm{max}}\right)$ was defined to prevent excessive ESS charge from ICE-G set and the dissipation of braking energy. Both, s_{cr} and $\sigma_{\mathrm{ESS}}^{\mathrm{lim}}$ were calibrated from an estimated duty cycle for a particular railway line and vehicle configuration. To avoid frequent switches between ESS charging and discharging operation modes that might cause its damage and degradation, a hysteresis cycle for the SoC, $\sigma_{\mathrm{ESS}}^{\mathrm{hyst}} \in \left(\sigma_{\mathrm{ESS}}^{\mathrm{min}}, \sigma_{\mathrm{ESS}}^{\mathrm{lim}}\right)$, was implemented by introducing a dynamic binary indicator $Flag(t) \in \{0,1\}$, with $Flag(0) = 0$. An optimal level of electrical power from the ICE-G set $P_{\mathrm{G}}^{\mathrm{opt}}$ [W] corresponds to its optimal efficiency region. Power flows corresponding to the different states and the triggers for the transition to each particular state were defined as follows.

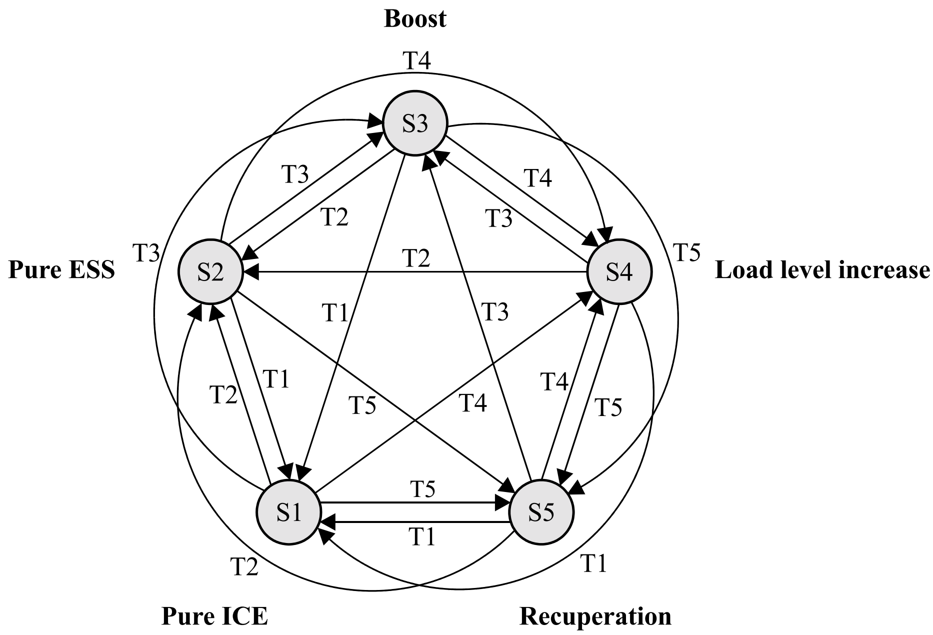

Figure 3.5: Finite state machine control for hybrid propulsion system.

Under the *pure ICE state* (S1), total demanded power $P_{\mathrm{dem}}(t) = P_{\mathrm{EM}}(t) + P_{\mathrm{aux}}(t)$ is provided by ICE-G set, and the ESS converter is switched off. Depending on the requested power level and ESS characteristics (maximum power), this state is active if ESS reaches its SoC limiting values and/or the vehicle is located within the critical track section, i.e.

$$\begin{aligned}\mathrm{T1}\colon &\left(P_{\mathrm{dem}}(t) \geq P_{\mathrm{G}}^{\mathrm{opt}} \wedge \left(\sigma_{\mathrm{ESS}}(t) = \sigma_{\mathrm{ESS}}^{\min} \vee s_{\mathrm{cr}} \leq s(t) < s_{\mathrm{ts}}\right)\right) \\ &\vee \left(0 \leq P_{\mathrm{dem}}(t) < P_{\mathrm{G}}^{\mathrm{opt}} \wedge P_{\mathrm{dem}}(t) \leq P_{\mathrm{ESS}}^{\max}(t) \wedge \sigma_{\mathrm{ESS}}(t) \geq \sigma_{\mathrm{ESS}}^{\mathrm{lim}} \wedge s_{\mathrm{cr}} \leq s(t) < s_{\mathrm{ts}}\right) \\ &\vee \left(P_{\mathrm{dem}}(t) < P_{\mathrm{G}}^{\mathrm{opt}} \wedge P_{\mathrm{dem}}(t) > P_{\mathrm{ESS}}^{\max}(t) \wedge \sigma_{\mathrm{ESS}}(t) \geq \sigma_{\mathrm{ESS}}^{\mathrm{lim}}\right)\end{aligned} \tag{3.30}$$

$$\mathrm{S1}\colon \begin{cases} P_{\mathrm{ESS}}(t) = 0 \\ P_{\mathrm{G}}(t) = P_{\mathrm{dem}}(t) \\ Flag(t) = Flag(t - \Delta t). \end{cases} \tag{3.31}$$

In the *pure ESS state* (S2), the ESS provides the total requested power, with ICE running with no load on idling speed, or switched off if the terminal stop is reached. This state is enabled outside of the critical track section and its activation depends on the SoC value and the implemented hysteresis, defined by

$$\begin{aligned}\mathrm{T2}\colon &\left(0 \leq P_{\mathrm{dem}}(t) \leq P_{\mathrm{ESS}}^{\max}(t)\right) \wedge \left(s(t) < s_{\mathrm{cr}} \vee s(t) = s_{\mathrm{ts}}\right) \\ &\wedge \left(Flag(t - \Delta t) = 0 \vee \left(Flag(t - \Delta t) = 1 \wedge \sigma_{\mathrm{ESS}}(t) \geq \sigma_{\mathrm{ESS}}^{\min} + \sigma_{\mathrm{ESS}}^{\mathrm{hyst}}\right)\right)\end{aligned} \tag{3.32}$$

$$\mathrm{S2}\colon \begin{cases} P_{\mathrm{ESS}}(t) = P_{\mathrm{dem}}(t) \\ P_{\mathrm{G}}(t) = 0 \\ Flag(t) = 0. \end{cases} \tag{3.33}$$

Similar as in the previous state, the *boost state* (S3) is enabled outside of the critical track section, and for particular SoC values and implemented hysteresis cycle. In this state, ESS provides support for the ICE-G set by providing a portion of high requested power, i.e.

$$\begin{aligned}\text{T3}: &P_{\text{dem}}(t) > P_{\text{G}}^{\text{opt}} \wedge P_{\text{dem}}(t) > P_{\text{ESS}}^{\max}(t) \wedge \sigma_{\text{ESS}}(t) > \sigma_{\text{ESS}}^{\min} \wedge (s(t) < s_{\text{cr}} \vee s(t) = s_{\text{ts}}) \\ &\wedge \left(Flag(t-\Delta t) = 0 \vee \left(Flag(t-\Delta t) = 1 \wedge \sigma_{\text{ESS}}(t) \geq \sigma_{\text{ESS}}^{\min} + \sigma_{\text{ESS}}^{\text{hyst}}\right)\right)\end{aligned} \tag{3.34}$$

$$\text{S3}: \begin{cases} P_{\text{ESS}}(t) = \min\left\{P_{\text{ESS}}^{\max}(t), P_{\text{aux}}(t), \left(P_{\text{dem}}(t) - P_{\text{ICE}}^{\text{opt}}\right)\right\} \\ P_{\text{G}}(t) = P_{\text{dem}}(t) - P_{\text{ESS}}(t) \\ Flag(t) = 0. \end{cases} \tag{3.35}$$

Under the *load level increase state* (S4), featured with low power demand, the ICE-G set provides the excess power which is used for recharging the ESS, defined by

$$\begin{aligned}\text{T4}: &\left(P_{\text{dem}}(t) < P_{\text{G}}^{\text{opt}} \wedge P_{\text{dem}}(t) > P_{\text{ESS}}^{\max}(t) \wedge \sigma_{\text{ESS}}(t) < \sigma_{\text{ESS}}^{\text{lim}}\right) \\ &\vee \Big(\left(0 \leq P_{\text{dem}}(t) < P_{\text{G}}^{\text{opt}} \wedge P_{\text{dem}}(t) \leq P_{\text{ESS}}^{\max}(t)\right. \\ &\wedge \left(\left(\sigma_{\text{ESS}}(t) < \sigma_{\text{ESS}}^{\text{lim}} \wedge s_{\text{cr}} \leq s(t) < s_{\text{ts}}\right) \vee \left(Flag(t-\Delta t) = 1 \wedge \sigma_{\text{ESS}}(t) < \sigma_{\text{ESS}}^{\min} + \sigma_{\text{ESS}}^{\text{hyst}}\right)\right)\Big)\end{aligned} \tag{3.36}$$

$$\text{S4}: \begin{cases} P_{\text{ESS}}(t) = \max\left\{P_{\text{ESS}}^{\min}(t), \left(P_{\text{dem}}(t) - P_{\text{G}}^{\text{opt}}\right)\right\} \\ P_{\text{G}}(t) = P_{\text{dem}}(t) - P_{\text{ESS}}(t) \\ Flag(t) = 1. \end{cases} \tag{3.37}$$

The *recuperation state* (S5) is active during braking, with the negative power values at the DC link, which is used for recharging the ESS. The power distributed to the ESS is limited with its maximum charging power, with the excess power dissipated at the braking rheostat, and ICE running with no load at idling speed, i.e.

$$\text{T5}: P_{\text{dem}}(t) < 0 \tag{3.38}$$

$$\text{S5}: \begin{cases} P_{\text{ESS}}(t) = \max\left\{P_{\text{ESS}}^{\min}(t), P_{\text{dem}}(t)\right\} \\ P_{\text{G}}(t) = 0 \\ Flag(t) = Flag(t-\Delta t). \end{cases} \tag{3.39}$$

FSM control for PHDEMU vehicle

The FSM control for PHDEMU is shown in Figure 3.6. The previously defined FSM control is extended with the additional state (S6) for the operational mode in stations equipped with charging facilities, together with the corresponding transition conditions.

The EMS is defined by introducing a binary indicator $b_{\text{el}}(s(t)) \in \{0,1\}$, to represent the track electrification status. Operational characteristics related to the critical track section were removed due to the existence of external power sources in terminal stops, resulting in the following transition triggers:

$$\begin{aligned}\text{T1}: b_{\text{el}}(s(t)) = 0 \wedge \Big(&\left(P_{\text{dem}}(t) \geq P_{\text{G}}^{\text{opt}} \wedge \sigma_{\text{ESS}}(t) = \sigma_{\text{ESS}}^{\min}\right) \\ &\vee \left(P_{\text{dem}}(t) < P_{\text{G}}^{\text{opt}} \wedge P_{\text{dem}}(t) > P_{\text{ESS}}^{\max}(t) \wedge \sigma_{\text{ESS}}(t) \geq \sigma_{\text{ESS}}^{\text{lim}}\right)\Big)\end{aligned} \tag{3.40}$$

$$\begin{aligned}\text{T2}: &b_{\text{el}}(s(t)) = 0 \wedge 0 \leq P_{\text{dem}}(t) \leq P_{\text{ESS}}^{\max}(t) \\ &\wedge \left(Flag(t-\Delta t) = 0 \vee \left(Flag(t-\Delta t) = 1 \wedge \sigma_{\text{ESS}}(t) \geq \sigma_{\text{ESS}}^{\min} + \sigma_{\text{ESS}}^{\text{hyst}}\right)\right)\end{aligned} \tag{3.41}$$

$$\begin{aligned}\mathrm{T3}\colon & b_{\mathrm{el}}\big(s(t)\big) = 0 \wedge P_{\mathrm{dem}}(t) > P_{\mathrm{G}}^{\mathrm{opt}} \wedge P_{\mathrm{dem}}(t) > P_{\mathrm{ESS}}^{\max}(t) \wedge \sigma_{\mathrm{ESS}}(t) > \sigma_{\mathrm{ESS}}^{\min} \\ & \wedge \Big(Flag(t-\Delta t) = 0 \vee \big(Flag(t-\Delta t) = 1 \wedge \sigma_{\mathrm{ESS}}(t) \geq \sigma_{\mathrm{ESS}}^{\min} + \sigma_{\mathrm{ESS}}^{\mathrm{hyst}}\big)\Big)\end{aligned} \tag{3.42}$$

$$\begin{aligned}\mathrm{T4}\colon & b_{\mathrm{el}}\big(s(t)\big) = 0 \wedge \Big(\big(P_{\mathrm{dem}}(t) < P_{\mathrm{G}}^{\mathrm{opt}} \wedge P_{\mathrm{dem}}(t) > P_{\mathrm{ESS}}^{\max}(t) \wedge \sigma_{\mathrm{ESS}}(t) < \sigma_{\mathrm{ESS}}^{\mathrm{lim}}\big) \\ & \vee \big(0 \leq P_{\mathrm{dem}}(t) < P_{\mathrm{G}}^{\mathrm{opt}} \wedge P_{\mathrm{dem}}(t) \leq P_{\mathrm{ESS}}^{\max}(t) \wedge Flag(t-\Delta t) = 1 \wedge \sigma_{\mathrm{ESS}}(t) < \sigma_{\mathrm{ESS}}^{\min} + \sigma_{\mathrm{ESS}}^{\mathrm{hyst}}\big)\Big)\end{aligned} \tag{3.43}$$

$$\mathrm{T5}\colon P_{\mathrm{dem}}(t) < 0 \tag{3.44}$$

$$\mathrm{T6}\colon b_{\mathrm{el}}\big(s(t)\big) = 1. \tag{3.45}$$

The power distribution for the states S1-S5 remained the same as in the previous case. Under the newly added *pure electric state* (S6), the ICE is switched off in case of a stop duration longer than 5 minutes, or switched to idle operation with no load otherwise. Depending on the maximum power from the grid $P_{\mathrm{pan}}^{\max}$ [W] and the maximum charging power of ESS, electric power from the grid is used for supplying the auxiliaries and recharging the ESS, i.e.

$$S6\colon \begin{cases} P_{\mathrm{ESS}}(t) = \max\{P_{\mathrm{ESS}}^{\min}(t), \big(P_{\mathrm{dem}}(t) - P_{\mathrm{pan}}^{\max}\big)\} \\ P_{\mathrm{G}}(t) = 0 \\ P_{\mathrm{pan}}(t) = P_{\mathrm{dem}}(t) - P_{\mathrm{ESS}}(t) \\ Flag(t) = Flag(t-\Delta t). \end{cases} \tag{3.46}$$

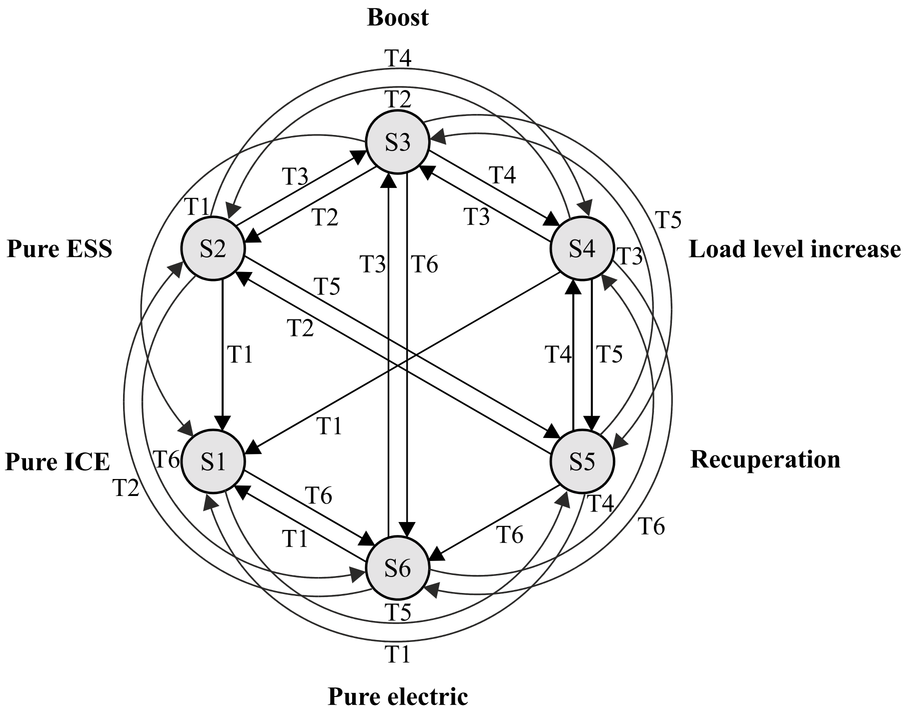

Figure 3.6: Finite state machine control for plug-in hybrid propulsion system.

3.4 Case study of the Dutch Northern regional railway lines

The simulation methodology proposed in the previous section was applied in estimating the energy consumption for each of the considered alternative propulsion systems, followed by the calculation of related GHG emissions and energy costs. The following sub-sections provide the description of the selected benchmark DEMU and railway line, followed by a detailed comparative analysis of the different scenarios.

3.4.1 Benchmark railway vehicle

A two-coach DEMU of the type Gelenktriebwagen (GTW) 2/6 from the Swiss manufacturer Stadler, currently employed on the network by the RU Arriva Nederland, was selected as the benchmark vehicle for this study. The power-module of GTW 2/6 is located between the two passenger coaches and contains two identical propulsion systems, shown in Figure 3.1a. Simulation parameters for a standard GTW 2/6 DEMU are given in Table 3.1. The EM, G, and ICE characteristic maps for the GTW 2/6 were reconstructed using data provided by Paukert (2011), with the available efficiency map of EM linearly scaled in order to comply with the maximum requested power for traction and auxiliaries and the maximum available power from ICE-G set at the DC link (Figure 3.7a), and an ICE-specific fuel consumption map (Figure 3.7b) reconstructed using similarly sized ICE and Willans lines technique (Pourabdollah et al., 2013).

Table 3.1: Standard GTW 2/6 DEMU simulation parameters.

Parameter	Unit	Value	Description
m_{tare}	t	70.4	Tare weight [1]
λ	-	0.05	Rotating mass factor [2]
m_{pax}	t	7	Total passengers weight [3]
r_0	N	1001	Davis equation coefficient (constant term) [2]
r_1	N/(km/h)	22.3	Davis equation coefficient (linear term) [2]
r_2	N/(km/h)^2	0.1	Davis equation coefficient (quadratic term) [2]
d_{w}	m	0.86	Powered wheel diameter [4]
i_{ag}	-	1.7218	Axle gear ratio [5]
η_{ag}	-	0.97	Axle gear efficiency [6]
v_{max}	km/h	140	Maximum velocity [4]
a_{max}	m/s^2	1.05	Maximum acceleration [2]
a_{min}	m/s^2	-1	Maximum deceleration [2]
$F_{\text{w}}^{\text{max}}$	kN	80	Maximum (starting) tractive effort at the wheel [4]
$P_{\text{w}}^{\text{max}}$	kW	600	Maximum power at the wheel [4]
$P_{\text{EM}}^{\text{rated}}$	kW	2×400	EM rated power [1]
$P_{\text{ICE}}^{\text{rated}}$	kW	2×390	ICE rated power [1]
$P_{\text{aux,const}}$	kW	50	Constant auxiliaries power [3]
p_{cool}	-	0.01	Cooling power coefficient [3]
ρ	g/l	825	Fuel density (diesel) [6]

Source/Note: [1] Giro Batalla and Feenstra (2012); [2] Personal communication with Arriva; [3] Assumed values; [4] Stadler (2005); [5] Derived from the ratio between the maximum rotational speed of the GTW's EM given by Giro Batalla and Feenstra (2012) and the maximum rotational speed of the wheel corresponding to the maximum vehicle speed; [6] Adopted from Pröhl (2017b).

Commercially available LB or DLC modules with proven railway applications were considered for DEMU hybridization in order to obtain as realistic estimations as possible. A Toshiba SCiB™ module, type 1–23, contains 24 lithium-ion cells, arranged in 2 parallel branches with 12 cells in series. The cells are based on a lithium nickel manganese cobalt oxide (NMC) chemistry with a lithium titanium oxide (LTO) anode, which offers a good compromise between energy density, power density, and achievable lifetime (Takami et al., 2013; Toshiba, 2021). Due to the unavailability of the open-circuit voltage characteristic as a function of SoC, the function from SAFT and UNEW (2017) was adopted and scaled according to voltage limits for the SCiB™ module (Figure 3.7c). A BMOD0063 module from the manufacturer Maxwell Technologies was selected as the DLC technology. It contains 48 cells, with 6 parallel series of 8 cells each, and it is especially suited for heavy-duty transport applications, such as trains and buses (Maxwell, 2021). Detailed characteristics of the selected LB and DLC modules are given in Table 3.2.

The total required number of modules was derived from the energy requirement of supplying the auxiliaries in terminal stops according to the extended layover time in terminal stops of 30 min, resulting in 28 LB modules and 179 DLC modules. Train weight was adjusted to account for the added ESSs. An additional weight of 1000 kg was assumed for the converters and other equipment and 150 kg for the pantograph. Since the additional mass affects both acceleration and braking performance, it was accounted for in the velocity profile calculation and simulations for each of the alternative vehicle configurations.

Table 3.2: Parameters of the selected lithium-ion battery and double-layer capacitor modules.

Parameter	**Unit**	**Value**	**Description**
LB module [1]			
Q_{LB}	Ah	45	Nominal capacity
$I_{\mathrm{LB}}^{\mathrm{cont,ch}}/I_{\mathrm{LB}}^{\mathrm{cont,dch}}$	A	-160/160	Minimum/maximum continuous current
$I_{\mathrm{LB}}^{\mathrm{peak,ch}}/I_{\mathrm{LB}}^{\mathrm{peak,dch}}$	A	-350/350	Minimum/maximum pulse current
$t_{\mathrm{peak}}^{\mathrm{dch}}/t_{\mathrm{peak}}^{\mathrm{dch}}$	s	10	Allowed time for pulse current
$U_{\mathrm{LB}}^{\mathrm{min}}/U_{\mathrm{LB}}^{\mathrm{max}}$	V	18/32.4	Minimum/maximum voltage
$R_{\mathrm{LB}}^{\mathrm{ch}}/R_{\mathrm{LB}}^{\mathrm{dch}}$	Ω	0.006	Internal resistance charge/discharge
$\sigma_{\mathrm{LB}}^{\mathrm{min}}/\sigma_{\mathrm{LB}}^{\mathrm{max}}$	%	10/90	Minimum/maximum SoC [2]
$E_{\mathrm{LB}}^{\mathrm{max}}$	kWh	1.24	Energy content
$E_{\mathrm{LB}}^{\mathrm{use}}$	kWh	0.922	Usable energy content [3]
m_{LB}	kg	15	Weight
DLC module [4]			
C_{DLC}	F	63	Rated capacitance
$I_{\mathrm{DLC}}^{\mathrm{max,ch}}/I_{\mathrm{DLC}}^{\mathrm{max,dch}}$	A	-240/240	Minimum/maximum continuous current
$U_{\mathrm{DLC}}^{\mathrm{min}}/U_{\mathrm{DLC}}^{\mathrm{max}}$	V	12.5/125	Minimum/maximum voltage
R_{DLC}	Ω	0.018	Internal resistance
E_{DLC}	kWh	0.14	Energy content
m_{DLC}	kg	61	Weight

Source/Note: [1] Extracted values from specifications and data sheets from Toshiba (2021) unless otherwise indicated; [2] Adopted values for simulation purposes; [3] Based on allowed SoC range; [4] Extracted values from specifications and data sheets from Maxwell (2021).

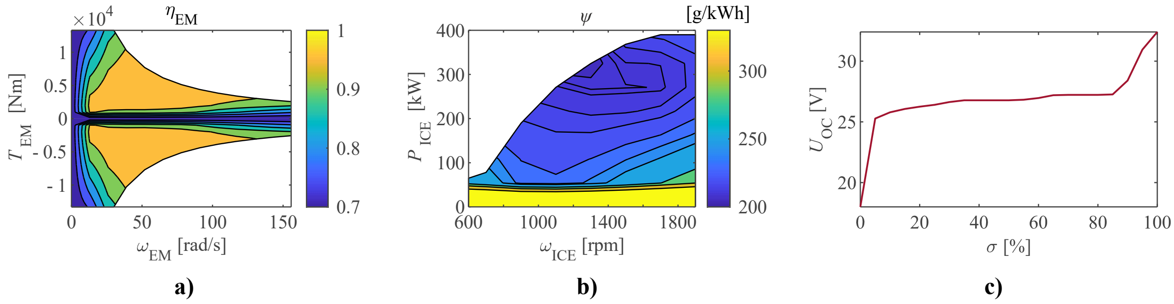

Figure 3.7: (a) Efficiency map of an electric motor; (b) Specific fuel consumption of an internal consumption engine; (c) Lithium-ion battery module open circuit voltage as a function of state-of-charge.

3.4.2 Benchmark railway line selection

The main railway line on the network between the cities Leeuwarden and Groningen was selected for the train simulations (Figure 3.8). Compared to the rest of the network, the provision of the two different services on this line (stopping and express) allowed for an impact assessment of the stopping frequency on the total energy consumption. Two different scenarios were considered for the plug-in hybrid concepts regarding the charging facilities location:

1. Charging facilities located only in terminal stations with long layover times;
2. Charging facilities located in terminal stations and an additional fast charging facility located in Buitenpost, a common short stop for the two services.

The vehicle round trip, based on the actual periodic timetable and rolling stock circulation plan (Table 3.3), was analysed to account for the difference in line resistances and maximum speed limits for the two opposite directions. A dwell time of 30s was presumed for all intermediate stops. For the scenarios including the additional charging location in Buitenpost, this time was extended to 2 min at this particular stop.

Table 3.3: Distance between stops and departure times for the vehicle round trip on the line Leeuwarden (Lw) - Groningen (Gn).

Station	**Distance (km)**	**Departure time (hh:mm)**			
		Stopping service		**Express service**	
		Lw → Gn	**Gn → Lw**	**Lw → Gn**	**Gn → Lw**
Leeuwarden	0	hh : 51	hh+2 : 40 (arrival)	hh : 44	hh+2 : 16 (arrival)
Leeuwarden C.	3.34	hh : 54	hh+2 : 35	-	-
Hurdegaryp	9.83	hh+1 : 01	hh+2 : 30	-	-
Feanwalden	14.00	hh+1 : 05	hh+2 : 25	-	-
De Westereen	17.24	hh+1 : 08	hh+2 : 20	-	-
Buitenpost	24.74	hh+1 : 16	hh+2 : 15	hh+1 : 00	hh+2 : 00
Grijskerk	35.71	hh+1 : 23	hh+2 : 06	-	-
Zuidhorn	42.35	hh+1 : 30	hh+2 : 01	-	-
Groningen	54.05	hh+1 : 39 (arrival)	hh+1 : 51	hh+1 : 18 (arrival)	hh+1 : 42

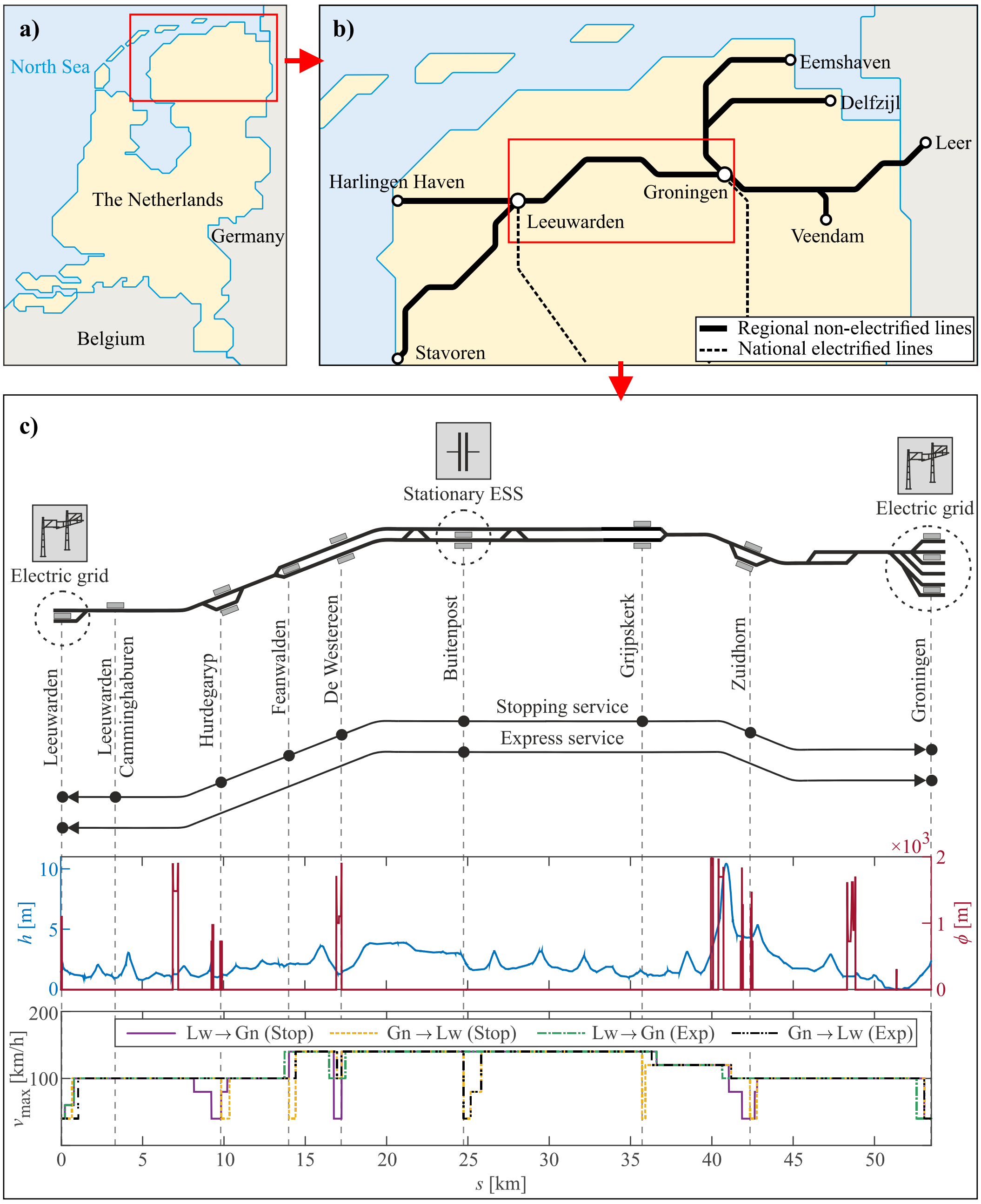

Figure 3.8: (a) Position and (b) schematic representation of the Northern lines in the Netherlands; and (c) track layout for the railway line Leeuwarden-Groningen with indicated locations for charging facilities, stops for stopping and express service, track geometry, and maximum allowed speed.

3.4.3 Comparative assessment results

Energy consumption for each of the alternative scenarios is estimated using the MATLAB®/Simulink© simulation model described in Section 3.3, with the adopted fixed time step $\Delta t = 0.1$s, the ode3 (Bogacki-Shampine) solver used for numerical integration, and implemented hysteresis cycles of $\sigma_{\mathrm{LB}}^{\mathrm{hyst}} = 5\%$ and $\sigma_{\mathrm{DLC}}^{\mathrm{hyst}} = 20\%$ for LB and DLC, respectively. Due to its causal nature, the proposed FSM control cannot guarantee the SoC sustenance. Therefore, each HDEMU and PHDEMU configuration is simulated twice, with the initial SoC set to $\sigma_{\mathrm{ESS}} = 50\%$, and then replaced with the final value obtained in the first simulation run. This allowed for a fair comparison between different configurations. The maximum power from the grid $P_{\mathrm{pan}}^{\mathrm{max}}$ was determined from the national railway traction grid characteristics, namely 1500V DC voltage and current limitation of 2000A (ProRail, 2020). To account for a difference in weight due to additional components, optimized vehicle speed profiles that comply with the timetable, vehicle, and track parameters were pre-calculated using a bisection algorithm (Leska et al., 2013) for each vehicle configuration. For the sake of brevity, detailed simulation results are given in Appendix A (Figures A.1-A.3), with the main results summarized in Table 3.4.

The obtained energy consumption was used afterwards in quantifying the total GHG emissions and energy costs, using a consumption-based approach (Kirschstein and Meisel, 2015), by multiplying the amount of fuel or electricity consumed with the corresponding emission factor and unit cost, respectively. A Well-to-Wheel approach (Hoffrichter et al., 2012) was adopted in deriving the emission factors to allow for a credible comparison between GHG emissions of different energy carriers, namely diesel fuel and electricity in our case, and to comply with the international norms (CEN, 2012). Emission factors and energy prices representative for the Netherlands and the year 2020 were used to reflect the analysed case study and to account for the most recent trends. An emission factor for diesel with 2.6% biofuel content of 3.23 kgCO_2e/l and for grey electricity reflecting a national power mix of 0.556 kgCO_2e/kWh (CO2emissiefactoren, 2021) were assumed. Since all national trains on the electrified lines run on the electricity produced from wind power since 2017 (EcoWatch, 2017), an alternative scenario considered the utilization of green electricity coming from the same source, with the emission factor equal to zero. For the calculation of energy costs, an average diesel price of 1.237 EUR/l (CBS, 2021) and a railway traction electricity price of 0.024137 EUR/kWh (ProRail, 2020) were adopted.

The estimated GHG emissions (Table 3.4) showed significant benefits from hybridization, primarily as a consequence of reduced diesel consumption. Both total GHG emissions for each alternative scenario and estimated relative emissions reduction compared to the standard DEMU are shown in Figure 3.9. Emission reductions compared to a standard DEMU vehicle range between 9.43% and 56.92%, depending on the type of service and vehicle/charging configuration. The results indicated the stopping pattern, ESS technology selection, and the charging facilities location had a considerable influence. In general, a positive effect from further conversion of a particular hybrid vehicle to its plug-in hybrid counterpart was observed. The DLC ESS demonstrated better performance compared to the LB ESS, both in hybrid and plug-in hybrid alternatives, mainly due to its higher power density and the ability to recuperate total available regenerative braking energy. While the additional charging location at the intermediate stop resulted in further emission reductions for the DLC-based ESS, it showed negative effects for the LB ESS. Finally, utilization of green instead of grey electricity contributed to a further emission reduction of ~6-8% and ~10-16% for PHDEMUs with LB and DLC-based ESS, respectively.

Similar to the GHG emissions, results on energy costs (Table 3.4 and Figure 3.10) indicated higher benefits from DLC-based configurations, with cost reductions of 31.87–55.46% compared to 9.69–27.97% savings for vehicles with LB ESS, and with plug-in hybrid vehicles showing better performance than their hybrid counterparts for each scenario. The same negative effect from an additional charging facility in the intermediate stop for PHDEMU with LB ESS was observed. In general, energy cost savings resulted predominantly from the reduction in diesel consumption and a high diesel-to-electricity price ratio.

Table 3.4: Energy consumption, GHG emissions and energy costs for standard, hybrid and plug-in hybrid vehicle configurations.

Service	**Configuration**	**ESS**	**Charging option** [1]	**Energy consumption**		**GHG emissions** [2] **[kgCO₂e]**	**Energy costs [EUR]**
				Fuel [l]	**Electricity [kWh]**		
Stopping	DEMU	-	-	106.31	-	343.38	131.51
	HDEMU	LB	-	92.01	-	297.19	113.82
		DLC	-	72.43	-	233.95	89.60
	PHDEMU	LB	TSs	75.77	41.01	267.54 (244.74)	94.72
			TSs+IS	75.84	47.44	271.34 (244.96)	94.96
		DLC	TSs	50.38	63.43	197.99 (162.73)	63.85
			TSs+IS	46.04	100.55	204.62 (148.71)	59.38
Express	DEMU	-	-	140.40	-	453.49	173.67
	HDEMU	LB	-	126.80	-	409.56	156.85
		DLC	-	87.11	-	281.37	107.76
	PHDEMU	LB	TSs	106.61	49.61	371.93 (344.35)	133.07
			TSs+IS	118.58	49.84	410.72 (383.01)	147.89
		DLC	TSs	61.98	83.48	246.61 (200.20)	78.68
			TSs+IS	60.49	104.81	253.66 (195.38)	77.36

Note: [1] TS – Terminal stop, IS – Intermediate stop; [2] The values in brackets are calculated for the scenarios that consider green electricity for ESS charging.

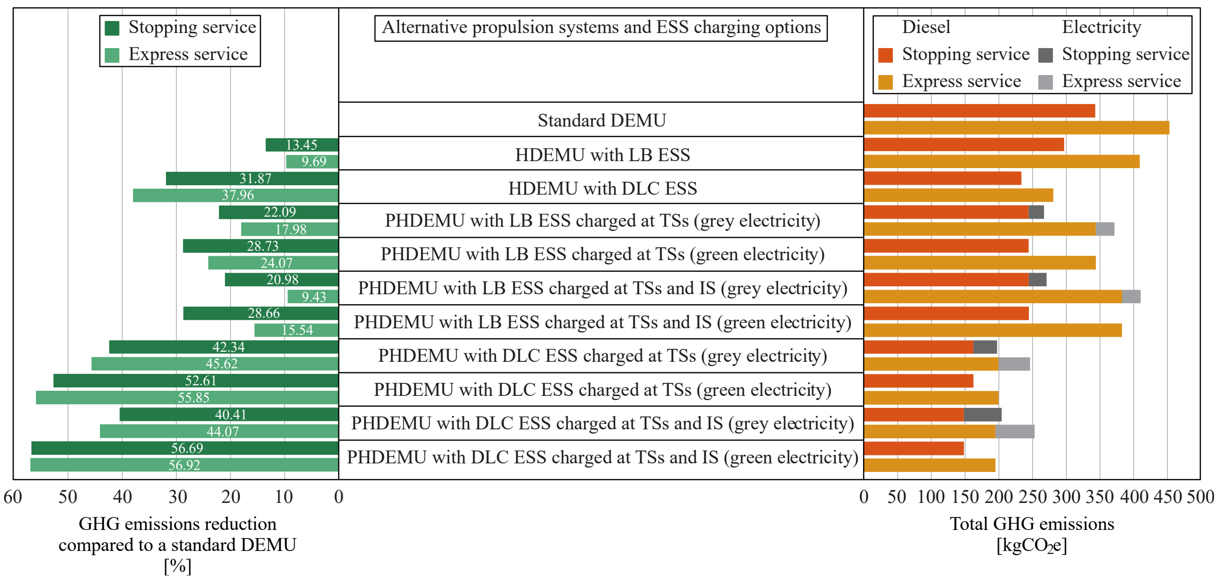

Figure 3.9: Total GHG emissions depending on the propulsion system, charging location, and electricity production configurations; and estimated potential reduction compared to a standard diesel-electric multiple unit.

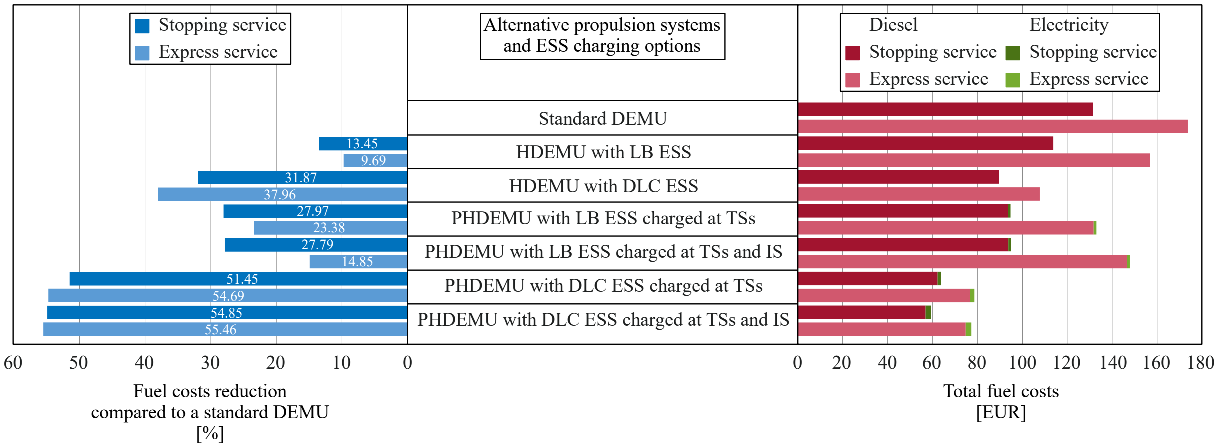

Figure 3.10: Estimated fuel costs for different propulsion system and charging location configurations; and potential reduction compared to a standard diesel-electric multiple unit.

3.5 Discussion

The results of the comparative analysis indicate promising potential benefits from the hybridization of a DEMU. A further conversion to its plug-in hybrid counterpart allowed for significantly greater energy savings and the reduction in GHG emissions and costs in all scenarios. The results also provided insight into numerous interrelated factors influencing the vehicle performance, which are further elaborated in this section.

The comparison of estimated energy consumption for the stopping and express service showed considerable impact of the stopping frequency and applied timetable. While frequent stops in the first case offered a higher amount of braking energy, they also required more energy for the high-power acceleration phases. Even though these energy levels were much lower for the considered express service with only one intermediate stop, the obtained total energy demand was higher in all analysed scenarios. This was mainly due to the short running times defined by the timetable, requiring vehicles running at the maximum speed and preventing them from using the benefits of coasting operation (see speed diagrams in Appendix A). Energy-efficient timetabling approaches (Scheepmaker et al., 2017) could potentially contribute to revising the existing timetable and reducing the overall energy demand for train operation.

The selection of ESS technology plays an important role in defining future powertrain solutions, as identified in the results for HDEMU and PHDEMU vehicles. The DLC-based ESS demonstrated significantly better performance compared to the LB, mainly as a consequence of the differences in their physical characteristics. Due to the low power density, the LB ESS could not cover high power fluctuations, both during traction and braking phases, causing a lack of support to the ICE and significant dissipation of braking energy. On the other hand, DLC allowed for recuperation of total regenerative braking energy and ICE operation in the most-efficient region. However, due to its low energy density, and considering the main criteria in sizing the ESS, it comes at the price of a high total weight, reaching almost 11 tonnes in this case. This raises the question of the feasibility of such a solution, requiring further investigation into the physical constraints (Hoffrichter et al., 2016), including the available volumetric space on the vehicle and maximum axle load as defined by EN 15528 (CEN, 2015), which, in our case, was 20 tonnes corresponding to the track category C for the Northern lines (ProRail, 2020). Combining the individual benefits of LBs and DLCs into a hybrid ESS (Peng et al., 2018) could be an effective approach in overcoming the limitation of a single-technology ESS. However, this raises significant challenges in terms of the optimal sizing, the complexity of energy management, and the integration of such a solution into the system.

The identified impact of infrastructure and vehicle characteristics, applied timetable, and technology selection imply the need for a comprehensive line-by-line and vehicle-by-vehicle analysis in the case of heterogeneous rolling stock fleets operating on multiple lines. Additionally, external factors and their variability, such as ambient temperature and number of passengers, should be considered. Variations in the number of passengers during the day, and the ambient temperature depending on the season, could potentially have a significant influence on the auxiliaries power load and the overall energy consumption.

Emissions from train operation not only arise due to the fuel or electricity consumption, but also result from a number of direct and indirect sources, including vehicle production and infrastructure construction (Esters and Marinov, 2014). Although international standards on emissions calculation and declaration (CEN, 2012) stipulate consideration of only Well-to-Wheel emissions, the emissions resulting from the production and disposal/replacement of additional system components, including ESSs and stationary charging facilities in our case, should be identified. For instance, recent studies estimated GHG emissions from battery production for electric cars to be in the span of 150–200 kgCO_2e per kWh of battery capacity (Romare and Dahllöf, 2017), contributing 31–46% to the total GHG impact from vehicle production (Ellingsen et al., 2016). Even though these relative contributions would be significantly lower for railway vehicles due to their much higher utilization and longer life cycle, further investigation in terms of detailed Life Cycle Assessment (LCA) (Jones et al., 2017) is needed in order to assess the overall environmental impact of a particular solution.

Similar to the GHG emissions, next to the fuel/energy-related costs, other investment costs will occur when rolling out a new propulsion system concept. These monetary costs are related to a particular technology and its lifetime, and include initial, maintenance, and replacement costs. Considering the obtained fuel savings for different solutions, high vehicle utilization, and foreseen operation for the next 15 years, it can be assumed that the investment costs would be compensated with the energy savings in a relatively short period of time. However, a comprehensive Life Cycle Costs (LCC) analysis (García Márquez et al., 2008) would allow for identification of overall costs and benefits in this investment decision process.

3.6 Conclusions

This chapter presented a comparative assessment of standard, hybrid, and plug-in hybrid propulsion system alternatives for regional diesel-electric multiple unit vehicles. The analysis encompassed the development of a detailed simulation model, which considered different energy storage technologies, namely lithium-ion battery and double-layer capacitor, and the real-time energy management strategies based on finite state machines. Focusing on the regional railway services in the Netherlands, we investigated the hypothetical conversion of a conventional benchmark vehicle found on the network, and provided a simulation-based assessment in terms of overall energy consumption, related greenhouse gas emissions, and monetary costs. With the energy storage systems sized to ensure emission-free and noise-free train operation in terminal stations, the results indicated higher potential benefits from implementing the double-layer capacitor instead of the lithium-ion battery, with an identified need for further investigation on its practical implementation due to the high associated weight. Compared to the standard vehicle, these benefits are reflected in emissions and cost reduction that exceeded 55% for certain scenarios. Positive effects from further conversion of a hybrid to a plug-in hybrid system were observed, with significant impacts of the stopping patterns (type of service), timetable, and the charging facilities configuration.

The presented research is part of a larger project aiming to identify optimal solutions for reducing the total Well-to-Wheel and life cycle emissions on the regional non-electrified network in the Northern Netherlands by analysing different technical, operational, and policy measures. In this context, extensions of the present work will consider remaining rolling stock and lines, as well as testing and validation of the proposed method using field test data. Further extensions to the current research will include investigation of hydrogen-powered propulsion systems and upstream processes related to the production of alternative fuels, such as biofuels and hydrogen, through a detailed Well-to-Wheel analysis. The overall impact of vehicle production or refurbishment will be evaluated through LCA and LCC approaches.

Chapter 4

Analysis of hydrogen-powered propulsion system alternatives for diesel-electric regional trains

Apart from minor updates, this chapter has been published as:

Kapetanović, M., Núñez, A., van Oort, N., Goverde, R.M.P. (2022). Analysis of hydrogen-powered propulsion system alternatives for diesel-electric regional trains. *Journal of Rail Transport Planning & Management*, 23, 100338.

4.1 Introduction

Regional non-electrified railway networks require the identification of alternative traction options to meet strict regulations and emission reduction targets imposed on the railway sector (Beatrice et al., 2013; UIC and CER, 2012). Hydrogen-based vehicle technologies are a potentially suitable alternative to typically employed diesel-electric multiple units (DEMUs) in regional passenger transport (Klebsch et al., 2020). Fuel cells (FCs) are a dominant technology for onboard power generation in hydrogen-related railway applications. FCs offer numerous advantages compared to internal combustion engines (ICEs), summoned primarily in high efficiency, quiet and emission-free operations at the point of use, with water vapour and heat as the only products (Sun et al., 2021). However, their main drawback is the slow dynamic response, which requires vehicle hybridization with an energy storage system (ESS) and accompanying energy management and control strategy (EMCS), which would cover power fluctuations and allow for the recuperation of braking energy (Siddiqui and Dincer, 2019).

Following rapid technology developments and availability of FC technologies, several fuel cell multiple units (FCMUs) have been introduced in the market by some of the major railway vehicle manufacturers, e.g., Coradia iLint from Alstom (Alstom, 2020), Mireo Plus H from Siemens (FuelCellWorks, 2020), and Stadler's Zillertalbahn narrow-gauge FCMU (IRJ, 2019). Furthermore, considering the service life of railway vehicles, typically spanning over 30 years, it could be advantageous to convert existing vehicles to their hydrogen-powered counterparts instead of replacing them with new commercially available alternatives. A prominent recent example for the regional train is UK's train HydroFLEX, in operation since 2019 (Calvert et al., 2021; Gallucci, 2019).

Although MAN produces hydrogen ICEs for busses (Knorr et al., 1998; MAN, 2020), no commercial railway vehicles are powered by a hydrogen ICE. However, another major ICE manufacturer Deutz recently announced the introduction of hydrogen ICEs in 2024, aimed at railway applications (Deutz, 2021). Hydrogen combustion in ICE does not produce greenhouse gas (GHG) emissions; however, local pollutants such as nitrogen oxides (NOx) are emitted due to high-temperature hydrogen combustion with air. Their main advantage is that they are based on well-established technology, as they mostly represent modifications of existing ICEs running on compressed natural gas (Akal et al., 2020), and have a service life three times longer than the FCs (Marin et al., 2010). Based on the previous experience with other technologies that found their place in railway applications, as a result of spillovers from other modes of transport such as busses and passenger cars, together with the relatively low price compared to the emerging technology as FCs, hydrogen ICEs could be considered as a carbon-neutral bridging solution towards totally-emission free railway transport.

The transition from conventional DEMUs to alternative systems is a complex dynamic decision-making process that involves various stakeholders and multiple aspects to be considered. It requires in-depth analyses that include identification of available technology, design, modelling, and assessment of potential alternatives, with respect to the particular case-related constraints imposed by infrastructure, technical and operational characteristics (e.g., track geometry, speed, and axle load limitations, implemented onboard power control of different power sources, maintaining existing timetables, etc.) (Kapetanović et al., 2021a). This chapter aims to support the design of hydrogen-powered propulsion systems by converting conventional DEMUs, and to present the comparative model-based assessment of different powertrain configurations in terms of overall energy consumption and produced GHG emissions. This research uses a case of the regional railway network in the Northern Netherlands and passenger services provided by Arriva, the largest regional railway undertaking in the Netherlands. The results of this research can serve as an essential input for decision-makers in the planning of future rolling stock investments and trains operations.

The remainder of the chapter is organized as follows. A literature review and chapter contributions are given in Section 4.2. Section 4.3 presents a detailed vehicle simulation model with implemented real-time power-distribution control for identified alternative propulsion systems. The propulsion systems design and a comparative assessment are provided in Section 4.4. We conclude this chapter with a final discussion and future research directions in Section 4.5.

4.2 Literature review

Considering the main aim of present chapter, this section reviews the scientific literature on hydrogen-powered railway vehicles, focusing primarily on a regional passengers' transport context and the four main interrelated aspects: design, modelling, control, and assessment of different propulsion systems.

As noted in the Introduction, FCs are the predominant technology in hydrogen-based propulsion system designs for railway vehicles, which is reflected in extensive literature covering different aspects of their development and deployment. Considering regional passengers transport, various studies analysed the available commercial FCMUs and the feasibility of their deployment on regional railway networks (Klebsch et al., 2020, 2019; Mueller et al., 2020), using mainly general vehicle characteristics published by the manufacturers (e.g., range, maximum power, etc.), and compared them with the general infrastructure-related requirements for the railway network in question. Although these studies provide rough estimations of FCMUs feasibility and potential benefits, a comprehensive investigation on the available FCMUs would require detailed simulation models coupled with infrastructure and vehicle-specific data, which are often difficult to obtain for the new vehicles. Additionally, field tests and trials (RailTech, 2020) require significant effort and would be a logical next step after completing detailed studies.

With regard to vehicles conversion/retrofit to their hydrogen-powered counterpart, selecting suitable technology is a crucial step in the vehicle powertrain design process. There are several types of FCs, differing in start-up time, efficiency, operating temperature, materials used for their manufacture, costs, etc., with detailed overview and comparison of different FC technologies provided by Bagotsky et al. (2015), Siddiqui and Dincer (2019), and Sun et al. (2021). In general, the polymer electrolyte membrane (or proton-exchange membrane) fuel cell (PEMFC) is the most commonly utilized FC technology, due to numerous advantages over other FC types, reflected in relatively short start-up and shutdown time, and low operating temperature (80 °C). Their main drawbacks are high cost due to the use of expensive metal catalysts, and the platinum catalyst poisoning effect (Carrette et al., 2001; Sopian and Wan Daud, 2006; Wang et al., 2011). The alkaline fuel cell (AFC) is another low-temperature FC technology with lower costs than the PEMFC; however, their sensitivity to CO_2 molecules leads to considerable deterioration of its performance (Kordesch et al., 2000). Phosphoric acid fuel cells (PAFCs) are featured with lower efficiency and higher operating temperature than previous FCs (200 °C), leading to a reduced platinum catalyst poisoning effect and thus longer lifetime (US Department of Energy, 2021). They are mainly employed in stationary power and heat generation systems (Chen et al., 2016). Solid oxide fuel cells (SOFCs) are high-temperature FCs (800-1000 °C), which allows for high power output (up to 2 MW) with high efficiency of 60%, but also causes low performance at lower temperatures, requires long start-up time, higher costs of materials, and sophisticated design and the assembly (Sun et al., 2021). Molten carbonate fuel cells (MCFCs) are another high-temperature FCs (600-650 °C), offering high output power (up to 3 MW), utilized mainly in stationary power generation systems (US Department of Energy, 2021). Considering the applicability to the railway sector, low-temperature PEMFC fits best to non-permanent demand cycles, and applications like light rail vehicles, commuter and regional trains, shunt/switch and underground mine locomotives, while high-temperature SOFC has been seen as a promising technology for freight or heavy haul locomotives, given their long operation time and steady duty cycles (Barbosa, 2019; Sun et al., 2021).

In addition to FCs as the main power source, various ESS technologies have emerged in the transport sector over the last decades, with batteries, double-layer capacitors (DLCs), and flywheels being the most represented solutions depending on the particular application and requirements (Vazquez et al., 2010). Due to their high energy-to-weight ratio, no memory effect, low self-discharge rates, rapid technology development, and commercial availability, lithium-ion batteries (LBs) are the most represented battery and ESS technology in railway applications (Meinert et al., 2015a). DLCs provide high power density and low energy density, making them suitable for peak power shaving and maximizing recuperation of braking energy. They are often coupled with LBs in a hybrid energy storage system (HESS), that combines individual benefits offered by the two technologies (Dittus et al., 2011; G. Zhang et al., 2019). Flywheels offer fast charging and discharging rates; however, they are featured with various safety issues (González-Gil et al., 2013), high weight and self-discharging rates. Thus, they are not considered in this study. Detailed characteristics of different ESS technologies are provided in reviews by Bagotsky et al. (2015) and Ghaviha et al. (2017).

Comprehensive and reliable mathematical models are required to assess the behaviour of system components and to obtain plausible results in terms of energy consumption and efficiency. Models of electrochemical power sources, such as FCs, batteries, and DLCs, can be generally divided into electrochemical models and equivalent electrical circuit models (Zhang et al., 2017). Different dimensions of electrochemical models use electrochemical equations in modelling and describing the distributed electrochemistry reactions in the electrodes and electrolytes. Piraino and Fragiacomo (2020) provided a comprehensive model that incorporates each powertrain component, such as energy sources, power electronics and drivetrain. Although these physics-based models can provide the information on the full dynamic behaviour of the system, they require detailed information and numerous parameters on the physical system, which are often difficult to obtain, and employ a set of partial differential equations, which make them too complex for fast simulation purposes (Ghaviha et al., 2019). On the other hand, different orders of equivalent electrical circuit models use different electrical components such as capacitors and resistors to obtain a response similar to the behaviour of the physical system (see Krastev and Tricoli, 2022). They provide high enough accuracy for power management applications, while avoiding unnecessary complexities of the electrochemical models (Fotouhi et al., 2016).

Since the energy management and control strategy (EMCS) is the main driver of the fuel economy for hybrid vehicles, most of the railway literature focuses on this particular aspect, i.e., its development for a particular predefined FCMU powertrain configuration. EMCSs can be generally classified into optimization-based and rule-based strategies, where former are further divided according to the optimization horizon in global optimization, instantaneous optimization, and real-time optimization (Xu et al., 2015a). Dynamic programming is a powerful method for solving global optimization problems (Kapetanović et al., 2021a). Ogawa et al. (2007) proposed an optimal EMCS based on dynamic programming for a FC/DLC railway vehicle, further used in deriving an optimal required capacity for a DLC. The main drawbacks hindering real-time application of dynamic programming are that it requires perfect information on future driving conditions, which is hard to achieve in reality, the long calculation time, and the inability to deal with variables that include counters (see Section 4.3.2) due to its nature of propagation backward in time. Therefore, these algorithms are often used as a benchmark in developing other causal controls. Tao et al. (2021) combined dynamic programming and state machine control in obtaining optimal power distribution between the FC and DLC for a tram vehicle, demonstrating significant benefits in terms of fuel economy, efficiency and durability. Regarding regional railway vehicles, Peng et al. (2020b) used dynamic programming in deriving a scalable, causal, adaptive EMCS for an FC/LB powertrain, achieving only 0.01-0.09% increase in fuel consumption compared to the optimal case.

The equivalent consumption minimization and Pontryagin's minimum principle strategies are suitable for instantaneous optimization problems. Torreglosa et al. (2011a) presented an equivalent consumption minimization strategy for an FC/battery hybrid tram, with the results showing significant benefits reflected in fuel savings compared to other causal controls, while at the same time maintaining the battery state-of-charge (SoC). A similar approach is proposed by W. Zhang et al. (2017) in a case of FC/LB/DLC tram. This method is also used as the basis in the development of dynamic power factor control for FC/LB locomotive (Hong et al., 2018). H. Zhang et al. (2019) proposed a firefly algorithm to optimize the parameters in equivalent consumption minimization strategy for an FC/LB/DLC tram. Liu et al. (2020) employed Pontryagin's minimum principle in defining the optimal EMCS and the optimal braking energy recovery strategy for an FC/DLC tram. Peng et al. (2020a) used the same method as a benchmark in deriving a causal real-time EMCS for a regional railway vehicle. In general, with the future driving conditions properly estimated, the previous two methods can be applied to real-time optimization problems. Some papers propose the use of meta-heuristics for power flows control. Li et al. (2018) employed a genetic algorithm in the case of an FC/LB/DLC low-floor tramcar, with an obtained fuel savings of 15% compared to the baseline rule-based control.

Rule-based strategies are based on event-triggered Boolean or fuzzy rules used in online (real-time) control applications, where rules can be designed according to powertrain characteristics or extracted from optimized algorithms. Garcia et al. (2010) proposed an adaptive rule-based control for a tram by considering eight states in distributing requested power between the FC and a nickel-metal hydride cell battery. A similar control based on a state machine for a hybrid FC/LB tram is proposed by Han et al. (2016). A two-mode multisource coordination EMCS based on self-convergence droop control for a FC/LB/DLC tram is presented by Han et al. (2018). A power-voltage equilibrium strategy based on droop control for an FC/LB/DLC hybrid was proposed by G. Zhang et al. (2019). Peng et al. (2018) used fuzzy logic in developing a sub-optimal control for an FC/LB/DLC tram by incorporating operational uncertainties, performance degradation and SoC balancing. A fuzzy logic controller for an FC/battery tram based on LB SoC, and FC and traction load was proposed by Torreglosa et al. (2011b). Although rule-based strategies typically cannot offer a proof of optimality, low computation cost and storage memory requirement make them especially suitable for the development of causal real-time controllers, offering at the same time promising benefits in terms of energy consumption reduction (Zhang et al., 2020).

Regarding the powertrain design, several studies reported on a conversion analysis of existing railway vehicles to their hydrogen counterparts. For instance, Washing and Pulugurtha (2016) presented a simulation-based analysis of energy use and emissions for a pure FC and a hybrid FC/LB alternative powertrain for a Siemens light rail vehicle operating in North Carolina. Analyses that employ similar simplified vehicle models are reported for locomotives by Miller et al. (2007) and Peng et al. (2014). Concerning the design of hydrogen-based regional vehicles, a conceptual design of FCMUs, both non-hybrid and hybrid with an LB, is presented by Hoffrichter et al. (2016). The authors investigate the feasibility of converting a standard DEMU from Stadler, by incorporating constraints related to the available weight and volume of the components, as well as the range requirements for the FCMUs. In terms of selection and sizing of powertrain components, the vehicle design is based on a simulated round trip and corresponding energy demand of a standard DEMU, with no detailed models that would capture the dynamics of electrochemical power sources (FC and LB), nor active EMCS implemented. A similar study for the British class 150 regional train is presented by Din and Hillmansen (2018). In contrast to the previous conceptual designs that focus more on the practical implementability of particular technology, while neglecting detailed powertrain and ECMS modelling, some papers employed optimization algorithms that consider the relationship between the EMCS in place and the optimal size of the powertrain components based on selected main criteria and constraints, and focusing mainly on locomotive applications. Such method based on the Krill herd optimization algorithm is presented by Guo et al. (2020) for a hybrid FC/LB locomotive. A Particle Swarm Optimization algorithm combined with several rule-based power controls for a hybrid FC/LB locomotive was presented by Sarma and Ganguly (2020; 2018).

From the literature review it can be noted that an extensive research has been reported on different aspects of hydrogen propulsion systems deployment in the railway sector, focusing mainly on ECMS development for a particular predefined powertrain configuration. However, several limitations and scientific lacks were identified among the prior research. Existing studies focus exclusively on FCs technology, with no reported detailed analyses on hydrogen ICEs, and with only a scarce number of comparative analyses between alternative powertrain configurations and ESS technologies. As a rare example, Hoffrichter et al. (2012) derived the Well-to-Wheel energy efficiencies and CO_2 emissions for electric, diesel and hydrogen (both pure ICE and pure FC) traction for railway vehicles, using the low and high heating values of the enthalpy of oxidation of the fuel. The theoretical analysis is based on a desk study using typical one-lumped efficiency values found in the literature for individual powertrain components. Furthermore, prior design methods rely mainly on simplified simulation models, neglecting the behaviour of individual powertrain components and the influence of the ECMS. It would be advantageous to integrate these aspects together with other significant drivers and physical/safety limitations in a comprehensive powertrain layout design. A recent analysis is provided by Fragiacomo and Piraino (2021) for an innovative vehicle-to-grid FC-based tram application. Regarding the type of vehicle analysed (market segment), urban railway vehicles (trams) are a predominant category in the literature, followed by locomotives, with a limited number of papers focusing on regional multiple unit railway vehicles. Although the main principles in powertrain design apply to different applications, freight locomotives and trams feature different technical characteristics, stopping patterns, and lower operational speeds, resulting in different energy and power demand, duty cycles, and related design parameters. For instance, Fragiacomo and Piraino (2019) analysed the use of hydrogen-hybrid powertrains including FCs, LBs and/or DLCs in four different contexts in Southern Italian railways, including detailed powertrain modelling, EMCS, and validation using real-world measurements, with the results indicating a significant impact of case related characteristics on both powertrain design and performance. One of the main challenges in realizing a comprehensive comparative design and reliable performance assessment is addressing the issues related to detailed data availability and high models complexity.

Considering the previously discussed main aspects, identified knowledge gaps, and the context of the present analysis, the following are defined as the contributions of this chapter:

1. A method to support the design of alternative hydrogen-powered propulsion systems for a regional railway vehicle, including both internal combustion engine and fuel cell system as the prime mover, and various energy storage systems based on lithium-ion battery and/or double-layer capacitor technologies.
2. A backward-looking quasi-static simulation model equipped with an achievable real-time energy management and control strategy applicable to all considered powertrain configurations. It allows for realistic systems performance evaluation, while requiring only main technology parameters typically published by manufacturers and avoiding issues related to the detailed data unavailability and/or confidentiality;
3. A feasibility study and comparative analysis of fuel economy and greenhouse gas emissions of alternative systems, applied in a case of a two-coach diesel-electric multiple unit employed on a regional railway network in the Netherlands. The results will provide the railway undertaking and decision-makers with an essential input for future investments planning.

4.3 Hydrogen-powered propulsion systems modelling and control

This section presents the approach used in modelling and control of hydrogen-based propulsion systems, which served as a basis for the overall design analysis. First, alternative propulsion system configurations for a conventional diesel-electric vehicle are introduced, followed by a detailed description of the simulation model that includes the dynamics of individual main system components, and a control strategy used in distributing the power flows between different power sources in the system.

4.3.1 Propulsion system configurations

The propulsion system of a standard DEMU (Figure 4.1a) is based on a series topology consisting of an internal combustion engine (ICE) and two electric machines (Spiryagin et al., 2014). ICE directly connected to an AC electric generator forms an engine-generator unit (EGU), which is further connected via the rectifier and inverter to an AC electric motor located on the driveshaft. The axle gear transmits the power from the electric motor shaft to the wheels with a constant gear ratio. Electric motor enables electro-dynamic braking and its operation as a generator, allowing for recuperation of braking energy. In standard DEMU vehicles, this energy is completely dissipated at the braking resistor (rheostat), connected to the DC link via a DC/DC converter. We assume total electrification of auxiliary systems connected to the existing DC link via a DC/AC inverter. Compared to other systems such as diesel-mechanical or diesel-hydraulic, the electric transmission system, in this case, allows for fully independent rotational speed of the ICE from the wheel and its operation in optimal region for a particular power demand level.

Conversion of standard DEMU to its hydrogen-powered counterpart can be achieved by replacing the prime mover of the system architecture, i.e., diesel ICE with hydrogen ICE (Figures 4.1a-d), or the EGU and corresponding rectifier with FC stack and unidirectional DC/DC converter (Figures 4.1e-g), together with hybridization by adding appropriately sized ESS that would enable recuperation of braking energy and its later use in powering traction and auxiliary systems. Considering non-steady duty cycles of regional passenger trains, rapid development, commercial availability and foreseen decrease in the price of PEMFCs, we limit the analysis in this chapter to this particular technology. Three different ESS configurations are considered in this study – LB (Figures 4.1b,e), DLC (Figures 4.1c,f), and HESS that combines both LB and DLC technologies (Figures 4.1d,g). Active control of each ESS technology is achieved via a corresponding bidirectional DC/DC converter. Due to the slow dynamic response of FCs, a non-hybrid configuration powered solely by FCs is not considered, as it would require a significant increase of the FC system size according to the peak power demand and high dissipation of hydrogen energy. This results in seven powertrain configurations shown in Figures 4.1a-g.

Compared to diesel fuel, hydrogen is featured with high flammability, and high complexity requirements to store, transport and handle (Dincer and Zamfirescu, 2016). In addition to the previous adjustments in the powertrain structure, converting diesel vehicles to hydrogen-powered counterparts requires replacing conventional fuel tank systems used for standard liquid fuels with an adequate onboard hydrogen storage system. Several technologies are available for onboard hydrogen storage, including high-pressure cylinders (typically 350 or 700 bar), metal hydride storage systems, or systems for liquefied hydrogen through cryo-compression at low temperatures (Madovi et al., 2021).

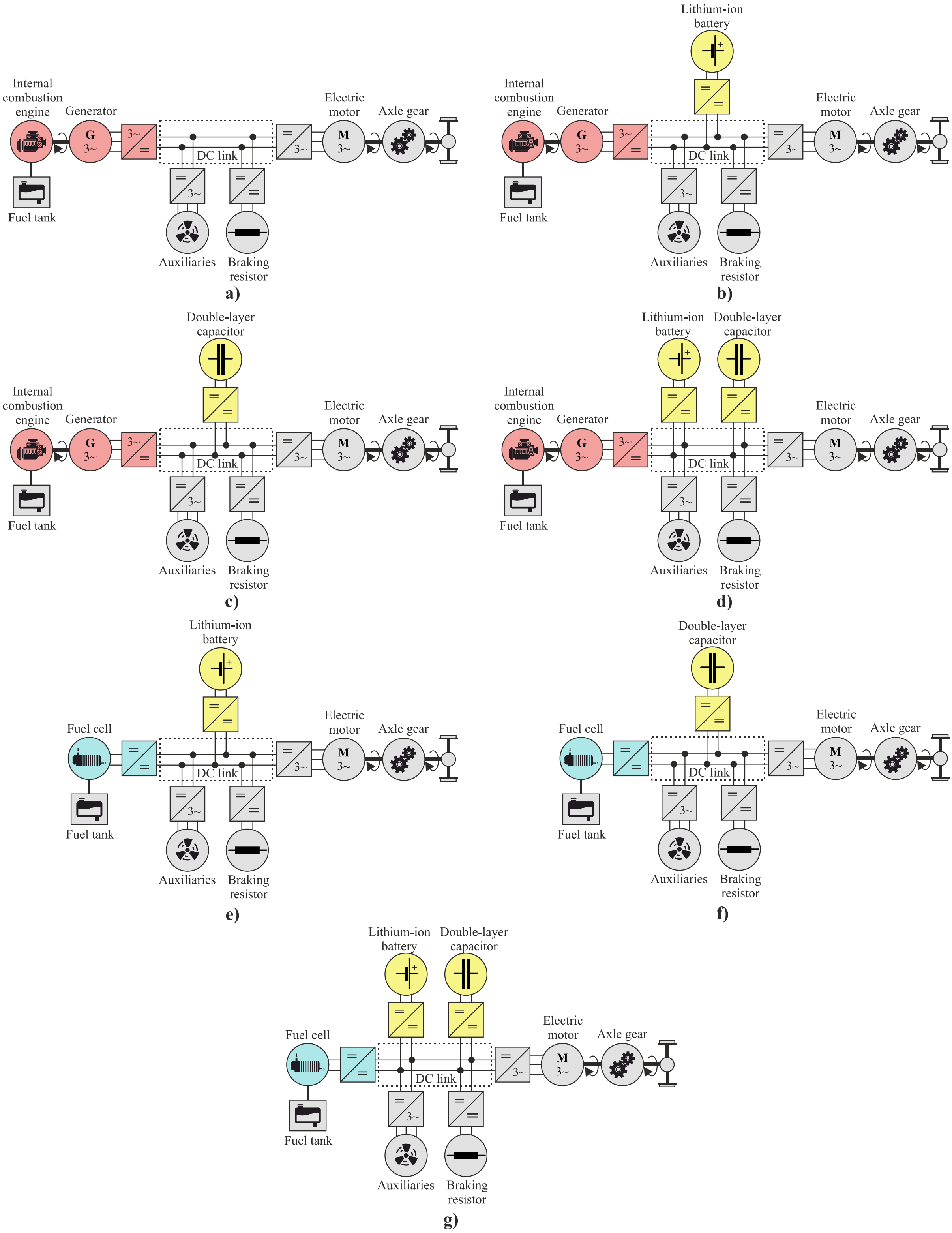

Figure 4.1: Schematic representation of alternative propulsion system configurations: (a) standard (non-hybrid); internal combustion engine-based hybrids with (b) lithium-ion battery, (c) double-layer capacitor, and (d) hybrid energy storage system; fuel cell-based hybrids with (e) lithium-ion battery, (f) double-layer capacitor, and (g) hybrid energy storage system.

4.3.2 Simulation model

The dynamics of alternative system architectures are modelled using a backward-looking quasi-static simulation approach (Kapetanović et al., 2021a; Leska et al., 2017; Pröhl, 2017b). The simulation model is developed with the MATLAB/Simulink tool and OPEUS Simulink toolbox (Pröhl, 2017a). We extend the Simulink toolbox and the model presented by Kapetanović et al. (2021b) with the FC module and corresponding EMCSs for each alternative system. The simulation model structure (Figure 4.2) reflects the physical system architectures from Figure 4.1, with the individual blocks representing components of the model for the hybrid system. Simulation of different configurations is achieved by disconnecting components not included in the respective system. Corresponding to the backward simulation approach, the inputs of the simulation model are the vehicle velocity and track geometry profiles. The energy-optimized velocity profile is pre-calculated using the bisection algorithm (Leska et al., 2013), that considers optimal switching points between the acceleration, cruising, coasting and braking phases, while complying with the scheduled running times, track speed limitations, vehicle weight and maximum tractive/braking effort characteristics. A constant passenger load is assumed in determining the vehicle weight. The main output is given by a cumulative fuel consumption during the trip. The arrows indicate the numerical evaluation order of the model components, opposed to the direction of the physical power flow. The power converters in regional railway vehicles are featured with high efficiency, typically above 98% (Giro Batalla and Feenstra, 2012) compared to the main components such as traction motors with efficiencies as low as 70% during low load/low speed operation (Pröhl, 2017a). Thus, following the approach of W. Zhang et al. (2017), only energy losses related to the main powertrain components are considered, with efficiencies of power converters assumed approximately 100%. Nevertheless, converters are considered for the power flows control according to the proposed EMCS (see Section 4.3.3). A braking resistor is used only for assessing the balance of power flows in the system. The description of the model components is provided in the remainder of this section.

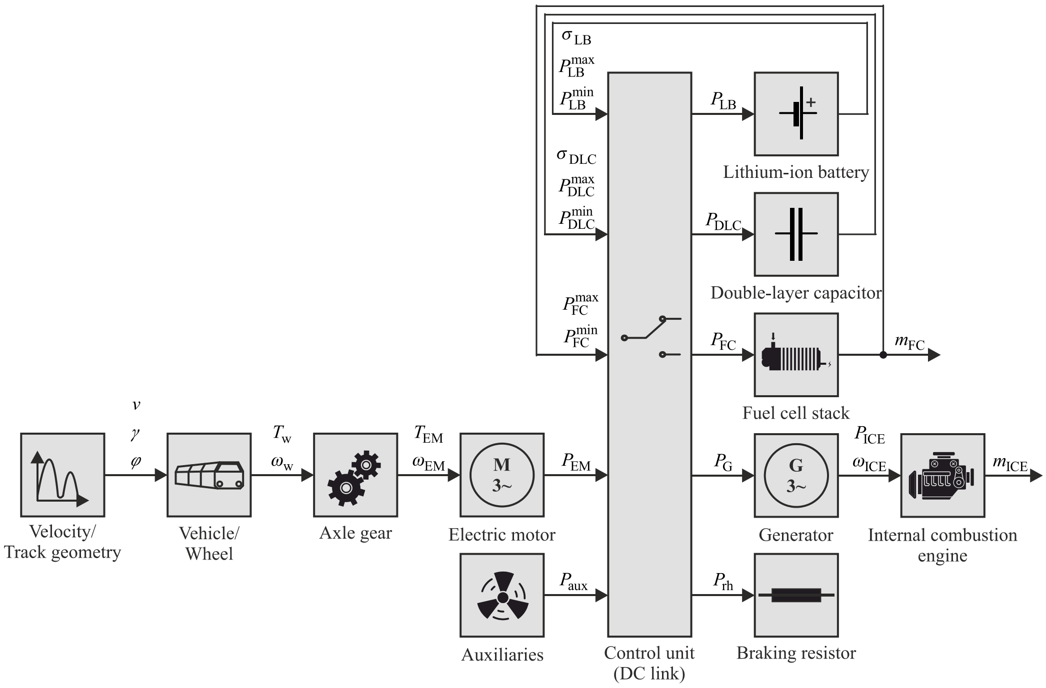

Figure 4.2: Structure of the backward-looking simulation model for the alternative hydrogen-based propulsion systems.

Traction load

Traction load represents the electrical power required by the electric traction motors at the DC link. According to the backward-looking approach, it is fully described by the velocity and track geometry profiles, and the power losses due to inefficiencies of the components along the traction chain, namely of the gearbox and of the electric motor. With the given velocity and track geometry profiles as input signals, longitudinal vehicle dynamics are described by the tractive or braking effort at the wheel F_{w} [N], expressed as

$$F_{\mathrm{w}}\big(v(t)\big) = m_{\mathrm{v}} \cdot a(t) + R_{\mathrm{v}}\big(v(t)\big) + R_{\mathrm{g}}\Big(\gamma\big(s(t)\big)\Big) + R_{\mathrm{c}}\Big(\phi\big(s(t)\big)\Big) \tag{4.1}$$

with

$$R_{\mathrm{v}}\big(v(t)\big) = r_0 + r_1 \cdot v(t) + r_2 \cdot v(t)^2 \tag{4.2}$$

$$R_{\mathrm{g}}\Big(\gamma\big(s(t)\big)\Big) = m_{\mathrm{v}} \cdot g \cdot \sin\Big(\gamma\big(s(t)\big)\Big) \tag{4.3}$$

$$R_{\mathrm{c}}\Big(\phi\big(s(t)\big)\Big) = \begin{cases} m_{\mathrm{v}} \cdot \dfrac{4.91}{\phi\big(s(t)\big) - 30} & \text{if } \phi\big(s(t)\big) < 300 \text{ m} \\ m_{\mathrm{v}} \cdot \dfrac{6.3}{\phi\big(s(t)\big) - 55} & \text{if } \phi\big(s(t)\big) \geq 300 \text{ m,} \end{cases} \tag{4.4}$$

where t [s] is the time; v [m/s] is the vehicle velocity; $s = \int_0^t v(\tau)d\tau$ [m] is the distance travelled; $a = dv/dt$ [m/s^2] is the acceleration; m_{v} [kg] is the total mass of the vehicle which takes into account the rotary inertia of the powertrain and the passengers weight, i.e. $m_{\mathrm{v}} = (1 + \lambda) \cdot m_{\mathrm{tare}} + m_{\mathrm{pax}}$, with λ denoting the dimensionless rotating mass factor, m_{tare} [kg] the vehicle tare weight, and m_{pax} [kg] the total weight of passengers; the vehicle resistances R_{v} [N] include roll resistance and air resistance, modelled as a quadratic function of the vehicle velocity using the Davis equation (Davis, 1926), with vehicle-specific coefficients r_0 [N], r_1 [N/(m/s)] and r_2 $\left[\mathrm{N/(m/s)^2}\right]$; R_{g} [N] is the grade resistance, with $g = 9.81$ [m/s^2] representing the gravitational acceleration, and γ [rad] the angle of the slope (Brünger and Dahlhaus, 2014); curve resistance R_{c} [N] is calculated using Roeckl's formula (Huerlimann and Nash, 2003), with ϕ [m] denoting the curve radius. With the given tractive/braking effort at the wheel, traction load is computed according to the numerical evaluation order of the model components shown in Figure 4.2, using the following equations (Leska et al., 2017; Pröhl, 2017a):

$$T_{\mathrm{w}}(t) = F_{\mathrm{w}}\big(v(t)\big) \cdot \frac{d_{\mathrm{w}}}{2} \tag{4.5}$$

$$\omega_{\mathrm{w}}(t) = 2 \cdot \frac{v(t)}{d_{\mathrm{w}}} \tag{4.6}$$

$$T_{\mathrm{EM}}(t) = \begin{cases} \dfrac{T_{\mathrm{w}}(t)}{i_{\mathrm{ag}} \cdot \eta_{\mathrm{ag}}} & \text{if } T_{\mathrm{w}}(t) \geq 0 \\ \dfrac{T_{\mathrm{w}}(t) \cdot \eta_{\mathrm{ag}}}{i_{\mathrm{ag}}} & \text{if } T_{\mathrm{w}}(t) < 0 \end{cases} \tag{4.7}$$

$$\omega_{\mathrm{EM}}(t) = \omega_{\mathrm{w}}(t) \cdot i_{\mathrm{ag}} \tag{4.8}$$

$$P_{\mathrm{EM}}(t) = \begin{cases} \dfrac{T_{\mathrm{EM}}(t) \cdot \omega_{\mathrm{EM}}(t)}{\eta_{\mathrm{EM}}\big(T_{\mathrm{EM}}(t), \omega_{\mathrm{EM}}(t)\big)} & \text{if } T_{\mathrm{EM}}(t) \geq 0 \\ T_{\mathrm{EM}}(t) \cdot \omega_{\mathrm{EM}}(t) \cdot \eta_{\mathrm{EM}}\big(T_{\mathrm{EM}}(t), \omega_{\mathrm{EM}}(t)\big) & \text{if } T_{\mathrm{EM}}(t) < 0, \end{cases} \tag{4.9}$$

where d_{w} [m] denotes the diameter of the powered wheel; T_{w} [Nm] is the torque at the wheel; ω_{w} [rad/s] is the rotational speed of the wheel; i_{ag} is the constant gear ratio; η_{ag} is the efficiency of the gearbox, assumed to be constant; T_{EM} [Nm] is the torque at the mechanical input of the axle gear provided by the electric motor; ω_{EM} [rad/s] is the rotational speed of the electric motor; $\eta_{\mathrm{EM}} = f_{\mathrm{EM}}(T_{\mathrm{EM}}, \omega_{\mathrm{EM}})$ is the efficiency of electric motor, determined by a linear 2D-interpolation in the efficiency map; and P_{EM} [W] is the resulting electric power of the traction motor.

Auxiliary load

In addition to the power required for traction, passenger trains are equipped with auxiliary consumers linked to the propulsion system operation or passengers' comfort. Auxiliary onboard systems include compressors, cooling equipment, heating, ventilation and air conditioning (HVAC), lighting, etc. We model the total auxiliaries power P_{aux} [W] as the sum of the constant term $P_{\mathrm{aux,const}}$ [W], representing constant consumers such as lighting and HVAC systems, and the variable term which accounts for the cooling power (Kapetanović et al., 2021b), i.e.

$$P_{\mathrm{aux}}(t) = P_{\mathrm{aux,const}} + p_{\mathrm{cool}} \cdot |P_{\mathrm{EM}}(t)|, \tag{4.10}$$

where coefficient p_{cool} represents the proportion of the total traction power required for cooling the main traction components.

Engine-generator unit

With the given requested electrical power from the EGU, P_{G} [W], the mechanical output power of the ICE P_{ICE} [W] is computed by

$$P_{\mathrm{ICE}} = \frac{P_{\mathrm{G}}}{\eta_{\mathrm{G}}}, \tag{4.11}$$

with the efficiency $\eta_{\mathrm{G}} = f_{\mathrm{G}}(T_{\mathrm{G}}, \omega_{\mathrm{ICE}})$ determined by a linear 2D-interpolation in the efficiency map of the generator. The cumulative fuel consumption of the ICE, M_{ICE} [kg], from the time instant 0 to t, follows from

$$M_{\mathrm{ICE}}(t) = \int_0^t m_{\mathrm{ICE}}(\tau)\, d\tau = \int_0^t P_{\mathrm{ICE}}(\tau) \cdot \psi(\tau) \cdot d\tau, \tag{4.12}$$

with the specific fuel consumption $\psi = f(P_{\mathrm{ICE}}, \omega_{\mathrm{ICE}})$ [kg/Ws] computed using a 2D-linear interpolation of the static engine map (Figure 4.5c), based on the instantaneous requested power and the optimal EGU rotational speed ω_{ICE} [rad/s] pre-calculated using the Nelder-Mead simplex method for different possible levels of requested power (Leska et al., 2012).

Fuel cell

A simplified model of a PEMFC is developed to assess hydrogen consumption, while including FC's dynamics and efficiency. With the given requested power from FC, $P_{\mathrm{FC}}(t)$, cumulative hydrogen consumption at time instant t is calculated by (Sarma and Ganguly, 2018):

$$M_{\mathrm{FC}}(t) = \int_0^t m_{\mathrm{FC}}(\tau)\, d\tau = \int_0^t \frac{P_{\mathrm{FC}}(t)}{LHV_{\mathrm{Hydrogen}} \cdot \eta_{\mathrm{FC}}\big(PLR(t)\big)} dt, \tag{4.13}$$

where $\eta_{\mathrm{FC}} = f_{\mathrm{FC}}\big(PLR(t)\big)$ is the FC efficiency, determined using an approximated function of the normalized FC electrical output power by the rated FC power $P_{\mathrm{FC}}^{\mathrm{rated}}$ [W], referred to as part-load ratio (PLR), i.e., $PLR = P_{\mathrm{FC}}/P_{\mathrm{FC}}^{\mathrm{rated}}$ (Maleki and Rosen, 2017):

$$\eta_{\mathrm{FC}}\big(PLR(t)\big) = \begin{cases} 0.2716, & \text{if } (PLR) < 0.05 \\ 0.9033 \cdot \big(PLR(t)\big)^5 - 2.996 \cdot \big(PLR(t)\big)^4 & \\ +3.6503 \cdot \big(PLR(t)\big)^3 - 2.0704 \cdot \big(PLR(t)\big)^2 & \text{if } (PLR) \geq 0.05. \\ +0.4623 \cdot \big(PLR(t)\big) + 0.3747 & \end{cases} \tag{4.14}$$

The FC efficiency curve (4.14) is depicted in Figure 4.3a. The slow dynamic response of the PEMFC auxiliary components imposes the limitation on the rate of change of PEMFC output power P_{FC} (Barbir, 2013). Based on the premise that the PEMFC requires 30s from a start-up to reaching 90% of its rated power (Pesaran et al., 2005), the limitation of the rate of change of PEMFC output power is defined by the following constraint

$$\left|\frac{dP_{\mathrm{FC}}}{dt}\right| \leq 0.03 \cdot P_{\mathrm{FC}}^{\mathrm{rated}} \left[\frac{\mathrm{W}}{\mathrm{s}}\right]. \tag{4.15}$$

Thus, the maximum and the minimum possible FC power at time instant t, $P_{\mathrm{FC}}^{\max}(t)$ and $P_{\mathrm{FC}}^{\min}(t)$, result from the power load of the FC in the previous time instant, $P_{\mathrm{FC}}(t - \Delta t)$, and the constraint (4.15).

Lithium-ion battery

A lithium-ion battery (LB) model is implemented for the equivalent electrical circuit shown in Figure 4.3b. It consists of an open circuit voltage source U_{OC} [V], which depends on the battery state-of-charge (SoC), in series with a constant internal resistance R_{LB} [Ω], which represents ohmic losses and depends on the direction of the ESS current I_{LB} [A] (i.e., whether the battery is being charged or discharged). With the given power provided from the battery P_{LB} [W], the battery current and terminal voltage U_{LB} [V] are determined by (Prohl and Aschemann, 2019):

$$I_{\mathrm{LB}}(t) = \frac{U_{\mathrm{OC}}\big(\sigma_{\mathrm{LB}}(t)\big) - \sqrt{U_{\mathrm{OC}}\big(\sigma_{\mathrm{LB}}(t)\big)^2 - 4 \cdot P_{\mathrm{LB}}(t) \cdot R_{\mathrm{LB}}\big(I_{\mathrm{LB}}(t)\big)}}{2 \cdot R_{\mathrm{LB}}\big(I_{\mathrm{LB}}(t)\big)} \tag{4.16}$$

$$U_{\mathrm{LB}}(t) = U_{\mathrm{OC}}\big(\sigma_{\mathrm{LB}}(t)\big) - R_{\mathrm{LB}}\big(I_{\mathrm{LB}}(t)\big) \cdot I_{\mathrm{LB}}(t). \tag{4.17}$$

With the initial SoC $\sigma_{\mathrm{LB}}(0)$, and nominal battery capacity Q_{LB} [As], the battery SoC at time instant t results from

$$\sigma_{\mathrm{LB}}(t) = \sigma_{\mathrm{LB}}(0) - \frac{1}{Q_{\mathrm{LB}}} \cdot \int_0^t I_{\mathrm{LB}}(\tau) d\tau. \tag{4.18}$$

The maximum (discharging) power $P_{\mathrm{LB}}^{\max}$ [W] and minimum (charging) power $P_{\mathrm{LB}}^{\min}$ [W] are limited by the maximum and minimum current, $I_{\mathrm{LB}}^{\max}$ [A] and $I_{\mathrm{LB}}^{\min}$ [A], while keeping the limits of the SoC $\sigma_{\mathrm{LB}} \in [\sigma_{\mathrm{LB}}^{\min}, \sigma_{\mathrm{LB}}^{\max}]$, battery voltage $U_{\mathrm{LB}} \in [U_{\mathrm{LB}}^{\min}, U_{\mathrm{LB}}^{\max}]$, and allowed short peak values (Kapetanović et al., 2021b):

$$P_{\mathrm{LB}}^{\max}(t) = \left(U_{\mathrm{OC}}\big(\sigma_{\mathrm{LB}}(t)\big) - R_{\mathrm{LB}}^{\mathrm{dch}} \cdot I_{\mathrm{LB}}^{\max}(t)\right) \cdot I_{\mathrm{LB}}^{\max}(t) \tag{4.19}$$

$$P_{\mathrm{LB}}^{\min}(t) = \left(U_{\mathrm{OC}}\big(\sigma_{\mathrm{LB}}(t)\big) - R_{\mathrm{LB}}^{\mathrm{ch}} \cdot I_{\mathrm{LB}}^{\min}(t)\right) \cdot I_{\mathrm{LB}}^{\min}(t) \tag{4.20}$$

with

$$I_{\mathrm{LB}}^{\max}(t) = \min\left\{\frac{U_{\mathrm{OC}}\big(\sigma_{\mathrm{LB}}(t)\big) - U_{\mathrm{LB}}^{\min}}{R_{\mathrm{LB}}^{\mathrm{dch}}}, \frac{\left(\sigma_{\mathrm{LB}}(t) - \sigma_{\mathrm{LB}}^{\min}\right) \cdot Q_{\mathrm{LB}}}{\Delta t}, I_{\mathrm{LB}}^{\mathrm{max,dch}}(t)\right\} \tag{4.21}$$

$$I_{\mathrm{LB}}^{\min}(t) = \max\left\{\frac{U_{\mathrm{OC}}\big(\sigma_{\mathrm{LB}}(t)\big) - U_{\mathrm{LB}}^{\max}}{R_{\mathrm{LB}}^{\mathrm{ch}}}, \frac{\left(\sigma_{\mathrm{LB}}(t) - \sigma_{\mathrm{LB}}^{\max}\right) \cdot Q_{\mathrm{LB}}}{\Delta t}, I_{\mathrm{LB}}^{\mathrm{max,ch}}(t)\right\}, \tag{4.22}$$

where Δt [s] is the simulation (integration) time step, and $I_{\mathrm{LB}}^{\mathrm{max,dch}}$ [A] and $I_{\mathrm{LB}}^{\mathrm{max,ch}}$ [A] are the maximum discharging and charging current, defined by the maximum permitted continuous values ($I_{\mathrm{LB}}^{\mathrm{cont,dch}}$ [A], $I_{\mathrm{LB}}^{\mathrm{cont,ch}}$ [A]) or the pulse values ($I_{\mathrm{LB}}^{\mathrm{peak,dch}}$ [A], $I_{\mathrm{LB}}^{\mathrm{peak,ch}}$ [A]) allowed for the limited time ($t_{\mathrm{peak}}^{\mathrm{dch}}$ [s], $t_{\mathrm{peak}}^{\mathrm{ch}}$ [s]) and controlled by the corresponding time counters ($t_{\mathrm{cnt}}^{\mathrm{dch}}$, $t_{\mathrm{cnt}}^{\mathrm{ch}}$), i.e.

$$I_{\mathrm{LB}}^{\mathrm{max,dch}}(t) = \begin{cases} I_{\mathrm{LB}}^{\mathrm{peak,dch}} & \text{if } t_{\mathrm{cnt}}^{\mathrm{dch}}(t) < t_{\mathrm{peak}}^{\mathrm{dch}} \\ I_{\mathrm{LB}}^{\mathrm{cont,dch}} & \text{if } t_{\mathrm{cnt}}^{\mathrm{dch}}(t) \geq t_{\mathrm{peak}}^{\mathrm{dch}} \end{cases} \tag{4.23}$$

$$I_{\mathrm{LB}}^{\mathrm{max,ch}}(t) = \begin{cases} I_{\mathrm{LB}}^{\mathrm{peak,ch}} & \text{if } t_{\mathrm{cnt}}^{\mathrm{ch}}(t) < t_{\mathrm{peak}}^{\mathrm{ch}} \\ I_{\mathrm{LB}}^{\mathrm{cont,ch}} & \text{if } t_{\mathrm{cnt}}^{\mathrm{ch}}(t) \geq t_{\mathrm{peak}}^{\mathrm{ch}}. \end{cases} \tag{4.24}$$

Double-layer capacitor

A double-layer capacitor (DLC) model is based on the equivalent circuit shown in Figure 4.3c. The circuit is comprised of an internal resistance R_{DLC} [Ω] in series with a capacitance C_{DLC} [F]. Due to the linear relationship between the voltage and SoC of DLC (Li et al., 2019), terminal voltage and current at time instant t can be determined by

$$U_{\mathrm{DLC}}\big(\sigma_{\mathrm{DLC}}(t)\big) = \sigma_{\mathrm{DLC}}(t) \cdot \left(U_{\mathrm{DLC}}^{\max} - U_{\mathrm{DLC}}^{\min}\right) + U_{\mathrm{DLC}}^{\min} \tag{4.25}$$

$$I_{\mathrm{DLC}}(t) = \frac{U_{\mathrm{DLC}}\big(\sigma_{\mathrm{DLC}}(t)\big) - \sqrt{U_{\mathrm{DLC}}\big(\sigma_{\mathrm{DLC}}(t)\big)^2 - 4 \cdot P_{\mathrm{DLC}}(t) \cdot R_{\mathrm{DLC}}}}{2 \cdot R_{\mathrm{DLC}}}, \tag{4.26}$$

where $U_{\mathrm{DLC}}^{\min}$ [V]and $U_{\mathrm{DLC}}^{\max}$ [V] are the minimum and maximum voltage of DLC, respectively. With the initial SoC $\sigma_{\mathrm{DLC}}(0)$, and using (4.25) and (4.26) the resulting SoC follows from

$$\sigma_{\mathrm{DLC}}(t) = \sigma_{\mathrm{DLC}}(0) - \frac{1}{C_{\mathrm{DLC}} \cdot \left(U_{\mathrm{DLC}}^{\max} - U_{\mathrm{DLC}}^{\min}\right)} \cdot \int_0^t I_{\mathrm{DLC}}(\tau) d\tau. \tag{4.27}$$

The maximum (discharging) and minimum (charging) power of the DLC is limited by the current of the DLC. Either the maximum current is reached in order to keep the voltage constrains $U_{\mathrm{DLC}} \in \left[U_{\mathrm{DLC}}^{\min}, U_{\mathrm{DLC}}^{\max}\right]$, or the maximum charging/discharging permitted current defined by the manufacturer ($I_{\mathrm{DLC}}^{\max,\mathrm{dch}}$ [A], $I_{\mathrm{DLC}}^{\max,\mathrm{ch}}$ [A]) is reached (Kapetanović et al., 2021b):

$$P_{\mathrm{DLC}}^{\max}(t) = U_{\mathrm{DLC}}\left(\sigma_{\mathrm{DLC}}(t)\right) \cdot I_{\mathrm{DLC}}^{\max}(t) \tag{4.28}$$

$$P_{\mathrm{DLC}}^{\min}(t) = U_{\mathrm{DLC}}\left(\sigma_{\mathrm{DLC}}(t)\right) \cdot I_{\mathrm{DLC}}^{\min}(t) \tag{4.29}$$

with

$$I_{\mathrm{DLC}}^{\max}(t) = \min\left\{\frac{\left(U_{\mathrm{DLC}}\left(\sigma_{\mathrm{DLC}}(t)\right) - U_{\mathrm{DLC}}^{\min}\right) \cdot C_{\mathrm{DLC}}}{\Delta t}, I_{\mathrm{DLC}}^{\max,\mathrm{dch}}\right\} \tag{4.30}$$

$$I_{\mathrm{DLC}}^{\min}(t) = \max\left\{\frac{\left(U_{\mathrm{DLC}}\left(\sigma_{\mathrm{DLC}}(t)\right) - U_{\mathrm{DLC}}^{\max}\right) \cdot C_{\mathrm{DLC}}}{\Delta t}, I_{\mathrm{DLC}}^{\max,\mathrm{ch}}\right\}. \tag{4.31}$$

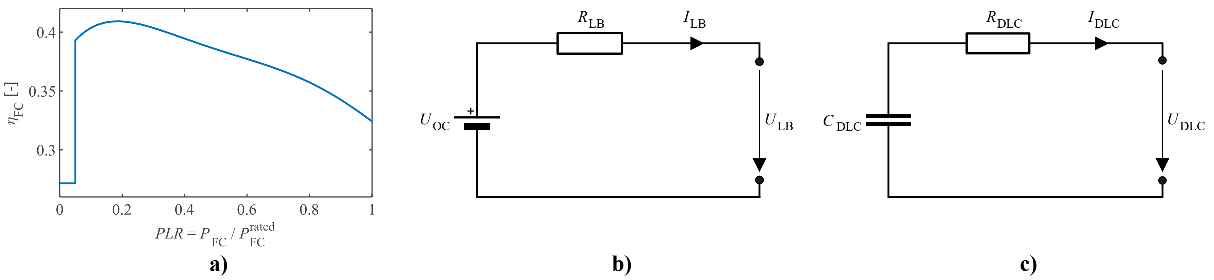

Figure 4.3: (a) Efficiency function curve of a fuel cell; equivalent electrical circuits for (b) lithium-ion battery, and (c) double-layer capacitor.

4.3.3 Energy management and control strategy

The aim of the EMCS implemented in the control unit (see Figure 4.2) is to distribute total instantaneous demanded power for traction and auxiliaries $P_{\mathrm{dem}}(t) = P_{\mathrm{EM}}(t) + P_{\mathrm{aux}}(t)$ between different power sources in the system, while complying with the following main requirements:

1. Improving fuel economy by maximizing regenerative braking energy and its later use in powering traction and auxiliary systems;
2. Increasing overall efficiency of the prime mover (ICE or FC) by avoiding low load operation;
3. Supporting the prime mover by an ESS during high power demand phases (acceleration);

4. Prolonging the LB life by giving priority to the DLC during charge/discharge processes for the HESS configurations.

To fulfil previous requirements, a real-time control based on a finite state machine (FSM) is proposed, allowing for realistic and achievable estimations of potential fuel savings for different configurations. FSM controls can be easily programmed in microcontrollers (Li et al., 2016), used for dispatching different power sources in the system by controlling their unidirectional or bidirectional converters, thus providing effective and implementable management of complex systems such as hybrid railway vehicles (Han et al., 2017; Yan et al., 2019). A five-state control is proposed (Figure 4.4), with states S1-S5 representing typical operation modes of a hybrid system (Kapetanović et al., 2021b), and with the corresponding triggers (conditions) T1–T5 covering all theoretically possible transitions between states, irrespective of the degree of hybridization, i.e., relative rated power ratio between the prime mover and the ESS. To define the operation modes for different states, an optimal level of electrical power from each prime mover is introduced, corresponding to its optimal efficiency region. These reference values are denoted by $P_{\mathrm{G}}^{\mathrm{opt}}$ [W] and $P_{\mathrm{FC}}^{\mathrm{opt}}$ [W], for EGU and FC, respectively. Excessive ESS charge from the prime mover and the dissipation of braking energy is avoided by introducing additional SoC reference values for each ESS $\in (\mathrm{LB}, \mathrm{DLC})$, denoted as $\sigma_{\mathrm{ESS}}^{\mathrm{lim}} \in (\sigma_{\mathrm{ESS}}^{\mathrm{min}}, \sigma_{\mathrm{ESS}}^{\mathrm{max}})$. To avoid frequent switches between ESS charging and discharging operation modes that might cause its damage and degradation, a hysteresis cycle for the SoC, $\sigma_{\mathrm{ESS}}^{\mathrm{hyst}} \in (\sigma_{\mathrm{ESS}}^{\mathrm{min}}, \sigma_{\mathrm{ESS}}^{\mathrm{lim}})$, is implemented by introducing a dynamic binary indicator $Flag(t) \in \{0,1\}$, with $Flag(0) = 0$.

For the sake of brevity, the power distribution and the triggers for transitions between different states are further presented only for the FCMU with HESS, as the most complex case. Analogously, the power distribution strategy for the remaining hybrid configurations represents a simplified case of the control (4.32)-(4.41). Single-technology ESS configurations are controlled by excluding parameters and terms related to the ESS technology not included in the observed system. For ICE-based configurations, all terms related to the FC system are replaced with the EGU-related equivalent, i.e., $P_{\mathrm{G}}(t), P_{\mathrm{G}}^{\mathrm{opt}}, P_{\mathrm{G}}^{\mathrm{idle}} = 0, P_{\mathrm{G}}^{\mathrm{min}} = 0, P_{\mathrm{G}}^{\mathrm{max}} = const.$

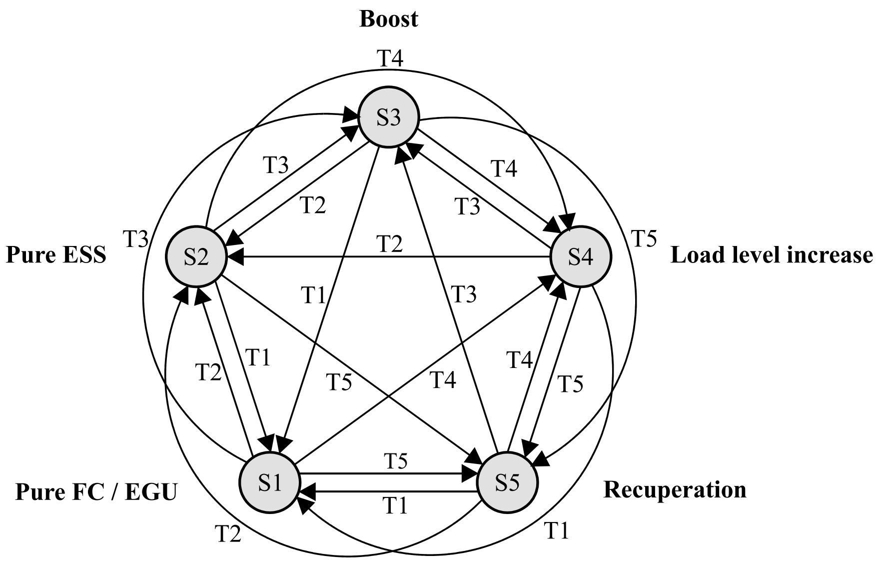

Figure 4.4: Power control based on a finite state machine, with indicated five states and corresponding transition triggers.

Under the *Pure FC state* (S1), total demanded power $P_{\mathrm{dem}}(t)$ is provided by FC system, and the ESS converters are switched off. Depending on the requested power level, FC output power limits, and ESS SoC and maximum power, this state is active under conditions defined by

$$\begin{aligned}\mathrm{T1}\colon & P_{\mathrm{FC}}^{\min}(t) \leq P_{\mathrm{dem}}(t) \leq P_{\mathrm{FC}}^{\max}(t) \\ & \wedge (P_{\mathrm{dem}}(t) = P_{\mathrm{FC}}^{\mathrm{opt}} \\ & \vee \left(P_{\mathrm{dem}}(t) > P_{\mathrm{FC}}^{\mathrm{opt}} \wedge \sigma_{\mathrm{DLC}}(t) = \sigma_{\mathrm{DLC}}^{\min} \wedge \sigma_{\mathrm{LB}}(t) = \sigma_{\mathrm{LB}}^{\min}\right) \\ & \vee \left(P_{\mathrm{dem}}(t) < P_{\mathrm{FC}}^{\mathrm{opt}} \wedge P_{\mathrm{dem}}(t) > \left(P_{\mathrm{DLC}}^{\max}(t) + P_{\mathrm{LB}}^{\max}(t)\right) \wedge \sigma_{\mathrm{DLC}}(t) \geq \sigma_{\mathrm{DLC}}^{\mathrm{lim}} \wedge \sigma_{\mathrm{LB}}(t) \geq \sigma_{\mathrm{LB}}^{\mathrm{lim}}\right)\Big)\end{aligned} \tag{4.32}$$

$$\mathrm{S1}\colon \begin{cases} P_{\mathrm{FC}}(t) = P_{\mathrm{dem}}(t) \\ P_{\mathrm{DLC}}(t) = 0 \\ P_{\mathrm{LB}}(t) = 0 \\ Flag(t) = Flag(t - \Delta t). \end{cases} \tag{4.33}$$

In the *Pure ESS state* (S2), the ESS provides the total requested power, with FC switched to idle. The corresponding conditions and power flows are defined by

$$\begin{aligned}\mathrm{T2}\colon & \left(0 \leq P_{\mathrm{dem}}(t) \leq \left(P_{\mathrm{DLC}}^{\max}(t) + P_{\mathrm{LB}}^{\max}(t)\right)\right) \\ & \wedge \left(Flag(t - \Delta t) = 0 \vee \left(Flag(t - \Delta t) = 1 \wedge \left(\sigma_{\mathrm{DLC}}(t) \geq \sigma_{\mathrm{DLC}}^{\mathrm{hyst}} \wedge \sigma_{\mathrm{LB}}(t) \geq \sigma_{\mathrm{LB}}^{\mathrm{hyst}}\right)\right)\right)\end{aligned} \tag{4.34}$$

$$\mathrm{S2}\colon \begin{cases} P_{\mathrm{FC}}(t) = \max\left\{P_{\mathrm{FC}}^{\min}(t), P_{\mathrm{FC}}^{\mathrm{idle}}\right\} \\ P_{\mathrm{DLC}}(t) = \min\{P_{\mathrm{DLC}}^{\max}(t), P_{\mathrm{dem}}(t)\} \\ P_{\mathrm{LB}}(t) = P_{\mathrm{dem}}(t) - P_{\mathrm{DLC}}(t) \\ Flag(t) = 0. \end{cases} \tag{4.35}$$

In the *Boost state* (S3), ESS provides support for the FC by providing a portion of high requested power that exceeds its maximum disposable power, i.e.

$$\begin{aligned}\mathrm{T3}\colon & \left(\left(P_{\mathrm{dem}}(t) < P_{\mathrm{FC}}^{\mathrm{opt}} \wedge P_{\mathrm{dem}}(t) > P_{\mathrm{FC}}^{\max}(t)\right) \vee P_{\mathrm{dem}}(t) > P_{\mathrm{FC}}^{\mathrm{opt}}\right) \\ & \wedge P_{\mathrm{dem}}(t) > \left(P_{\mathrm{DLC}}^{\max}(t) + P_{\mathrm{LB}}^{\max}(t)\right) \wedge \left(\sigma_{\mathrm{DLC}}(t) > \sigma_{\mathrm{DLC}}^{\min} \vee \sigma_{\mathrm{LB}}(t) > \sigma_{\mathrm{LB}}^{\min}\right) \\ & \wedge \left(Flag(t - \Delta t) = 0 \vee \left(Flag(t - \Delta t) = 1 \wedge \sigma_{\mathrm{DLC}}(t) \geq \sigma_{\mathrm{DLC}}^{\mathrm{hyst}} \wedge \sigma_{\mathrm{LB}}(t) \geq \sigma_{\mathrm{LB}}^{\mathrm{hyst}}\right)\right)\end{aligned} \tag{4.36}$$

$$\mathrm{S3}\colon \begin{cases} P_{\mathrm{FC}}(t) = \min\left\{\max\left\{\left(P_{\mathrm{dem}}(t) - P_{\mathrm{DLC}}^{\max}(t) - P_{\mathrm{LB}}^{\max}(t)\right), P_{\mathrm{FC}}^{\min}(t), P_{\mathrm{FC}}^{\mathrm{opt}}\right\}, P_{\mathrm{FC}}^{\max}(t)\right\} \\ P_{\mathrm{DLC}}(t) = \min\left\{\left(P_{\mathrm{dem}}(t) - P_{\mathrm{FC}}(t)\right), P_{\mathrm{DLC}}^{\max}(t)\right\} \\ P_{\mathrm{LB}}(t) = P_{\mathrm{dem}}(t) - P_{\mathrm{FC}}(t) - P_{\mathrm{DLC}}(t) \\ Flag(t) = 0. \end{cases} \tag{4.37}$$

Under the *Load level increase state* (S4), featured with low power demand, the FC provides the excess power which is used for recharging the ESS, defined by

$$\begin{aligned}\mathrm{T4}\colon & \left(P_{\mathrm{dem}}(t) < P_{\mathrm{FC}}^{\mathrm{opt}} \wedge P_{\mathrm{dem}}(t) \leq P_{\mathrm{FC}}^{\max}(t) \wedge P_{\mathrm{dem}}(t) > \left(P_{\mathrm{DLC}}^{\max}(t) + P_{\mathrm{LB}}^{\max}(t)\right) \wedge \left(\sigma_{\mathrm{DLC}}(t) < \sigma_{\mathrm{DLC}}^{\mathrm{lim}} \vee \sigma_{\mathrm{LB}}(t) < \sigma_{\mathrm{LB}}^{\mathrm{lim}}\right)\right) \\ & \vee \left(0 \leq P_{\mathrm{dem}}(t) < P_{\mathrm{FC}}^{\mathrm{opt}} \wedge P_{\mathrm{dem}}(t) \leq P_{\mathrm{FC}}^{\max}(t) \wedge P_{\mathrm{dem}}(t) \leq \left(P_{\mathrm{DLC}}^{\max}(t) + P_{\mathrm{LB}}^{\max}(t)\right)\right. \\ & \wedge Flag(t - \Delta t) = 1 \wedge \left(\sigma_{\mathrm{DLC}}(t) < \sigma_{\mathrm{DLC}}^{\mathrm{hyst}} \vee \sigma_{\mathrm{LB}}(t) < \sigma_{\mathrm{LB}}^{\mathrm{hyst}}\right)\Big)\end{aligned} \tag{4.38}$$

$$
\text{S4:}\begin{cases}
P_{\mathrm{FC}}(t) = \min\{\max\{P_{\mathrm{FC}}^{\min}(t), P_{\mathrm{FC}}^{\mathrm{opt}}\}, P_{\mathrm{FC}}^{\max}(t)\} \\
P_{\mathrm{DLC}}(t) = \begin{cases}
\max\{(P_{\mathrm{dem}}(t) - P_{\mathrm{FC}}(t)), P_{\mathrm{DLC}}^{\min}(t)\} & \text{if } \left(P_{\mathrm{dem}}(t) > (P_{\mathrm{DLC}}^{\max}(t) + P_{\mathrm{LB}}^{\max}(t)\right) \wedge \sigma_{\mathrm{DLC}}(t) < \sigma_{\mathrm{DLC}}^{\mathrm{lim}}) \\
 & \vee \left(P_{\mathrm{dem}}(t) \leq (P_{\mathrm{DLC}}^{\max}(t) + P_{\mathrm{LB}}^{\max}(t)) \wedge Flag(t - \Delta t) = 1 \wedge \sigma_{\mathrm{DLC}}(t) < \sigma_{\mathrm{DLC}}^{\mathrm{hyst}}\right) \\
0 & \text{if } \left(P_{\mathrm{dem}}(t) > (P_{\mathrm{DLC}}^{\max}(t) + P_{\mathrm{LB}}^{\max}(t)\right) \wedge \sigma_{\mathrm{DLC}}(t) \geq \sigma_{\mathrm{DLC}}^{\mathrm{lim}}) \\
 & \vee \left(P_{\mathrm{dem}}(t) \leq (P_{\mathrm{DLC}}^{\max}(t) + P_{\mathrm{LB}}^{\max}(t)) \wedge Flag(t - \Delta t) = 1 \wedge \sigma_{\mathrm{DLC}}(t) \geq \sigma_{\mathrm{DLC}}^{\mathrm{hyst}}\right)
\end{cases} \\
P_{\mathrm{LB}}(t) = \begin{cases}
\max\{(P_{\mathrm{dem}}(t) - P_{\mathrm{FC}}(t) - P_{\mathrm{DLC}}(t)), P_{\mathrm{LB}}^{\min}(t)\} & \text{if } \left(P_{\mathrm{dem}}(t) > (P_{\mathrm{DLC}}^{\max}(t) + P_{\mathrm{LB}}^{\max}(t)\right) \wedge \sigma_{\mathrm{LB}}(t) < \sigma_{\mathrm{LB}}^{\mathrm{lim}}) \\
 & \vee \left(P_{\mathrm{dem}}(t) \leq (P_{\mathrm{DLC}}^{\max}(t) + P_{\mathrm{LB}}^{\max}(t)) \wedge Flag(t - \Delta t) = 1 \wedge \sigma_{\mathrm{LB}}(t) < \sigma_{\mathrm{LB}}^{\mathrm{hyst}}\right) \\
0 & \text{if } \left(P_{\mathrm{dem}}(t) > (P_{\mathrm{DLC}}^{\max}(t) + P_{\mathrm{LB}}^{\max}(t)\right) \wedge \sigma_{\mathrm{LB}}(t) \geq \sigma_{\mathrm{LB}}^{\mathrm{lim}}) \\
 & \vee \left(P_{\mathrm{dem}}(t) \leq (P_{\mathrm{DLC}}^{\max}(t) + P_{\mathrm{LB}}^{\max}(t)) \wedge Flag(t - \Delta t) = 1 \wedge \sigma_{\mathrm{LB}}(t) \geq \sigma_{\mathrm{LB}}^{\mathrm{hyst}}\right)
\end{cases} \\
Flag(t) = 1.
\end{cases} \tag{4.39}
$$

The *Recuperation state* (S5) is active during braking, with the negative power values at the DC link used for recharging the ESS. The power distributed to the ESS is limited with its maximum charging power, with the excess power dissipated at the braking rheostat, and FC switched to idle and corresponding DC/DC converter switched off, i.e.

$$
\text{T5:}\, P_{\mathrm{dem}}(t) < 0 \tag{4.40}
$$

$$
\text{S5:}\begin{cases}
P_{\mathrm{DLC}}(t) = \max\{P_{\mathrm{DLC}}^{\min}(t), P_{\mathrm{dem}}(t)\} \\
P_{\mathrm{LB}}(t) = \max\{P_{\mathrm{LB}}^{\min}(t), (P_{\mathrm{dem}}(t) - P_{\mathrm{DLC}}(t))\} \\
P_{\mathrm{FC}}(t) = \max\{P_{\mathrm{FC}}^{\min}(t), P_{\mathrm{FC}}^{\mathrm{idle}}\} \\
Flag(t) = Flag(t - \Delta t).
\end{cases} \tag{4.41}
$$

4.4 Design and analysis of alternative propulsion systems

This section presents conceptual design and comparative assessment of the seven propulsion system configurations shown in Figure 4.1. The systems design comprises sizing of individual components for a benchmark standard DEMU vehicle employed on a selected benchmark route, based on estimated duty cycle coupled with the additional design criteria reflecting main physical and operation constraints. Alternative configurations are then compared in terms of fuel consumption and produced GHG emissions.

4.4.1 Benchmark vehicle selection

A two-coach version DEMU from the series Gelenktriebwagen (GTW 2/6), currently utilized in the Northern lines (Stadler, 2005), is selected as the benchmark vehicle for this study. GTW is a series of single-decker articulated DEMU regional trains manufactured by Stadler, with hundreds of vehicles in several configurations employed on regional railway lines across Europe and the United States (Stadler, 2021). This is reflected in their high representation in the literature as a reference vehicle on various analyses (Hoffrichter et al., 2016; Kapetanović et al., 2021a, 2021b). Required main input parameters for the selected benchmark vehicle are provided in Table 4.1. The maximum tractive effort curve, used for pre-calculating the velocity profile as the main simulation input, is shown in Figure 4.5a, with negative values assumed for braking. The efficiency map of an electric motor (Figure 4.5b) is reconstructed from the normalized efficiency maps provided by Paukert (2011) and Pröhl (2017b). The same sources are used in reconstructing the efficiency map of a generator and the specific consumption map of a diesel ICE (Figure 4.5c), where similarly sized ICE is scaled to the one found in GTW 2/6 DEMU using Willans lines technique (Pourabdollah et al., 2013). With the premise of maintaining the power characteristics (i.e., ICE output power), the specific consumption map of a hydrogen ICE is reconstructed by linearly scaling the specific consumption map of a diesel

ICE using the relation: $\psi_{\text{Hydrogen}}(P_{\text{ICE}}, \omega_{\text{ICE}}) = \psi_{\text{Diesel}}(P_{\text{ICE}}, \omega_{\text{ICE}}) \cdot LHV_{\text{Diesel}}/LHV_{\text{Hydrogen}}$, where $LHV_{\text{Diesel}} = 43.1$ MJ/kg and $LHV_{\text{Hydrogen}} = 120$ MJ/kg are the low heating values for diesel and hydrogen, respectively (JRC, 2020a).

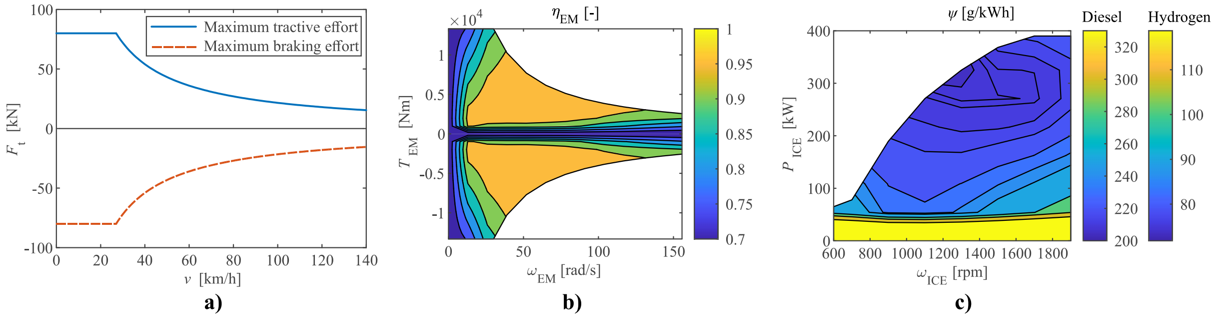

Figure 4.5: (a) Maximum tractive and braking effort; (b) reconstructed efficiency map of an electric motor; and (c) specific fuel consumption map of an internal combustion engine for the Stadler GTW 2/6 multiple-unit vehicle.

Table 4.1: Characteristics and simulation parameters for the standard GTW 2/6 diesel-electric multiple unit. [a)]

Parameter	**Unit**	**Value**
Vehicle tare weight [b)]	t	70.4
Rotating mass factor [c)]	-	0.05
Total passengers weight [d)]	t	7
Davis equation coefficient (constant term) [c)]	N	1001
Davis equation coefficient (linear term) [c)]	N/(km/h)	22.3
Davis equation coefficient (quadratic term) [c)]	N/(km/h)^2	0.1
Powered wheel diameter [e)]	m	0.86
Axle gear ratio [f)]	-	1.7218
Axle gear efficiency [g)]	-	0.97
Maximum velocity [e)]	km/h	140
Maximum acceleration [c)]	m/s^2	1.05
Maximum deceleration [c)]	m/s^2	-1
Maximum (starting) tractive effort [e)]	kN	80
Maximum power at the wheel [e)]	kW	600
Rated power of an electric motor [b)]	kW	2×400
Rated power of an internal combustion engine [b)]	kW	2×390
Constant auxiliaries power [d)]	kW	50
Cooling power coefficient [d)]	-	0.01

Note/Source: [a)] Vehicle parameters also reported by Kapetanović et al. (2021b); [b)] Giro Batalla and Feenstra (2012); [c)] Personal communication with Arriva employees; [d)] Assumed values; [e)] Stadler (2005); [f)] Determined from the ratio between the maximum rotational speed of the GTW's electric motor given by Giro Batalla and Feenstra (2012) and the maximum rotational speed of the wheel corresponding to the maximum vehicle speed; [g)] Adopted from Pröhl (2017b).

4.4.2 Benchmark route selection

The railway line that connects the cities Leeuwarden and Groningen is selected for the train simulations. This 54.051 km long line with seven intermediate stops is the main line in the observed regional network, with the highest utilization level. Due to the difference in line resistances (see Figures 4.6a,b) and maximum speed limits for the two opposite directions (Figure 4.6c), the vehicle round trip is analysed, based on the actual periodic timetable and vehicle circulation plan (Figure 4.6d). A dwell time of 30 seconds is assumed at intermediate stops, based on empirical observations, while layover times at the terminal stops are 11 minutes in Leeuwarden and 12 minutes in Groningen.

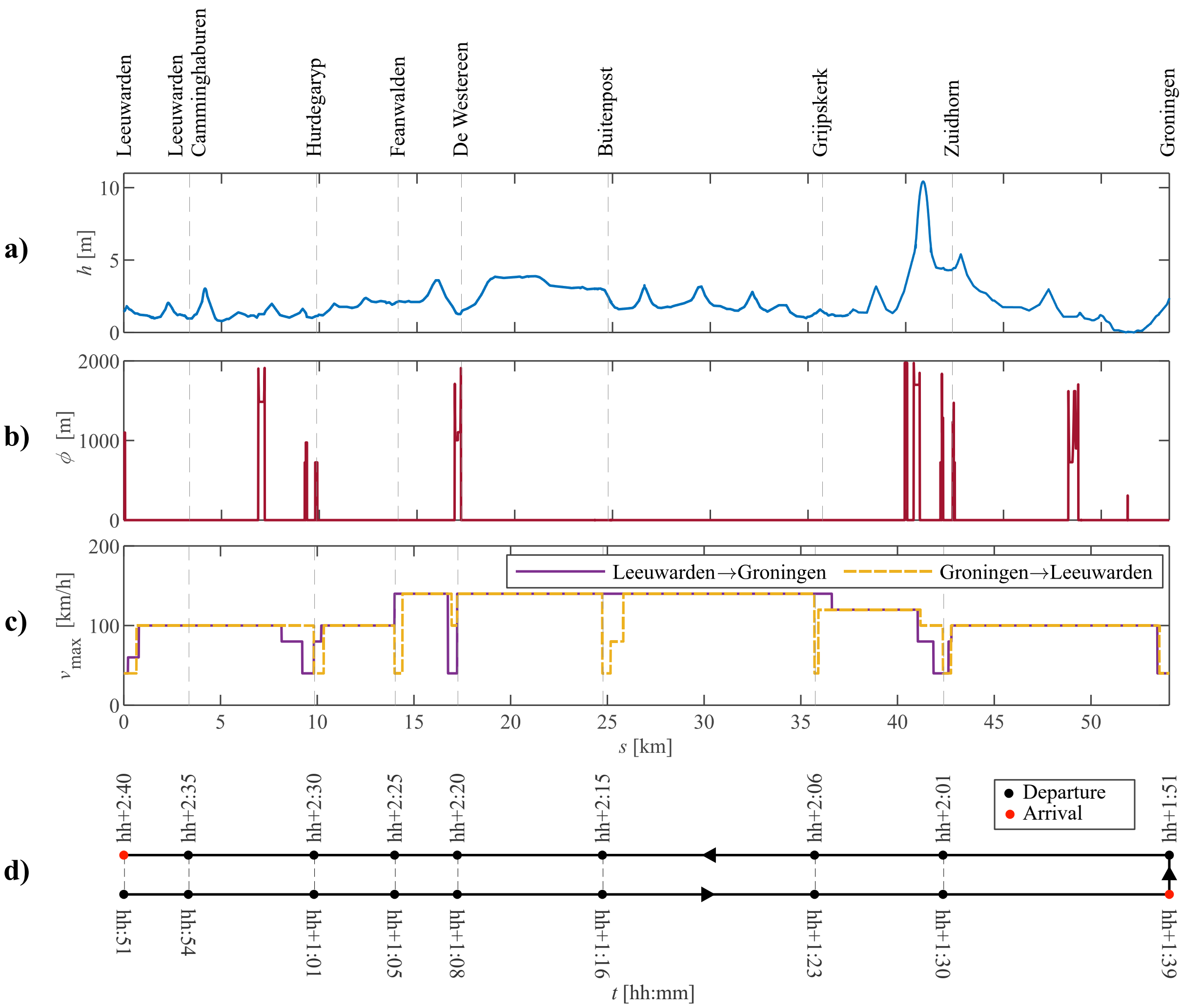

Figure 4.6: Railway line Leeuwarden – Groningen: (a) Track height compared to Normal Amsterdam Level; (b) position and dimeter of track curves; (c) maximum allowed speed; and (d) train departure times for the two opposite directions.

4.4.3 Technology selection

The design approach described in Section 4.3.1 is conducted using the following assumptions and selected technology. Due to the unavailability of data for a hydrogen ICE, we assume the possibility of converting the existing diesel ICE, or replacing it with hydrogen ICE with identical characteristics in terms of rated power, weight and dimensions. Commercially available technology for LBs, DLCs, FCs and hydrogen storage are considered, thus allowing for realistic estimations. Existing modules are then combined in series/parallel in order to meet the power and energy requirements. FC module FCmove™-HD from Ballard is considered as the replacement technology for EGU. This Ballard's latest platform for heavy-duty power modules based on the FCgen®-LCS stack offers benefits reflected in lower life cycle costs, simplified system integration and high performance (Ballard, 2021). SCiB™ module, type 1-23, of Japanese manufacturer Toshiba, is selected as the LB technology. The module contains 24 lithium-ion cells, arranged in 2 parallel branches with 12 cells in series. The cells are based on lithium nickel manganese cobalt oxide (NMC) chemistry with a lithium titanium oxide (LTO) anode, and offer a good compromise between energy density, power density and achievable lifetime (Takami et al., 2013; Toshiba, 2021). Due to the unavailability of the open-circuit voltage characteristic as a function of SoC, data from (SAFT and UNEW, 2017) is adopted and scaled according to voltage limits for the SCiB™ module (Figure 4.7). The BMOD0063 module from the manufacturer Maxwell Technologies is selected as DLC technology. It contains 48 cells, with 6 parallel series of 8 cells each. This commercially available module is especially suited for heavy-duty transport applications, such as trains and busses (Maxwell, 2021; Schmid et al., 2017). Luxfer G-Stor™ H2 are the type 3 cylinders for the storage of compressed hydrogen with demonstrated applications in railway vehicles (Luxfer, 2020a). We consider the model W322H35 with 350 bar of pressure since it offers high storage capacity and relatively low weight (Luxfer, 2020b). Detailed characteristics of the selected propulsion system components are given in Table 4.2.

Table 4.2: Parameters of different propulsion system components.

Parameter	Unit	Value
Fuel cell module [a]		
Rated power	kW	70
Idle power	kW	8
Volume	m^3	0.61362
Weight	kg	250
Lithium-ion battery module [b, c]		
Nominal capacity	Ah	45
Minimum/maximum continuous current	A	-160/160
Minimum/maximum pulse current	A	-350/350
Allowed time for pulse current	s	10
Minimum/maximum voltage	V	18/32.4
Internal resistance charge/discharge	Ω	0.006/0.006
Minimum/maximum state-of-charge [d]	%	10/90
Energy content	kWh	1.24
Usable energy content [e]	kWh	0.922
Minimum/maximum power at mean state-of-charge [f]	kW	-4.130/4.437
Volume	m^3	0.00857
Weight	kg	15
Double-layer capacitor module [b, g]		
Rated capacitance	F	63
Minimum/maximum continuous current	A	-240/240
Minimum/maximum voltage	V	12.5/125
Internal resistance	Ω	0.018
Energy content	kWh	0.14
Minimum/maximum power at mean state-of-charge [h]	kW	-16.5/16.5
Volume	m^3	0.00546
Weight	kg	61
Hydrogen storage [i]		
Storage capacity	kg	7.8
Volume	m^3	0.418
Tank weight	kg	141

Note/Source: [a] Extracted/calculated from specifications and data sheets from Ballard (2021); [b] Also reported by Kapetanović et al. (2021b); [c] Extracted/calculated values from specifications and data sheets from Toshiba (2021) unless otherwise indicated; [d] Adopted values for simulation purposes; [e] Based on allowed SoC range; [f] Calculated for continuous values using (4.19)-(4.22); [g] Extracted/calculated values from specifications and data sheets from Maxwell (2021) unless otherwise indicated; [h] Calculated using (4.28)-(4.31); [i] Extracted/calculated from specifications and data sheets from Luxfer (2020b).

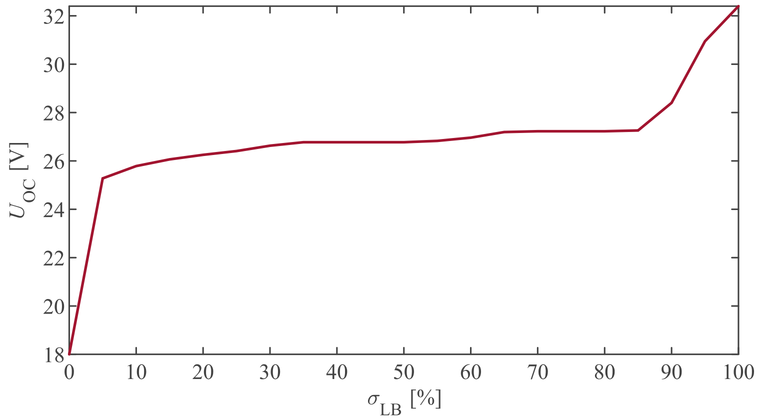

Figure 4.7: Reconstructed open circuit voltage function for a lithium-ion battery module.

4.4.4 Powertrain components sizing for alternative system configurations

The first step in designing alternative configurations is to define the benchmark criteria in sizing powertrain components. In order to derive power and energy requirements for the new systems, simulation of the round trip for the benchmark DEMU is performed by evaluating the simulation model from Figure 4.2, with the total demanded power provided solely by EGU. Figure 4.8 shows the speed profile as the main simulation input, power profiles at the wheel and the DC link, and cumulative energy and fuel consumption during the trip, with an estimated total diesel consumption of 87.78 kg. Overall results in terms of average and peak power, and cumulative energy demand, are summarized in Table 4.3. As can be noted, the braking energy and the difference between the average and peak power values indicate significant potential for hybridization.

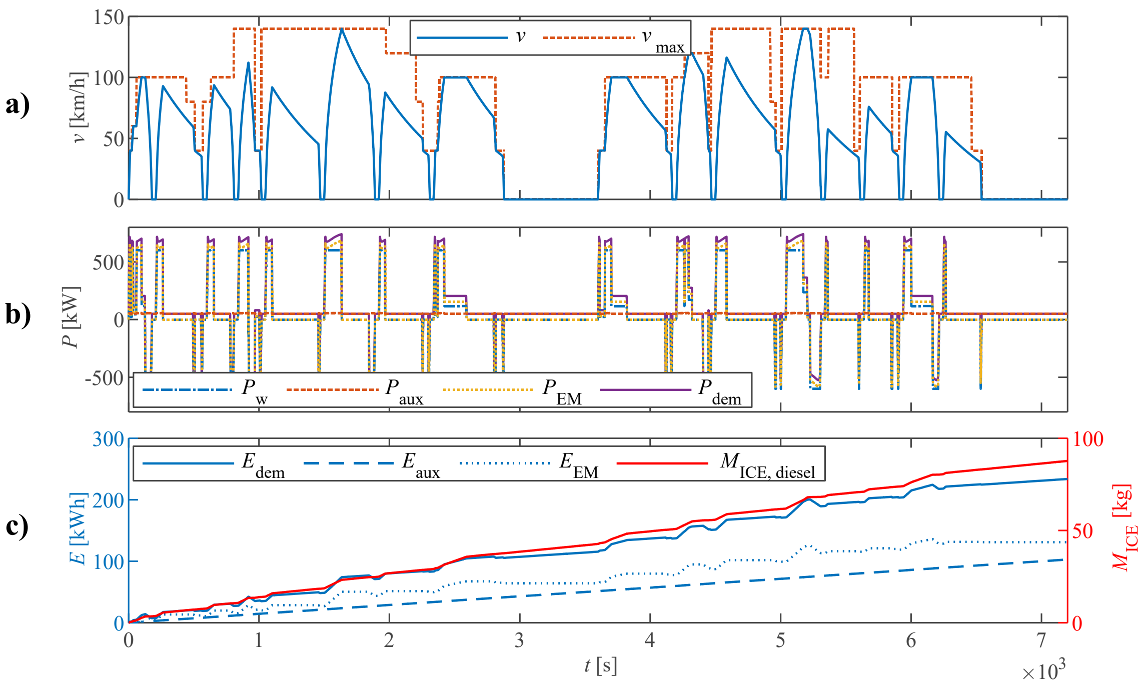

Figure 4.8: Simulation results for a benchmark diesel-electric multiple unit: (a) velocity profile; (b) power profiles at the DC link; (d) cumulative energy consumption at the DC link and cumulative consumption of diesel.

Table 4.3: Summary of round trip duty cycle characteristics (DC link) for the benchmark diesel-electric multiple unit.

Event	Average power [kW]	Peak power [kW]	Duration [s]	Cumulative energy [kWh]
Round trip (Engine-generator unit)	149.1	741.5	7200	298.3
Round trip (DC link)	116.8	741.5	7200	233.7
Acceleration	657.3	741.5	1060	193.1
Gradeability	191.7	363.9	678	36.1
Braking	-456.2	-526.0	510	-64.6

To prevent compromising the current timetable, power sources in place, both prime movers and ESSs, should be able to provide the same power and energy required for traction and auxiliaries, and at the same time to allow for the recuperation of the available braking energy. However, the maximum size for the components is conditioned by the maximum allowed weight to satisfy the axle load limitations and the maximum available volumetric space. According to the difference between alternative systems configurations described in Section 4.3.1, additional weight and volumetric space become available after removing the diesel EGUs and diesel fuel tank. Furthermore, the main criteria influencing fuel storage sizing is maintaining the vehicle range and current timetable, in this case, reflected in operation without refuelling during one day, i.e. nine round trips. Figure 4.9 shows the graphical representation of a Stadler GTW 2/6 DEMU with indicated space and weight limitations for the propulsion system and hydrogen fuel storage, generated based on the information from Giro Batalla and Feenstra (2012), Hoffrichter et al. (2016), Stadler (2005), and personal communication with Arriva. The derived benchmark criteria are summarized in Table 4.4.

Due to unavailability of the data related to the safety requirements for different powertrain components, and technical specifications and dimensions of corresponding power converters, safety distances, and weight and volumetric space requirements for power electronics devices are not accounted. Since the considered commercial FC, LB and DLC modules already have integrated main auxiliary components (e.g. cooling, monitoring, and cell voltage management), the weight and volumetric space required for auxiliary systems are omitted in the analysis. Nevertheless, we assume that the requirements for both safety distances and any additional auxiliary components can be compensated with the additional available space under the floor (Schmid et al., 2017) and/or by reducing the passenger capacity and utilizing part of the passenger compartments, as applied in the UK's HydroFLEX regional train (Calvert et al., 2021). Furthermore, we assume that required power electronics devices can be integrated into the existing insulated-gate bipolar transistor (IGBT) converter (ABB, 2018) and/or by utilizing the previously discussed additional space. Regarding traction motors, maintaining the two existing traction motors is considered for all powertrain configurations, without changes in their number or characteristics.

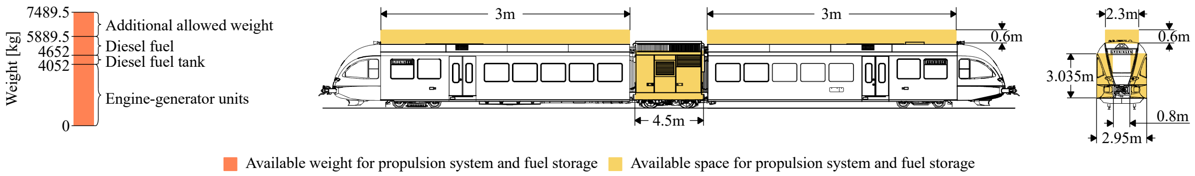

Figure 4.9: Graphical representation of a Stadler GTW 2/6 diesel-electric multiple unit with space and weight limitations for propulsion system and hydrogen fuel storage.

Table 4.4: Benchmark criteria in sizing powertrain components.

Parameter	Value	Unit
Energy demand		
Energy at DC link for 9 round trips (without regenerative braking)	2684.7	kWh
Energy at DC link for 9 round trips (with regenerative braking)	2103.3	kWh
Average energy during single acceleration	10.7	kWh
Average energy during single braking	-3.6	kWh
Mass		
Engine-generator units [a)]	4052	kg
Diesel fuel tank empty mass [b)]	600	kg
Diesel fuel (1500 litres) [c)]	1237.5	kg
Additional allowed mass (considering total mass limit of 72t) [d)]	1600	kg
Total allowed mass	7489.5	kg
Volume		
Engine-generator units [b)]	5	m^3
Diesel fuel tank	1.5	m^3
Additional space available at the roof [d)]	8.28	m^3
Total available space	14.78	m^3

Note/Source: [a)] Giro Batalla and Feenstra (2012); [b)] Approximate values based on personal communication with Arriva employees; [c)] Calculated from the fuel tank capacity provided by Giro Batalla and Feenstra (2012), and diesel fuel density of 0.825 kg/litre (Pröhl, 2017a); [d)] Adopted for GTW 2/6 from Hoffrichter et al. (2016).

Coupling previously defined benchmark criteria with the parameters for different technologies allows for determining the size of each of the components for alternative system configurations. Sizing is realized in the following order: (1) prime mover (EGU or FC), (2) ESS, and (3) hydrogen storage system. Regarding the ICE-based configurations, we assume identical number and characteristics of the EGUs to those found in the standard vehicle. For FC-based configurations, the number of FC modules is defined to satisfy gradeability power, following the recommendation of Garcia et al. (2010). Criteria in dimensioning ESS systems for ICE-based configurations include the peak braking power and average energy for braking. For FC-based alternatives, peak power and average energy values for both braking and acceleration are considered, to account for slow dynamics of an FC system and ensure maintaining tractive characteristics of a vehicle. ESS size is thus determined as the minimum number of modules required to satisfy all of the previously defined criteria. For HESS configurations, LB is sized according to the average power and energy level, while DLC covers the remaining peak power.

Finally, the size of the hydrogen storage system is determined using the following approach. First, the initial number of hydrogen cylinders is derived from the energy required at the DC link for nine round trips (Table 4.4), divided by the efficiency of the prime mover. For the EGU, an efficiency of 28.4% is determined from the ratio of the energy content of the total diesel fuel consumed and cumulative electrical energy provided by the EGU (Table 4.3), while for the FC the value of 37.8% is adopted as the average efficiency for the operation range between idling and rated FC power (Eq. (14) and Table 4.2), giving an initial size of 37, 29 and 22 cylinders for standard (non-hybrid), ICE-based hybrid and FC-based hybrid system, respectively. Due to the difference in vehicle weight, and the influence of the EMCS on the final fuel consumption, the final number of cylinders for each propulsion system is determined using an alternating coordination algorithm (Silvas et al., 2016) as follows. Using the initial hydrogen storage system size and the model described in Section 4.3, hydrogen consumption is evaluated and required number of cylinders for nine round trips is recalculated. In the case of an adjusted number of cylinders, the procedure is repeated until the hydrogen consumption and corresponding required vehicle range have converged.

A summary of obtained alternative system configurations is given in Table 4.5. As noted, only FCMU with LB satisfies both mass and volume constraints, while the remaining two FC-based configurations exceed only mass limit. Both limits are exceeded for all four ICE-based configurations. Nevertheless, assuming the possibility of increasing axle-load limitation by, e.g., replacing the existing with higher-load axles and/or redistributing the components and vehicle centre of gravity, they are further evaluated in terms of potential fuel savings and reduction of GHG emissions. In case the latter solution is not viable, results are further derived for reduced vehicle range scenarios.

Table 4.5: Characteristics of alternative system configurations complying with the maximum range requirement.

Component	**Number of components per configuration**						
	1	**2**	**3**	**4**	**5**	**6**	**7**
Engine-generator unit	2	2	2	2	-	-	-
Fuel cell module	-	-	-	-	6	6	6
Lithium-ion battery module	-	128	-	111	157	-	149
Double-layer capacitor module	-	-	32	5	-	77	6
Hydrogen fuel cylinder	37	27	29	27	23	25	23
Total mass required [kg]	9557.6	9989.6	10319.2	10039.6	7277.4	9917.0	7523.4
Mass constraint met	No	No	No	No	Yes	No	No
Total volume required [m^3]	20.47	17.38	17.30	17.26	14.64	14.55	14.61
Volume constraint met	No	No	No	No	Yes	Yes	Yes

4.4.5 Comparative assessment

Vehicle configurations complying with the maximum range requirement

Previously defined alternative configurations are assessed in terms of hydrogen consumption using the presented model and corresponding parameters for each scenario. Figure 4.10 shows the simulation results for the FCMU equipped with a HESS, as the most complex case. Results include vehicle speed profile, power profiles from different components in the system, ESS SoC, and cumulative fuel consumption during the trip. An example of a selected track segment between the two consecutive stops Buitenpost and Grijpskerk shows the system dynamics and power distribution between present sources according to ECMS-defined states. The slow dynamics feature of the FC system is emphasized during the acceleration and braking phases. For the sake of brevity, detailed simulation results for all scenarios are given in Figure 4.11, with the estimated hydrogen consumption summarized in Table 4.6.

As expected, results indicate the highest fuel consumption for non-hybrid configuration with ICE as the prime mover, due to dissipation of braking energy and total demanded power provided solely by EGU. FCMU with LB demonstrated the highest fuel-saving potential, with consumption reduced by 37.9% compared to the standard vehicle. A very similar performance is reached by FCMU equipped with HESS. Although this configuration did not satisfy the mass constraint, the excess of ~34 kg, in this case, can be considered negligible. Despite the limitation of the FC system in terms of slow dynamic response, the overall results indicate significantly better performance of FCMUs compared to the ICE-powered vehicles, mainly due to the higher efficiency of FC systems compared to the EGUs. Regarding hybrid configurations, vehicles equipped with LB demonstrated the highest potential benefits, followed by the HESS, while configuration hybridized solely with the DLC demonstrated higher fuel consumption for both ICE and FC-based vehicles.

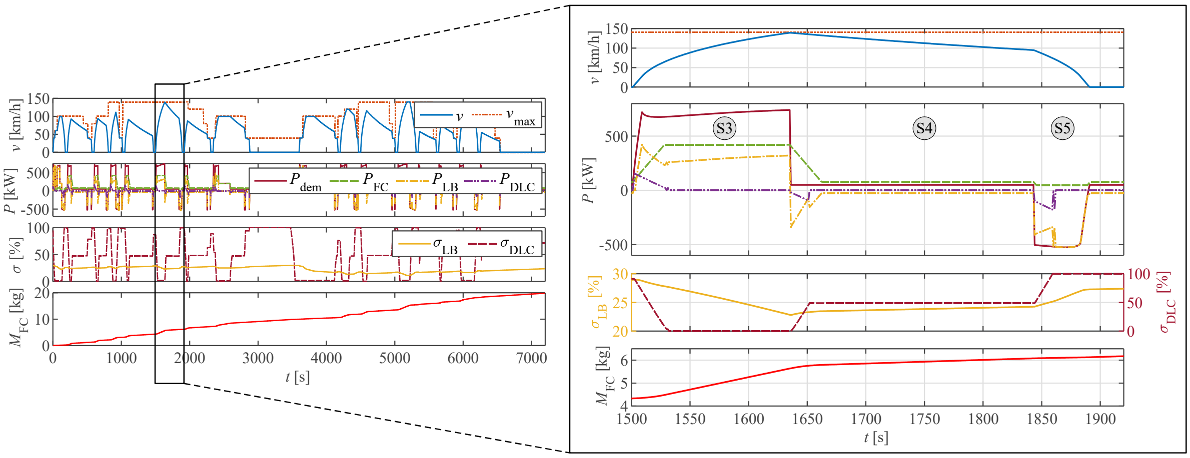

Figure 4.10: Simulation results for a fuel cell multiple unit vehicle equipped with a hybrid energy storage system.

Table 4.6: Estimated hydrogen consumption per round trip for alternative system configurations complying with the maximum range requirement.

Config.	**Prime mover**	**Energy storage system**	**Hydrogen consumption [kg]**
1	Internal combustion engine	-	31.87
2	Internal combustion engine	Lithium-ion battery	22.85
3	Internal combustion engine	Double-layer capacitor	24.95
4	Internal combustion engine	Hybrid energy storage system	23.28
5	Fuel cell	Lithium-ion battery	19.80
6	Fuel cell	Double-layer capacitor	21.02
7	Fuel cell	Hybrid energy storage system	19.83

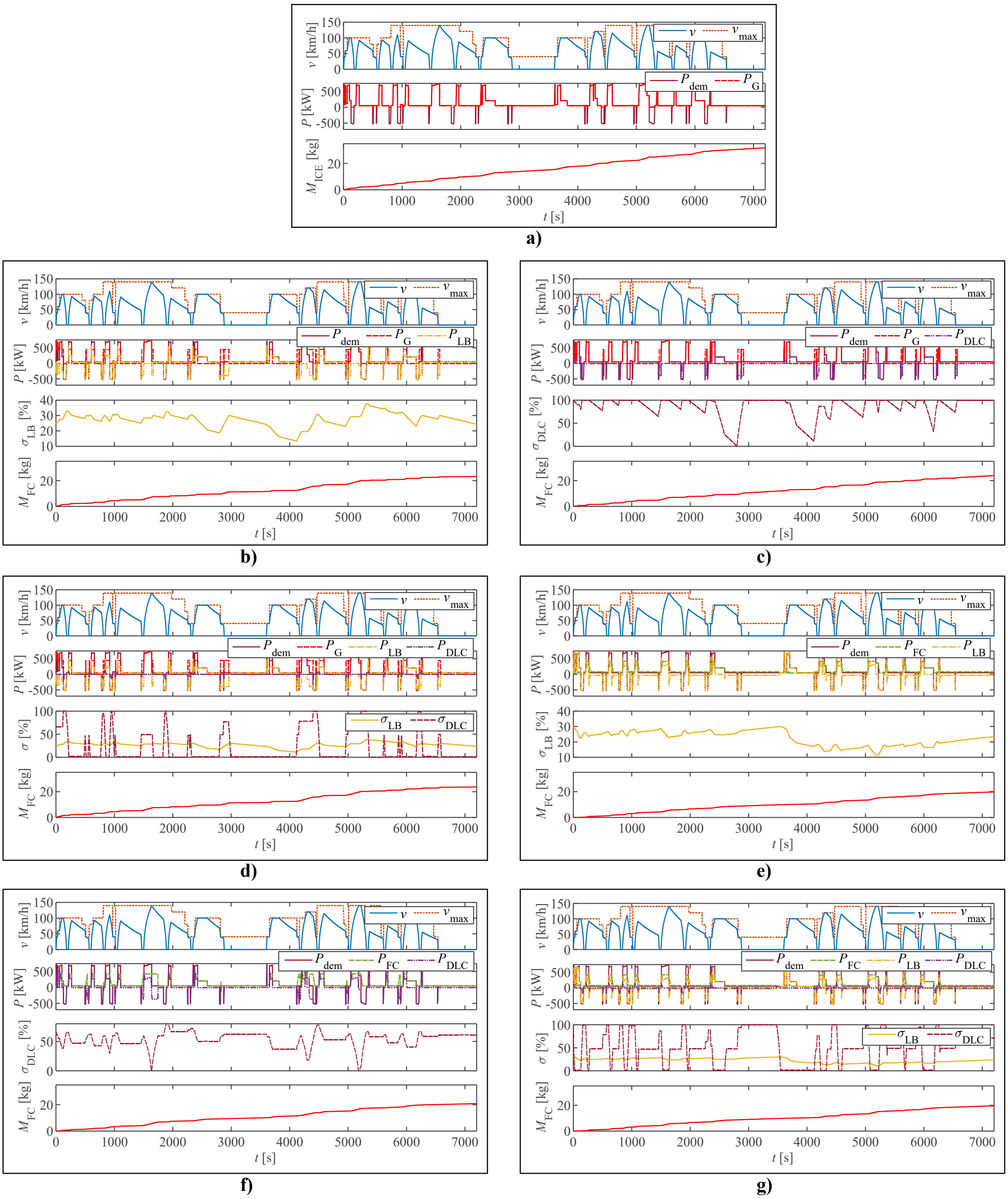

Figure 4.11: Simulation results for alternative propulsion systems complying with the maximum range requirement: (a) standard (non-hybrid); internal combustion engine-based hybrids with (b) lithium-ion battery, (c) double-layer capacitor, and (d) hybrid energy storage system; fuel cell-based hybrids with (e) lithium-ion battery, (f) double-layer capacitor, and (g) hybrid energy storage system.

Vehicle configurations complying with weight and volumetric space constraints

In case that defined vehicle weight and volumetric space constraints cannot be relaxed, we further adjust the vehicle configurations by reducing the size of the hydrogen storage system, while maintaining the previously defined propulsion system components. The adjusted hydrogen storage system size is determined as the maximum number of cylinders that satisfies both vehicle mass and volumetric space constraints. Since this leads to reduced vehicle range, we assume an efficient refuelling system in place, that would prevent compromising the current timetable and vehicle circulation plan.

Characteristics and estimated hydrogen consumption for adjusted vehicle configurations are summarized in Table 4.7. Due to reduced vehicle weight, affecting the acceleration and braking performance, additional fuel savings are obtained. Compared to the previous scenario, these savings range between 0.25% for FCMU with HESS up to 3.77% for ICE-based hybrid with DLC. At the same time, vehicle range is reduced to 2 up to 8 round trips, depending on the configuration. Again, FCMU with LB and HESS demonstrated the highest fuel economy, with a slightly lower consumption of HESS-equipped vehicle in this case (0.1%).

Table 4.7: Characteristics and estimated hydrogen consumption for alternative system configurations complying with weight and volumetric space constraints.

	Configuration						
	1	2	3	4	5	6	7
Number of hydrogen fuel cylinders	23	10	9	9	23	8	22
Hydrogen consumption per trip [kg]	31.06	22.13	24.01	22.67	19.80	20.32	19.78
Fuel savings compared to the full range [%]	2.54	3.15	3.77	2.62	0.00	3.33	0.25
Vehicle range (number of round trips)	5	3	2	3	9	3	8

Preliminary validation of energy use

Available historical data on actual fuel consumption provided by the railway undertaking for the Dutch Northern lines shows an average annual consumption of diesel per vehicle-distance travelled of 0.94 l/km and 0.95 l/km, in 2019 and 2020, respectively. This is a 3-4% lower diesel consumption compared to our estimations for a standard diesel-electric vehicle, i.e., a total consumption of 87.78 kg (106.4 l) for a round trip, giving an average consumption of 0.98 l/km. This difference can be attributed to various factors, including the variation in duty cycles linked to different lines in the network, passengers load and auxiliary systems consumption over different seasons and time of the day. In addition, our estimations are based on the assumption that all auxiliary systems are active during layover times, while in reality this is not always the case.

Furthermore, the onboard system used for train drivers training that registers fuel consumption during each trip (excluding the layover time) showed an average diesel fuel consumption for GTW 2/6 DEMUs in a range 0.66-0.86 l/km and 0.70-0.92 l/km for the Leeuwarden-Groningen and Groningen-Leeuwarden directions, respectively. With the layover time omitted, our estimations are within the given range for both directions, i.e., 36.86 kg (0.83 l/km) for the Leeuwarden-Groningen trip, and 40.65 kg (0.91 l/km) for the Groningen-Leeuwarden trip.

In addition, although there are numerous factors affecting the estimates, including the observed technology, size, and operation context, the model estimations are compared to the scientific findings in the literature that considers similar use cases, i.e., regional railway transport and multiple-unit vehicles. Our estimations on fuel consumption for a standard

DEMU, and relative savings for ICE-based hybrid powertrains compared to the standard vehicle, are close or within the range of the estimations in scientific studies that considered various geographical contexts, technologies and test conditions, c.f., Lanneluc et al. (2017); Leska et al. (2017); Meinert et al. (2015a); Poline et al. (2019); Schmid et al. (2017). Regarding FC-based systems, it can be noted that our estimations on hydrogen consumption of 0.37-0.39 kg/km, depending on the ESS configuration, are similar to, or within the range of the estimations found in studies on regional hybrid trains, c.f., Din and Hillmansen (2018); Hoffrichter et al. (2016); Peng et al. (2020a).

Greenhouse gas emissions

Although hydrogen as fuel leads to zero direct GHG emissions, its overall environmental impact heavily depends on its production pathway. Therefore, it is important to adopt the so-called "Well-to-Wheel" approach, where the emissions from upstream processes related to hydrogen production are accounted. This allows for a plausible and fair comparison of GHG emissions linked to the alternative hydrogen-based scenarios and the benchmark diesel-driven vehicle. To assess the influence of hydrogen production, we include two common hydrogen production pathways – steam methane reforming (SMR) and electrolysis of water. Corresponding emission factors are derived from the latest JEC report (JRC, 2020b), and represent the amount of GHG emissions expressed in kilograms of CO_2-equivalents per kilogram of fuel expended (kgCO_2e/kg). Considered production of hydrogen from SMR includes typical EU natural gas supply transported to EU by pipeline (1900 km), distributed inside the EU (500 km) through high-pressure trunk lines and a low-pressure grid, small scale reforming at a retail site, and hydrogen compression to 88 MPa, with a corresponding emission factor of 13.128 kgCO_2e/kg. The electrolysis scenario considers hydrogen produced from a central electrolysis with medium voltage electricity, hydrogen transport by pipeline and compression to 88 MPa. To account for future trends, the electricity used is based on predicted EU-mix electricity supply relevant for 2030, resulting in a hydrogen emission factor of 14.208 kgCO_2e/kg. Electrolysis using electricity produced solely from renewables, e.g., wind energy, is not considered, as it would practically lead to net-zero emissions for all scenarios. Furthermore, it is expected that such a production process leads to a significantly higher price of hydrogen compared to the SMR, with a current hydrogen price of 2 Euros per kilogram (Klebsch et al., 2019). The baseline scenario considers diesel fuel produced from crude oil from typical EU supply transported by sea, refined in EU (marginal production), with typical EU distribution and retail, resulting in a Well-to-Wheel emission factor of 3.970 kgCO_2e/kg.

Overall GHG emissions for the two production scenarios are obtained by multiplying the estimated hydrogen consumption given in Tables 4.6 and 4.7 with corresponding emission factors. The results are then compared to the baseline estimate for a diesel-driven vehicle in terms of relative change in GHG emissions (Figure 4.12). As noted, conversion to a standard hydrogen ICE-based configuration would potentially lead to a significant increase of GHG emissions compared to diesel baseline (~17-30%). Another configuration that showed an increase of 1.72% compared to the baseline is the maximum range ICE-based hybrid with DLC. A reduction of GHG emissions is achieved in all remaining scenarios, with the highest savings reached by FCMU with LB or HESS, as the most fuel-efficient configurations.

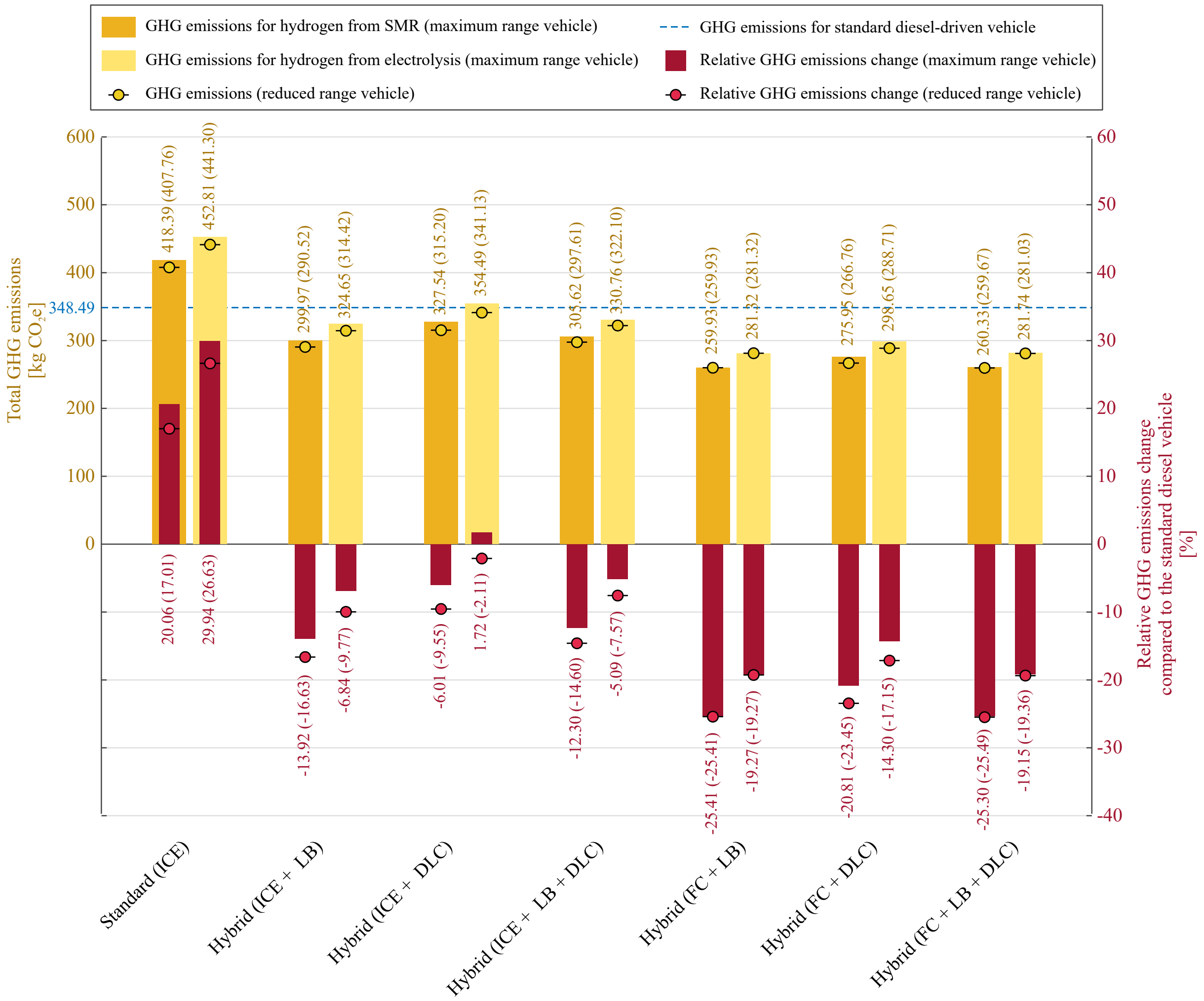

Figure 4.12: Estimated greenhouse gas (GHG) emissions and relative GHG emissions change compared to the standard diesel vehicle.

4.5 Conclusions

This chapter presented a comparative assessment of hydrogen-powered propulsion systems with an internal combustion engine or fuel cells as the prime mover, hybridized with different energy storage system configurations, based on lithium-ion batteries and double-layer capacitors. The analysis encompassed the technology identification, design, modelling and assessment of alternative powertrains, with respect to the particular case-related constraints imposed by the infrastructure, technical and operational requirements. Focusing on the regional railways in the Northern Netherlands, we investigated the possibilities of converting a conventional benchmark vehicle used in current operations, and provided a simulation-based assessment in terms of overall hydrogen consumption.

According to the results, the highest fuel-saving potential was found for the fuel cell-based hybrid propulsion systems with lithium-ion battery or a hybrid energy storage system that combines both energy storage system technologies, while at the same time complying with the volumetric space and weight limitations. Additionally, the previous two configurations demonstrated the highest greenhouse gas emissions reduction compared to the benchmark diesel-driven vehicle, i.e., between 25.3-25.5% for hydrogen produced by steam methane reforming, and between 19.2-19.4%, if hydrogen obtained through electrolysis of water is used.

Overall, our results indicate promising potential benefits from adopting hydrogen-based technology and provide decision-makers with valuable input in defining a roadmap for the railway transport development in the Northern Netherlands. Future research efforts will include the application of the proposed method to the remaining lines and rolling stock in the network while addressing limitations of the present study resulting primarily from a wide range of data sources used and a degree of variability in parameters and assumptions adopted. Regarding the variability of parameters, one of the main challenges in practical implementation is the consideration of real-life phenomena such as fuel cell deterioration and battery degradation due to aging, which can affect the system's performance. Another system engineering challenge is incorporating safety requirements and vehicle/components geometrics, which require more detailed analyses including, for instance, developing detailed 3D CAD models.

The presented research is part of a wider-scope project realized in collaboration with Arriva, aiming to investigate the overall environmental impacts from novel technology adoption and possibilities to reduce the carbon footprint from trains operation. In this context, extensions of the present research will include further investigation of alternative fuels and upstream processes related to their production through a detailed Well-to-Wheel analysis. The environmental impacts of technology production and vehicle retrofit will be evaluated by a Life Cycle Assessment (LCA) approach, as introduced by Jones et al. (2017). Furthermore, a comprehensive Life Cycle Costs (LCC) analysis, based on Zhang et al. (2016) will be realized to assess the fixed investment costs for both onboard hydrogen technologies and stationary infrastructure required for refuelling. As shown by Logan et al. (2020), railways should also be observed in a wider transport system context. Therefore, future research could consider network-wide operational measures (Dunbar et al., 2017), or policy interventions with the potential to increase the modal shift from individual road transport to rail.

The methodology provided in this chapter offers numerous possibilities for other railway market segments. The high level of generality and ability to capture main technology, infrastructure and operation characteristics allow for its application in urban and freight rail transport, as well as in different contexts of regional railway transport, where, for instance, different vehicle features, speed limits and/or track geometry profiles determine corresponding duty cycles and the final outcomes of the analysis. Thus, our findings provide decision-makers with a valuable tool in assessing future investments planning, including the identification of suitable powertrain technology and potential benefits in terms of fuel economy and reduction of emissions.

Chapter 5

Energy use and greenhouse gas emissions of traction alternatives for regional railways

Apart from minor updates, this chapter has been submitted as:

Kapetanović, M., Núñez, A., van Oort, N., Goverde, R.M.P. (2023). Energy use and greenhouse gas emissions of traction alternatives for regional railways. (*Under review*).

5.1 Introduction

Approximately one-quarter of the total greenhouse gas (GHG) emissions emitted in the European Union (EU) are attributed to transport, with climate neutrality for this sector requiring a 90% reduction of its emissions by 2050 (EC, 2019). A modal shift from road and aviation to rail is one of the main instruments in achieving this goal, with further synergetic electrification of railways and electricity production from renewables (EC, 2011). The national railway network in the Netherlands features one of the highest electrification rates in the EU, with over 75% electrified lines (EC, 2018) and traction electricity claimed to be completely produced from wind power (EcoWatch, 2017). In 2018, electricity accounted for 85% of the total energy demand in the Dutch railway sector (IEA, 2020). The remaining 15% is attributed mainly to diesel trains operating on non-electrified regional lines, for which passenger transport accounted for an estimated 55-60% of total diesel consumption (CE Delft, 2020). Considering the scale and high utilization of the Dutch railway network, even when the share of diesel traction is relatively low, the resulting GHG emissions are in the order of millions of kilograms per year. New railway technologies allow the reduction of these emissions; however, finding the most suitable solution imposes a significant challenge to railway undertakings (RUs) and policy makers. The fair evaluation of solutions requires assessment methods that capture the complexities of railway systems, including the dynamic interlinks between infrastructure and operations, context-specific information in the decision-making process, and involvement of multiple stakeholders.

Due to the relatively low utilization of regional lines, complete electrification is often not economically viable. In addition, the planning and construction phases can take several years or even decades (Klebsch et al., 2019). Therefore, solutions for improving energy efficiency and reducing GHG emissions are being sought in advanced catenary-free propulsion systems and alternative low-carbon fuels. The former primarily relates to vehicle hybridization with intelligent energy storage systems (ESSs) that allow the utilization of braking energy by traction and auxiliary systems, which results in reduced energy use and produced emissions (Klebsch et al., 2018). Similar to the automotive sector's long-term strategy to completely phase-out internal combustion engines (ICEs), several established manufacturers rolled-out fuel-cell multiple unit (FCMU) and battery-electric multiple unit (BEMU) vehicles into the rail market (Klebsch et al., 2020). Although these vehicles allow for (locally) emission-free train operation, their readiness to operate on existing networks is subjected to local requirements and constraints (Mueller et al., 2020).

In addition to the advanced energy-efficient powertrains, the use of alternative fuels aims to reduce emissions from direct combustion and those related to their production and supply. A number of alternatives to fossil diesel have emerged in the transport sector, including first and second-generation biofuels, hydrogen, and synthetic or e-fuels (Andersson and Börjesson, 2021). Despite the variety of novel propulsion systems and energy carriers, more studies are needed on energy use and environmental impacts from their synergetic implementations in the railway sector. In the railway literature, different methods have been proposed, including meta-analyses (Hoffrichter et al., 2012), top-down approaches (Gangwar and Sharma, 2014), and the application of high-level models (Knörr et al., 2018). However, to the best of our knowledge, a method that also includes both the complexity of the advanced propulsion systems and the local conditions that pertain to the particular geographical scope or use case is not yet available. Relaxing conservative assumptions such as uniform conditions or including the analysis of potentially influential factors such as infrastructure characteristics and ambient conditions are needed to avoid biased conclusions.

This chapter focuses on the Northern lines in the Netherlands (in Dutch, *Noordelijke lijnen*), a common name for the seven non-electrified railway lines that constitute the regional rail network in the provinces of Friesland and Groningen. Arriva, Dutch largest regional RU, operates passenger trains on the network. As part of the new 15-year concession that started in December 2020, the RU committed to significantly reduce the overall GHG emissions on the network (Arriva, 2019). Near-term solutions include gradual retrofitting and hybridization of existing diesel-electric multiple units (DEMUs) (Arriva, 2020) and the introduction of new bi-mode hybrid vehicles with ICEs compatible with hydrotreated vegetable oil (HVO) (Stadler, 2020). Given the range of available propulsion system technologies, energy carriers, and their production pathways, it is essential to understand the overall energy demand and GHG emissions attributed to each alternative. This information would enable a consistent and credible comparative analysis, which is crucial in policy decision-making and long-term planning of energy efficient and low- or zero-emission regional railway transport. The key contributions of this chapter are the following:

1. We propose a comparative analysis of implementations of various (hybrid) propulsion systems combined with prominent low-emission energy carriers while including commercially mature and novel technologies and energy carrier production pathways.
2. The analysis adopts a bottom-up approach, with direct fuel and/or electricity consumption estimated via a simulation model that captures relevant factors influencing direct energy use and, thus, the resulting overall energy demand and emissions.

3. We showcase the method in the real-world case of regional rail passenger transport in the Netherlands. We use energy carriers pathways and emission factors relevant to European and Dutch contexts and provide the RU and policy-makers with new essential information for planning future rolling stock and infrastructure investments.
4. We also provide new estimates of primary energy use and GHG emissions (see Appendix B), which can benefit future research, especially in comparable cases when detailed vehicle, infrastructure and/or operational parameters are unavailable.

This chapter is structured as follows. Section 5.2 reviews existing approaches in quantifying energy use and GHG emissions, focusing on railway studies. The methodology and detailed description of considered alternatives and scenarios are presented in Section 5.3. Our comparative analysis of total energy use and GHG emissions for the Dutch case study is given in Section 5.4. Section 5.5 concludes this chapter with the main findings and outlines future research directions.

5.2 Literature review

Various approaches are used in assessing energy use and GHG emissions from transport, differing in scope, background methodology, and assumptions. In this section, we provide a review of the literature on different approaches, focusing primarily on railway transport.

Life Cycle Assessment (LCA), as the most thorough method, encompasses the entire life cycle of a product, process, or activity, typically starting with the raw materials extraction and treatment, followed by construction/manufacture, operation, maintenance, down to end-of-life processes (Kapetanović et al., 2019). Traditionally product-oriented, LCA can provide a set of environmental impact indicators such as global warming potential, ozone depletion, human toxicity, and acidification (Curran, 2012). With local specifications typically not considered and assumed uniform conditions, assessing GHG emissions in such analysis could lead to biased conclusions, as they highly depend on the context and the case-specific energy sources (Nocera and Cavallaro, 2016).

While in some cases, the construction-related processes of railway infrastructure led to considerable environmental impacts (Banar and Özdemir, 2015; Stripple and Uppenberg, 2010), a number of LCA studies showed that GHG emissions that result from train production, maintenance, recycling and/or disposal usually have minor contribution when compared to the train operation stage (Andrade and D'Agosto, 2016; Chan et al., 2013; Del Pero et al., 2015; Shinde et al., 2018). This is mainly due to the relatively long service life of railway vehicles, which typically spans thirty or more years, and the required infrastructure considered as already in place. Regarding hybridized regional DEMU vehicles, which are the main subject in this chapter, an LCA study by Meynerts et al. (2018) on hybridized diesel vehicle with and without additional recharging stations showed that the operation phase accounts for the largest portion of emissions released over the vehicle's life cycle. They also reported a negligible impact from the production phase, mainly attributed to the battery production. The authors suggest that further progress could be made by increasing the efficiency in braking energy utilization and using green electricity for battery recharging.

A Well-to-Wheel (WTW) approach is a sub-class of the LCA, focusing on the vehicle operation phase and the life cycle of an energy carrier (e.g., diesel, electricity), commonly referred to as the fuel cycle. A WTW analysis is subdivided into the Well-to-Tank (WTT) phase, related to the production and distribution pathway of an energy carrier, and the Tank-to-Wheel (TTW) phase, linked to the energy expended and tailpipe emissions released directly by the vehicle over its drive cycle. Therefore, a clear distinction is made between the energy use and GHG emissions attributed to the primary energy source and the vehicle powertrain efficiency

(Nocera and Cavallaro, 2016). In contrast to the LCA approach, in which vehicle upstream and end-of-life stages are influenced by the processes of external parties, e.g., vehicle manufacturers, the WTW system boundary reflects the sphere of influence of transport operators where they can actively influence energy use and GHG emissions, for instance by employing novel propulsion systems and/or alternative transport fuels (Dreier et al., 2018). Moreover, European standards such as EN16258 (CEN, 2012) stipulate the WTW system boundary in calculating and declaring energy use and GHG emissions from transport while excluding other vehicle life cycle stages. Therefore, this study limits its analysis to the WTW system boundary.

Extensive research on WTW energy use and GHG emissions linked to alternative powertrain configurations and transport fuels has been carried out for cars (Küng et al., 2018; Yazdanie et al., 2016, 2014), buses (Dreier et al., 2018; Mao et al., 2020; Pourahmadiyan et al., 2021; Soukhov and Mohamed, 2022) and heavy-duty road transport (Gustafsson et al., 2021; Kuttler and Pichlmaier, 2021; Mojtaba Lajevardi et al., 2019). However, only a few studies have considered the railway sector.

Hoffrichter et al. (2012) evaluated WTW energy efficiency and CO_2 emissions linked to the electricity-, diesel- and hydrogen-powered trains using existing estimations in the literature and meta-analysis for each energy pathway component. They found that a fuel cell system running on hydrogen as a compressed gas obtained by steam methane reforming (SMR) features a WTW efficiency of 25%, comparable to diesel and electric scenarios in the UK and US. They suggest that the mentioned hydrogen fuel cell alternative could contribute to a CO_2 emissions reduction of approximately 19% compared to the diesel scenario and about 3% compared to US electricity. The case of diesel-based propulsion demonstrated that alternatives featured by a high WTW efficiency do not necessarily account for low emissions.

Esters and Marinov (2014) analysed different resistance-based methods for calculating emissions for various train types in the UK (conventional, high-speed, and freight) and propulsion systems (diesel, electric, and bi-mode). The results for a trip on a hypothetical flat and straight track indicated that diesel trains feature lower emissions compared to their electric counterparts as a consequence of the high carbon intensity of the electricity in the UK. Despite time efficiency, high-speed trains release more emissions due to the energy use being proportional to the square of speed. The authors also predict redundancy of bi-mode trains in the future, keeping in mind the electrification trends, and recommend biodiesel (blends) as an alternative to diesel fuel.

Gangwar and Sharma (2014) quantified the WTW emissions for diesel- and electricity-powered locomotives in India. Their study identified higher accumulated emissions for electric locomotives due to predominantly coal-based electricity production. The authors highlight the requirement of a well-balanced mix of both traction alternatives by considering different aspects such as environmental efficiency, economic sustainability, and equity.

Washing and Pulugurtha (2015) estimated WTW efficiencies of electric and hydrogen light rail in Charlotte, North Carolina (US). A fuel cell vehicle running on SMR-produced hydrogen showed WTW efficiency of 16.6–19.6%, while electric trains featured WTW efficiency of 25.3%. The authors attribute this difference to the inefficiencies of the fuel cell system and hydrogen production process and the significantly lower feedstock energy required by the electric trains. The study also confirmed the substantial influence of the main electricity production source on the efficiency of the electric train by observing other regions, i.e., 24.6% in Cleveland, Ohio (predominantly coal-based) and 50.3% in Portland, Oregon (predominantly hydroelectric power).

Railway-related WTW studies focus mainly on conventional (non-hybrid) powertrain topologies and biodiesel and/or hydrogen as the only alternatives to diesel fuel. Significant fuel savings from hybridization of diesel trains have been demonstrated in various European projects

(EC, 2005; Hillmansen et al., 2009, 2008; Marsilla, 2013) and studies (Cipek et al., 2019; Meinert et al., 2015a, 2015b). Despite the range of alternative fuels that emerged in the transport sector (Dincer et al., 2016; Dincer and Zamfirescu, 2016), no scientific study on the comparative assessment of WTW energy use and GHG emissions from the synergetic implementation of such solutions is available in the railway literature. In assessing the energy consumption, which directly influences the produced emissions, literature has contributed with simulation models such as ARTEMIS (Boulter and McCrae, 2007), EcoTransit (Knörr et al., 2018) and EcoPassenger (Knörr and Hüttermann, 2016). However, these models do not include hybrid configurations, featuring multiple power sources, their interaction, and simultaneous operation. Moreover, analysis of real-world cases requires consideration of numerous local factors that influence vehicle performance, such as track geometry, scheduled running times, passenger load, ambient conditions, etc.

5.3 Methodology

This chapter proposes a comparative assessment of energy demand and produced GHG emissions from implementing advanced propulsion systems combined with various alternative energy carriers in the regional railway transport. The following subsections provide a description of the general framework developed for assessing energy use and GHG emissions, the considered alternative propulsion systems including their modelling and control, the considered energy carriers and their production pathways, and external factors that influence the vehicle performance.

5.3.1 Framework for the assessment of overall energy use and greenhouse gas emissions

For assessing the overall energy use and produced GHG emissions, a WTW analysis is applied, allowing for a fair comparison between different scenarios by accounting for the energy use and emissions linked to both stages of WTT (energy carrier producing and distributing, e.g., from the feedstock extraction/harvesting to the fuelling station and/or pantograph) and TTW (energy use in the train during operation, e.g., from the onboard fuel storage system, pantograph and/or battery system to the motion power at the wheel). A WTW analysis is an effective tool for assessing the magnitude of the impact of measures instituted by decision-makers in a regional railway transport system (e.g., RUs), particularly for the estimation of energy use and GHG emissions reduction.

The WTW analysis in this chapter is based on a consumption-based approach (CEN, 2012; CLECAT, 2012; Kirschstein and Meisel, 2015). In this approach, the energy demand and GHG emissions are calculated from the fuel or electricity consumed in a vehicle operation, i.e., by multiplying the given amount with the corresponding energy and emission factors, respectively. To compare different energy carriers, the quantity of the energy used is expressed in a common unit of megajoule (MJ), while the quantity of GHG emissions is expressed in kilograms of CO_2 equivalents (kgCO_2e), accounting for the impact of all the main GHGs such as carbon dioxide (CO_2), methane (CH_4) and nitrous oxide (N_2O) (IPCC, 2007). With the measured or estimated fuel and/or electricity consumption, energy use and GHG emissions can be computed using the following relationships:

$$E_s = \sum_{i=1}^{n} C_i \cdot e_{s,i} \tag{5.1}$$

$$GHG_s = \sum_{i=1}^{n} C_i \cdot g_{s,i} \tag{5.2}$$

where

- E_s is the energy demand related to a particular scope $s \in \{\text{WTT, TTW, WTW}\}$, expressed in MJ, where $E_{\text{WTW}} = E_{\text{WTT}} + E_{\text{TTW}}$;
- C_i is the estimated powertrain consumption of energy carrier i during a trip, expressed in liters (l) for liquid fuels, kilograms (kg) for gaseous fuels, and kilowatt hours (kWh) for electricity;
- $e_{s,i}$ is the energy factor related to a scope s and energy carrier i, expressed in MJ/l, MJ/kg and MJ/kWh for liquid fuels, gaseous fuels and electricity, respectively, and where $e_{\text{WTW},i} = e_{\text{WTT},i} + e_{\text{TTW},i}$;
- GHG_s is the produced GHG emissions related to a scope s, expressed in $kgCO_2e$, where $GHG_{\text{WTW}} = GHG_{\text{WTT}} + GHG_{\text{TTW}}$;
- $g_{s,i}$ is the GHG emissions factor related to a scope s and energy carrier i, expressed in $kgCO_2e$/l, $kgCO_2e$/kg and $kgCO_2e$/kWh for liquid fuels, gaseous fuels and electricity, respectively, where $g_{\text{WTW},i} = g_{\text{WTT},i} + g_{\text{TTW},i}$;
- n is the total number of energy carriers used for train propulsion (maximum 2 in this study).

While the consumption-based approach is straightforward in ex-post evaluations for the transport that took place already with fuel consumption known, assessment of energy demand and emissions for potential future solutions requires the application of reliable forecasting models. This process is especially challenging for hybrid propulsion systems due to the simultaneous operation of multiple power sources. Therefore, this study proposes implementing a comprehensive simulation model for assessing the direct fuel and/or electricity consumption from train operation (TTW stage), which is then used to calculate primary (WTW) energy use and GHG emissions.

The methodological framework for estimating WTW energy use and GHG emissions is provided in Figure 5.1, with arrows indicating the information flow and/or computation sequence. The simulation model captures the main factors that affect vehicle dynamics and provides cumulative fuel and/or electricity consumption during the trip as the main output. The required inputs include rolling stock data (technical specifications of the vehicle and system components, implemented onboard energy management strategy), infrastructure characteristics (speed limits, track geometry, electrification status), train operation attributes (timetable and vehicle circulation plan), and external factors (vehicle occupancy and ambient conditions). The obtained direct fuel and/or electricity consumption is then coupled with corresponding energy use and GHG emissions factors using (5.1)-(5.2) to compute the energy use and GHG emissions linked to each TTW and WTT stage. Finally, the overall WTW energy use and produced GHG emissions are given as the sum of the TTW and WTT estimates.

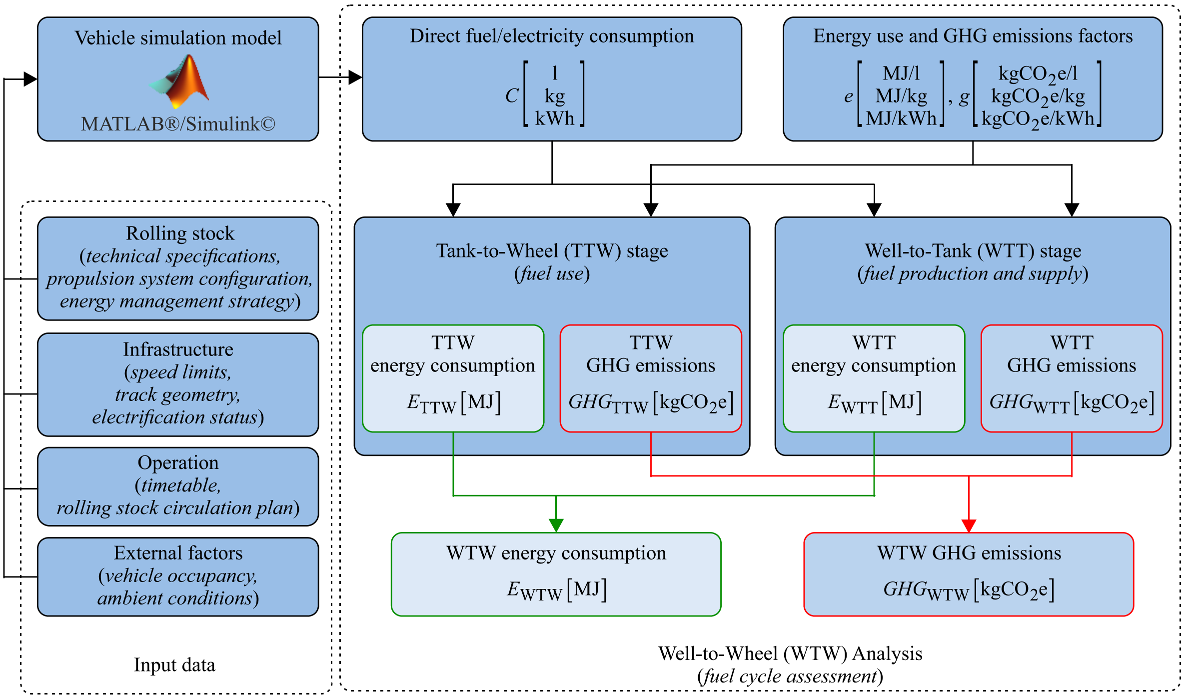

Figure 5.1: Methodological framework for the assessment of Well-to-Wheel energy use and greenhouse gas emissions of regional trains.

5.3.2 Alternative propulsion systems

In general, a propulsion system represents a set of different components that, through their interaction, provide motion power to the wheels (Spiryagin et al., 2014). This study focuses on diesel-electric multiple unit vehicles as the baseline, featuring a serial topology and electric transmission system in place. The presence of a DC link between the prime mover (i.e., engine-generator unit, EGU) and the electric motor allows for relatively simple hybridization and/or customization of the propulsion system configuration by adding and/or removing the power sources. Table 5.1 provides an overview of analysed alternative systems, with indicated corresponding power sources. Considered alternatives to a conventional diesel-electric system are hybrid-electric, plug-in hybrid-electric, fuel cell hybrid-electric, and battery-electric. Figure 5.2 shows the simplified schematic layouts of the five configurations considered in this chapter.

Table 5.1: Overview of alternative propulsion systems with corresponding power sources.

Propulsion system	**Power source**			
	Internal combustion engine	**Pantograph (external grid)**	**Fuel cell system**	**Energy storage system**
Diesel-electric	✓			
Hybrid-electric	✓			✓
Plug-in hybrid-electric	✓	✓		✓
Fuel cell hybrid-electric			✓	✓
Battery-electric		✓		✓

In a *conventional (diesel-electric)* system used as a baseline (Figure 5.2a), the EGU (ICE coupled with an AC electric generator) supplies an AC electric traction motor via a rectifier and an inverter, as well as the auxiliary onboard consumers such as heating, ventilation and air conditioning (HVAC) systems, lighting, compressors, etc. The gearbox located at the drive shaft transmits the output mechanical power of the motor to the wheels at a constant transmission ratio. In this system, regenerated braking energy provided by the motor is completely dissipated at the braking resistors, typically mounted on the roof of the vehicle.

Conversion to its *hybrid-electric* counterpart (Figure 5.2b) can be achieved by connecting an energy storage system (ESS) to the DC link via a bi-directional DC/DC converter. The ESS enables the recuperation of regenerative braking energy, which can support the ICE in supplying the traction and/or auxiliary consumers, eventually leading to an improved fuel economy compared to conventional (diesel-electric) vehicles. Various ESS technologies, such as batteries, supercapacitors, and flywheels, have emerged in the transport sector, featuring different benefits, limitations, and main applications (Ghaviha et al., 2017). Lithium-ion batteries are considered ESS technology in this study due to their rapid technology advancements, market availability, and ongoing implementation in the current Dutch fleet.

A *plug-in hybrid-electric* system (Figure 5.2c) requires the installation of a pantograph and accompanying power converter that complies with the electricity type (AC or DC) and voltage of the external grid, and adjusts the input voltage to the DC link. The system expands the functionalities of the aforementioned hybrid-electric system and the benefits of the ESS by providing additional charging directly from the external electric power grid during stabling periods (Meynerts et al., 2018). This potentially contributes to a further improvement of ICE fuel economy and the overall energy use and environmental performance.

A *fuel cell hybrid-electric* system (Figure 5.2d) can be obtained by replacing the prime mover in the hybrid-electric system, i.e., EGU and the corresponding AC/DC converter, with the hydrogen fuel cell stack and unidirectional DC/DC converter. Featuring a slow response and low dynamics, fuel cells require the implementation of an ESS that would cover high fluctuations in demanded power for traction and auxiliaries. Since fuel cells cannot absorb energy as ESSs, unidirectional converters protect the fuel cells from the high voltage at the DC link during braking phases by switching off. Hydrogen fuel cells offer various benefits compared to the ICE technology, reflected in higher efficiency, reduced noise and eliminated tailpipe emissions (both GHGs and local pollutants) (Sun et al., 2021).

In a *battery-electric* system (Figure 5.2e), the required power is provided either from the external grid via a pantograph, where available, or from the large battery ESS when the train runs on non-electrified track sections. The ESS is recharged from both the external grid and from the regenerative braking energy (Klebsch et al., 2020). Powertrain energy losses are fully attributed to inefficiencies of the electrical components, namely of the ESS, electric motors and power converters, which generally feature higher efficiencies than ICEs and fuel cell systems (Klebsch et al., 2019).

Other propulsion system configurations and operation modes, such as bi-mode or three-mode, are not considered, as they are derived from the five scenarios above, with expected estimations yielding within the intervals of the original systems. Furthermore, they would add a new dimension and increase the complexity of the present analysis. For instance, the performance of a bi-mode train (pure diesel vs. pure electric) highly depends on the length of the electrified track sections.

Note that in addition to the main powertrain components, vehicles might also differ in their fuel storage systems, depending on the energy carrier in use. While for liquid fuels such as biofuels, the same fuel tanks as for diesel can be used, gaseous and cryo-compressed fuels require the replacement of conventional fuel tanks with cylinders that comply with the requirements for their storage. The difference in vehicle weight between alternatives due to added and/or replaced components should be explicitly considered in the analysis, as it potentially influences the vehicle dynamics and overall performance.

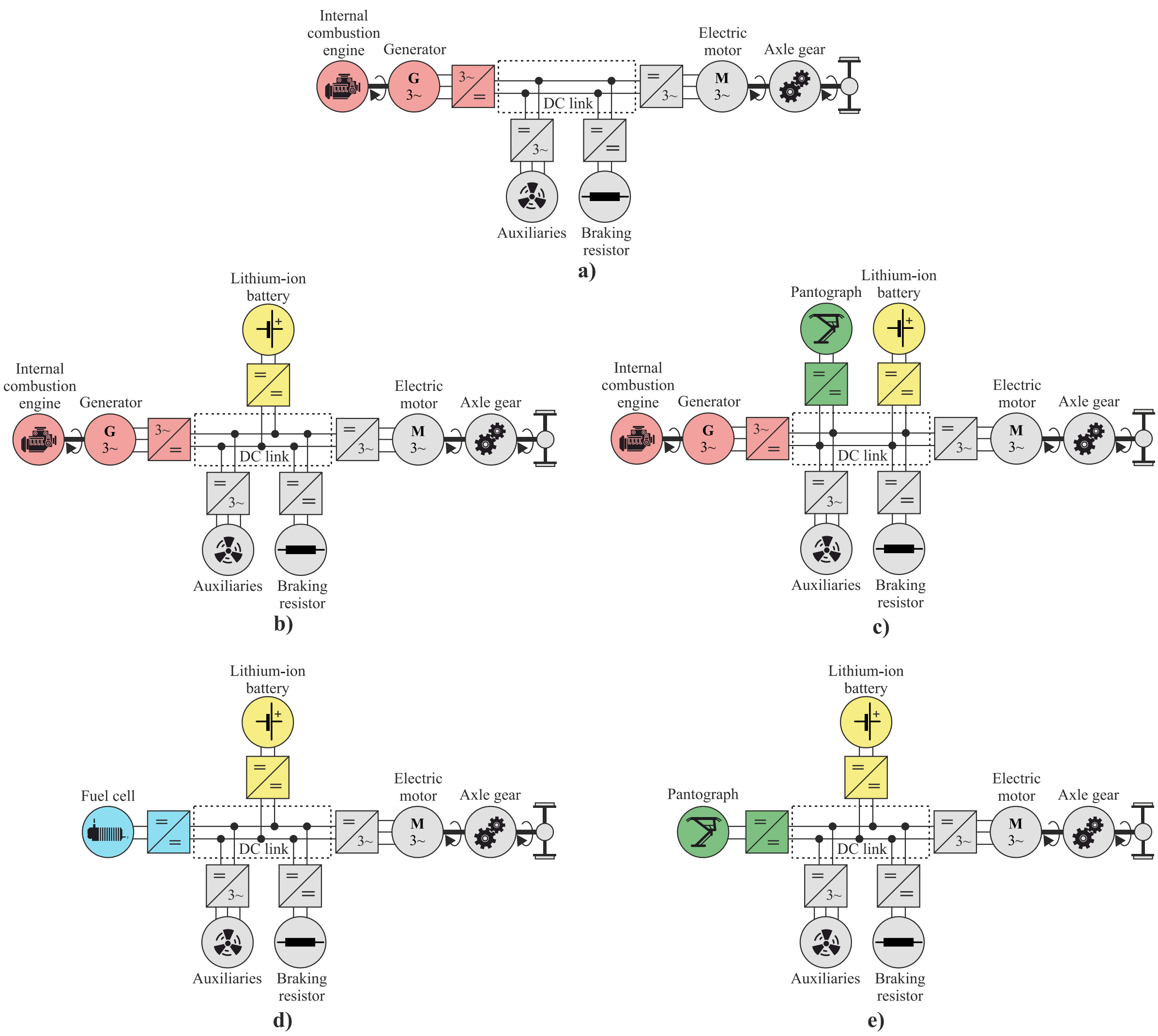

Figure 5.2: Schematics for alternative propulsion systems: (a) conventional (diesel-electric), (b) hybrid-electric, (c) plug-in hybrid-electric, (d) fuel cell hybrid-electric, and (e) battery-electric.

Modelling propulsion systems

A crucial step in assessing the WTW energy demand and GHG emissions is estimating the fuel and/or electricity consumption from train operation. This chapter uses a comprehensive simulation model built on a backward-looking quasi-static simulation approach (Pröhl, 2017b). The model is developed in MATLAB®/Simulink© (The MathWorks Inc., 2021) using the OPEUS Simulink library and simulation tool (Pröhl, 2017a) – an outcome of the knowledge accrued in European projects MERLIN (CORDIS, 2021), Cleaner-D (CleanER-D, 2020) and OPEUS (Shift2Rail, 2021). Compared to commercial simulation software such as LMS Imagine.Lab Amesim from Siemens (Schmid et al., 2017), its modular structure and programming environment allowed for relatively easy development or customization of railway vehicle's propulsion system configurations and onboard power management implementation (Pröhl, 2017c). The model was validated in a number of studies, c.f., Kapetanović et al. (2022, 2021a, 2021b), Leska et al. (2017), Meinert et al. (2015a, 2015b), Prohl and Aschemann (2019).

Figure 5.3 shows the structure of the backward-looking simulation model, with indicated low-order models of individual components, and the sequence of their evaluation opposed to the direction of the physical power flow. The alternative propulsion systems are simulated by disconnecting power sources not included in the respective system. The model captures technical characteristics and efficiencies of the system components, infrastructure and operation (timetable) attributes, and provides cumulative fuel and/or electricity consumption during the trip as the main output. As one of the main input signals, the energy-optimized velocity profile is pre-calculated using the bisection algorithm (Leska et al., 2013). The algorithm considers optimal transitions between the acceleration, cruising, coasting and braking phases, while complying with the scheduled running times, track geometry and speed limitations, vehicle weight, and maximum tractive/braking effort characteristics. According to the energy management and control strategy (EMCS), the control unit distributes the requested power for traction and auxiliaries between the power sources in place. For a detailed description of low-order models and implemented dynamic equations, readers are referred to the work of Kapetanović et al. (2022, 2021a, 2021b).

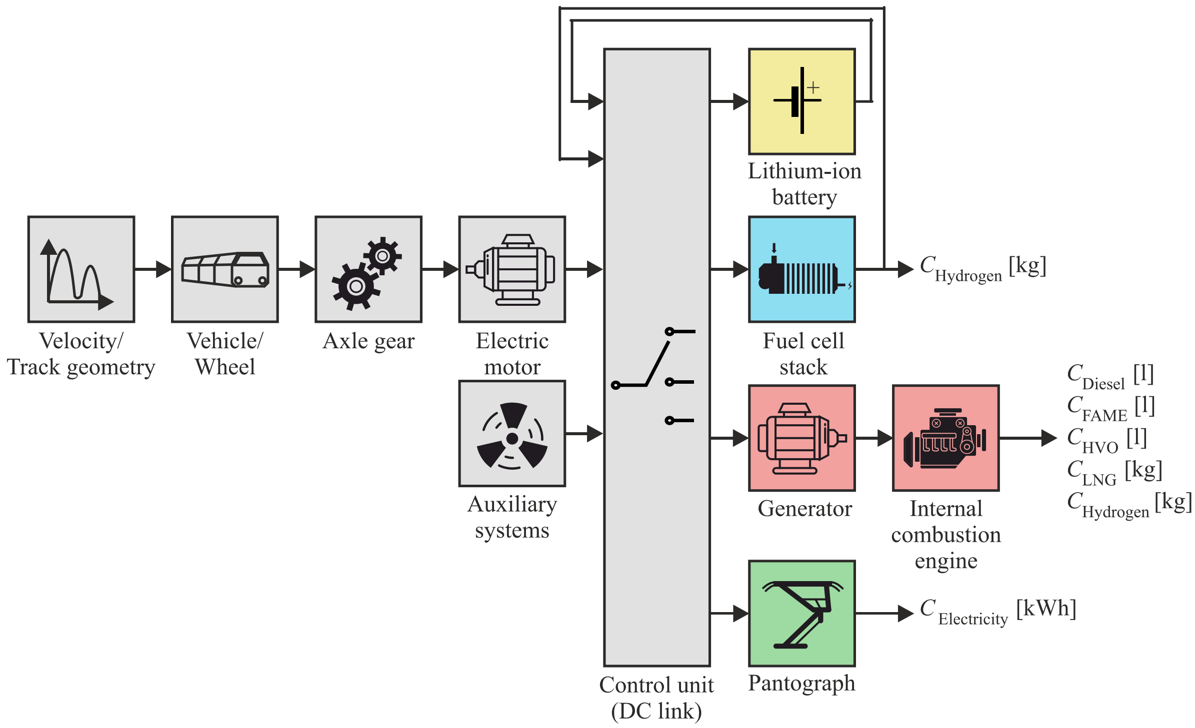

Figure 5.3: Structure of the backward-looking quasi-static simulation model for estimating cumulative fuel and/or electricity consumption of alternative propulsion systems.

Energy management and control strategy

While estimating system dynamics for conventional (diesel-electric) and battery-electric vehicles is straightforward, the main driver of fuel economy in hybrid vehicles is the implemented EMCS, i.e., how the requested power for traction and auxiliary consumers is distributed between the multiple power sources which operate simultaneously. To allow for realistic and achievable estimates, we adopt the real-time EMCS based on a finite state machine control (FSMC) for hybrid-electric, plug-in hybrid-electric and fuel-cell hybrid-electric vehicles from Kapetanović et al. (2022, 2021b). FSMCs offer relatively easy programmability of microcontrollers (Li et al., 2016), making them especially suited for the control of complex systems such as hybrid vehicle powertrains (Han et al., 2017; Yan et al., 2019).

Adopted FSMC allows the ESS to support the prime mover (EGU or fuel cell system) during high power demand (boost mode), e.g., during acceleration, while avoiding low load operation during coasting phases (load level increase mode), thus improving the overall efficiency of the prime mover. For hybrid-electric trains, it explicitly considers the emission-free and noise-free operation requirement in terminal stops with longer stabling periods by switching off the EGU and supplying the auxiliary systems solely from the ESS during the layover.

To assess the impact of the EMCS on energy performance, we introduce an alternative zero-emission station control (ZESC). This control is a simplified FSMC and reflects the strategy implemented in the current fleet. It also assumes ESS utilization in supplying the auxiliary systems in terminal stations with the ICE switched off. If needed, the ESS is charged primarily from regenerative braking energy, with additional energy provided from the EGU in the last track sections (load level increase mode). According to this strategy, the ESS provides no active support to the EGU (boost mode) during the vehicle trip. It should be noted that plug-in hybrid-electric, fuel cell hybrid-electric and battery-electric systems, by default, provide emission-free and noise-free trains operation at terminal stops.

5.3.3 Energy carriers

A range of energy carriers has emerged over the last decade(s) as alternatives to fossil diesel. For the present WTW analysis, the most prominent energy carriers are selected, considering their applicability to the railway sector and with respect to the 15-year analysis perspective. Considered energy carriers include biodiesel, commonly referred to as fatty acid methyl esters (FAME), as the first-generation biofuel; hydrotreated vegetable oil (HVO) as the second-generation biofuel; liquefied natural gas (LNG); hydrogen; and electricity. Although synthetic or e-fuels offer numerous benefits reflected in low emissions, compatibility with current ICE technologies, and no significant infrastructure requirements, they are expected to remain prohibitively expensive until 2050 (Agora Verkehrswende et al., 2018). Thus, they are omitted in this study.

For deriving the energy use and GHG emission factors for selected energy carriers and corresponding production paths, we reference the JEC's well-to-wheel report (JRC, 2020a, 2020b), as the latest and the most comprehensive source disposable. JEC is a product of collaboration between the European Commission's Joint Research Centre (JRC), European Council for Automotive R&D (EUCAR) and Conservation of Clean Air and Water in Europe (CONCAWE). In contrast to other widely used databases such as the North American GREET (Greenhouse gases, Regulated Emissions, and Energy use in Transportation) (ANL, 2020) and GHGenius (S&T, 2020), or UK's Defra (DEFRA, 2012), JEC's report encompasses data reflecting energy production pathways in Europe, which are pertinent to our research. Derived energy use and GHG emissions factors for the considered energy carriers are given in Table 5.2, with indicated primary sources and corresponding production and distribution paths. For comparing the impact of upstream processes for different energy carriers, Figure 5.4 shows (a) the WTT energy use per unit of energy content of a final fuel/electricity consumed in the TTW stage, e.g., energy used for the raw material extraction and processing, final fuel production and distribution, and energy losses due to electricity transmission, and (b) GHGs emitted from the use of fossil energy in these processes.

Considered diesel fuel is produced from crude oil from typical EU supply (mainly North Sea, North and West Africa), transported mainly by sea, refined in EU (marginal production), and with typical EU distribution (road tanker, pipeline, train or barge) and retail. Production and conditioning of crude oil at source contributes to about 50% of the overall WTT energy use and produced GHG emissions, followed by the refining processes (about 40%) (JRC, 2020b).

Compared to fossil fuels, biofuels are produced from renewable sources such as biomass, significantly reducing overall GHG emissions due to the CO_2 captured by plants during their growth. FAME produced from rapeseed (Rapeseed Methylester) as the main feedstock for biofuels in the EU, with meal export as animal feed, is considered. Rapeseed production, particularly rape cultivation, is a dominant contributor to the WTT GHG emissions, mostly through N_2O emissions associated with nitrogen fertilizer (JRC, 2020b).

Although HVO can be produced by deep-hydrotreating oils using the same feedstock as FAME, the use of HVO avoids the detrimental effects of ester-type biofuels (Aatola et al., 2009). In addition to the rapeseed-based HVO, we include the alternative production pathway based on processing waste cooking oil, which features significantly lower WTT energy demand and GHG emissions (see Figure 5.4). HVO produced from waste cooking oil also helps in addressing the land use issues, and is becoming an increasingly used alternative to fossil diesel by public transport companies (Neste, 2016).

Natural gas is the fossil fuel with the lowest GHG emissions, used either as compressed natural gas (CNG) or LNG. We limit our analysis to LNG as a preferred alternative for railway applications due to its advantages related to range, costs, volumetric space and refuelling requirements (Peredel'skii et al., 2005; Dincer and Zamfirescu, 2016). We consider LNG produced from remote natural gas liquefied at source (mainly the Arabian Gulf), LNG transported by sea and distributed by road.

Although hydrogen and electricity eliminate tailpipe GHG emissions, their production pathways can significantly reduce the potential benefits of their implementation (see Figure 5.4). Hydrogen can be used in both, ICEs (Deutz, 2021; MAN, 2020) and fuel cells (Sun et al., 2021), with steam methane reforming (SMR) and electrolysis of water being the main production alternatives. For the SMR scenario, we consider EU-mix piped natural gas transported by a 1900 km pipeline to the EU and 500 km inside the EU, distributed through high-pressure trunk lines and low-pressure grid, and reformed at the retail site using a small-scale reformer. For the electrolysis scenarios, either medium voltage electricity based on EU production mix for 2030 with retail site electrolysis, or electricity from wind energy with central electrolysis and pipeline transport are analysed. Finally, hydrogen compression to 88 MPa is considered in all scenarios.

Same as for hydrogen production, medium-voltage grey electricity with a predicted EU production mix for 2030 and green electricity produced from wind power are considered. As shown in Figure 5.4, wind power-based electricity is the only energy carrier that features net-zero GHG emissions while offering the lowest WTT energy use, resulting mainly from the distribution losses in the grid.

Table 5.2: Energy use and greenhouse gas (GHG) emissions factors for the considered energy carriers.

Energy carrier	**Energy use**				**GHG emissions**			
	Unit	e_{WTT}	e_{TTW} [g]	e_{WTW}	**Unit**	g_{WTT}	g_{TTW}	g_{WTW}
Diesel [a]	MJ/l	9.323	35.859	45.182	$kgCO_2e/l$	0.678	2.625	3.303
FAME [b]		36.750	33.108	69.858		1.602	0.000	1.602
HVO [c] (rapeseed)		38.438	34.320	72.758		1.781	0.000	1.781
HVO (waste cooking oil)		5.491	34.320	39.811		0.381	0.000	0.381
LNG [d]	MJ/kg	8.838	49.100	57.938	$kgCO_2e/kg$	0.815	2.769	3.584
Hydrogen [e] (SMR)		112.800	120.000	232.800		13.128	0.000	13.128
Hydrogen (elec. EU2030-mix)		326.400	120.000	446.400		14.232	0.000	14.232
Hydrogen (elec. wind)		104.400	120.000	224.400		1.140	0.000	1.140
Electricity [f] (EU2030-mix)	MJ/kWh	4.536	3.600	8.136	$kgCO_2e/kWh$	0.259	0.000	0.259
Electricity (wind)		0.252	3.600	3.852		0.000	0.000	0.000

Source: Energy use and GHG emissions factors adopted/derived from (JRC, 2020b):

a) Produced from crude oil from typical EU supply, transported by sea, refined in the EU (marginal production), and with typical EU distribution and retail. Diesel final fuel density is 0.832 kg/l.

b) Produced from rapeseed (Rapeseed Methylester) as the main feedstock for biofuels in the EU, with meal export as animal feed. FAME fuel density is 0.890 kg/l.

c) Produced from either rapeseed with meal export as animal feed, or from waste cooking oil. HVO fuel density is 0.780 kg/l.

d) Produced from remote natural gas liquefied at the source, LNG is transported by sea and distributed by road, used as LNG in the vehicle.

e) Produced from either SMR or electrolysis of water. For the SMR scenario, assumed EU-mix piped natural gas supply, transport to EU by pipeline (1900 km), transport inside EU (500 km), distribution through high-pressure trunk lines and low-pressure grid, small scale reformer at retail site, hydrogen compression to 88 MPa. For the electrolysis scenarios, production using either medium voltage electricity based on EU2030-mix with retail site electrolysis, or electricity from wind energy with central electrolysis and pipeline transport and hydrogen compression to 88 MPa in both scenarios.

f) Medium voltage electricity based on EU2030-mix, or produced from wind energy.

g) Represents low heating value (LHV) of a fuel.

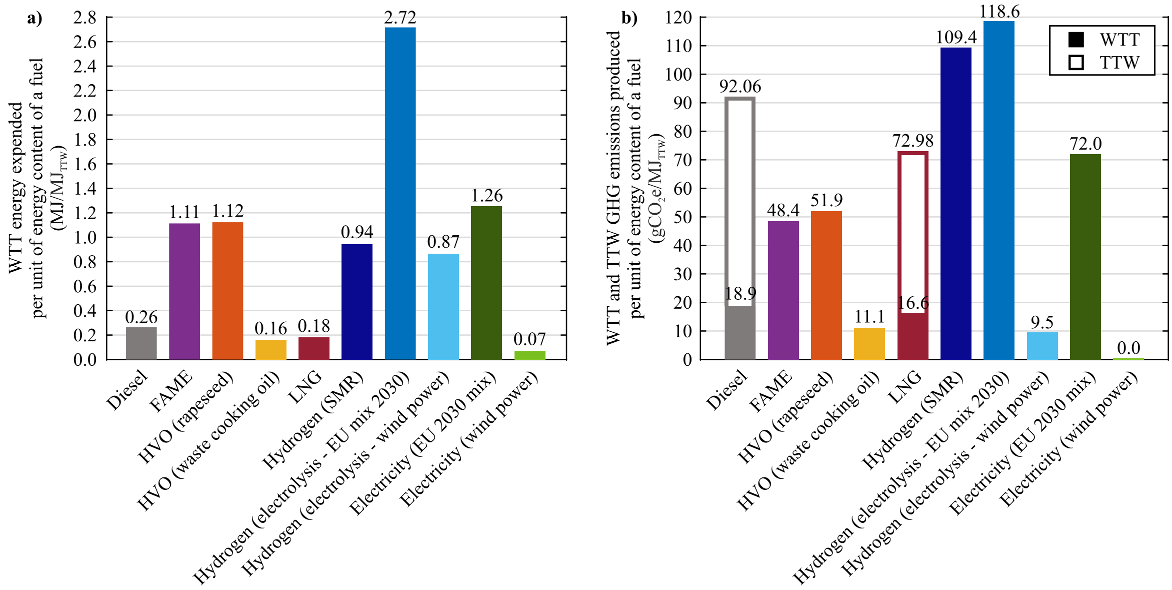

Figure 5.4: Well-to-Tank (WTT) (a) energy expended and (b) GHG emissions per unit of energy content of a fuel consumed in Tank-to-Wheel (TTW) stage.

5.4 Case study of the Dutch Northern lines

This section presents the application of the proposed methodology to a case study of the regional non-electrified railway network and multiple unit vehicles in the Netherlands. First, the input parameters are provided for the rolling stock, railway lines and passenger transport services, followed by a comparative assessment of different scenarios.

5.4.1 Rolling stock fleet

The rolling stock fleet of the Northern lines consists of three types of multiple units from the Swiss manufacturer Stadler (Figure 5.5). GTW (abb. for *Gelenktriebwagen*, in English, *articulated multiple-unit train*) DEMUs include two-coach GTW2/6 and three-coach GTW2/8 configurations (Stadler, 2005). Currently at their mid-life stage, with the foreseen operation until 2035, these vehicles are being retrofitted and hybridized with a lithium-ion battery ESS (Arriva, 2020). As of 2021, the fleet is being extended with bi-mode hybrid-electric DEMUs, based on the newly developed two-coach platform WINK (abb. for *Wandelbarer Innovativer Nahverkehrs-Kurzzug*, in English, *convertible innovative commuter short train*) (Stadler, 2020). These vehicles are already equipped with a pantograph, allowing for a bi-mode operation, and a lithium-ion battery ESS. The main characteristics of the rolling stock are given in Table 5.3.

The approach described in Section 5.3.2 is followed in further conceptual vehicles retrofitting to assess potential future powertrain solutions. Commercially available technologies with proven applications in the railway sector are selected while maintaining the vehicle weight limits to the current fleet to prevent exceeding the maximum axle load. We assume to maintain the number and attributes in terms of weight and rated power of ICEs and electric motors to those found in the current fleet in all considered scenarios. The efficiency maps of electric motors and generators are reconstructed using normalized efficiency maps provided by Paukert (2011) and Pröhl (2017b). Similarly sized diesel ICEs from the same sources are scaled to those found in GTWs and WINK vehicles by employing Willans lines technique (Pourabdollah et al., 2013), with the specific consumption maps for alternative fuels further linearly scaled according to the low heating value of the fuel (Kapetanović et al., 2022).

The current fleet is equipped with two battery packs based on SCiB™ technology from Toshiba (Toshiba, 2021). The present ESS configuration (size) is considered for hybrid-electric and plug-in hybrid-electric scenarios. Identical additional battery packs are considered for further vehicles conversion to their fuel-cell hybrid-electric and battery-electric counterparts. Fuel cell modules FCmove™-HD from Ballard (2021) are considered as the replacement technology for EGUs, with their number defined to satisfy gradeability power (Garcia et al., 2010), i.e., the power load at the DC link at the maximum constant speed (140 km/h). The maximum number of battery packs is then derived according to the remaining power and energy demand and overall weight limits. The maximum weight criteria is also adopted for determining the number of battery packs in battery-electric configurations.

Current fuel tanks are kept for the FAME and HVO scenarios, with their overall weight used as a benchmark for the LNG and hydrogen storage systems. Fuel tanks with 383 kg capacity from Enric (2021) are considered as LNG storage system, and Luxfer G-Stor™ H2, model W322H35 cylinders with 7.8 kg capacity, as the storage system for compressed hydrogen (Luxfer, 2020a, 2020b).

Finally, to assess the effects of the ongoing refurbishment and hybridization of GTW DEMUs, the analysis also includes the pre-refurbishment standard (diesel-electric) vehicles configurations. The list of vehicle parameters, number and characteristics of individual components used in the simulations are provided in Appendix B (Table B.1 and Figures

B.1-B.5). Due to the existence of a non-disclosure agreement with Stadler, some data are treated as confidential and marked as such.

a)
b)
c)

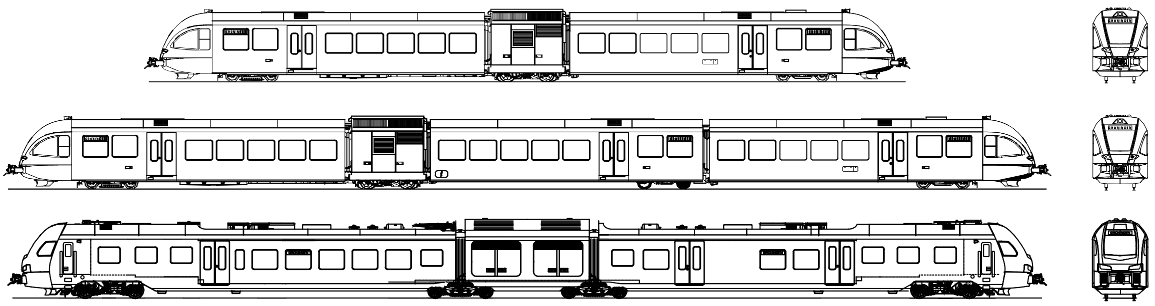

Figure 5.5: Graphical representation of Stadler's multiple unit vehicles employed on the Northern lines: (a) GTW 2/6, (b) GTW 2/8, and (c) WINK (Stadler, 2020, 2005).

Table 5.3: Main characteristics of multiple unit vehicles on the Northern lines.

Characteristic	**Vehicle**		
	GTW2/6	**GTW2/8**	**WINK**
Number of vehicles	14	37	18
Maximum speed (km/h)	140	140	140
Length (m)	40.890	55.937	55.550
Width (m)	2.950	2.950	2.820
Height (m)	4.035	4.035	4.120
Seating capacity	106	165	153
Maximum capacity (seating and standing)	196	295	273

Source: Stadler (2020, 2005); Personal communication with Arriva.

5.4.2 Regional railway network and passenger services

The Northern lines encompass a seven-branches rail network in the Dutch provinces Friesland and Groningen, providing sixteen passenger transport services, as shown in Figure 5.6. As can be noted, some services share the same route and terminal stations, yet differ in stopping patterns, e.g., at the Leeuwarden – Groningen line. This situation results in different duty cycles, corresponding power demand and energy consumption, linked to the same vehicle and route. Therefore, it is necessary to include all the services in the analysis to obtain overall performance. Furthermore, the simulations are carried out for both directions to account for the difference in track geometry, speed limits, running times, and layover times in terminal stops. The distance between stops and scheduled running times according to the current timetable provided by Arriva are given in Appendix B (Table B.2).

For the plug-in hybrid-electric system scenarios, we consider the installation of charging facilities in all twelve terminal stations (see Figure 5.6). For the battery-electric system scenarios, we consider the continuous partial tracks electrification starting from stations Leeuwarden and Groningen, as the only two stations connected to the rest of the electrified national railway network. Using the simulation model, the length of the electrified tracks is derived from the minimum number of electrified track sections required to maintain the ESS state-of-charge above the lower threshold for each vehicle series separately, as shown in Figure 5.7. To comply with the national traction power supply, a 1.5 kV DC system with 2 kA traction current (ProRail, 2020) is considered for both charging facilities and partial tracks electrification.

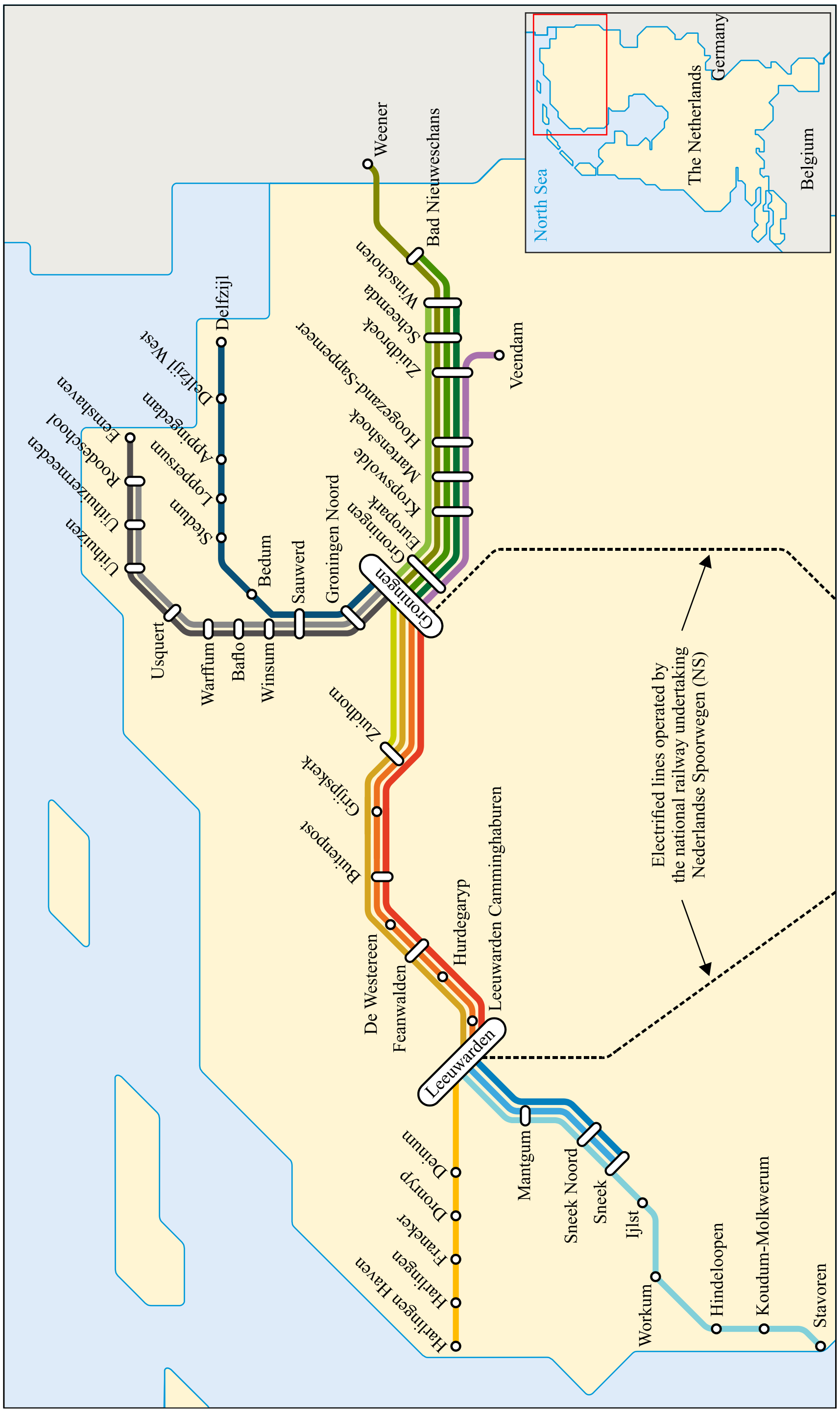

Figure 5.6: Regional railway network and passenger transport services in the Northern Netherlands.

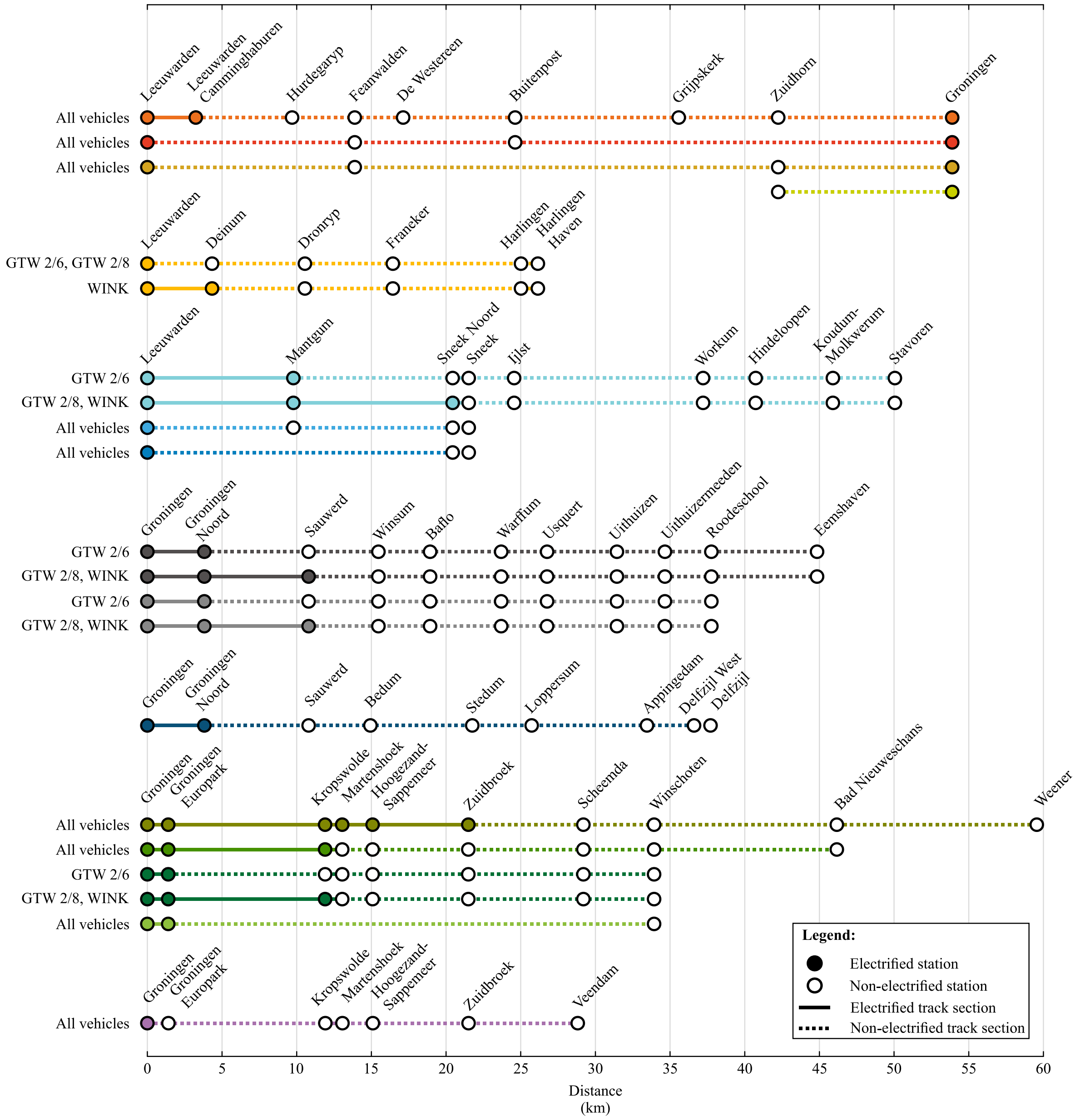

Figure 5.7: Required electrification for the operation of battery-electric regional trains for each vehicle series and transport service in the network.

5.4.3 Overview of scenarios and external factors

A schematic overview of the analysed scenarios is provided in Figure 5.8, indicating the pathways from the main energy sources through production processes into energy carriers (WTT), and their use with the respective propulsion systems and multiple unit vehicles (TTW). Within the WTT phase, different line colours are used to distinguish the considered energy carriers and corresponding alternative production pathways, presented in Section 5.3.3. For instance, different shades of blue denote the three hydrogen production scenarios, while different shades of green distinguish between the grey electricity based on the 2030 production mix for the EU and the green electricity produced from wind power. As depicted in the TTW stage, all six propulsion system configurations are evaluated for both GTW vehicle series, while the standard diesel-electric system is omitted for the new WINK vehicles, as these are manufactured as hybrids.

In addition to fixed factors such as track topology, external factors (for instance, ambient temperature and passengers load) have a degree of variability that can potentially have a great impact on the train's energy consumption (Bomhauer-Beins, 2019). The ambient conditions are taken into account via the auxiliary systems consumption (e.g., HVAC), provided by the vehicle manufacturer, where each vehicle trip is simulated separately for the summer and winter season operation. Furthermore, to assess the influence of the passengers load on vehicle's performance, each scenario is simulated separately for the case of an empty and fully loaded vehicle, with the weight of the vehicle kept constant during the trip.

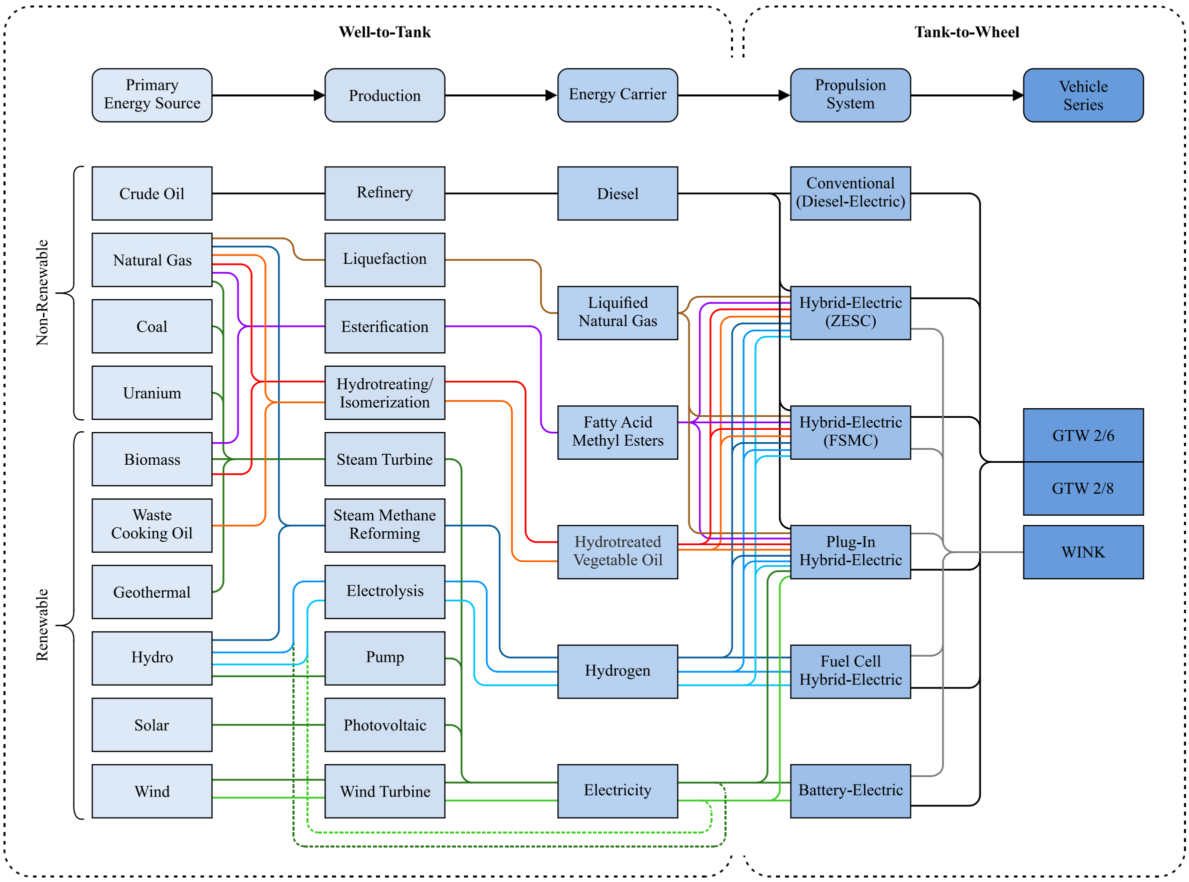

Figure 5.8: Overview of the analysed scenarios: primary energy sources, production processes and relevant energy carriers used in the propulsion of different powertrain configurations.

5.4.4 Comparative assessment results

This section presents the comparative assessment of alternative traction options for the analysed Dutch case study. Following the methodology presented in Section 5.3, the consumption of fuel and/or electricity for each vehicle, propulsion system, energy carrier, passenger load and ambient conditions scenario is computed for each individual trip using the simulation model (Appendix B: Tables B.3-B.5), and corresponding WTT, TTW and WTW energy use and GHG emissions are calculated using (5.1)-(5.2) (Appendix B: Tables B.6-B.11). Table 5.4 provides the summary of the estimated average fuel and/or electricity consumption per distance travelled from simulated trips in the Northern lines. In the following subsections, commonly used indicators of energy use and GHG emissions per distance (in MJ/km and kgCO_2e/km) and seat-distance (in kJ/skm and gCO_2e/skm) are derived to allow for the overall comparison between different scenarios.

Tank-to-Wheel stage

The overall (WTW) energy use and GHG emissions are directly proportional to the energy use in the TTW stage, with the efficiency of the individual components in the powertrain and the EMCS being the main drivers of the fuel economy. Table 5.5 provides the overall estimates of TTW energy use per distance and seat-distance for each considered scenario. To compare the TTW energy use associated with the alternative propulsion systems, the overall mean values are further aggregated over alternative energy carriers (Figure 5.9). The relative difference compared to the current hybrid-electric system with ZESC as a benchmark is derived (Figure 5.10).

The retrofit of conventional (diesel-electric) powertrains to their diesel-powered hybrid-electric counterpart with ZESC demonstrated positive effects on fuel economy, with estimated average direct energy use per distance and seat-distance reduced by 8.5% (from 35.5 MJ/km to 32.4 MJ/km, and 334.6 kJ/skm to 306.0 kJ/skm) for GTW 2/6 and 6.5% (from 38.1 MJ/km to 35.7 MJ/km, and 231.1 kJ/skm to 216.2 kJ/skm) for GTW 2/8 vehicles (see Table 5.5). Thus, significant economic benefits are obtained in addition to the emission-free and noise-free operation at terminal stops by switching-off ICEs and supplying auxiliary systems from the ESS, despite the increased overall vehicle weight.

As one of the potential future solutions, the implementation of FSMC instead of ZESC in hybrid-electric vehicles is associated with diverse impacts on fuel economy, depending on the vehicle series and energy carrier scenarios. While it resulted in the average energy savings of 0.54% for GTW 2/6 and 0.09% for GTW 2/8 vehicles, an increase of 3.38% is obtained for WINK vehicles (see Figure 5.10). The latter implies high energy demand for auxiliary systems during layovers, with the additional energy required from the ICEs for charging the ESS exceeding the benefits obtained from the enabled boost mode in this case, i.e., supporting the ICEs during acceleration phases by using stored regenerative braking energy.

The significant impact of train operation during layovers is most evident in the case of the plug-in hybrid-electric concept, where the external power grid is used for both supplying the auxiliaries and charging the ESS, thus providing additional energy to support the prime mover during trips. Compared to the baseline, the implementation of this system led to the average reduction of TTW energy use per distance and seat-distance of approximately 23%, 20%, and 13% for GTW 2/6, GTW 2/8 and WINK vehicles, respectively.

Despite the limitation of fuel cells reflected in slow dynamics, the fuel cell hybrid-electric system demonstrated a reduction of TTW energy use of approximately 10% for both GTW vehicles and 7% for WINK vehicles, mainly due to the higher energy efficiency of a fuel cell system compared to the ICEs. Lastly, the battery-electric system offered the highest reduction of direct energy use by approximately 66% for GTW 2/6, 65% for GTW 2/8, and 59% for WINK vehicles, with eliminated energy losses linked to inefficiencies of both ICE and fuel cell technologies.

Table 5.4: Overall estimates of fuel and/or electricity consumption from trains operation.

Vehicle	Prop. system	Energy carrier	Unit	Mean	Max	Min
GTW 2/6	DE	Diesel	l/km	0.989	1.595	0.723
	HE (ZESC)	Diesel		0.905	1.236	0.696
		FAME		0.979	1.334	0.753
		HVO		0.945	1.286	0.726
		LNG	kg/km	0.660	0.899	0.508
		Hydrogen		0.270	0.368	0.208
	HE (FSMC)	Diesel	l/km	0.900	1.236	0.699
		FAME		0.974	1.339	0.757
		HVO		0.941	1.292	0.730
		LNG	kg/km	0.656	0.903	0.510
		Hydrogen		0.268	0.369	0.209
	PIHE	Diesel / Electricity	l/km, kWh/km	0.560 / 1.368	0.823 / 4.004	0.179 / 0.280
		FAME / Electricity		0.605 / 1.367	0.888 / 4.004	0.196 / 0.280
		HVO / Electricity		0.586 / 1.356	0.859 / 4.004	0.205 / 0.280
		LNG / Electricity	kg/km, kWh/km	0.408 / 1.372	0.598 / 4.005	0.131 / 0.278
		Hydrogen / Electricity		0.167 / 1.362	0.245 / 4.004	0.054 / 0.280
	FCHE	Hydrogen	kg/km	0.243	0.391	0.187
	BE	Electricity	kWh/km	3.073	9.167	0.000
GTW 2/8	DE	Diesel	l/km	1.063	1.669	0.749
	HE (ZESC)	Diesel		0.995	1.304	0.734
		FAME		1.079	1.414	0.795
		HVO		1.039	1.361	0.767
		LNG	kg/km	0.729	0.952	0.536
		Hydrogen		0.298	0.390	0.219
	HE (FSMC)	Diesel	l/km	0.995	1.302	0.743
		FAME		1.078	1.410	0.804
		HVO		1.037	1.360	0.776
		LNG	kg/km	0.728	0.953	0.543
		Hydrogen		0.298	0.389	0.222
	PIHE	Diesel / Electricity	l/km, kWh/km	0.654 / 1.387	0.948 / 4.118	0.222 / 0.280
		FAME / Electricity		0.707 / 1.386	1.027 / 4.118	0.236 / 0.281
		HVO / Electricity		0.680 / 1.400	0.989 / 4.118	0.229 / 0.280
		LNG / Electricity	kg/km, kWh/km	0.478 / 1.381	0.692 / 4.118	0.163 / 0.280
		Hydrogen / Electricity		0.195 / 1.394	0.283 / 4.118	0.065 / 0.280
	FCHE	Hydrogen	kg/km	0.268	0.421	0.196
	BE	Electricity	kWh/km	3.465	9.936	0.000
WINK	HE (ZESC)	Diesel	l/km	1.263	1.591	0.898
		FAME		1.369	1.712	0.972
		HVO		1.319	1.657	0.938
		LNG	kg/km	0.921	1.157	0.655
		Hydrogen		0.378	0.472	0.268
	HE (FSMC)	Diesel	l/km	1.305	1.609	0.949
		FAME		1.416	1.739	1.027
		HVO		1.363	1.676	0.992
		LNG	kg/km	0.953	1.171	0.692
		Hydrogen		0.391	0.480	0.283
	PIHE	Diesel / Electricity	l/km, kWh/km	0.882 / 2.123	1.209 / 7.770	0.340 / 0.398
		FAME / Electricity		0.956 / 2.123	1.310 / 7.766	0.368 / 0.399
		HVO / Electricity		0.925 / 2.109	1.273 / 7.782	0.368 / 0.399
		LNG / Electricity	kg/km, kWh/km	0.645 / 2.115	0.883 / 7.766	0.247 / 0.399
		Hydrogen / Electricity		0.266 / 2.097	0.364 / 7.769	0.101 / 0.398
	FCHE	Hydrogen	kg/km	0.352	0.604	0.227
	BE	Electricity	kWh/km	5.121	16.689	0.000

Legend: DE = Diesel-electric, HE = Hybrid-electric, PIHE = Plug-in hybrid-electric, FCHE = Fuel cell hybrid-electric, BE = Battery-electric, ZESC = Zero-emission station control, FSMC - Finite state machine control, FAME = Fatty Acid Methyl Ester, HVO = Hydrotreated vegetable oil, LNG = Liquefied natural gas.

Table 5.5: Overall estimates of Tank-to-Wheel (TTW) energy use per distance and seat-distance.

Vehicle	Propulsion system	Energy carrier	Overall estimates per distance (MJ/km)			Overall estimates per seat-distance (kJ/skm)			Rel. range[a] (%)
			Mean	Max	Min	Mean	Max	Min	
GTW 2/6	DE	Diesel	35.468	57.201	25.943	334.600	539.636	244.743	88
	HE (ZESC)	Diesel	32.435	44.329	24.942	305.994	418.197	235.303	60
		FAME	32.397	44.152	24.932	305.631	416.524	235.205	59
		HVO	32.446	44.150	24.932	306.092	416.511	235.206	59
		LNG	32.401	44.147	24.931	305.667	416.477	235.202	59
		Hydrogen	32.399	44.149	24.945	305.652	416.497	235.328	59
	HE (FSMC)	Diesel	32.278	44.329	25.059	304.513	418.197	236.407	60
		FAME	32.242	44.334	25.050	304.166	418.241	236.322	60
		HVO	32.299	44.330	25.050	304.707	418.206	236.323	60
		LNG	32.193	44.328	25.053	303.709	418.187	236.345	60
		Hydrogen	32.186	44.334	25.065	303.646	418.247	236.461	60
	PIHE	Diesel / Electricity	25.021	34.037	15.749	236.044	321.106	148.576	73
		FAME / Electricity	24.938	34.084	15.737	235.265	321.548	148.466	74
		HVO / Electricity	25.007	33.948	15.748	235.920	320.260	148.566	73
		LNG / Electricity	24.955	33.990	15.751	235.423	320.658	148.595	73
		Hydrogen / Electricity	24.955	34.021	15.751	235.426	320.957	148.594	73
	FCHE	Hydrogen	29.180	46.918	22.413	275.284	442.620	211.440	84
	BE	Electricity	11.062	33.001	0.000	104.357	311.329	0.000	298
GTW 2/8	DE	Diesel	38.132	59.866	26.857	231.102	362.827	162.770	87
	HE (ZESC)	Diesel	35.665	46.764	26.318	216.154	283.416	159.506	57
		FAME	35.718	46.802	26.317	216.474	283.649	159.498	57
		HVO	35.669	46.724	26.320	216.175	283.175	159.517	57
		LNG	35.789	46.725	26.324	216.906	283.184	159.542	57
		Hydrogen	35.732	46.762	26.318	216.556	283.407	159.501	57
	HE (FSMC)	Diesel	35.671	46.675	26.632	216.189	282.878	161.408	56
		FAME	35.690	46.682	26.632	216.304	282.918	161.403	56
		HVO	35.602	46.678	26.637	215.771	282.899	161.438	56
		LNG	35.730	46.777	26.639	216.548	283.498	161.451	56
		Hydrogen	35.710	46.673	26.636	216.426	282.866	161.429	56
	PIHE	Diesel / Electricity	28.433	39.335	17.659	172.320	238.396	107.026	76
		FAME / Electricity	28.393	39.343	17.700	172.076	238.440	107.272	76
		HVO / Electricity	28.389	39.284	17.581	172.056	238.086	106.554	76
		LNG / Electricity	28.432	39.363	17.660	172.314	238.563	107.031	76
		Hydrogen / Electricity	28.379	39.369	17.680	171.992	238.602	107.152	76
	FCHE	Hydrogen	32.133	50.575	23.505	194.748	306.513	142.455	84
	BE	Electricity	12.475	35.769	0.000	75.605	216.784	0.000	287
WINK	HE (ZESC)	Diesel	45.281	57.059	32.195	295.955	372.936	210.423	55
		FAME	45.335	56.683	32.177	296.309	370.475	210.305	54
		HVO	45.271	56.858	32.188	295.889	371.619	210.380	54
		LNG	45.232	56.809	32.137	295.636	371.298	210.048	55
		Hydrogen	45.383	56.619	32.178	296.621	370.057	210.316	54
	HE (FSMC)	Diesel	46.789	57.708	34.035	305.808	377.174	222.452	51
		FAME	46.867	57.590	34.016	306.318	376.407	222.326	50
		HVO	46.776	57.518	34.033	305.725	375.934	222.438	50
		LNG	46.771	57.517	33.967	305.691	375.926	222.008	50
		Hydrogen	46.948	57.552	34.009	306.852	376.154	222.284	50
	PIHE	Diesel / Electricity	39.259	53.164	25.443	256.593	347.477	166.291	71
		FAME / Electricity	39.294	53.227	25.444	256.821	347.889	166.299	71
		HVO / Electricity	39.331	53.180	25.420	257.067	347.584	166.144	71
		LNG / Electricity	39.262	53.181	25.403	256.612	347.589	166.032	71
		Hydrogen / Electricity	39.463	53.191	25.420	257.928	347.651	166.147	70
	FCHE	Hydrogen	42.195	72.488	27.252	275.783	473.778	178.118	107
	BE	Electricity	18.437	60.079	0.000	120.504	392.675	0.000	326

Legend: DE = Diesel-electric, HE = Hybrid-electric, PIHE = Plug-in hybrid-electric, FCHE = Fuel cell hybrid-electric, BE = Battery-electric, ZESC = Zero-emission station control, FSMC - Finite state machine control, FAME = Fatty Acid Methyl Ester, HVO = Hydrotreated vegetable oil, LNG = Liquefied natural gas.

Note: [a] Calculated as $\big((\text{Max-Min})/\text{Mean}\big)\cdot 100\%$.

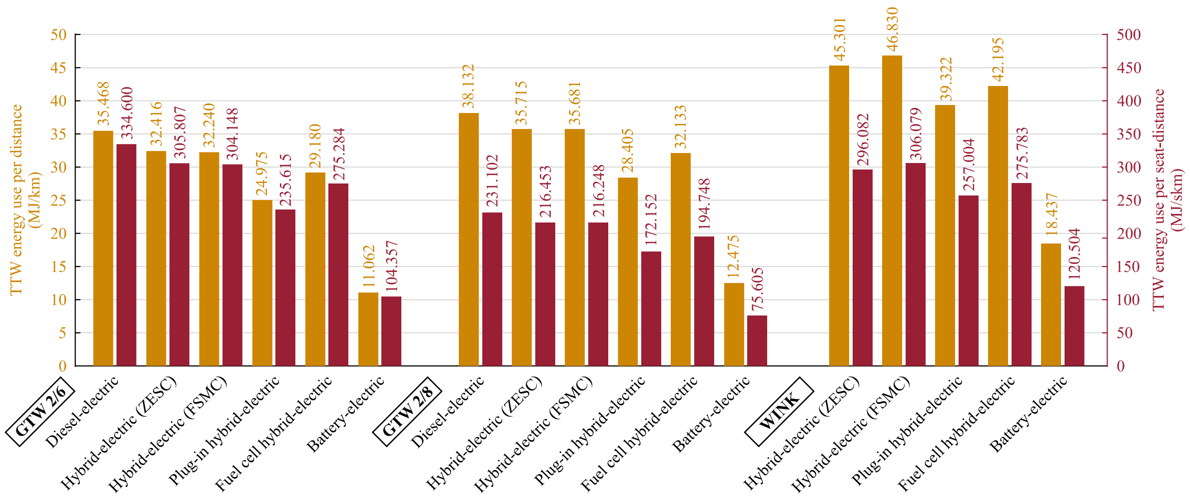

Figure 5.9: Tank-to-Wheel (TTW) energy use per distance and seat-distance for the multiple unit vehicles and corresponding propulsion systems, based on the overall mean values aggregated over alternative energy carriers.

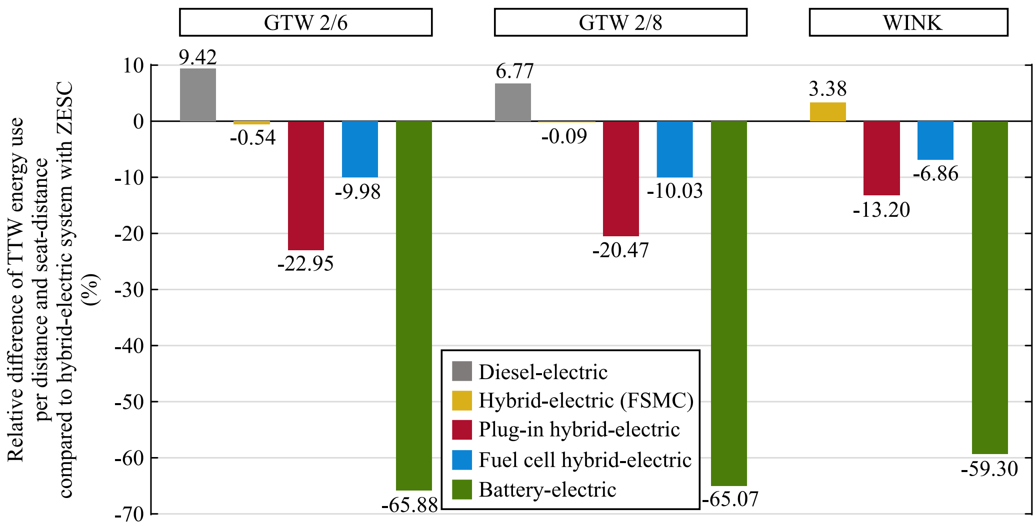

Figure 5.10: Comparison of Tank-to-Wheel (TTW) energy use between alternative propulsion systems, based on hybrid-electric system with ZESC as a benchmark, and the overall mean values aggregated over alternative energy carriers.

The selection of performance indicators is of high importance in calculating and reporting energy use and environmental impacts from trains operation, especially in the case of heterogeneous fleets. Figure 5.11 shows the relative difference in TTW energy use per distance and seat-distance travelled between different vehicle series, using GTW 2/6 as a benchmark. The two-coach GTW 2/6 multiple units showed the lowest energy use and GHG emissions in each scenario when estimates per vehicle-distance were used. With an identical propulsion system to that of GTW 2/6, the three-coach GTW 2/8 vehicles feature both higher weight and capacity, leading to higher energy use per vehicle-distance, but at the same time to the lowest estimates per seat-distance travelled among all three vehicle series. The new WINK vehicles feature the highest overall weight, power demand for traction and auxiliaries compared to GTW configurations, resulting in the overall highest average energy use per vehicle-distance, and diverse results if performance per seat-distance is considered.

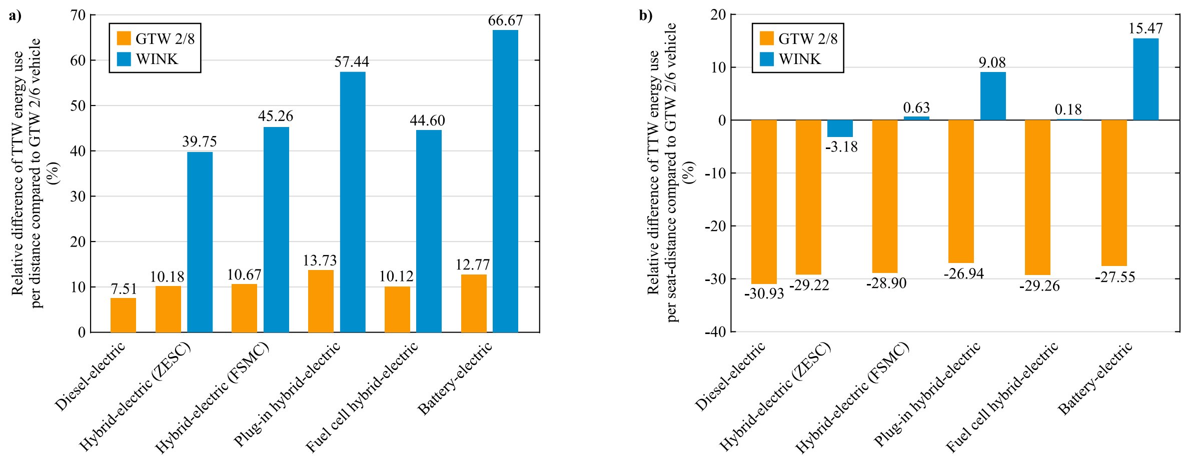

Figure 5.11: Comparison of Tank-to-Wheel (TTW) energy use between different vehicle series for the alternative propulsion systems, based on the overall mean values per (a) distance and (b) seat-distance, with GTW 2/6 as a benchmark.

Well-to-Tank stage

The estimations of overall (WTW) energy use and GHG emissions per vehicle-distance and seat-distance for each vehicle series, propulsion system and energy carrier scenario are shown in Figures 5.12 and 5.13, respectively, with distinguished WTT and TTW stages. In contrast to the TTW stage, the contribution of the WTT stage to the WTW energy use and GHG emissions depends on the energy carriers' primary source(s) and their production pathways (see Table 5.2 and Figure 5.4).

Regarding fossil fuels, the WTT stage has a minor contribution to both WTW energy use (diesel: 20.6%, LNG: 15.3%) and GHG emissions (diesel: 20.5%, LNG: 22.7%) when used in conventional and hybrid-electric vehicles. The influence of the primary energy source and production pathway is notable in the case of non-fossil fuels, for which WTT accounts for the overall GHG emissions. For instance, for hybrid-electric vehicles, the WTT stage contributes to 52.9% of HVO's WTW energy use if produced from rapeseed (similar to FAME: 52.6%), compared to 13.8% if HVO produced from waste cooking oil is used, which at the same time leads to 78.6% lower GHG emissions. Although both FAME and HVO from rapeseed have higher WTW energy use than considered fossil fuels, they significantly reduced overall GHG emissions in all scenarios.

The impact of the WTT stage on the overall estimates is most evident in the case of hydrogen, contributing to 48.5% (SMR), 73.1% (electrolysis using EU2030-mix electricity) and 46.5% (electrolysis using green electricity from wind power) of WTW energy use for hybrid-electric and fuel cell hybrid-electric scenarios. Hydrogen usage is associated with the increased WTW energy use in all scenarios compared to the baseline, with EU2030-mix-based electrolysis having the overall highest energy use. This production pathway and SMR also have the highest WTW GHG emissions in all scenarios, with only wind power electrolysis-based hydrogen leading to significantly reduced GHG emissions.

Regarding electricity used in battery-electric systems, the WTT stage contributes to 55.8% of overall energy use for EU2030-mix scenario, and only 6.5% for wind power-based production. Lastly, the contribution of the WTT stage in the case of plug-in hybrid-electric vehicles depends on the combination of fuel used with electricity and the associated production path.

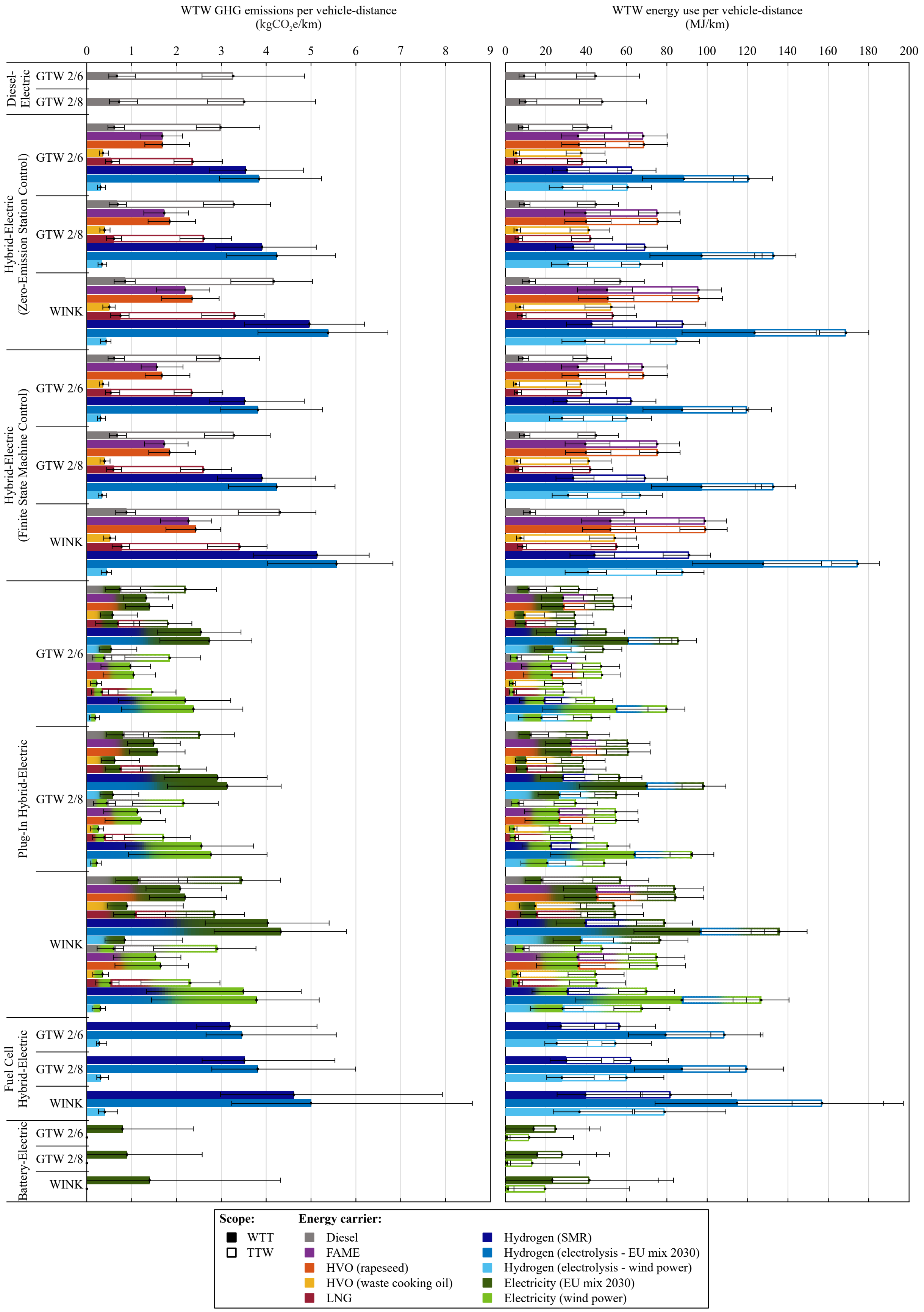

Figure 5.12: Well-to-Tank (WTT), Tank-to-Wheel (TTW) and Well-to-Wheel (WTW) estimations of energy use and greenhouse gas (GHG) emissions per vehicle-distance for regional multiple unit vehicles in the Northern lines.

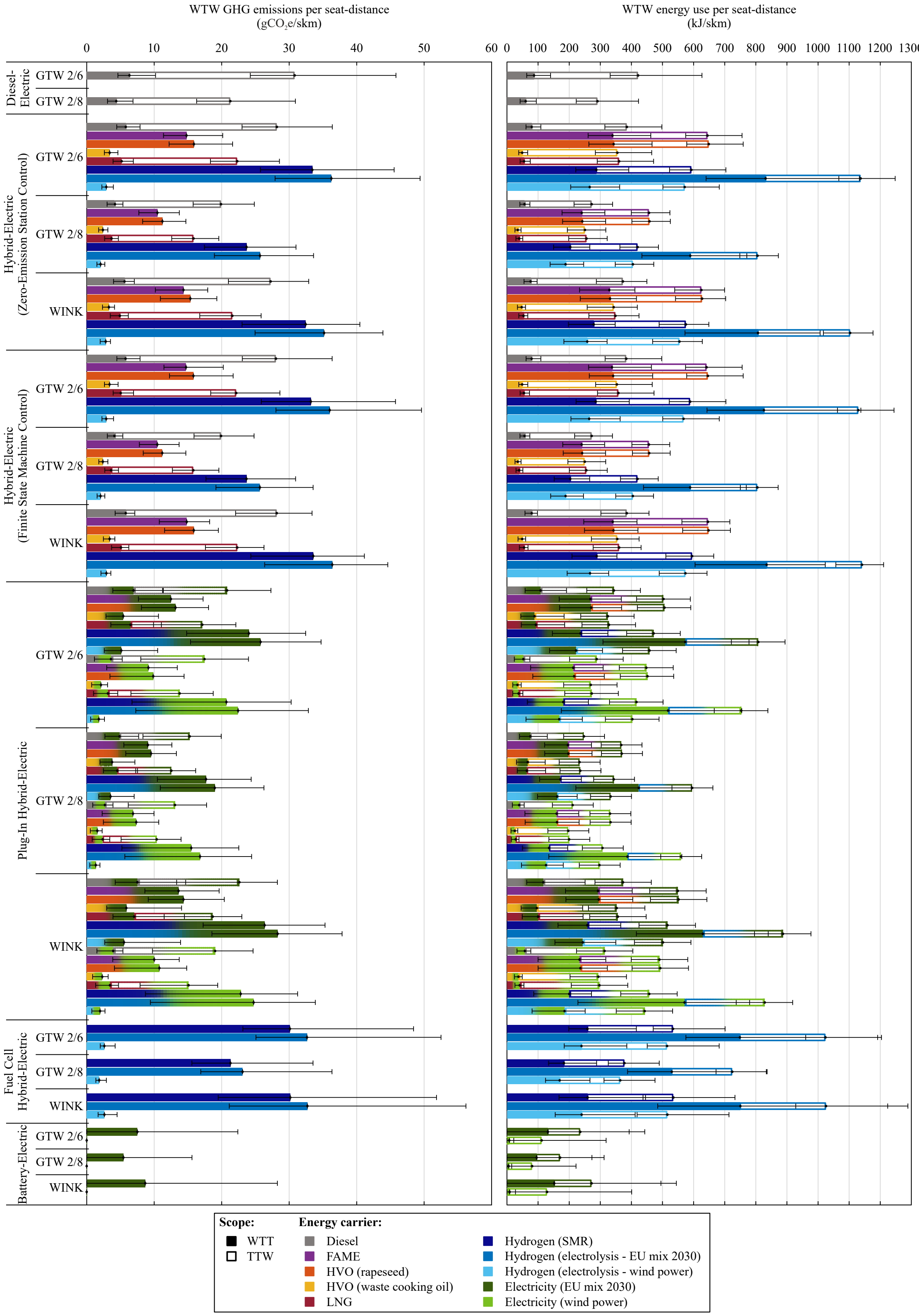

Figure 5.13: Well-to-Tank (WTT), Tank-to-Wheel (TTW) and Well-to-Wheel (WTW) estimations of energy use and greenhouse gas (GHG) emissions per seat-distance for regional multiple unit vehicles in the Northern lines.

Relative change of Well-to-Wheel energy use and greenhouse gas emissions

Using the present diesel-powered hybrid-electric system with ZESC as a benchmark, the relative change in WTW energy use and GHG emissions is derived using the overall mean estimates for each vehicle series, as shown in Figure 5.14 and Table B.12 (Appendix B).

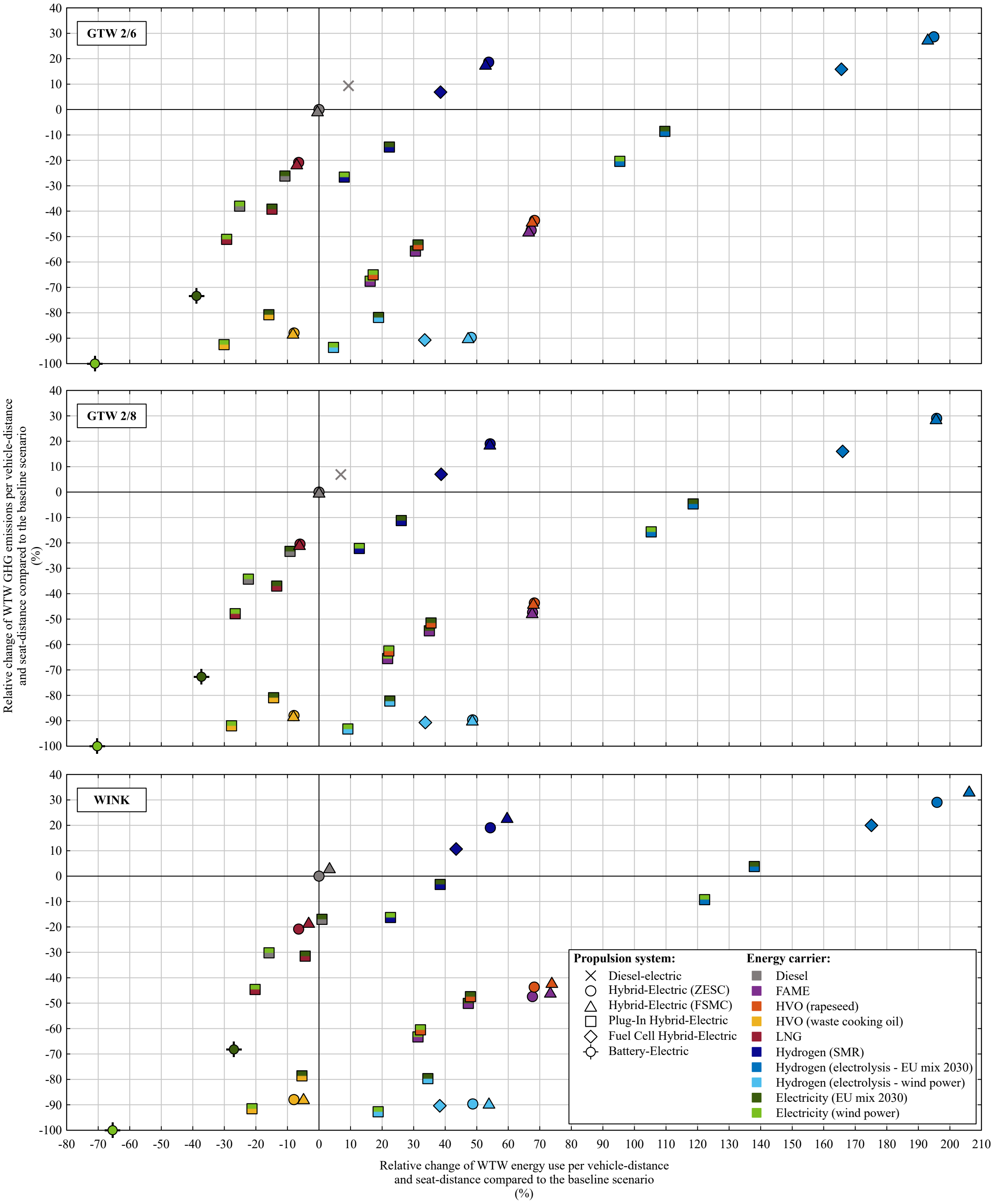

Figure 5.14: Estimated relative change in Well-to-Wheel (WTW) energy use and greenhouse gas (GHG) emissions per vehicle-distance and seat-distance compared to the baseline scenario (hybrid-electric vehicle with Zero-Emission Station Control (ZESC) and diesel as a fuel) for different multiple unit vehicles in the Northern lines.

When using wind power-based electricity, the battery-electric system is the only configuration leading to zero-emission train operation from the WTW perspective while at the same time offering the highest reduction of overall energy use by about 65-71%, depending on the vehicle series. When using electricity based on the EU2030 production mix, these savings are reduced to about 27-39% in WTW energy use and around 68-73% in WTW GHG emissions.

The plug-in hybrid-electric concept significantly reduced overall energy use and emissions when combining diesel, LNG or waste cooking oil-based HVO with electricity. The remaining configurations that reduce energy use and GHG emissions are hybrid-electric systems running on LNG or HVO from waste cooking oil. The latter leads to approximately 88% lower WTW emissions than the baseline for each vehicle type.

When produced from SMR or EU2030-mix-based electrolysis, hydrogen demonstrated negative effects in both aspects, irrespective of the prime mover technology, i.e., in both ICEs (hybrid-electric) or fuel cell systems. However, when produced via green electricity, it offers a GHG reduction of approximately 90% for hybrid-electric and fuel cell hybrid-electric configurations, with further reduction of up to 92-93% if combined with green electricity in plug-in hybrid-electric systems.

5.5 Conclusions

This chapter provided a comprehensive comparative assessment of WTW energy use and GHG emissions for various powertrain technologies for regional trains in the Netherlands, with considered range of energy carriers and their production pathways in the Dutch and European contexts. Emission-free and noise-free train operation in terminal stops is imposed as the main requirement in the design of alternative systems. As a critical step in ex-ante evaluations, direct fuel and/or electricity consumption is assessed in the vehicle operation (TTW) stage by employing a detailed backward-looking quasi-static simulation model for different rolling stock series and passenger services on the network. The obtained estimations are combined with various energy carriers' production pathways linked to the WTT stage in the comparative assessment.

Overall, the production pathway of the energy carrier is the most significant contributor to the overall energy use and produced emissions, followed by the efficiency of the powertrain. Due to eliminated energy losses linked to the inefficiencies of ICE and fuel cell technologies, the battery-electric system demonstrated the highest reduction of WTW energy use while offering zero-carbon trains operation if green electricity is used. However, this system requires partial track electrification in addition to the retrofit of vehicles.

Although recognized as a prominent long-term alternative to diesel for non-electrified railway networks, hydrogen adoption can be justified only if green hydrogen obtained from renewable sources is used. Fuel cell hybrid-electric configurations demonstrated more energy savings than hybrid-electric systems due to improved powertrain efficiency while eliminating local pollutants and noise emissions.

The plug-in hybrid-electric concept offers exploitation of external charging facilities in terminal stops, providing additional energy to support the ICEs during trips and thus improving overall efficiency. It performed better than the current hybrid electric system in all scenarios regarding WTW energy use and GHG emissions. In addition to green hydrogen and green electricity, HVO produced from waste cooking oil showed the highest energy savings and GHG emissions reduction in each corresponding scenario.

The outcomes of this study resulted in various valuable insights for policy makers and railway undertakings regarding potential measures to reduce WTW energy use and GHG emissions. In the short term, focusing on the energy carrier production pathway, as the main contributor to the overall energy and environmental performance, would be an effective approach. In this regard, fuels such as HVO from waste cooking oil could be considered an instantly implementable cost-effective transition solution toward carbon-neutral regional railways. Focusing on such ICE-based propulsion systems with infrastructure already in place would allow for significant positive effects in the short term while allowing for a smooth transition and development of supporting infrastructure required for more energy-efficient and environment-friendly technologies. Furthermore, depending on the performance indicator adopted, i.e., energy use and/or GHG emissions per vehicle-distance or per seat-distance, the estimations obtained in this study can serve as an input in planning the rolling stock deployment on the network, leading to improved overall energy efficiency and/or reduced carbon footprint of trains operation.

Future research efforts will take on a broader perspective on sustainability by applying Life Cycle Assessment (LCA) and Life Cycle Costing (LCC) methods while also considering policy mechanisms such as carbon taxes in facilitating the transition towards carbon-neutral railways operation.

Chapter 6

Conclusions

This thesis is devoted to improving environmental sustainability of regional railway services, with focus on the Dutch non-electrified regional railway network in the provinces Friesland and Groningen, commonly referred as the Northern lines. The main objective is to *identify and assess potential solutions in reducing overall (Well-to-Wheel) energy use and greenhouse gas emissions from the operation of regional trains, focussing primarily on alternative propulsion systems and energy carriers*. Several research questions were posed in Chapter 1 to achieve the research objective, which are answered throughout Chapters 2 to 5. In this chapter, Section 6.1 presents the main findings, while Sections 6.2 and 6.3 provide recommendations for practice and future research directions, respectively.

6.1 Main findings

To achieve the main research objective, five research questions were defined. The answers to these questions are summarized as follows.

– *How to model the dynamic behaviour of alternative propulsion systems and estimate corresponding energy consumption?* (Chapters 2-4)

  A backward-looking quasi-static simulation model is gradually developed throughout Chapters 2 to 4 to encompass various alternative (hybrid) propulsion systems for the conventional diesel-electric topology. First, the model of a hybrid-electric system with an internal combustion engine (ICE) as the prime mover coupled with a lithium-ion battery (LB) is introduced in Chapter 2. The model is further extended in Chapter 3 with a double-layer capacitor (DLC) as an alternative energy storage system (ESS) technology, together with implemented plug-in hybrid-electric concept. In Chapter 4, a fuel cell hybrid-electric system is introduced, with additional hybrid ESS configuration that combines both, LB and DLC technologies. Low-order models of individual main components (modules) along the traction chain are coupled with suitable energy management and control strategy (EMCS) to address the high complexity of hybrid systems reflected in simultaneous operation of multiple power sources. The requirement of emission-free and noise-free operation in terminal stations with longer stabling periods in incorporated in the design of both, propulsion systems and the EMCS.

The backward-looking approach enables estimation and comparative assessment of powertrain dynamics for a range of propulsion systems by capturing main, typically available vehicle, infrastructure and operation parameters influencing energy performance of a train. Energy-optimized velocity profile used as the main input for the simulation offers phased-out influence of the driver's behaviour, lower complexity and faster execution time compared to the forward-looking approach. Furthermore, in contrast to the energetic macroscopic representation approach it does not require field test data, which are often unavailable.

– *How to determine the optimal size of the energy storage system for a hybridized diesel-electric railway vehicle?* (Chapter 2)

In Chapter 2, a bi-level multi-objective optimization approach is developed for determining the optimal size of the LB-based ESS in a hybrid-electric vehicle, by integrating the ESS sizing and control optimization levels. The proposed framework includes most relevant design aspects, such as the requirement of achieving emissions-free and noise-free operation in stations, the trade-off (preference) between lower fuel consumption and hybridization cost, technical constraints related to battery voltage and maximum allowed mass, and the influence of the EMCS. Using derived LB parameters at the cell level, a nested coordination framework is employed, where a brute force search finds the optimal battery size using dynamic programming for full EMCS optimization for each feasible solution. In this way, the global minimum for fuel consumption for each battery configuration is achieved.

The results of a case study for selected vehicle, railway line and LB technology, demonstrated fuel savings and related greenhouse gas (GHG) emissions reduction ranging between 29.6% and 34.5% compared to the conventional diesel-electric vehicle, depending on the ESS size and configuration. A non-linear dependence between better fuel economy and lower hybridization cost is identified. When using an alternative sub-optimal rule-based control, these savings are reduced to 7%-19.2%, demonstrating a significant impact of the EMCS on the results, reflected in higher fuel consumption and increased LB size together with corresponding costs.

Overall, results indicated significant potential benefits of hybridization, while stipulating the need for the integration of different design and optimization levels, and further performance improvement of real-time controllers towards the global optimum. Although the focus of this study was on a particular case of diesel-electric multiple units and a specific Dutch scenario, the presented methodology allows for fair generalization and relatively easy adaptation to other railway networks and vehicles, regardless of the geographical context, vehicle and/or services type, ESS technology, etc.

– *What are the potential energy savings from the implementation of hybrid and plug-in hybrid propulsion system concepts in diesel-electric trains?* (Chapter 3)

In Chapter 3, a simulation-based analysis of hybrid and plug-in hybrid propulsion system concepts for diesel-electric multiple unit vehicles is presented. The analysis encompassed LBs or DLCs as alternative ESS technologies, and newly developed causal and easy-to-implement real-time power control for each concept. The proposed ECMSs are based on a finite state machine control (FSMC), with different states and corresponding transition triggers defined to satisfy the requirements of removing emissions and noise in terminal stops by switching off the ICE and supplying auxiliary systems from an ESS or electric power grid, and improving fuel economy by maximizing use of regenerative braking energy, avoiding low load ICE operation, and supporting ICE by an ESS during high power demand phases (acceleration).

The results for the benchmark vehicle and railway line showed considerable fuel savings compared to the conventional diesel-electric vehicle, leading to the GHG emissions reduction of 9.43–56.92% and direct energy costs reduction of 9.69–55.46%, depending on the type of service (express or stopping), energy storage technology selection (LB or DLC), electricity production (green or grey electricity), and charging facilities configuration (charging in terminal stations with or without additional charging possibility during short intermediate stops). Overall, positive effects from further conversion of a hybrid to a plug-in hybrid system were observed, with significant impacts of the stopping patterns (type of service), timetable, and the charging facilities configuration. The DLC-based ESS allowed for recuperation of total regenerative braking energy and ICE operation in the most-efficient region, providing notably better vehicle performance compared to the LB in all scenarios. However, the main criteria in sizing the ESS resulted in its high weight reaching almost 11 tonnes in this case, which requires further investigation of the practical implementability of such solution by including various physical constraints in the design process.

– *How to develop a conceptual design of hydrogen-powered propulsion systems for the conversion of diesel-electric trains?* (Chapter 4)

A conceptual design of hydrogen-powered propulsion systems for the conversion of diesel-electric trains is proposed in Chapter 4. An ICE and a fuel cell system are considered as the alternative prime mover configurations, coupled with LB, DLC or a hybrid ESS that combines both technologies. The analysis encompassed technology identification, design, modelling and assessment of alternative powertrains in terms of feasibility, fuel economy and produced emissions. Case-related constraints imposed by the infrastructure, technical and operational requirements are incorporated in the system design, while extending the simulation model and FSMC presented in Chapter 3 to the new system layouts. Slow dynamic response feature of a fuel cell system is coupled with estimated power and energy demand in sizing the ESS, with fuel cell system size derived from the gradeability power. The hydrogen storage system size is determined according to the requirement of a daily operation without refuelling. The feasibility of obtained propulsion systems is investigated by considering available weight and volumetric space constraints.

According to the comparative assessment results, the highest fuel-efficiency was obtained for the fuel cell-based hybrid propulsion systems with LB or a hybrid ESS. Additionally, the previous two configurations demonstrated the highest GHG emissions reduction compared to the benchmark diesel-driven vehicle, between 25.3-25.5% for hydrogen produced by steam methane reforming, and 19.2-19.4%, for hydrogen obtained through electrolysis of water. Remaining configurations are featured with higher hydrogen consumption, while at the same time requiring reduced fuel storage and thus reduced vehicle range. This brings the challenge of implementing efficient refuelling system comparable to that for diesel vehicles, which would prevent compromising timetable fulfilment and daily operation. Furthermore, transition to non-hybrid powertrain powered solely by hydrogen ICE demonstrated significant increase of GHG emissions compared to diesel baseline, confirming the necessity for hybrid systems implementation.

– *How to estimate Well-to-Wheel energy demand and greenhouse gas emissions from the implementation of alternative propulsion systems and energy carriers?* (Chapter 5)

  In Chapter 5, a framework for the estimation of Well-to-Wheel (WTW) energy use and GHG emissions attributed to the implementation of alternative propulsion systems in conjunction with a range of energy carriers is introduced. Considered alternative propulsion systems for a conventional diesel-electric vehicle include hybrid-electric, plug-in hybrid-electric, fuel cell hybrid-electric and battery-electric. Biodiesel, commonly referred as fatty acid methyl esters (FAME) as the first generation biofuel, hydrotreated vegetable oil (HVO) as the second generation biofuel, liquefied natural gas (LNG), hydrogen, and electricity are considered as alternative energy carriers to diesel. A bottom-up consumption-based approach is employed, with direct fuel and/or electricity consumption assessed in the Tank-to-Wheel (TTW) stage by employing a backward-looking quasi-static simulation model presented in Chapters 3 and 4, further extended with a battery-electric system, and a new simplified FSMC for hybrid configurations to reflect the current EMCS. Obtained estimations are then combined with various energy carriers' production pathways linked to the Well-to-Tank (WTT) stage in the overall comparative assessment using energy and GHG emission factors relevant for the Dutch and European context.

  The case study encompassed different multiple units and passenger services currently operated by Arriva in the Northern lines. Commercially available technologies are considered in the vehicles' conceptual retrofit to alternative propulsion systems, while maintaining the overall weight and tractive characteristics. Estimations are obtained for each vehicle and service, while including the influence of the external factors affecting energy consumption such as passenger load and ambient conditions. Overall, battery-electric is the only configuration leading to zero-emission trains operation from the WTW perspective when using wind power-based electricity, while at the same time offering the highest reduction of overall energy use by 65-71% compared to the current hybrid-electric system. Positive effects in both aspects are obtained for plug-in hybrid-electric concept in scenarios that combine the external charging in terminal stops with diesel, LNG or waste cooking oil-based HVO. Furthermore, reduction of both, energy use and GHG emissions is identified for hybrid-electric systems running on LNG or HVO from waste cooking oil, with latter leading to about 88% lower WTW emissions compared to the current system. Depending on the application, hydrogen offers the reduction of GHG emissions ranging between 90-93% if produced from electrolysis using green electricity. However, if produced from non-renewable sources, it demonstrated negative effects in both aspects, irrespective of the prime mover technology.

6.2 Recommendations for practice

This thesis has led to several practical recommendations that can be adopted by railway undertaking(s) and policy makers in planning energy-efficient and low or zero-emission railway transport. These recommendations are elaborated as follows.

The simulation model developed throughout Chapters 2 to 4 can be used in predicting the effects on energy efficiency and produced GHG emissions resulting from the implementation of various propulsion systems in conventional diesel-electric multiple units. It allows for a comprehensive comparative assessment of alternative traction options, providing a valuable input for decision-makers in the strategic planning of future rolling stock and low or zero-emission regional services. The modular structure enables relatively simple modifications of existing topologies, and further development of, for instance, bi-mode or three-mode systems. Furthermore, the easy manipulation of input parameters allows for considering powertrain components of different manufacturers. This can help in the essential economic and cost/benefit analysis in identifying optimal solution in terms of performance and costs.

In addition to the rolling stock planning, the model can help in assessing measures linked to the infrastructure and operations. Infrastructure measures can include, for instance, increasing the speed limits on some track sections, which may result in different speed profiles and corresponding energy consumption. Measures related to the trains operation may significantly impact the energy and environmental performance of railway services. These measures include, for example, modifications of railway services (line planning), adjustments of timetable and/or rolling stock circulation plans, etc. The model and methods developed in this thesis can also be employed in wider scope optimization frameworks, such as energy-efficient timetabling, that would integrate the energy and emissions performance in the planning process. It is important to note that implementing most of the measures discussed above involve multiple stakeholders, namely railway undertakings, infrastructure managers and vehicle/equipment manufacturers. Therefore, close collaboration between the stakeholders, information exchange, and overcoming data confidentiality issues is of utmost importance in achieving more environment-friendly regional railway transport.

The WTW analysis presented in Chapter 5 provides several valuable insights for policy decision-makers and railway operators regarding potential measures aimed at reducing overall energy use and GHG emissions. WTW approach allows for a fair comparison between different solutions by accounting for the energy demand and emissions linked to both stages of WTT and TTW. It is an effective tool in assessing the magnitude of the impact of the measures made by decision-makers in a regional railway transport system such as the adoption of novel propulsion systems and/or alternative transport fuels, while at the same time complying with European standards on calculation and declaration of energy use and GHG emissions from transport services. The production pathway of the energy carrier is identified as the most significant contributor to the overall energy use and produced emissions. Thus, focusing on this aspect and systems with infrastructure already in place could be an effective approach in reaching significant energy and GHG emissions savings in the short-term. In this regard, replacing diesel with fuels such as HVO from waste cooking oil could be considered as an instantly implementable cost-effective solution. This approach would facilitate a smooth transition toward more energy efficient and environment friendly solutions, while providing the time for novel technologies to mature and reach economy of scale required for their wider adoption, as well as the time required for the development of the supporting infrastructure.

6.3 Future research

This thesis provided the modelling and analysis of various potential solutions for improving environmental sustainability of regional railway transport. However, presented models and methods are subject to several limitations which require further research in order to improve the quality of the results. This section points out several directions for future research, which are elaborated as follows.

As identified, ECMS is the main driver of the fuel economy in hybrid vehicles. Therefore, a first suggestion for future research is to develop an optimization-based real-time EMCS that would provide fuel savings that converge to the global optimum. In this context, controls derived from dynamic programming can be used either to obtain a reference fuel consumption or to obtain optimal power split trajectories that can later be used in defining implementable real-time control strategies. Heuristic rule-based controls, or combining the equivalent consumption minimisation method with dynamic programming or optimal control theory are promising approaches in this regard. Special focus in modelling both the propulsion systems and EMCSs will be on incorporating real-life phenomena such as fuel cell deterioration and battery degradation due to aging, which can affect the system's performance.

Emissions from trains operation not only arise due to the fuel or electricity consumption, but also result from a number of direct and indirect sources, including vehicles/equipment production, infrastructure construction, and end-of-life activities such as recycling and/or disposal. Even though these activities are expected to have a minor contribution due to the high utilization and long useful life of railway vehicles, further investigation is needed in order to understand the overall environmental impact of a particular solution and technology. Therefore, a further step will be extending the scope of the analysis with remaining life cycle stages and other environmental impact indicators next to the GHG emissions in a detailed Life Cycle Assessment (LCA) study.

When rolling out a new traction concept, other investment costs will occur next to the direct (operational) energy-related costs. These monetary costs depend on a particular technology, required supporting infrastructure and corresponding lifetime, and include initial, maintenance, and replacement costs. To identify the overall costs and benefits in this investment decision process, a comprehensive Life Cycle Costs (LCC) analysis is required. Furthermore, integrating optimization algorithms in LCA and LCC studies can help decision-makers in solving design problems linked to the new traction concepts, for instance, in the development of an optimal tracks electrification layout for battery-electric trains, or in introducing vehicle-to-grid applications for battery-electric of fuel cell hybrid-electric vehicles.

Appendix A

Simulation results for standard, hybrid and plug-in hybrid regional railway vehicles

This appendix presents the simulation results for the case study in Chapter 3. Figure A.1 shows the vehicle speed profile, power profiles and resulting fuel consumption for a standard diesel-electric multiple unit vehicle. Simulation results for hybrid and plug-in hybrid multiple unit vehicle are visualized in Figure A.2 and Figure A.3, respectively.

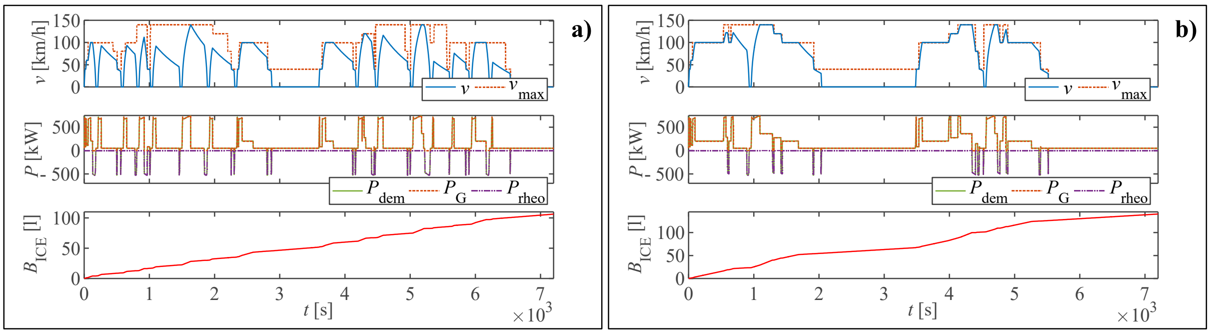

Figure A.1: Simulation results for a standard DEMU vehicle on (a) stopping service and (b) express service.

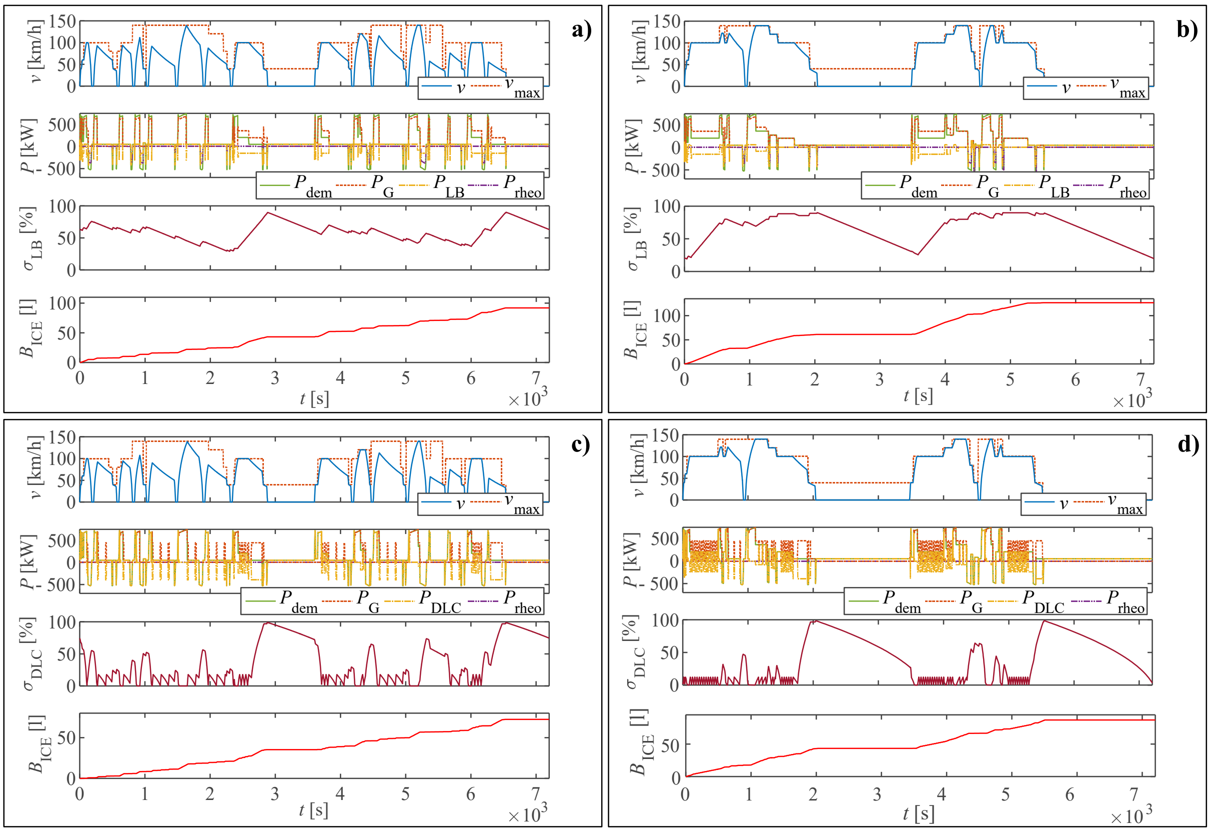

Figure A.2: Simulation results for a HDEMU vehicle on stopping and express service, respectively: (a-b) with LB ESS; (c-d) with DLC ESS.

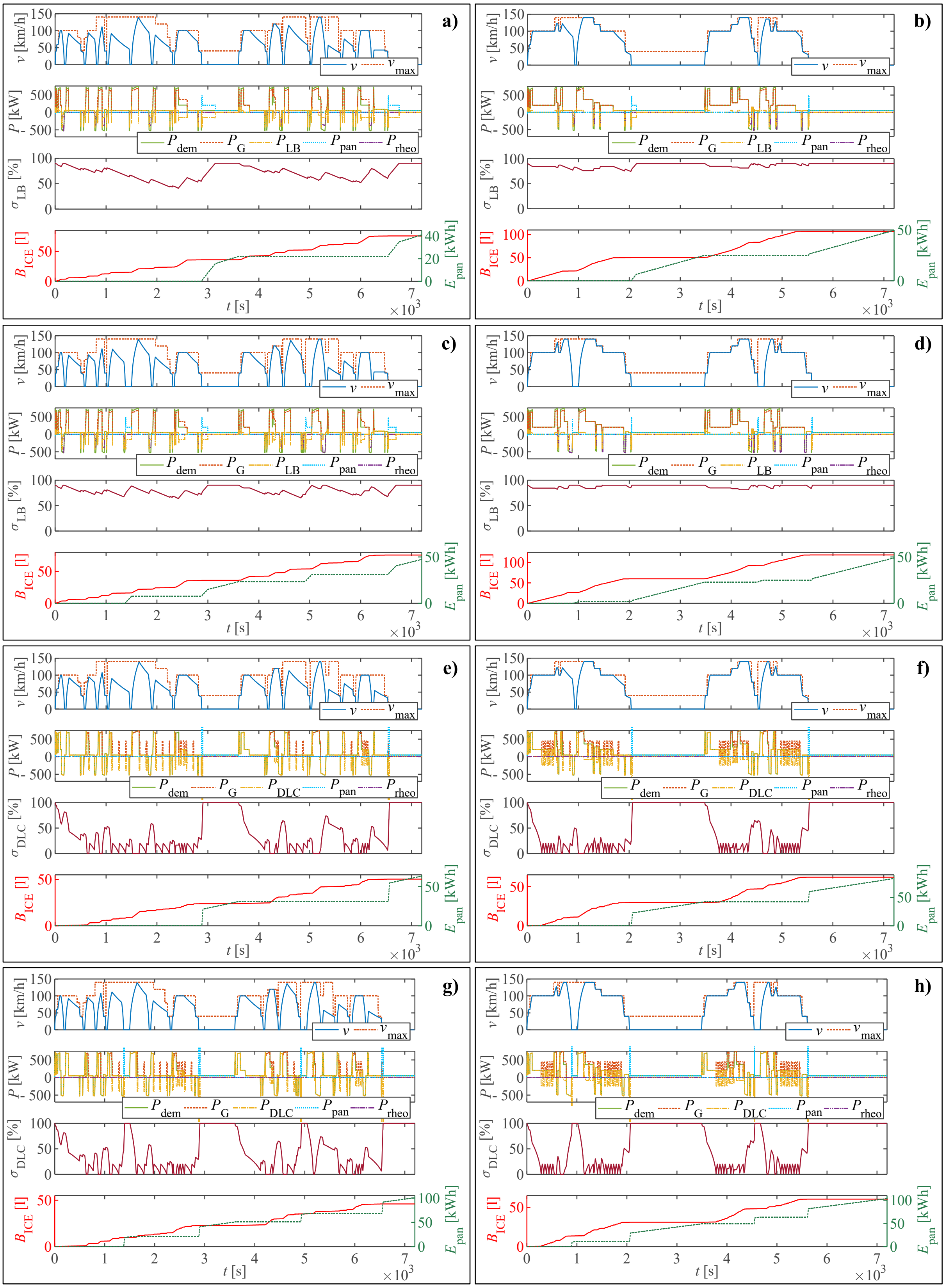

Figure A.3: Simulation results for a PHDEMU vehicle on stopping and express service, respectively: (a-b) LB ESS with charging at TSs; (c-d) LB ESS with charging at TSs and IS; (e-f) DLC ESS with charging at TSs; (g-h) DLC ESS with charging at TSs and IS.

Appendix B

Well-to-Wheel analysis input data and main results

This appendix presents the main input data and results for the case study in Chapter 5. Table B.1 lists vehicle parameters for different rolling stock series and propulsion systems used in the simulations. Figures B.1-B.5 visualize reconstructed maps and functions for the main powertrain components. The distance between stops, departure and arrival times for different passenger services are given in Table B.2. Estimated consumption of fuel and/or electricity for the analysed scenarios is provided in Tables B.3-B.5, for GTW2/6, GTW2/8 and WINK multiple unit vehicles, respectively. Tables B.6-B.11 show the overall estimates of WTT, TTW and WTW energy use, and WTT, TTW and WTW GHG emissions, respectively. Table B.12 provides the estimations of average relative change WTW energy use and GHG emissions compared to the baseline scenario.

Table B.1: Vehicle, propulsion systems and simulation parameters.

General vehicle parameters	GTW2/6	GTW2/8	WINK
Vehicle length [a,b]	40.890	55.973	55.500
Vehicle width [a,b] (m)	2.950	2.950	2.820 [c]
Vehicle height [a,b] (m)	4.035	4.035	4.120
Vehicle tare weight [d,e] (t)	-	-	-
Rotating mass factor [d,e] (%)	-	-	-
Davis equation coefficient (constant term) [d,e] (N)	-	-	-
Davis equation coefficient (linear term) [d,e] (N/(km/h))	-	-	-
Davis equation coefficient (quadratic term) [d,e] ($N/(km/h)^2$)	-	-	-
Powered wheel diameter [a,b] (m)	0.86	0.86	0.87
Axle gear ratio [d] (-)	-	-	-
Axle gear efficiency [d] (%)	-	-	-
Maximum velocity [a,b] (km/h)	140	140	140
Maximum acceleration [d] (m/s2)	-	-	-
Maximum deceleration [f] (m/s2)	-1	-1	-1
Number of seats [a,b,g]	106	165	153
Max. passengers capacity [g]	196	295	273
Passengers weight (max. occupancy) [h] (t)	13.720	20.650	19.110
Auxiliaries power (summer) [d] (kW)	-	-	-
Auxiliaries power (winter) [d] (kW)	-	-	-
Diesel generator set			
Internal combustion engine rated power [d] (kW)	-	-	-
Internal combustion engine weight [d] (kg)	-	-	-
Generator weight [d] (kg)	-	-	-
Fuel cell module			
Rated power [i] (kW)	70	70	70
Idle power [i] (kW)	8	8	8
Weight [i] (kg)	250	250	250
Lithium-ion battery			
Nominal capacity [d] (Ah)	-	-	-
Minimum/maximum continuous current [d] (A)	-	-	-
Minimum/maximum pulse current [d] (A)	-	-	-
Allowed time for pulse current [d] (s)	-	-	-
Minimum voltage [d] (V)	-	-	-
Maximum voltage [d] (V)	-	-	-
Internal resistance charge [d] (Ω)	-	-	-
Internal resistance discharge [d] (Ω)	-	-	-
Minimum SoC [d] (%)	-	-	-
Maximum SoC [d] (%)	-	-	-
Energy content [d] (kWh)	-	-	-
Weight [d] (kg)	-	-	-
Parameters depending on the propulsion system and/or energy carrier			
Number of engine-generator units			
Conventional, Hybrid-Electric, Bi-Mode Hybrid-Electric	2	2	2
Number of fuel cell modules			
Fuel Cell Hybrid-Electric	7	7	8
Number of lithium-ion batteries			
Hybrid-Electric, Bi-Mode Hybrid-Electric	2	2	2
Fuel Cell Hybrid-Electric	6	6	7
Battery-Electric	12	12	14
Empty fuel tank weight (kg)			
Diesel, FAME, HVO [d,j]	-	-	-
LNG [k]	990	990	1485
Hydrogen [l]	1692	1692	2820

(Table B.1 continued on the next page)

(Table B.1 continued from the previous page)

Total fuel weight (kg)			
Diesel, FAME, HVO [j]	-	-	-
LNG [k]	766.0	766.0	1149.0
Hydrogen [l]	93.6	93.6	156.0

Source/Note:

a) Stadler (2005).

b) Stadler (2020).

c) Width of the power module is 2.980m.

d) Obtained from internal communication with Stadler Bussnang AG. Information is subject to a Non-Disclosure Agreement (NDA).

e) Values provided for the current rolling stock, i.e. retrofitted hybrid-electric GTW and bi-mode hybrid-electric WINK vehicles. Vehicle tare weight is adjusted for each considered scenario according to the change in the propulsion system components. For plug-in hybrid-electric configuration, additional pantograph weight of 150kg is assumed for GTW2/6 and GTW2/8 vehicles. Rotating mass factor is inverse linearly scaled with the change in vehicle tare weight depending on the propulsion system configuration, while assuming no change in overall rotating masses. Mass-dependent constant and linear term in Davis equation are linearly scaled with the change in vehicle tare weight, with mass-independent quadratic term remained unchanged.

f) Assumed values.

g) Obtained from internal communication with Arriva Personenvervoer Nederland B.V.

h) Based on assumed average passenger weight of 70 kg.

i) Adopted/derived from Ballard (2021).

j) Current diesel fuel tank considered for FAME and HVO fuels. Total fuel weight calculated according to the fuels density with considered full tanks.

k) LNG fuel tanks with 383kg capacity and 495kg empty weight from Enric (2021). Considered 2 fuel tanks for GTW and 3 fuel tanks for WINK vehicles.

l) Luxfer G-Stor H2, model W322H35 cylinders with 7.8kg capacity and 141kg empty weight (Luxfer (2020a,2020b). Considered 12 cylinders for GTW and 20 cylinders for WINK vehicles.

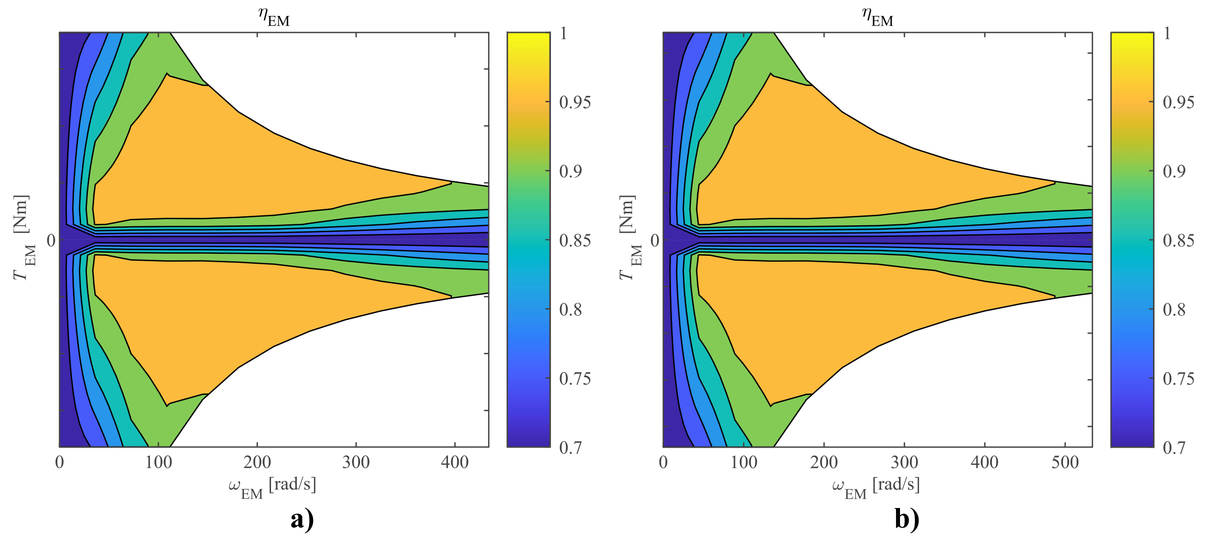

Figure B.1: Efficiency map of electric motor for (a) GTW2/6 and GTW2/8, and (b) WINK multiple unit vehicles.

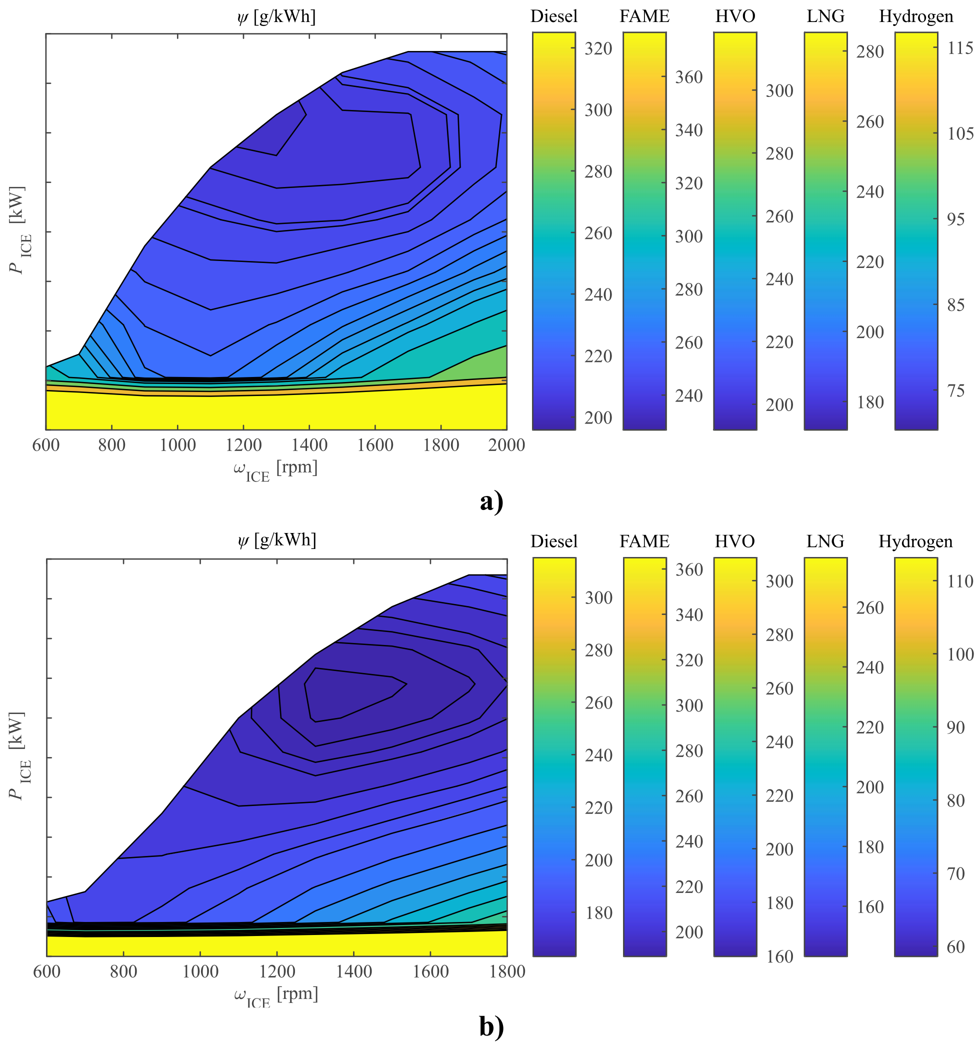

Figure B.2: Specific fuel consumption map for (a) GTW2/6 and GTW2/8, and (b) WINK multiple unit vehicles.

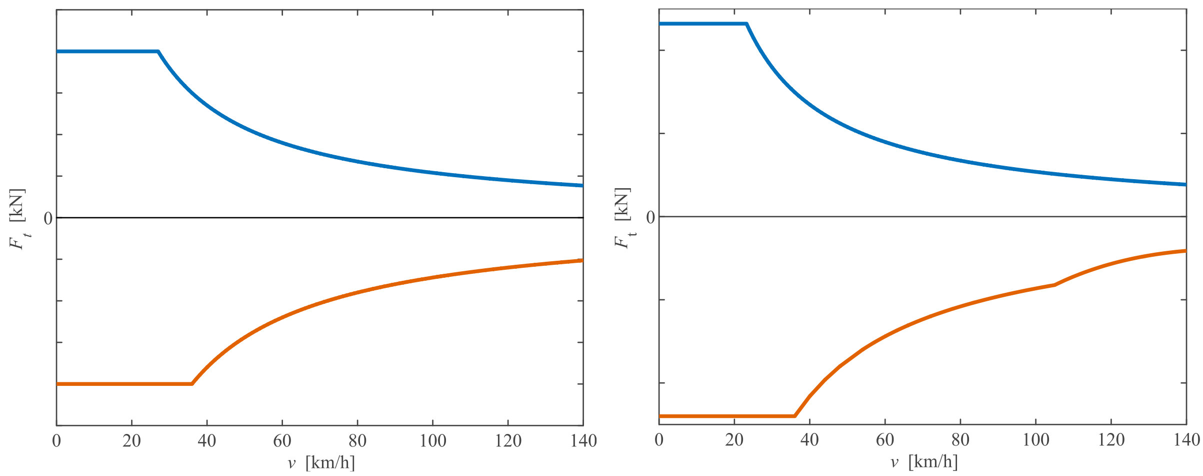

a) **b)**

Figure B.3: Maximum tractive effort (blue) and braking effort (orange) curve for (a) GTW2/6 and GTW2/8, and (b) WINK multiple unit vehicles.

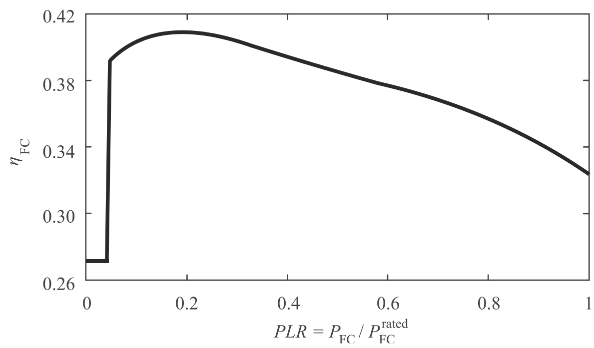

Figure B.4: Normalized efficiency function for fuel cell module.

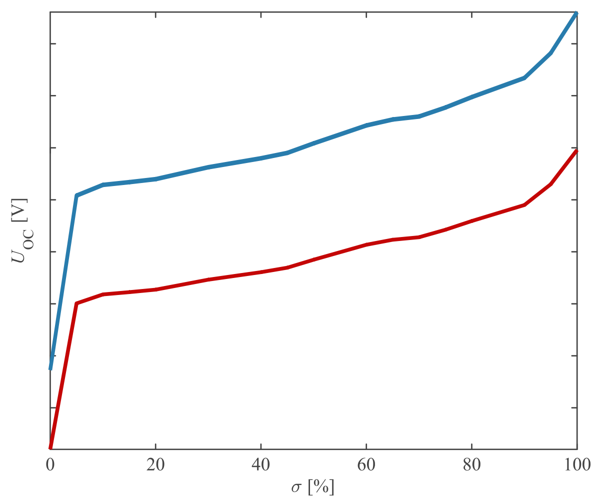

Figure B.5: Open circuit voltage as a function of battery state-of-charge for GTW2/6 and GTW2/8 (red), and WINK (blue) multiple unit vehicles.

Table B.2: Distance between stops, arrival and departure times for the passenger services in the Northern lines.

Stop	Distance (km)	Arrival (hh:mm:ss)	Departure (hh:mm:ss)	Stop	Distance (km)	Arrival (hh:mm:ss)	Departure (hh:mm:ss)
(1) Leeuwarden → Groningen (stopping)				(2) Groningen → Leeuwarden (stopping)			
Leeuwarden	0		hh:51:00	Groningen	0		hh:54:00
Leeuwarden Camminghaburen	3.242	hh:53:30	hh:54:00	Zuidhorn	11.647	hh:1:02:00	hh+1:03:00
Hurdegaryp	9.691	hh:59:00	hh+1:00:00	Grijpskerk	18.310	hh+1:07:30	hh+1:08:00
Feanwalden	13.886	hh+1:04:00	hh+1:05:00	Buitenpost	19.263	hh+1:15:00	hh+1:16:00
De Westereen	17.127	hh+1:07:30	hh+1:08:00	De Westereen	36.763	hh+1:20:30	hh+1:21:00
Buitenpost	24.627	hh+1:13:30	hh+1:14:00	Feanwalden	40.004	hh+1:25:00	hh+1:26:00
Grijpskerk	35.581	hh+1:20:30	hh+1:21:00	Hurdegaryp	44.199	hh+1:29:00	hh+1:30:00
Zuidhorn	42.243	hh+1:26:30	hh+1:27:00	Leeuwarden Camminghaburen	50.648	hh+1:35:30	hh+1:36:00
Groningen	53.890	hh+1:36:00	*hh+1:54:00*	Leeuwarden	53.890	hh+1:40:00	*hh+1:47:00*
(3) Leeuwarden → Groningen (express variant 1)				(4) Groningen → Leeuwarden (express variant 1)			
Leeuwarden	0		hh:17:00	Groningen	0		hh:39:00
Leeuwarden Camminghaburen	3.284	-	-	Zuidhorn	11.647	-	-
Hurdegaryp	9.733	-	-	Grijpskerk	18.310	-	-
Feanwalden	13.928	hh:25:00	hh:26:00	Buitenpost	29.263	hh:55:30	hh:56:00
De Westereen	17.169	-	-	De Westereen	36.763	-	-
Buitenpost	24.669	hh:32:30	hh:33:00	Feanwalden	40.004	hh+1:03:00	hh+1:04:00
Grijpskerk	35.623	-	-	Hurdegaryp	44.199	-	-
Zuidhorn	42.285	-	-	Leeuwarden Camminghaburen	50.648	-	-
Groningen	53.932	hh:51:00	*hh+1:09:00*	Leeuwarden	53.932	hh+1:13:00	*hh+1:21:00*
(5) Leeuwarden → Groningen (express variant 2)				(6) Groningen → Leeuwarden (express variant 2)			
Leeuwarden	0		hh:47:00	Groningen	0		hh:09:00
Leeuwarden Camminghaburen	3.284	-	-	Zuidhorn	11.647	hh:16:30	hh:17:00
Hurdegaryp	9.733	-	-	Grijpskerk	18.310	-	-
Feanwalden	13.928	hh:55:00	hh:56:00	Buitenpost	29.263	-	-
De Westereen	17.169	-	-	De Westereen	36.763	-	-
Buitenpost	24.669	-	-	Feanwalden	40.004	hh:33:00	hh:34:00
Grijpskerk	35.623	-	-	Hurdegaryp	44.199	-	-
Zuidhorn	42.285	hh+1:11:30	hh+1:12:00	Leeuwarden Camminghaburen	50.648	-	-
Groningen	53.932	hh+1:21:00	*hh+1:39:00*	Leeuwarden	53.932	hh:43:00	*hh:51:00*
(7) Zuidhorn → Groningen				(8) Groningen → Zuidhorn			
Zuidhorn	0		hh:57:00	Groningen	0		hh:24:00
Groningen	11.647	hh+1:06:00	*hh+1:24:00*	Zuidhorn	11.647	hh:33:00	*hh:57:00*
(9) Leeuwarden → Harlingen Haven				(10) Harlingen Haven → Leeuwarden			
Leeuwarden	0		hh:20:00	Harlingen Haven	0		hh:12:00
Deinum	4.332	hh:24:30	hh:25:00	Harlingen	1.114	hh:15:00	hh:16:00
Dronryp	10.549	hh:30:00	hh:31:00	Franeker	9.681	hh:23:00	hh:24:00
Franeker	16.438	hh:36:00	hh:37:00	Dronryp	15.600	hh:29:00	hh:30:00
Harlingen	25.019	hh:44:30	hh:45:00	Deinum	21.817	hh:35:30	hh:36:00
Harlingen Haven	26.149	hh:48:00	*hh+1:12:00*	Leeuwarden	26.149	hh:41:00	*hh:50:00*
(11) Leeuwarden → Sneek (stopping)				(12) Sneek → Leeuwarden (stopping)			
Leeuwarden	0		hh:53:00	Sneek	0		hh:18:00
Mantgum	9.776	hh+1:00:00	hh+1:01:00	Sneek Noord	1.077	hh:20:00	hh:21:00
Sneek Noord	20.440	hh+1:08:00	hh+1:09:00	Mantgum	11.741	hh:29:00	hh:30:00
Sneek	21.517	hh+1:12:00	*hh+1:18:00*	Leeuwarden	21.517	hh:38:00	*hh:53:00*

(Table B.2 continued on the next page)

(Table B.2 continued from the previous page)

(13) Leeuwarden → Sneek (express)				(14) Sneek → Leeuwarden (express)			
Leeuwarden	0		hh:07:00	Sneek	0		hh:06:00
Mantgum	9.776	-	-	Sneek Noord	1.077	hh:08:00	hh:09:00
Sneek Noord	20.440	hh:21:00	hh:22:00	Mantgum	11.741	-	-
Sneek	21.517	hh:25:00	*hh:36:00*	Leeuwarden	21.517	hh:24:00	*hh:53:00*
(15) Leeuwarden → Stavoren				(16) Stavoren → Leeuwarden			
Leeuwarden	0		hh:23:00	Stavoren	0		hh:18:00
Mantgum	9.777	hh:30:00	hh:31:00	Koudum-Molkwerum	4.152	hh:21:30	hh:22:00
Sneek Noord	20.441	hh:38:00	hh:39:00	Hindeloopen	9.320	hh:26:30	hh:27:00
Sneek	21.518	hh:42:00	hh:46:00	Workum	12.773	hh:30:00	hh:31:00
Ijlst	24.599	hh:48:30	hh:49:00	Ijlst	25.455	hh:39:30	hh:40:00
Workum	37.210	hh:59:00	hh+1:00:00	Sneek	28.536	hh:44:00	hh:48:00
Hindeloopen	40.734	hh+1:02:30	hh+1:03:00	Sneek Noord	29.613	hh:50:00	hh:51:00
Koudum-Molkwerum	45.902	hh+1:07:30	hh+1:08:00	Mantgum	40.277	hh:59:00	hh+1:00:00
Stavoren	50.054	hh+1:13:00	*hh+1:18:00*	Leeuwarden	50.054	hh+1:08:00	*hh+1:23:00*
(17) Groningen → Roodeschool				(18) Roodeschool → Groningen			
Groningen	0		hh:22:00	Roodeschool	0		hh:27:00
Groningen Noord	3.814	hh:25:30	hh:26:00	Uithuizermeeden	3.110	hh:30:00	hh:31:00
Sauwerd	10.799	hh:31:00	hh:32:00	Uithuizen	6.323	hh:34:30	hh:35:00
Winsum	15.473	hh:36:00	hh:37:00	Usquert	10.977	hh:40:00	hh:41:00
Baflo	18.934	hh:40:30	hh:41:00	Warffum	14.074	hh:45:00	hh:46:00
Warffum	23.691	hh:46:00	hh:47:00	Baflo	18.831	hh:51:30	hh:52:00
Usquert	26.764	hh:50:00	hh:51:00	Winsum	22.292	hh:55:30	hh:56:00
Uithuizen	31.442	hh:55:30	hh:56:00	Sauwerd	26.966	hh+1:01:00	hh+1:02:00
Uithuizermeeden	34.655	hh+1:00:00	hh+1:01:00	Groningen Noord	33.951	hh+1:07:00	hh+1:08:00
Roodeschool	37.765	hh+1:05:00	*hh+1:27:00*	Groningen	37.750	hh+1:13:00	*hh+1:22:00*
(19) Groningen → Eemshaven				(20) Eemshaven → Groningen			
Groningen	0		hh:22:00	Eemshaven	0		hh:19:00
Groningen Noord	3.814	hh:25:30	hh:26:00	Roodeschool	7.077	hh:26:00	hh:27:00
Sauwerd	10.799	hh:31:00	hh:32:00	Uithuizermeeden	10.187	hh:30:00	hh:31:00
Winsum	15.473	hh:36:00	hh:37:00	Uithuizen	13.400	hh:34:30	hh:35:00
Baflo	18.934	hh:40:30	hh:41:00	Usquert	18.054	hh:40:00	hh:41:00
Warffum	23.691	hh:46:00	hh:47:00	Warffum	21.151	hh:45:00	hh:46:00
Usquert	26.764	hh:50:00	hh:51:00	Baflo	25.908	hh:51:30	hh:52:00
Uithuizen	31.442	hh:55:30	hh:56:00	Winsum	29.369	hh:55:30	hh:56:00
Uithuizermeeden	34.655	hh+1:00:00	hh+1:01:00	Sauwerd	34.043	hh+1:01:00	hh+1:02:00
Roodeschool	37.765	hh+1:05:00	hh+1:06:00	Groningen Noord	41.028	hh+1:07:00	hh+1:08:00
Eemshaven	44.842	hh+1:13:00	*hh+1:19:00*	Groningen	44.827	hh+1:13:00	*hh+1:22:00*
(21) Groningen → Delfzijl				(22) Delfzijl → Groningen			
Groningen	0		hh:18:00	Delfzijl	0		hh:00:00
Groningen Noord	3.810	hh:21:30	hh:22:00	Delfzijl West	1.104	hh:01:30	hh:02:00
Sauwerd	10.795	hh:27:00	hh:28:00	Appingedam	4.255	hh:05:30	hh:06:00
Bedum	14.935	hh:31:30	hh:32:00	Loppersum	11.975	hh:12:00	hh:13:00
Stedum	21.755	hh:37:30	hh:38:00	Stedum	15.954	hh:16:30	hh:17:00
Loppersum	25.734	hh:42:00	hh:43:00	Bedum	22.773	hh:22:30	hh:23:00
Appingedam	33.454	hh:48:30	hh:49:00	Sauwerd	26.914	hh:26:30	hh:27:00
Delfzijl West	36.605	hh:52:30	hh:53:00	Groningen Noord	33.899	hh:32:30	hh:33:00
Delfzijl	37.709	hh:55:00	*hh+1:00:00*	Groningen	37.694	hh:39:00	*hh:48:00*

(Table B.2 continued on the next page)

(Table B.2 continued from the previous page)

(23) Groningen → Veendam				(24) Veendam → Groningen			
Groningen	0		hh:29:00	Veendam	0		hh:02:00
Groningen Europark	1.412	hh:31:30	hh:32:00	Zuidbroek	7.311	hh:07:30	hh:08:00
Kropswolde	11.917	hh:39:30	hh:40:00	Hoogezand-Sappemeer	13.723	hh:13:30	hh:14:00
Martenshoek	13.062	hh:41:30	hh:42:00	Martenshoek	15.756	hh:16:30	hh:17:00
Hoogezand-Sappemeer	15.097	hh:44:30	hh:45:00	Kropswolde	17.106	hh:18:30	hh:19:00
Zuidbroek	21.507	hh:50:00	hh:51:00	Groningen Europark	27.406	hh:26:30	hh:27:00
Veendam	28.818	hh:58:00	*hh+1:02:00*	Groningen	28.818	hh:31:00	*hh:47:00*
(25) Groningen → Winschoten (stopping)				(26) Winschoten → Groningen (stopping)			
Groningen	0		hh:47:00	Winschoten	0		hh:10:00
Groningen Europark	1.397	hh:49:30	hh:50:00	Scheemda	4.733	hh:14:00	hh:15:00
Kropswolde	11.902	hh:57:30	hh:58:00	Zuidbroek	12.438	hh:20:30	hh:21:00
Martenshoek	13.047	hh:59:30	hh+1:00:00	Hoogezand-Sappemeer	18.850	hh:25:30	hh:26:00
Hoogezand-Sappemeer	15.082	hh+1:02:30	hh+1:03:00	Martenshoek	20.883	hh:28:30	hh:29:00
Zuidbroek	21.492	hh+1:07:00	hh+1:08:00	Kropswolde	22.233	hh:31:30	hh:32:00
Scheemda	29.197	hh+1:15:00	hh+1:16:00	Groningen Europark	32.533	hh:39:30	hh:40:00
Winschoten	33.930	hh+1:21:00	*hh+2:10:00*	Groningen	33.945	hh:43:00	*hh:59:00*
(27) Groningen → Winschoten (express)				(28) Winschoten → Groningen (express)			
Groningen	0		hh:07:00	Winschoten	0		hh:55:00
Groningen Europark	1.397	hh:10:00	hh:11:00	Scheemda	4.733	hh:59:00	hh+1:00:00
Kropswolde	11.902	-	-	Zuidbroek	12.438	-	-
Martenshoek	13.047	-	-	Hoogezand-Sappemeer	18.850	-	-
Hoogezand-Sappemeer	15.082	-	-	Martenshoek	20.883	-	-
Zuidbroek	21.492	-	-	Kropswolde	22.233	-	-
Scheemda	29.197	hh:29:00	hh:30:00	Groningen Europark	32.533	hh+1:19:00	hh+1:20:00
Winschoten	33.930	hh:35:00	*hh:55:00*	Groningen	33.945	hh+1:23:00	*hh+1:29:00*
(29) Groningen → Bad Nieuweschans				(30) Bad Nieuweschans → Groningen			
Groningen	0		hh:53:00	Bad Nieuweschans	0		hh:00:00
Groningen Europark	1.397	hh:55:30	hh:56:00	Winschoten	12.305	hh:09:00	hh:10:00
Kropswolde	11.902	hh+1:03:30	hh+1:04:00	Scheemda	17.038	hh:14:00	hh:15:00
Martenshoek	13.047	hh+1:05:30	hh+1:06:00	Zuidbroek	24.743	hh:20:30	hh:21:00
Hoogezand-Sappemeer	15.082	hh+1:08:30	hh+1:09:00	Hoogezand-Sappemeer	31.155	hh:25:30	hh:26:00
Zuidbroek	21.492	hh+1:14:00	hh+1:15:00	Martenshoek	33.188	hh:28:30	hh:29:00
Scheemda	29.197	hh+1:22:00	hh+1:24:00	Kropswolde	34.538	hh:31:30	hh:32:00
Winschoten	33.930	hh+1:29:00	hh+1:31:00	Groningen Europark	44.838	hh:39:30	hh:40:00
Bad Nieuweschans	46.166	hh+1:41:00	*hh+2:05:00*	Groningen	46.250	hh:43:00	*hh:47:00*
(31) Groningen → Weener				(32) Weener → Groningen			
Groningen	0		hh:17:00	Weener	0		hh:18:00
Groningen Europark	1.397	hh:19:30	hh:20:00	Bad Nieuweschans	13.389	hh:27:00	hh:28:00
Kropswolde	11.902	hh:27:30	hh:28:00	Winschoten	25.694	hh:38:00	hh:40:00
Martenshoek	13.047	hh:29:30	hh:30:00	Scheemda	30.427	hh:44:00	hh:45:00
Hoogezand-Sappemeer	15.082	hh:32:30	hh:33:00	Zuidbroek	38.132	hh:50:30	hh:51:00
Zuidbroek	21.492	hh:37:30	hh:38:00	Hoogezand-Sappemeer	44.544	hh:55:30	hh:56:00
Scheemda	29.197	hh:44:30	hh:45:00	Martenshoek	46.577	hh:58:30	hh:59:00
Winschoten	33.930	hh:49:30	hh:50:00	Kropswolde	47.927	hh+1:01:30	hh+1:02:00
Bad Nieuweschans	46.166	hh:59:00	hh+1:01:00	Groningen Europark	58.227	hh+1:09:30	hh+1:10:00
Weener	59.555	hh+1:10:00	*hh+1:18:00*	Groningen	59.639	hh+1:13:00	*hh+1:17:00*

Table B.3: Estimated consumption of different energy carriers for GTW 2/6 vehicle.

Propulsion system	Energy carrier	Season	Load (%)	Consumption per service															
DE	Diesel			(1)	(2)	(3)	(4)	(5)	(6)	(7)	(8)	(9)	(10)	(11)	(12)	(13)	(14)	(15)	(16)
	(l)	Win.	0	51.495	48.445	49.557	40.064	48.225	42.014	16.297	18.370	30.733	24.081	19.854	21.772	20.960	27.595	43.964	45.630
		Win.	100	54.353	51.644	50.861	40.796	48.863	42.803	16.637	18.579	31.553	25.318	20.565	22.325	21.396	27.929	46.114	47.577
		Sum.	0	50.189	47.270	48.284	39.018	47.032	40.983	15.629	17.703	29.722	23.340	19.255	21.051	20.302	26.437	42.696	44.215
		Sum.	100	53.033	50.458	49.598	39.759	47.673	41.781	15.965	17.917	30.539	24.464	19.964	21.609	20.743	26.768	44.846	46.161
				(17)	(18)	(19)	(20)	(21)	(22)	(23)	(24)	(25)	(26)	(27)	(28)	(29)	(30)	(31)	(32)
		Win.	0	42.939	34.896	40.391	40.074	33.309	34.363	23.404	31.188	50.316	34.338	33.378	27.114	45.350	37.106	52.068	49.30905
		Win.	100	44.410	37.614	41.993	42.433	34.745	36.174	24.493	32.531	52.780	35.998	33.515	27.897	46.804	39.338	55.735	51.972
		Sum.	0	41.450	33.986	39.049	38.868	32.311	33.222	22.685	30.251	48.595	33.306	32.218	26.292	43.731	36.053	50.554	47.913
		Sum.	100	42.957	36.525	40.686	42.248	33.799	35.031	23.781	31.594	51.030	34.964	32.274	27.077	45.289	38.239	54.194	50.571
HE	Diesel			(1)	(2)	(3)	(4)	(5)	(6)	(7)	(8)	(9)	(10)	(11)	(12)	(13)	(14)	(15)	(16)
(ZESC)	(l)	Win.	0	48.205	48.137	46.964	38.515	45.165	40.684	14.145	12.993	27.029	22.239	18.676	19.812	19.239	23.418	43.592	42.500
		Win.	100	52.368	52.019	48.506	39.487	45.571	41.797	14.398	12.963	27.348	23.025	19.402	20.128	19.532	23.848	45.762	45.043
		Sum.	0	46.802	47.085	45.695	37.513	43.804	39.780	13.312	12.703	25.287	21.631	18.173	19.179	18.609	22.782	42.418	41.063
		Sum.	100	50.957	50.949	47.400	38.578	44.631	40.895	13.643	12.672	26.124	22.462	18.898	19.607	19.028	23.198	44.588	44.588
				(17)	(18)	(19)	(20)	(21)	(22)	(23)	(24)	(25)	(26)	(27)	(28)	(29)	(30)	(31)	(32)
		Win.	0	37.982	32.984	38.882	37.486	32.191	31.677	22.532	28.580	38.120	31.697	30.292	26.110	40.591	36.993	51.912	49.915
		Win.	100	40.008	34.674	41.095	39.268	34.572	33.782	23.725	30.253	39.746	33.486	30.891	26.898	42.218	39.137	54.639	52.841
		Sum.	0	36.485	32.115	37.743	36.563	31.353	30.455	21.896	26.830	37.155	30.747	28.700	25.064	38.684	36.010	50.368	48.590
		Sum.	100	38.493	33.783	39.932	38.317	33.634	32.458	23.086	28.525	38.809	32.267	29.304	25.864	40.356	38.154	53.312	51.516
HE	FAME			(1)	(2)	(3)	(4)	(5)	(6)	(7)	(8)	(9)	(10)	(11)	(12)	(13)	(14)	(15)	(16)
(ZESC)	(l)	Win.	0	52.128	52.126	50.629	41.847	48.846	43.950	15.258	12.270	28.876	24.114	20.558	21.794	20.841	26.072	47.208	46.016
		Win.	100	56.778	56.299	52.383	43.013	49.852	45.155	15.532	13.926	29.862	25.478	21.368	21.568	21.348	25.751	49.600	48.614
		Sum.	0	50.614	50.988	48.986	40.613	46.916	42.631	14.415	13.622	27.678	23.071	19.663	20.613	20.303	24.173	45.937	44.459
		Sum.	100	55.249	55.140	50.759	41.759	47.913	43.850	14.777	13.610	28.657	24.329	20.484	20.538	20.811	24.448	48.329	47.046
				(17)	(18)	(19)	(20)	(21)	(22)	(23)	(24)	(25)	(26)	(27)	(28)	(29)	(30)	(31)	(32)
		Win.	0	41.080	35.201	42.044	40.797	35.164	34.301	24.418	30.946	41.254	34.336	33.154	28.277	44.074	40.027	55.971	54.382
		Win.	100	43.428	37.641	44.592	43.290	37.168	37.032	25.716	32.763	43.050	36.318	33.468	29.096	45.732	42.376	59.139	57.298
		Sum.	0	39.410	34.317	40.766	39.651	34.201	32.988	23.729	29.048	40.284	33.309	31.428	27.146	42.118	38.964	54.538	52.902
		Sum.	100	41.786	36.721	43.332	42.089	36.186	35.598	25.025	30.891	42.027	35.285	31.756	27.972	43.716	41.303	57.703	55.856
HE	HVO			(1)	(2)	(3)	(4)	(5)	(6)	(7)	(8)	(9)	(10)	(11)	(12)	(13)	(14)	(15)	(16)
(ZESC)	(l)	Win.	0	50.323	50.196	48.804	40.370	47.192	42.404	14.721	13.447	27.854	23.888	19.828	20.899	20.105	24.398	45.539	44.367
		Win.	100	54.673	54.353	49.953	41.417	48.093	43.559	14.983	13.433	28.777	24.517	20.580	21.526	20.584	24.845	47.853	47.503
		Sum.	0	48.856	49.098	47.221	39.179	45.327	41.127	13.908	13.141	26.703	22.694	18.962	19.760	19.586	23.249	44.313	42.867
		Sum.	100	53.199	53.235	48.425	40.237	46.222	42.301	14.255	13.128	27.614	23.413	19.725	20.396	20.069	23.625	46.627	45.889
				(17)	(18)	(19)	(20)	(21)	(22)	(23)	(24)	(25)	(26)	(27)	(28)	(29)	(30)	(31)	(32)
		Win.	0	39.700	34.636	40.639	39.831	33.834	33.478	23.544	29.86603	39.820	33.138	31.957	27.298	42.569	38.662	54.239	52.486
		Win.	100	41.617	36.174	42.944	41.019	36.092	35.402	24.730	31.601	41.556	35.036	32.288	28.106	44.141	40.864	57.036	55.209
		Sum.	0	38.076	33.633	39.393	38.813	32.918	32.130	22.880	28.042	38.812	31.858	30.290	26.206	40.724	37.596	52.627	51.059
		Sum.	100	40.099	35.262	41.743	40.002	35.167	34.019	24.063	29.805	40.622	33.763	30.632	27.024	42.245	39.830	55.650	53.817
HE	LNG			(1)	(2)	(3)	(4)	(5)	(6)	(7)	(8)	(9)	(10)	(11)	(12)	(13)	(14)	(15)	(16)
(ZESC)	(kg)	Win.	0	35.196	35.148	34.136	28.221	32.955	29.617	10.290	9.398	19.474	16.207	13.866	14.602	14.052	17.055	31.839	31.109
		Win.	100	38.214	37.858	35.333	28.996	33.625	30.449	10.472	9.390	20.077	16.893	14.407	14.529	14.433	17.379	33.450	33.217
		Sum.	0	34.174	34.380	33.029	27.385	31.652	28.728	9.722	9.186	18.666	15.519	13.262	13.810	13.690	16.254	30.985	30.043
		Sum.	100	37.183	37.078	34.239	28.173	32.315	29.571	9.963	9.177	19.263	16.194	13.807	13.833	14.070	16.529	32.596	32.089
				(17)	(18)	(19)	(20)	(21)	(22)	(23)	(24)	(25)	(26)	(27)	(28)	(29)	(30)	(31)	(32)
		Win.	0	27.608	23.660	28.379	27.374	23.709	23.188	16.455	20.869	27.840	23.176	22.125	19.077	29.722	27.251	37.724	36.458
		Win.	100	29.104	25.327	30.029	28.742	25.260	24.667	17.304	22.133	29.042	24.491	22.777	19.649	30.842	28.562	39.949	38.622
		Sum.	0	26.521	23.087	27.523	26.701	23.069	22.238	15.991	19.591	27.190	22.284	20.960	18.313	28.410	26.504	36.758	35.491
		Sum.	100	27.994	24.706	29.144	27.931	24.575	23.748	16.838	20.871	28.390	23.601	21.791	18.896	29.517	27.839	38.928	37.650

(Table B.3 continued on the next page)

(Table B.3 continued from the previous page)

HE (ZESC)	H2 (kg)			(1)	(2)	(3)	(4)	(5)	(6)	(7)	(8)	(9)	(10)	(11)	(12)	(13)	(14)	(15)	(16)
		Win.	0	14.395	14.357	13.891	11.552	13.485	12.123	4.210	3.845	7.966	6.636	5.672	5.976	5.749	6.979	13.027	12.844
		Win.	100	15.658	15.479	14.284	11.872	13.749	12.446	4.285	3.842	8.225	6.998	5.888	5.950	5.888	7.104	13.683	13.421
		Sum.	0	13.978	14.043	13.452	11.211	12.952	11.759	3.978	3.758	7.635	6.351	5.424	5.652	5.601	6.645	12.677	12.386
		Sum.	100	15.236	15.160	13.848	11.534	13.213	12.088	4.077	3.755	7.894	6.683	5.643	5.667	5.740	6.755	13.332	12.989
				(17)	(18)	(19)	(20)	(21)	(22)	(23)	(24)	(25)	(26)	(27)	(28)	(29)	(30)	(31)	(32)
		Win.	0	11.310	9.754	11.583	11.271	9.692	9.627	6.734	8.539	11.409	9.478	9.052	7.805	12.131	11.055	15.440	15.002
		Win.	100	11.886	10.203	12.258	11.772	10.434	10.111	7.091	9.041	11.878	10.030	9.345	8.041	12.629	11.698	16.319	15.818
		Sum.	0	10.868	9.473	11.247	10.957	9.430	9.207	6.544	8.017	11.151	9.196	8.575	7.493	11.563	10.761	15.045	14.594
		Sum.	100	11.438	9.929	11.900	11.461	10.164	9.714	6.901	8.527	11.595	9.664	8.871	7.731	12.073	11.402	15.923	15.420
HE (FSMC)	Diesel (l)			(1)	(2)	(3)	(4)	(5)	(6)	(7)	(8)	(9)	(10)	(11)	(12)	(13)	(14)	(15)	(16)
		Win.	0	47.600	46.532	47.644	39.647	44.801	41.234	14.145	12.993	26.110	21.346	20.819	20.070	20.350	23.404	43.496	42.591
		Win.	100	51.473	50.606	47.498	40.471	45.592	42.651	14.398	12.963	26.890	22.735	21.427	19.503	19.843	23.822	45.697	45.282
		Sum.	0	45.657	44.857	46.061	37.689	43.190	39.366	13.517	12.703	24.282	19.952	20.522	18.597	19.746	22.716	41.909	40.456
		Sum.	100	49.664	48.840	45.833	38.724	44.028	41.010	13.711	12.672	25.061	21.191	21.122	18.655	19.562	23.099	43.939	43.200
				(17)	(18)	(19)	(20)	(21)	(22)	(23)	(24)	(25)	(26)	(27)	(28)	(29)	(30)	(31)	(32)
		Win.	0	37.939	34.745	37.501	38.227	31.950	31.186	21.749	28.800	38.095	31.808	31.662	26.736	41.580	35.785	51.996	47.996
		Win.	100	40.141	35.575	39.647	39.404	33.910	33.149	22.808	30.434	39.724	33.005	32.186	27.358	42.795	37.739	53.339	50.701
		Sum.	0	36.421	33.063	35.601	35.999	30.895	29.919	20.557	27.413	37.117	29.819	30.427	25.575	38.424	34.161	50.082	46.120
		Sum.	100	38.588	33.831	37.807	37.277	32.612	31.387	21.654	28.926	38.773	31.289	31.083	25.793	39.070	36.172	51.809	48.726
HE (FSMC)	FAME (l)			(1)	(2)	(3)	(4)	(5)	(6)	(7)	(8)	(9)	(10)	(11)	(12)	(13)	(14)	(15)	(16)
		Win.	0	51.421	50.360	51.596	42.776	48.314	44.403	15.318	14.072	28.449	23.175	22.144	21.616	21.698	26.079	47.326	46.097
		Win.	100	55.863	54.153	53.265	43.688	49.282	45.725	15.596	14.062	29.356	24.961	22.855	21.489	21.524	25.753	49.510	48.664
		Sum.	0	49.578	48.628	49.885	40.806	46.203	42.828	14.336	13.758	26.553	21.882	21.829	20.243	21.390	24.967	45.359	43.426
		Sum.	100	53.809	52.454	51.402	41.944	47.155	44.234	14.628	13.747	27.470	23.495	22.540	20.198	21.218	24.904	47.621	46.062
				(17)	(18)	(19)	(20)	(21)	(22)	(23)	(24)	(25)	(26)	(27)	(28)	(29)	(30)	(31)	(32)
		Win.	0	42.735	35.997	41.618	41.461	34.109	34.137	23.569	31.451	39.475	34.394	34.061	28.953	45.006	38.593	55.323	53.079
		Win.	100	44.251	38.626	43.345	44.088	36.639	37.105	24.703	33.382	41.196	35.805	34.885	29.628	46.346	40.877	58.062	55.017
		Sum.	0	40.001	33.758	39.526	38.920	32.768	32.395	22.227	29.590	38.312	32.268	32.010	27.703	41.011	37.274	53.221	50.850
		Sum.	100	41.334	36.496	41.014	41.555	35.090	35.312	23.449	31.215	40.034	33.942	32.983	27.930	42.320	39.436	56.050	53.151
HE (FSMC)	HVO (l)			(1)	(2)	(3)	(4)	(5)	(6)	(7)	(8)	(9)	(10)	(11)	(12)	(13)	(14)	(15)	(16)
		Win.	0	49.628	48.512	49.794	41.270	46.680	42.841	14.779	13.577	27.441	23.915	21.360	20.971	20.929	24.401	45.627	44.440
		Win.	100	53.783	52.308	50.441	42.078	48.044	47.537	15.044	13.565	28.316	23.993	22.022	21.145	20.767	24.848	47.789	47.681
		Sum.	0	47.879	46.760	48.144	39.365	44.609	41.333	13.832	13.272	25.619	22.510	21.055	19.419	20.634	23.639	43.715	41.864
		Sum.	100	51.830	51.225	48.292	40.391	46.022	45.558	14.110	13.261	26.488	22.588	21.711	19.781	20.475	24.031	45.942	45.963
				(17)	(18)	(19)	(20)	(21)	(22)	(23)	(24)	(25)	(26)	(27)	(28)	(29)	(30)	(31)	(32)
		Win.	0	40.840	36.128	39.745	41.090	33.098	33.677	22.725	30.355	38.593	33.191	32.883	27.970	43.129	37.261	54.698	50.436
		Win.	100	42.654	37.706	40.981	41.733	35.724	35.109	23.760	32.202	39.634	34.549	33.636	28.518	44.477	39.390	55.983	52.248
		Sum.	0	38.188	34.307	37.758	38.965	31.791	31.771	21.430	28.562	37.540	31.134	30.111	26.760	38.782	35.991	52.340	48.162
		Sum.	100	39.327	35.524	38.944	39.487	34.171	32.932	22.556	30.118	38.581	32.753	31.778	26.885	40.014	37.987	54.042	50.143
HE (FSMC)	LNG (kg)			(1)	(2)	(3)	(4)	(5)	(6)	(7)	(8)	(9)	(10)	(11)	(12)	(13)	(14)	(15)	(16)
		Win.	0	34.718	33.979	34.814	28.845	32.596	29.917	10.330	9.489	19.193	15.610	14.931	14.653	14.644	17.060	31.926	31.243
		Win.	100	37.608	36.418	35.945	29.454	33.241	30.731	10.515	9.482	19.754	16.193	15.389	14.483	14.614	17.381	33.411	33.355
		Sum.	0	33.313	32.754	33.642	27.518	31.171	28.858	9.668	9.277	17.916	14.677	14.717	13.571	14.438	16.523	30.605	29.678
		Sum.	100	36.229	35.382	34.686	28.281	31.806	29.821	9.863	9.269	18.475	15.325	15.170	13.618	14.397	16.815	32.117	32.155
				(17)	(18)	(19)	(20)	(21)	(22)	(23)	(24)	(25)	(26)	(27)	(28)	(29)	(30)	(31)	(32)
		Win.	0	28.787	24.506	27.540	27.903	23.175	23.081	15.876	21.206	26.639	23.265	22.885	19.549	30.370	26.823	37.504	34.565
		Win.	100	29.657	26.008	29.006	29.262	24.780	24.427	16.638	22.540	27.714	24.118	23.559	19.963	31.097	27.562	39.303	36.605
		Sum.	0	26.570	23.027	26.209	26.278	22.266	21.524	14.966	19.957	25.854	21.824	21.031	18.701	27.696	25.691	35.856	33.120
		Sum.	100	27.697	24.572	27.458	27.509	23.838	23.245	15.710	21.098	26.977	22.861	22.665	18.809	29.933	26.556	37.999	35.128
HE (FSMC)	H2 (kg)			(1)	(2)	(3)	(4)	(5)	(6)	(7)	(8)	(9)	(10)	(11)	(12)	(13)	(14)	(15)	(16)
		Win.	0	14.192	13.873	13.931	11.807	13.338	12.250	4.227	3.883	7.851	6.369	6.109	5.998	5.985	6.980	13.054	12.871
		Win.	100	15.404	14.888	14.409	12.057	13.589	12.561	4.303	3.880	8.094	6.878	6.297	5.930	5.936	7.105	13.664	13.433
		Sum.	0	13.694	13.372	13.324	11.265	12.756	11.813	3.956	3.796	7.328	6.015	6.023	5.556	5.901	6.758	12.512	12.447
		Sum.	100	14.836	14.465	13.806	11.577	13.002	12.194	4.036	3.793	7.573	6.440	6.207	5.575	5.852	6.871	13.134	12.713
				(17)	(18)	(19)	(20)	(21)	(22)	(23)	(24)	(25)	(26)	(27)	(28)	(29)	(30)	(31)	(32)
		Win.	0	11.801	9.941	11.310	11.282	9.478	9.708	6.500	8.679	10.891	9.496	9.472	7.992	12.571	10.671	15.260	14.415
		Win.	100	12.301	10.391	11.812	11.698	10.380	10.028	6.824	9.210	11.371	9.882	9.579	8.179	12.810	11.289	16.013	14.983
		Sum.	0	10.901	9.328	10.766	10.588	9.105	9.064	6.127	8.165	10.585	8.907	8.670	7.646	12.087	10.305	14.678	13.766
		Sum.	100	11.396	9.809	11.279	11.061	9.994	9.403	6.438	8.619	11.050	9.366	9.051	7.710	12.324	10.871	15.477	14.398

(Table B.3 continued on the next page)

(Table B.3 continued from the previous page)

PIHE	Diesel			(1)	(2)	(3)	(4)	(5)	(6)	(7)	(8)
	(l)	Win.	0	36.450 / 61.859	35.444 / 30.107	37.093 / 62.023	26.478 / 34.530	34.448 / 61.966	28.632 / 34.511	2.311 / 46.402	3.925 / 42.356
	/	Win.	100	40.698 / 61.927	38.971 / 30.118	37.630 / 61.648	27.692 / 34.577	35.305 / 61.957	29.909 / 34.611	2.650 / 46.638	4.026 / 42.285
	E	Sum.	0	35.161 / 59.049	33.962 / 29.128	36.850 / 55.444	25.340 / 33.343	33.080 / 59.292	27.210 / 33.354	2.287 / 42.581	3.837 / 37.969
	(kWh)	Sum.	100	39.375 / 58.833	37.561 / 29.136	36.441 / 59.309	26.476 / 33.363	34.140 / 58.803	28.613 / 33.423	2.573 / 43.032	3.834 / 38.460
				(9)	(10)	(11)	(12)	(13)	(14)	(15)	(16)
		Win.	0	12.004 / 69.427	9.775 / 38.881	12.651 / 23.717	7.206 / 45.750	11.237 / 31.549	4.562 / 75.569	30.993 / 21.353	35.839 / 58.157
		Win.	100	12.915 / 69.379	10.536 / 38.858	13.185 / 24.661	6.785 / 53.064	11.698 / 31.746	4.991 / 75.600	33.386 / 21.348	38.566 / 58.064
		Sum.	0	10.987 / 65.811	8.596 / 37.581	12.487 / 20.992	7.188 / 40.724	11.061 / 28.192	3.845 / 71.501	29.228 / 20.692	34.302 / 55.958
		Sum.	100	11.935 / 65.908	9.453 / 37.588	13.164 / 21.136	6.764 / 48.010	11.298 / 29.080	4.383 / 70.943	31.560 / 20.797	36.786 / 55.954
				(17)	(18)	(19)	(20)	(21)	(22)	(23)	(24)
		Win.	0	24.572 / 67.121	21.372 / 38.966	29.308 / 25.811	32.002 / 39.027	23.619 / 21.333	25.889 / 38.817	10.990 / 17.342	19.444 / 60.322
		Win.	100	26.317 / 67.041	23.514 / 38.928	31.214 / 25.826	33.944 / 38.927	26.161 / 21.309	28.083 / 38.854	11.918 / 17.302	21.277 / 60.531
		Sum.	0	22.909 / 63.843	19.863 / 37.788	27.466 / 25.002	30.222 / 37.847	22.281 / 20.639	24.621 / 37.664	10.955 / 16.950	18.339 / 57.768
		Sum.	100	24.793 / 63.783	21.924 / 37.750	29.429 / 24.961	32.100 / 37.748	25.155 / 20.662	26.872 / 37.635	11.881 / 16.902	19.979 / 57.580
				(25)	(26)	(27)	(28)	(29)	(30)	(31)	(32)
		Win.	0	17.997 / 100.991	16.576 / 58.353	20.039 / 42.928	18.613 / 27.092	29.638 / 69.444	25.249 / 17.273	46.941 / 34.674	41.183 / 17.272
		Win.	100	19.616 / 100.468	17.922 / 60.371	20.350 / 46.093	18.386 / 26.785	30.926 / 69.741	26.767 / 17.280	49.016 / 34.655	43.457 / 17.280
		Sum.	0	16.838 / 93.802	15.284 / 55.591	19.706 / 38.138	16.829 / 26.017	27.495 / 66.725	23.738 / 16.583	44.885 / 33.567	39.104 / 16.703
		Sum.	100	18.251 / 93.792	16.801 / 57.056	20.331 / 39.207	18.328 / 26.259	28.986 / 66.401	25.256 / 16.704	47.022 / 33.546	41.286 / 16.704
PIHE	FAME			(1)	(2)	(3)	(4)	(5)	(6)	(7)	(8)
	(l)	Win.	0	39.527 / 61.973	38.344 / 30.107	39.060 / 61.910	28.651 / 34.538	37.312 / 61.945	31.004 / 34.506	2.503 / 46.403	4.251 / 42.357
	/	Win.	100	44.086 / 61.926	42.401 / 30.113	40.770 / 61.712	29.981 / 34.575	38.207 / 61.849	32.400 / 34.538	2.870 / 46.640	4.360 / 42.298
	E	Sum.	0	38.103 / 59.286	36.736 / 29.126	37.672 / 59.060	27.423 / 33.353	35.829 / 59.285	29.459 / 33.348	2.477 / 42.583	4.156 / 37.970
	(kWh)	Sum.	100	42.636 / 58.820	40.881 / 29.132	39.446 / 59.320	28.666 / 33.361	36.946 / 58.693	31.021 / 33.362	2.786 / 43.034	4.153 / 38.471
				(9)	(10)	(11)	(12)	(13)	(14)	(15)	(16)
		Win.	0	12.992 / 69.425	9.690 / 38.884	13.706 / 23.637	7.806 / 45.746	12.168 / 31.560	4.936 / 75.597	33.520 / 21.354	38.913 / 58.158
		Win.	100	13.998 / 69.397	10.641 / 38.854	14.282 / 24.597	7.349 / 53.077	12.664 / 31.549	5.406 / 75.455	36.130 / 21.361	41.801 / 58.067
		Sum.	0	11.887 / 65.819	8.851 / 37.774	13.525 / 20.922	7.786 / 40.732	11.977 / 28.205	4.225 / 71.322	31.608 / 20.692	37.158 / 55.924
		Sum.	100	12.993 / 65.717	9.626 / 37.671	14.260 / 21.059	7.326 / 48.023	12.219 / 28.933	4.742 / 71.078	34.192 / 20.797	39.870 / 55.946
				(17)	(18)	(19)	(20)	(21)	(22)	(23)	(24)
		Win.	0	26.761 / 66.895	23.582 / 38.968	31.814 / 25.815	34.284 / 39.040	25.429 / 21.323	28.106 / 38.936	11.885 / 17.417	21.071 / 60.322
		Win.	100	28.838 / 67.038	23.484 / 38.854	34.141 / 25.898	36.103 / 38.930	28.153 / 21.312	30.219 / 38.730	12.927 / 17.304	23.086 / 60.529
		Sum.	0	25.042 / 63.779	21.942 / 37.791	29.967 / 24.973	32.531 / 37.861	24.197 / 20.797	26.778 / 37.708	11.847 / 17.025	19.868 / 57.767
		Sum.	100	27.179 / 63.778	21.464 / 37.581	32.193 / 25.030	33.967 / 37.751	26.801 / 20.621	28.863 / 37.592	12.886 / 16.904	21.685 / 57.566
				(25)	(26)	(27)	(28)	(29)	(30)	(31)	(32)
		Win.	0	19.403 / 100.963	17.956 / 58.406	21.757 / 42.621	20.160 / 27.091	32.023 / 69.418	26.776 / 17.272	50.871 / 34.675	44.665 / 17.272
		Win.	100	20.748 / 100.845	19.427 / 60.262	22.216 / 44.166	20.001 / 26.889	33.833 / 69.767	29.074 / 17.281	52.887 / 34.645	46.938 / 17.280
		Sum.	0	18.183 / 93.672	16.554 / 55.651	20.883 / 39.143	18.227 / 26.016	29.707 / 66.700	25.178 / 16.703	48.640 / 33.568	42.406 / 16.704
		Sum.	100	19.396 / 93.693	18.169 / 57.077	22.191 / 37.321	19.941 / 26.363	31.717 / 66.426	27.445 / 16.707	50.599 / 33.537	44.570 / 16.703
PIHE	HVO			(1)	(2)	(3)	(4)	(5)	(6)	(7)	(8)
	(l)	Win.	0	38.081 / 61.841	36.980 / 30.107	38.760 / 61.995	27.643 / 34.614	35.964 / 61.838	29.835 / 34.499	2.415 / 46.400	4.101 / 42.370
	/	Win.	100	42.343 / 61.951	40.064 / 30.119	40.586 / 61.579	28.926 / 34.566	36.896 / 61.850	31.224 / 34.547	2.769 / 46.631	4.206 / 42.301
	E	Sum.	0	36.703 / 59.137	35.434 / 29.127	38.501 / 55.431	26.458 / 33.427	34.548 / 59.158	28.357 / 33.345	2.389 / 42.580	4.009 / 37.981
	(kWh)	Sum.	100	40.956 / 58.819	38.564 / 29.139	39.246 / 59.303	27.657 / 33.353	35.622 / 58.890	29.867 / 33.362	2.688 / 43.025	4.006 / 38.474
				(9)	(10)	(11)	(12)	(13)	(14)	(15)	(16)
		Win.	0	12.542 / 69.433	9.325 / 38.873	13.215 / 23.910	6.899 / 54.245	11.736 / 31.536	10.325 / 52.820	32.307 / 21.342	36.146 / 57.871
		Win.	100	13.536 / 69.399	11.146 / 38.947	13.776 / 24.680	7.087 / 53.150	12.093 / 31.846	5.212 / 75.522	34.883 / 21.472	39.111 / 57.817
		Sum.	0	11.479 / 65.818	8.538 / 37.765	13.050 / 21.153	6.867 / 49.218	11.557 / 28.172	10.056 / 47.848	30.461 / 20.680	34.338 / 55.475
		Sum.	100	12.564 / 65.730	10.040 / 37.688	13.754 / 21.155	7.067 / 48.094	11.686 / 29.146	4.536 / 71.111	33.029 / 20.867	37.185 / 55.507
				(17)	(18)	(19)	(20)	(21)	(22)	(23)	(24)
		Win.	0	25.724 / 67.101	22.362 / 38.964	30.659 / 25.810	32.985 / 38.964	24.720 / 21.334	26.555 / 38.737	11.483 / 17.345	20.312 / 60.326
		Win.	100	27.239 / 66.395	22.825 / 38.835	32.199 / 25.825	33.816 / 38.854	27.070 / 21.439	29.205 / 38.793	12.455 / 17.299	22.156 / 60.530
		Sum.	0	23.980 / 63.849	20.779 / 37.787	28.739 / 25.002	31.106 / 37.787	23.303 / 20.643	25.220 / 37.592	11.445 / 16.954	19.157 / 57.772
		Sum.	100	25.645 / 63.190	21.035 / 37.654	30.378 / 24.965	31.765 / 37.582	25.763 / 20.745	27.956 / 37.668	12.415 / 16.898	20.790 / 57.579
				(25)	(26)	(27)	(28)	(29)	(30)	(31)	(32)
		Win.	0	19.212 / 100.321	17.318 / 58.429	20.938 / 42.787	19.447 / 27.090	31.692 / 69.445	27.117 / 17.273	49.098 / 34.673	42.220 / 17.273
		Win.	100	19.912 / 100.871	18.747 / 60.477	21.397 / 44.017	19.326 / 26.809	32.533 / 69.730	28.071 / 17.279	51.162 / 34.644	45.380 / 17.279
		Sum.	0	17.744 / 93.889	15.969 / 55.647	20.570 / 38.014	17.583 / 26.016	29.318 / 66.725	25.848 / 16.704	46.949 / 33.567	40.306 / 16.704
		Sum.	100	18.610 / 93.705	17.563 / 57.190	21.373 / 37.172	19.266 / 26.283	30.493 / 66.402	26.473 / 16.704	49.083 / 33.536	43.116 / 16.704

(Table B.3 continued on the next page)

(Table B.3 continued from the previous page)

PIHE	LNG			(1)	(2)	(3)	(4)	(5)	(6)	(7)	(8)
	(kg)	Win.	0	26.593 / 61.859	25.797 / 30.115	27.057 / 62.008	19.337 / 34.530	25.175 / 61.841	20.913 / 34.510	1.688 / 46.402	2.866 / 42.371
	/	Win.	100	29.686 / 61.930	28.677 / 30.114	27.447 / 61.862	20.208 / 34.568	25.819 / 61.846	21.846 / 34.612	1.935 / 46.641	2.940 / 42.285
	E	Sum.	0	25.655 / 59.049	24.715 / 29.134	26.888 / 55.385	18.506 / 33.343	24.159 / 59.254	19.875 / 33.353	1.670 / 42.582	2.802 / 37.982
	(kWh)	Sum.	100	28.712 / 58.812	27.651 / 29.134	26.589 / 59.304	19.322 / 33.354	24.931 / 58.867	20.897 / 33.423	1.879 / 43.035	2.800 / 38.459
				(9)	(10)	(11)	(12)	(13)	(14)	(15)	(16)
		Win.	0	8.766 / 69.445	6.547 / 38.874	9.239 / 23.822	4.715 / 51.885	8.207 / 31.526	3.320 / 75.590	22.644 / 21.332	24.474 / 57.871
		Win.	100	9.450 / 69.367	7.784 / 38.947	9.629 / 24.672	4.955 / 52.938	8.535 / 31.637	3.645 / 75.598	24.390 / 21.347	27.940 / 58.069
		Sum.	0	8.024 / 65.821	5.968 / 37.752	9.120 / 21.093	4.703 / 46.830	8.078 / 28.172	2.818 / 71.397	21.353 / 20.664	24.357 / 55.481
		Sum.	100	8.731 / 65.917	7.010 / 37.687	9.614 / 21.148	4.940 / 47.885	8.239 / 28.990	3.200 / 71.215	23.073 / 20.797	26.586 / 55.948
				(17)	(18)	(19)	(20)	(21)	(22)	(23)	(24)
		Win.	0	18.051 / 66.907	14.795 / 38.855	21.459 / 25.811	23.341 / 39.027	17.414 / 21.429	18.968 / 38.737	8.026 / 17.341	14.197 / 60.322
		Win.	100	19.262 / 66.444	16.932 / 38.928	22.736 / 25.826	23.866 / 38.835	19.269 / 21.346	20.010 / 38.731	8.704 / 17.303	15.517 / 60.453
		Sum.	0	16.890 / 63.795	13.426 / 37.583	20.203 / 25.002	21.922 / 37.847	16.556 / 20.742	18.040 / 37.591	8.002 / 16.949	13.389 / 57.768
		Sum.	100	18.166 / 63.115	15.735 / 37.749	21.450 / 24.961	22.332 / 37.654	18.346 / 20.650	19.086 / 37.591	8.677 / 16.903	14.586 / 57.419
				(25)	(26)	(27)	(28)	(29)	(30)	(31)	(32)
		Win.	0	13.116 / 100.985	12.170 / 58.209	14.494 / 44.589	13.594 / 27.091	21.619 / 69.418	18.114 / 17.281	34.273 / 34.672	32.003 / 17.277
		Win.	100	13.927 / 100.921	13.081 / 60.717	14.980 / 43.918	13.487 / 26.888	22.779 / 69.741	19.624 / 17.283	35.603 / 34.645	31.771 / 17.282
		Sum.	0	12.274 / 93.779	11.198 / 55.565	14.234 / 39.820	12.290 / 26.016	20.058 / 66.700	16.988 / 16.703	32.771 / 33.566	30.590 / 16.603
		Sum.	100	13.024 / 93.729	12.285 / 57.265	14.963 / 37.076	13.446 / 26.362	21.355 / 66.401	18.524 / 16.709	34.065 / 16.709	30.192 / 16.708
PIHE	H2			(1)	(2)	(3)	(4)	(5)	(6)	(7)	(8)
	(kg)	Win.	0	10.900 / 61.834	10.593 / 30.108	11.071 / 62.004	7.906 / 34.539	10.293 / 61.846	8.553 / 34.515	0.691 / 46.403	1.173 / 42.357
	/	Win.	100	12.167 / 61.844	11.696 / 30.112	11.605 / 61.610	8.281 / 34.640	10.561 / 61.831	8.934 / 34.536	0.792 / 46.640	1.203 / 42.299
	E	Sum.	0	10.497 / 59.271	10.148 / 29.126	11.002 / 55.382	7.567 / 33.354	9.885 / 59.160	8.127 / 33.358	0.683 / 42.582	1.147 / 37.970
	(kWh)	Sum.	100	11.770 / 58.766	11.276 / 29.131	11.222 / 59.323	7.919 / 33.424	10.208 / 58.752	8.547 / 33.352	0.769 / 43.034	1.146 / 38.471
				(9)	(10)	(11)	(12)	(13)	(14)	(15)	(16)
		Win.	0	3.577 / 69.448	2.839 / 38.855	3.780 / 23.793	2.154 / 45.629	3.358 / 31.552	1.362 / 75.595	9.264 / 21.347	10.691 / 58.161
		Win.	100	3.863 / 69.397	2.859 / 38.960	3.940 / 24.671	2.235 / 46.557	3.492 / 31.524	1.491 / 75.458	9.976 / 21.354	11.196 / 57.652
		Sum.	0	3.271 / 65.853	2.514 / 37.586	3.731 / 21.063	2.148 / 40.618	3.306 / 28.193	1.166 / 71.321	8.735 / 20.685	10.232 / 55.958
		Sum.	100	3.585 / 65.717	2.698 / 37.910	3.934 / 21.146	2.228 / 41.552	3.371 / 28.883	1.308 / 70.820	9.432 / 20.797	10.650 / 55.354
				(17)	(18)	(19)	(20)	(21)	(22)	(23)	(24)
		Win.	0	7.472 / 67.104	6.381 / 38.971	8.884 / 25.811	9.124 / 38.753	7.020 / 21.359	7.752 / 38.936	3.284 / 17.344	5.808 / 60.332
		Win.	100	7.707 / 66.375	6.894 / 38.930	9.206 / 25.826	9.714 / 38.854	7.821 / 21.353	8.393 / 38.865	3.566 / 17.304	6.353 / 60.575
		Sum.	0	6.965 / 63.843	5.941 / 37.794	8.326 / 25.002	8.519 / 37.492	6.683 / 20.802	7.385 / 37.708	3.274 / 16.953	5.479 / 57.766
		Sum.	100	7.330 / 63.172	6.353 / 37.751	8.679 / 24.961	9.130 / 37.581	7.512 / 20.797	8.035 / 37.646	3.555 / 16.905	5.974 / 57.541
				(25)	(26)	(27)	(28)	(29)	(30)	(31)	(32)
		Win.	0	5.371 / 100.955	4.980 / 58.227	6.003 / 42.596	5.562 / 27.092	8.902 / 69.429	7.752 / 17.280	14.025 / 34.673	12.106 / 17.280
		Win.	100	5.701 / 100.892	5.353 / 60.699	6.081 / 45.880	5.518 / 26.803	9.306 / 69.767	8.028 / 17.282	14.567 / 34.643	13.000 / 17.281
		Sum.	0	5.031 / 93.700	4.582 / 55.580	5.751 / 39.257	5.029 / 26.017	8.273 / 66.720	7.398 / 16.704	13.411 / 33.567	11.547 / 16.704
		Sum.	100	5.332 / 93.693	5.027 / 57.247	6.074 / 39.025	5.502 / 26.278	8.723 / 66.426	7.582 / 16.710	13.929 / 33.535	12.362 / 16.711

FCHE	H2			(1)	(2)	(3)	(4)	(5)	(6)	(7)	(8)	(9)	(10)	(11)	(12)	(13)	(14)	(15)	(16)
	(kg)	Win.	0	12.717	12.557	12.677	10.120	12.225	10.865	3.412	3.749	7.189	6.231	4.528	5.501	4.694	6.823	10.999	11.388
		Win.	100	14.058	13.624	13.222	10.391	12.410	11.138	3.495	3.788	7.395	6.340	4.717	5.415	4.771	6.916	11.523	12.185
		Sum.	0	12.692	12.132	12.486	10.073	12.122	10.320	3.330	3.718	7.184	6.085	4.430	4.415	4.621	6.675	10.852	11.272
		Sum.	100	13.815	13.625	13.174	10.376	12.331	11.063	3.413	3.761	7.389	6.236	4.613	5.400	4.709	6.769	11.378	11.999
				(17)	(18)	(19)	(20)	(21)	(22)	(23)	(24)	(25)	(26)	(27)	(28)	(29)	(30)	(31)	(32)
		Win.	0	10.343	8.602	9.822	10.082	8.116	8.727	5.951	7.425	12.988	8.270	8.413	6.461	11.490	9.117	14.243	12.479
		Win.	100	10.834	9.061	10.354	10.559	8.659	9.107	6.233	7.843	13.266	8.685	8.614	6.594	11.721	9.661	14.733	13.193
		Sum.	0	10.252	8.530	9.730	9.837	8.043	8.650	5.914	7.347	11.977	8.206	8.181	6.344	11.026	9.020	13.990	12.324
		Sum.	100	10.733	8.919	10.252	10.361	8.554	9.058	6.197	7.765	12.384	8.631	8.385	6.493	11.282	9.562	14.583	13.054
BE	E			(1)	(2)	(3)	(4)	(5)	(6)	(7)	(8)	(9)	(10)	(11)	(12)	(13)	(14)	(15)	(16)
	(kWh)	Win.	0	167.131	158.895	169.559	138.601	161.618	145.159	105.056	0.000	0.000	163.508	0.000	130.275	0.000	153.352	24.827	258.125
		Win.	100	181.759	172.224	173.147	141.880	165.352	149.027	106.767	0.000	0.000	170.052	0.000	134.510	0.000	156.537	26.447	271.148
		Sum.	0	157.996	151.081	161.931	132.406	153.996	138.958	96.319	0.000	0.000	150.261	0.000	121.507	0.000	142.290	23.892	241.466
		Sum.	100	172.611	164.396	165.515	135.679	157.728	142.823	97.997	0.000	0.000	156.780	0.000	125.711	0.000	145.474	25.519	254.478
				(17)	(18)	(19)	(20)	(21)	(22)	(23)	(24)	(25)	(26)	(27)	(28)	(29)	(30)	(31)	(32)
		Win.	0	12.655	223.176	12.655	235.210	12.624	195.946	0.000	165.791	4.309	257.634	4.600	193.450	29.226	231.078	71.899	270.478
		Win.	100	13.582	235.401	13.582	245.807	13.580	210.239	0.000	175.795	4.613	267.857	4.748	198.157	30.748	238.496	76.955	283.274
		Sum.	0	12.206	205.988	12.206	218.019	12.178	183.205	0.000	154.314	3.978	238.537	4.195	181.763	27.812	215.110	69.291	256.338
		Sum.	100	13.133	218.210	13.133	228.612	13.131	197.487	0.000	164.310	4.285	248.749	4.343	186.483	29.341	222.473	74.349	268.527

Legend: DE = Diesel-electric, HE = Hybrid-electric, PIHE = Plug-in hybrid-electric, FCHE = Fuel cell hybrid-electric, BE = Battery-electric, ZESC = Zero-emission station control, FSMC = Finite state machine control, FAME = Fatty Acid Methyl Ester, HVO = Hydrotreated vegetable oil, LNG = Liquefied natural gas, H2 = Hydrogen, E = Electricity.

Table B.4: Estimated consumption of different energy carriers for GTW 2/8 vehicle.

Propulsion system	Energy carrier	Season	Load (%)	Consumption per service															
DE	Diesel			(1)	(2)	(3)	(4)	(5)	(6)	(7)	(8)	(9)	(10)	(11)	(12)	(13)	(14)	(15)	(16)
	(l)	Win.	0	55.971	53.441	51.630	41.574	49.595	43.489	17.021	18.821	32.252	25.821	21.090	22.741	21.860	28.515	47.426	48.905
		Win.	100	62.515	60.804	54.093	43.553	51.205	45.893	17.597	19.242	33.753	27.053	22.446	23.642	22.574	29.149	50.982	52.476
		Sum.	0	54.882	52.082	50.239	40.393	48.237	42.324	16.256	18.088	31.120	24.902	20.397	21.943	21.112	27.179	45.970	47.297
		Sum.	100	60.957	59.382	52.694	42.369	49.841	44.458	16.835	18.513	32.607	26.354	21.745	22.845	21.830	27.815	49.514	50.838
				(17)	(18)	(19)	(20)	(21)	(22)	(23)	(24)	(25)	(26)	(27)	(28)	(29)	(30)	(31)	(32)
		Win.	0	45.554	37.909	43.186	43.672	36.041	37.102	25.181	33.518	54.149	37.082	34.251	28.488	47.990	40.226	57.772	53.668
		Win.	100	49.023	40.596	46.852	46.917	40.076	40.567	27.084	36.408	56.646	40.099	35.495	29.851	50.444	43.764	62.036	58.378
		Sum.	0	43.860	36.668	41.650	42.217	36.928	35.851	24.377	32.441	52.020	35.920	32.793	27.552	46.258	39.024	55.881	52.075
		Sum.	100	47.371	39.350	45.357	45.261	38.845	39.293	26.269	35.310	54.644	38.903	34.107	28.922	48.778	42.526	60.323	56.748
HE	Diesel			(1)	(2)	(3)	(4)	(5)	(6)	(7)	(8)	(9)	(10)	(11)	(12)	(13)	(14)	(15)	(16)
(ZESC)	(l)	Win.	0	55.259	55.431	49.384	40.850	47.055	42.867	14.636	13.025	28.419	23.933	20.453	20.442	20.245	24.330	47.876	47.091
		Win.	100	62.093	62.727	52.372	43.391	48.926	45.383	15.083	13.167	30.019	25.513	21.772	21.333	20.965	24.980	51.732	50.665
		Sum.	0	53.666	54.175	47.511	39.583	45.085	41.532	13.914	12.677	27.187	22.884	19.545	19.407	19.668	23.000	46.516	45.432
		Sum.	100	60.438	61.414	50.504	42.125	46.946	44.043	14.505	12.817	28.775	24.459	20.882	20.297	20.384	23.552	50.360	49.022
				(17)	(18)	(19)	(20)	(21)	(22)	(23)	(24)	(25)	(26)	(27)	(28)	(29)	(30)	(31)	(32)
		Win.	0	42.147	36.556	43.371	41.893	36.559	36.113	24.807	32.000	41.353	35.137	31.703	27.759	44.830	41.169	57.334	55.458
		Win.	100	45.903	38.846	47.484	44.339	41.125	40.243	27.097	34.301	44.248	39.266	32.736	29.468	46.909	45.882	62.437	61.450
		Sum.	0	40.338	35.302	41.931	40.610	35.457	34.557	24.077	30.143	40.231	34.060	29.965	26.614	42.508	40.023	55.792	53.922
		Sum.	100	44.161	37.599	46.078	43.030	39.994	38.740	26.353	32.473	43.208	37.871	30.997	28.306	44.890	44.663	60.875	59.840
HE	FAME			(1)	(2)	(3)	(4)	(5)	(6)	(7)	(8)	(9)	(10)	(11)	(12)	(13)	(14)	(15)	(16)
(ZESC)	(l)	Win.	0	59.892	60.630	54.397	44.238	50.926	46.519	15.852	14.108	30.771	25.963	22.180	22.956	21.943	26.345	51.881	51.057
		Win.	100	67.387	68.005	57.753	46.983	52.985	49.134	16.339	14.260	32.524	27.654	23.617	23.110	22.754	27.102	56.081	54.824
		Sum.	0	58.169	59.262	52.323	42.870	48.800	45.064	15.071	13.730	29.444	24.825	21.201	21.693	21.312	24.913	50.413	49.260
		Sum.	100	65.597	66.581	55.689	45.608	50.839	47.677	15.713	13.881	31.177	26.494	22.649	21.988	22.125	25.541	54.594	53.040
				(17)	(18)	(19)	(20)	(21)	(22)	(23)	(24)	(25)	(26)	(27)	(28)	(29)	(30)	(31)	(32)
		Win.	0	45.642	38.975	46.989	44.883	40.011	38.953	26.871	34.717	44.769	38.059	34.447	30.064	48.594	44.558	62.247	60.154
		Win.	100	49.701	42.105	51.419	48.322	44.031	43.400	29.357	37.134	47.964	42.504	35.535	31.962	51.887	49.727	67.549	66.549
		Sum.	0	43.776	37.681	45.514	43.509	38.798	37.321	26.082	32.704	43.555	36.891	32.573	28.826	46.080	43.317	60.475	58.488
		Sum.	100	47.819	40.896	49.897	46.806	42.851	41.815	28.551	35.142	46.833	40.993	33.655	30.701	49.444	48.405	65.856	64.805
HE	HVO			(1)	(2)	(3)	(4)	(5)	(6)	(7)	(8)	(9)	(10)	(11)	(12)	(13)	(14)	(15)	(16)
(ZESC)	(l)	Win.	0	57.967	57.888	51.588	42.681	49.108	44.828	15.292	13.612	29.693	25.107	21.368	21.353	21.179	25.425	50.040	49.668
		Win.	100	64.928	65.483	54.670	45.319	51.110	47.417	15.761	13.777	31.307	27.167	22.781	22.303	21.925	26.097	54.054	52.582
		Sum.	0	56.033	56.577	49.635	41.361	47.057	43.426	14.539	13.245	28.406	24.009	20.422	20.275	20.569	24.063	48.620	47.841
		Sum.	100	63.218	64.112	52.721	43.995	49.028	46.014	15.157	13.410	30.011	25.946	21.843	21.226	21.318	24.596	52.618	51.139
				(17)	(18)	(19)	(20)	(21)	(22)	(23)	(24)	(25)	(26)	(27)	(28)	(29)	(30)	(31)	(32)
		Win.	0	43.825	37.491	45.118	43.261	38.578	37.049	25.914	33.480	43.173	36.738	33.511	28.994	46.826	43.068	60.044	57.987
		Win.	100	47.904	40.661	49.567	46.511	42.494	42.005	28.292	35.828	46.193	41.027	34.244	30.869	49.979	47.869	65.101	63.935
		Sum.	0	42.038	36.478	43.708	41.865	37.373	35.573	25.152	31.542	42.003	35.610	31.700	27.797	44.402	41.869	58.335	56.381
		Sum.	100	46.166	39.436	48.176	45.027	41.308	40.506	27.514	33.916	45.104	39.571	32.426	29.650	47.623	46.596	63.467	62.259
HE	LNG			(1)	(2)	(3)	(4)	(5)	(6)	(7)	(8)	(9)	(10)	(11)	(12)	(13)	(14)	(15)	(16)
(ZESC)	(kg)	Win.	0	40.378	40.810	36.617	29.840	34.340	31.325	10.689	11.016	20.761	17.864	14.942	14.965	14.771	17.777	34.966	34.277
		Win.	100	45.409	45.844	38.245	31.683	35.729	33.128	11.016	9.617	21.903	18.644	15.910	15.571	15.351	18.248	37.785	36.948
		Sum.	0	39.212	39.889	35.218	28.915	32.905	30.349	10.162	10.886	19.861	17.015	14.281	14.207	14.349	16.814	33.973	33.087
		Sum.	100	44.203	44.885	36.884	30.753	34.272	32.150	10.594	9.361	20.995	17.857	15.258	14.819	14.926	17.194	36.782	35.750
				(17)	(18)	(19)	(20)	(21)	(22)	(23)	(24)	(25)	(26)	(27)	(28)	(29)	(30)	(31)	(32)
		Win.	0	30.669	26.595	31.712	30.234	26.711	25.926	18.142	23.403	30.206	25.677	23.457	20.283	32.771	30.079	41.946	40.554
		Win.	100	33.394	28.398	34.705	32.416	29.707	29.234	19.755	25.032	32.289	28.689	23.993	21.586	34.928	33.526	45.533	44.895
		Sum.	0	29.350	25.845	30.616	29.354	25.929	24.876	17.607	22.047	29.441	24.890	22.194	19.542	31.128	29.240	40.751	39.430
		Sum.	100	32.120	27.488	33.635	31.459	28.879	28.165	19.212	23.697	31.529	27.676	22.726	20.733	33.282	32.635	44.391	43.718

(Table B.4 continued on the next page)

(Table B.4 continued from the previous page)

HE (ZESC)	H2 (kg)			(1)	(2)	(3)	(4)	(5)	(6)	(7)	(8)	(9)	(10)	(11)	(12)	(13)	(14)	(15)	(16)
		Win.	0	16.509	16.589	15.005	12.206	14.054	12.825	4.373	3.889	8.493	7.162	6.124	6.323	6.061	7.271	14.315	14.148
		Win.	100	18.580	18.748	15.918	12.974	14.617	13.557	4.508	3.935	8.970	7.632	6.504	6.377	6.353	7.482	15.474	15.134
		Sum.	0	16.034	16.213	14.432	11.828	13.466	12.424	4.158	3.785	8.125	6.848	5.853	5.977	5.886	6.876	13.908	13.632
		Sum.	100	18.086	18.355	15.349	12.595	14.021	13.155	4.335	3.830	8.598	7.310	6.237	6.067	6.165	7.057	15.063	14.642
				(17)	(18)	(19)	(20)	(21)	(22)	(23)	(24)	(25)	(26)	(27)	(28)	(29)	(30)	(31)	(32)
		Win.	0	12.543	10.734	12.974	12.525	11.033	10.674	7.421	9.571	12.369	10.512	9.586	8.303	13.419	12.289	17.130	16.599
		Win.	100	13.682	11.580	14.213	13.309	12.291	12.036	8.102	10.247	13.222	11.728	9.811	8.823	14.302	13.705	18.659	18.360
		Sum.	0	12.005	10.430	12.526	12.163	10.689	10.236	7.203	9.016	12.055	10.189	9.066	7.960	12.746	11.947	16.669	16.140
		Sum.	100	13.159	11.263	13.774	12.907	11.953	11.588	7.879	9.698	12.911	11.312	9.291	8.474	13.628	13.341	18.192	17.879
HE (FSMC)	Diesel (l)			(1)	(2)	(3)	(4)	(5)	(6)	(7)	(8)	(9)	(10)	(11)	(12)	(13)	(14)	(15)	(16)
		Win.	0	55.727	54.423	49.470	41.530	46.959	43.702	14.700	13.141	29.322	23.889	22.121	20.472	20.770	24.334	48.242	47.788
		Win.	100	62.128	61.353	52.488	43.843	48.718	46.265	15.160	13.276	30.786	25.198	23.573	21.243	21.161	24.983	51.569	50.938
		Sum.	0	52.382	52.141	47.070	40.055	44.679	42.026	14.030	12.794	26.341	22.142	21.510	19.259	20.144	23.440	46.033	44.863
		Sum.	100	59.076	59.542	50.464	42.424	46.607	44.608	14.750	12.929	27.982	23.783	22.912	20.091	20.749	23.967	49.446	48.468
				(17)	(18)	(19)	(20)	(21)	(22)	(23)	(24)	(25)	(26)	(27)	(28)	(29)	(30)	(31)	(32)
		Win.	0	43.438	38.188	42.923	43.591	36.811	36.500	24.241	32.284	39.809	34.982	32.919	28.258	45.877	40.065	56.279	52.918
		Win.	100	47.328	39.971	46.497	45.713	41.030	40.533	26.403	35.082	42.632	39.812	33.752	30.347	47.393	45.449	61.830	59.763
		Sum.	0	40.650	35.694	40.554	40.614	35.193	34.100	22.626	30.489	38.413	33.053	31.136	27.108	41.833	38.370	54.254	50.849
		Sum.	100	44.191	37.504	44.304	42.797	39.901	38.330	24.996	33.385	41.318	37.957	32.156	29.275	42.678	43.774	59.073	57.324
HE (FSMC)	FAME (l)			(1)	(2)	(3)	(4)	(5)	(6)	(7)	(8)	(9)	(10)	(11)	(12)	(13)	(14)	(15)	(16)
		Win.	0	60.364	59.540	55.326	44.979	50.824	47.431	15.921	14.233	31.766	25.756	23.992	22.987	22.604	26.349	52.345	51.810
		Win.	100	67.456	66.526	58.357	47.481	52.754	50.088	16.422	14.379	33.348	27.516	25.636	23.017	22.958	27.106	55.907	55.060
		Sum.	0	56.755	57.070	52.677	43.382	48.357	45.609	15.196	13.857	28.544	24.015	23.327	21.274	21.916	25.372	49.889	48.644
		Sum.	100	64.132	64.574	56.048	45.943	50.451	48.289	15.978	14.003	30.327	25.724	24.864	21.770	22.511	25.984	53.611	52.384
				(17)	(18)	(19)	(20)	(21)	(22)	(23)	(24)	(25)	(26)	(27)	(28)	(29)	(30)	(31)	(32)
		Win.	0	46.580	40.420	46.007	44.048	40.519	39.365	26.234	35.050	43.089	37.876	35.681	30.608	49.711	43.389	61.315	57.433
		Win.	100	51.230	43.445	50.346	47.381	43.633	43.456	28.675	37.982	46.221	42.982	36.587	32.932	52.600	49.316	66.937	64.718
		Sum.	0	43.434	37.938	43.342	41.192	38.830	36.607	24.506	33.076	41.578	35.785	33.831	29.362	47.373	41.544	58.961	55.136
		Sum.	100	47.830	40.881	47.962	44.798	42.132	41.032	27.106	36.140	44.788	40.994	34.884	31.740	50.403	47.496	63.934	62.103
HE (FSMC)	HVO (l)			(1)	(2)	(3)	(4)	(5)	(6)	(7)	(8)	(9)	(10)	(11)	(12)	(13)	(14)	(15)	(16)
		Win.	0	58.207	56.845	51.679	43.398	49.012	45.701	15.359	13.733	30.648	24.885	23.116	21.383	21.818	25.429	50.464	50.841
		Win.	100	65.019	64.034	54.820	45.798	50.901	48.338	15.841	13.890	32.131	27.290	24.628	22.247	22.128	26.100	53.911	53.146
		Sum.	0	54.695	54.461	49.177	41.859	46.636	43.947	14.660	13.368	27.545	23.205	22.475	20.106	21.153	24.499	48.103	47.935
		Sum.	100	61.826	62.133	52.699	44.318	48.675	46.606	15.412	13.527	29.187	25.445	23.937	21.016	21.699	25.041	51.686	50.579
				(17)	(18)	(19)	(20)	(21)	(22)	(23)	(24)	(25)	(26)	(27)	(28)	(29)	(30)	(31)	(32)
		Win.	0	45.469	38.702	44.169	42.947	38.980	37.019	25.309	33.779	41.544	36.756	34.166	29.538	47.898	41.876	59.137	55.361
		Win.	100	48.902	41.310	48.029	45.974	41.996	42.342	27.616	36.634	44.500	41.608	35.311	31.826	50.710	47.439	64.531	62.011
		Sum.	0	42.033	36.260	41.936	40.221	37.385	34.466	23.634	31.899	40.089	34.619	32.384	28.372	43.683	40.169	56.862	53.213
		Sum.	100	45.670	38.756	45.789	43.394	40.539	40.410	26.101	34.861	43.122	39.659	33.594	30.655	45.994	45.660	61.640	59.497
HE (FSMC)	LNG (kg)			(1)	(2)	(3)	(4)	(5)	(6)	(7)	(8)	(9)	(10)	(11)	(12)	(13)	(14)	(15)	(16)
		Win.	0	40.716	40.089	37.254	30.338	34.297	31.936	10.736	11.096	21.440	18.028	16.158	14.995	15.154	17.780	35.238	34.460
		Win.	100	45.356	44.823	38.331	32.013	35.572	33.771	11.072	9.696	22.451	18.520	17.215	15.537	15.487	18.251	37.662	37.139
		Sum.	0	38.341	38.419	35.469	29.261	32.609	30.710	10.247	10.967	19.259	16.728	15.707	14.104	14.697	17.127	33.630	32.535
		Sum.	100	43.005	43.519	36.855	30.974	34.027	32.562	10.773	9.443	20.413	17.316	16.731	14.679	15.186	17.503	36.114	35.343
				(17)	(18)	(19)	(20)	(21)	(22)	(23)	(24)	(25)	(26)	(27)	(28)	(29)	(30)	(31)	(32)
		Win.	0	31.616	27.630	31.200	30.013	26.939	25.908	17.748	23.608	28.975	25.687	23.899	20.692	33.240	29.258	41.323	38.677
		Win.	100	34.441	29.212	33.752	32.404	29.362	29.270	19.240	25.602	31.111	29.134	24.699	22.257	35.428	33.182	45.117	43.689
		Sum.	0	29.573	25.842	29.461	28.201	25.754	24.121	16.555	22.297	28.015	24.196	22.672	19.877	30.015	28.042	39.754	37.217
		Sum.	100	32.136	27.416	32.164	30.570	28.340	27.634	18.206	24.364	30.146	27.784	23.531	21.436	32.143	32.003	43.096	41.931
HE (FSMC)	H2 (kg)			(1)	(2)	(3)	(4)	(5)	(6)	(7)	(8)	(9)	(10)	(11)	(12)	(13)	(14)	(15)	(16)
		Win.	0	16.633	16.336	15.262	12.411	14.025	13.074	4.393	3.923	8.774	7.106	6.620	6.333	6.243	7.272	14.444	14.372
		Win.	100	18.598	18.344	16.086	13.109	14.565	13.821	4.530	3.967	9.195	7.592	7.047	6.352	6.329	7.483	15.427	15.202
		Sum.	0	15.667	15.608	14.531	11.971	13.344	12.571	4.193	3.820	7.878	6.626	6.434	5.863	6.053	7.002	13.765	13.639
		Sum.	100	17.604	17.802	15.449	12.684	14.055	13.325	4.408	3.864	8.359	7.123	6.841	6.008	6.207	7.177	14.794	14.469
				(17)	(18)	(19)	(20)	(21)	(22)	(23)	(24)	(25)	(26)	(27)	(28)	(29)	(30)	(31)	(32)
		Win.	0	12.921	11.094	12.744	12.865	11.154	10.667	7.247	9.655	11.864	10.462	9.776	8.468	13.603	11.954	16.801	15.846
		Win.	100	14.111	11.920	13.830	13.011	12.264	12.158	7.895	10.480	12.737	11.866	10.097	9.088	14.496	13.590	18.484	17.845
		Sum.	0	12.090	10.420	12.038	12.012	10.703	9.983	6.766	9.113	11.465	9.892	9.259	8.133	12.979	11.449	16.207	15.225
		Sum.	100	13.097	11.166	13.150	12.270	11.925	11.477	7.469	9.972	12.344	11.318	9.618	8.766	13.891	13.080	17.660	17.140

(Table B.4 continued on the next page)

(Table B.4 continued from the previous page)

PIHE	Diesel			(1)	(2)	(3)	(4)	(5)	(6)	(7)	(8)
	(l)	Win.	0	43.786 / 62.808	43.491 / 30.460	38.994 / 62.790	28.853 / 34.949	36.553 / 62.813	31.350 / 34.957	2.920 / 47.962	4.002 / 44.799
	/	Win.	100	51.038 / 62.599	50.453 / 30.473	43.528 / 62.440	32.104 / 34.881	38.624 / 62.665	34.157 / 34.881	3.794 / 47.154	4.098 / 46.149
	E	Sum.	0	42.057 / 59.289	41.809 / 29.297	37.697 / 59.356	27.489 / 33.535	35.081 / 59.439	29.973 / 33.613	2.758 / 43.960	3.995 / 39.218
	(kWh)	Sum.	100	49.328 / 58.702	48.769 / 29.304	42.230 / 59.397	29.956 / 33.577	37.294 / 58.768	32.406 / 33.577	3.318 / 44.480	4.085 / 40.570
				(9)	(10)	(11)	(12)	(13)	(14)	(15)	(16)
		Win.	0	13.961 / 70.641	10.939 / 39.410	13.619 / 27.037	6.987 / 55.773	12.092 / 32.912	6.023 / 74.530	36.137 / 21.629	40.719 / 58.798
		Win.	100	15.629 / 70.640	12.695 / 39.355	14.539 / 27.484	8.326 / 50.639	12.365 / 34.750	9.970 / 54.636	39.796 / 21.625	43.365 / 58.635
		Sum.	0	12.917 / 66.345	9.564 / 37.864	13.590 / 22.881	6.948 / 49.837	11.203 / 31.352	4.694 / 72.267	33.544 / 20.817	38.528 / 56.287
		Sum.	100	14.692 / 66.330	11.422 / 37.836	14.514 / 24.898	8.295 / 44.669	12.296 / 30.030	8.741 / 51.783	37.493 / 20.921	41.614 / 55.770
				(17)	(18)	(19)	(20)	(21)	(22)	(23)	(24)
		Win.	0	28.764 / 67.507	24.220 / 39.156	33.689 / 26.112	35.710 / 39.305	29.184 / 21.571	30.251 / 39.306	13.357 / 17.488	23.012 / 61.295
		Win.	100	32.907 / 67.829	27.207 / 39.304	38.205 / 26.131	38.256 / 39.305	33.364 / 21.713	34.562 / 39.324	15.482 / 17.477	25.489 / 60.988
		Sum.	0	26.956 / 63.656	22.112 / 37.792	31.651 / 25.107	33.218 / 37.902	27.897 / 20.919	28.681 / 37.840	12.495 / 16.902	21.500 / 58.271
		Sum.	100	31.018 / 64.091	24.955 / 37.796	35.956 / 25.085	35.797 / 37.807	32.103 / 21.012	33.158 / 37.827	14.407 / 16.842	24.152 / 57.969
				(25)	(26)	(27)	(28)	(29)	(30)	(31)	(32)
		Win.	0	21.129 / 103.341	20.557 / 59.747	20.672 / 49.413	18.436 / 26.757	33.970 / 70.894	29.196 / 17.482	51.756 / 35.010	46.884 / 17.482
		Win.	100	24.188 / 102.819	24.790 / 59.795	21.556 / 49.614	19.653 / 26.586	36.898 / 70.586	34.057 / 17.469	56.447 / 34.964	53.603 / 17.469
		Sum.	0	19.586 / 95.030	18.700 / 57.389	20.647 / 41.266	18.402 / 26.104	32.202 / 66.277	27.274 / 16.796	49.342 / 33.961	44.050 / 16.796
		Sum.	100	22.711 / 94.652	23.130 / 57.351	21.530 / 41.495	19.602 / 25.915	35.196 / 65.860	32.196 / 16.702	54.152 / 33.642	51.005 / 16.702
PIHE	FAME			(1)	(2)	(3)	(4)	(5)	(6)	(7)	(8)
	(l)	Win.	0	47.574 / 62.807	46.534 / 30.456	43.815 / 62.795	31.251 / 34.959	39.562 / 62.816	33.984 / 34.958	3.162 / 47.965	4.335 / 44.798
	/	Win.	100	55.357 / 62.776	54.652 / 30.547	45.768 / 62.349	34.769 / 34.881	41.826 / 62.727	36.988 / 34.881	4.110 / 47.152	4.438 / 46.132
	E	Sum.	0	45.659 / 59.289	44.701 / 29.290	42.443 / 59.357	29.751 / 33.536	38.019 / 59.263	32.510 / 33.617	2.988 / 43.963	4.327 / 39.217
	(kWh)	Sum.	100	53.367 / 58.903	52.836 / 29.375	44.340 / 59.206	32.440 / 33.578	40.383 / 58.825	35.089 / 33.578	3.592 / 44.478	4.424 / 40.556
				(9)	(10)	(11)	(12)	(13)	(14)	(15)	(16)
		Win.	0	15.143 / 70.648	12.606 / 39.304	14.734 / 27.186	7.553 / 55.789	13.119 / 32.694	6.525 / 74.400	39.083 / 21.636	43.446 / 58.780
		Win.	100	16.988 / 70.645	13.306 / 39.304	15.746 / 27.484	9.000 / 50.668	13.363 / 34.813	10.799 / 54.637	43.073 / 21.722	47.020 / 58.642
		Sum.	0	14.009 / 66.352	11.176 / 37.792	14.708 / 22.999	7.508 / 49.850	12.148 / 31.152	5.072 / 72.181	36.280 / 20.823	41.063 / 55.941
		Sum.	100	15.980 / 66.288	11.908 / 37.805	15.717 / 24.892	8.964 / 44.697	13.287 / 30.088	9.911 / 51.265	40.589 / 20.991	45.119 / 55.777
				(17)	(18)	(19)	(20)	(21)	(22)	(23)	(24)
		Win.	0	31.268 / 68.038	26.567 / 39.155	36.725 / 26.112	38.710 / 39.303	31.022 / 21.753	31.842 / 39.313	14.549 / 17.491	24.932 / 61.409
		Win.	100	35.657 / 67.171	29.611 / 39.305	41.247 / 26.134	41.126 / 39.305	36.209 / 21.586	37.505 / 39.325	16.765 / 17.476	27.608 / 61.036
		Sum.	0	29.354 / 64.228	24.167 / 37.792	34.568 / 25.107	35.952 / 37.900	29.826 / 20.971	30.291 / 37.852	13.569 / 16.898	23.302 / 58.388
		Sum.	100	33.630 / 63.363	27.285 / 37.790	38.795 / 25.084	38.438 / 37.790	34.728 / 20.783	35.986 / 37.827	15.637 / 16.846	26.126 / 58.095
				(25)	(26)	(27)	(28)	(29)	(30)	(31)	(32)
		Win.	0	22.873 / 103.299	22.214 / 59.787	22.354 / 49.372	19.997 / 26.832	35.624 / 70.516	31.677 / 17.479	56.019 / 35.010	50.679 / 17.479
		Win.	100	26.156 / 102.938	26.835 / 59.799	23.331 / 49.508	21.255 / 26.568	38.778 / 70.647	36.994 / 17.476	61.102 / 34.964	58.077 / 17.538
		Sum.	0	21.194 / 95.011	20.206 / 57.422	22.327 / 41.227	19.931 / 26.179	33.180 / 67.189	29.695 / 16.808	53.384 / 33.692	47.707 / 16.808
		Sum.	100	24.564 / 94.642	25.048 / 57.311	23.303 / 41.389	21.194 / 25.894	36.513 / 66.808	34.936 / 16.701	58.614 / 33.642	55.264 / 16.776
PIHE	HVO			(1)	(2)	(3)	(4)	(5)	(6)	(7)	(8)
	(l)	Win.	0	45.820 / 62.816	44.814 / 30.460	42.226 / 62.789	30.155 / 34.957	38.131 / 62.792	32.758 / 35.024	3.052 / 47.967	4.182 / 44.811
	/	Win.	100	53.219 / 62.613	52.662 / 30.471	44.050 / 62.461	33.494 / 34.881	40.341 / 62.608	35.691 / 34.869	3.964 / 47.155	4.282 / 46.150
	E	Sum.	0	44.008 / 59.240	43.056 / 29.297	40.897 / 59.373	28.707 / 33.533	36.655 / 59.206	31.319 / 33.678	2.882 / 43.965	4.174 / 39.218
	(kWh)	Sum.	100	51.425 / 58.715	50.914 / 29.308	42.661 / 59.358	31.240 / 33.577	38.952 / 58.129	33.862 / 33.566	3.467 / 44.481	4.269 / 40.571
				(9)	(10)	(11)	(12)	(13)	(14)	(15)	(16)
		Win.	0	14.616 / 70.628	11.407 / 39.330	14.197 / 26.978	7.286 / 55.870	12.667 / 32.756	6.295 / 74.611	37.657 / 21.595	41.902 / 58.808
		Win.	100	16.409 / 70.639	13.729 / 39.306	15.195 / 27.409	8.682 / 50.651	12.955 / 34.819	7.877 / 70.790	41.443 / 21.611	45.282 / 58.634
		Sum.	0	13.500 / 66.401	9.985 / 37.793	14.169 / 22.806	7.245 / 49.905	11.734 / 31.199	4.933 / 72.234	35.042 / 20.914	39.587 / 55.968
		Sum.	100	15.420 / 66.306	12.527 / 37.841	15.160 / 24.890	8.650 / 44.679	12.883 / 30.093	5.771 / 71.593	39.036 / 20.918	43.452 / 55.769
				(17)	(18)	(19)	(20)	(21)	(22)	(23)	(24)
		Win.	0	30.550 / 68.023	27.125 / 39.306	35.817 / 26.112	37.717 / 39.307	29.891 / 21.758	31.138 / 39.309	13.928 / 17.491	24.029 / 61.407
		Win.	100	34.130 / 67.774	28.107 / 39.305	39.657 / 26.131	39.603 / 39.305	34.948 / 21.586	35.619 / 39.337	16.157 / 17.476	26.578 / 61.093
		Sum.	0	28.548 / 64.293	25.001 / 37.904	33.599 / 25.107	35.143 / 37.904	28.743 / 20.976	29.668 / 37.849	12.990 / 16.901	22.463 / 58.386
		Sum.	100	32.290 / 64.039	25.765 / 37.790	37.441 / 25.084	36.977 / 37.791	33.513 / 20.783	34.071 / 37.822	15.054 / 16.844	25.145 / 58.217
				(25)	(26)	(27)	(28)	(29)	(30)	(31)	(32)
		Win.	0	22.052 / 103.286	21.439 / 59.705	21.599 / 49.428	19.275 / 26.756	35.468 / 70.896	30.576 / 17.554	54.030 / 35.009	49.003 / 17.550
		Win.	100	25.264 / 102.939	25.740 / 60.049	22.524 / 49.625	20.468 / 26.593	37.370 / 70.655	35.513 / 17.468	58.874 / 34.964	55.855 / 17.468
		Sum.	0	20.426 / 95.016	19.509 / 57.396	21.573 / 41.280	19.210 / 26.103	33.623 / 66.288	28.561 / 16.868	51.534 / 33.691	46.108 / 16.869
		Sum.	100	23.736 / 94.643	24.045 / 57.493	22.495 / 41.507	20.416 / 25.923	35.207 / 66.815	33.584 / 16.697	56.478 / 33.642	53.159 / 16.690

(Table B.4 continued on the next page)

(Table B.4 continued from the previous page)

PIHE	LNG			(1)	(2)	(3)	(4)	(5)	(6)	(7)	(8)
	(kg)	Win.	0	32.021 / 62.778	31.790 / 30.461	28.475 / 62.824	21.075 / 34.960	26.644 / 62.813	22.950 / 34.960	2.132 / 47.962	2.911 / 44.813
	/	Win.	100	37.287 / 62.670	36.831 / 30.464	30.757 / 62.432	23.448 / 34.869	28.158 / 62.580	24.943 / 34.881	2.771 / 47.153	2.993 / 46.134
	E	Sum.	0	30.732 / 59.368	30.558 / 29.297	27.507 / 59.479	20.064 / 33.537	25.619 / 59.191	21.963 / 33.620	2.015 / 43.960	2.906 / 39.234
	(kWh)	Sum.	100	36.029 / 58.770	35.618 / 29.304	29.789 / 59.330	21.877 / 33.566	27.189 / 58.686	23.662 / 33.577	2.422 / 44.479	2.983 / 40.557
				(9)	(10)	(11)	(12)	(13)	(14)	(15)	(16)
		Win.	0	10.212 / 70.648	7.821 / 39.304	9.935 / 27.187	5.609 / 49.353	8.855 / 32.825	4.403 / 74.457	26.316 / 21.608	29.017 / 58.693
		Win.	100	11.409 / 70.636	9.620 / 39.308	10.633 / 27.478	6.081 / 50.662	9.009 / 34.828	7.282 / 54.639	29.018 / 21.716	31.685 / 58.634
		Sum.	0	9.429 / 66.448	6.989 / 37.865	9.917 / 23.000	5.587 / 43.413	8.204 / 31.265	3.508 / 71.963	24.482 / 20.914	27.459 / 55.892
		Sum.	100	10.725 / 66.334	8.770 / 37.844	10.607 / 25.002	6.057 / 44.692	8.958 / 30.105	6.426 / 51.526	27.344 / 20.991	30.406 / 55.769
				(17)	(18)	(19)	(20)	(21)	(22)	(23)	(24)
		Win.	0	21.323 / 67.520	18.368 / 39.303	24.927 / 26.112	26.409 / 39.302	21.312 / 21.599	22.490 / 39.304	9.764 / 17.489	16.837 / 61.302
		Win.	100	23.843 / 67.830	19.860 / 39.305	27.715 / 26.131	27.442 / 39.272	23.943 / 21.586	24.916 / 39.338	11.243 / 17.316	18.624 / 61.089
		Sum.	0	19.946 / 63.672	16.910 / 37.900	23.383 / 25.107	24.563 / 37.899	20.357 / 20.917	21.475 / 37.847	9.126 / 16.901	15.739 / 58.271
		Sum.	100	22.558 / 64.086	18.197 / 37.790	26.165 / 25.085	25.645 / 37.864	22.935 / 20.783	23.835 / 37.822	10.522 / 16.839	17.633 / 58.103
				(25)	(26)	(27)	(28)	(29)	(30)	(31)	(32)
		Win.	0	15.687 / 103.010	14.999 / 59.795	15.192 / 47.780	13.484 / 26.764	24.658 / 70.869	21.325 / 17.479	37.808 / 35.008	34.216 / 17.479
		Win.	100	17.654 / 103.053	18.126 / 59.999	15.743 / 49.658	14.332 / 26.582	26.974 / 70.586	24.905 / 17.475	41.237 / 34.963	39.104 / 17.475
		Sum.	0	14.618 / 94.641	13.716 / 57.102	15.174 / 39.646	13.439 / 26.113	23.335 / 66.267	19.924 / 16.797	36.049 / 33.689	32.212 / 16.808
		Sum.	100	16.584 / 94.752	16.963 / 57.282	15.724 / 41.538	14.294 / 25.910	25.713 / 65.860	23.533 / 16.694	39.560 / 33.641	37.198 / 16.694
PIHE	H2			(1)	(2)	(3)	(4)	(5)	(6)	(7)	(8)
	(kg)	Win.	0	13.097 / 62.784	12.757 / 30.454	11.651 / 62.794	8.624 / 34.949	10.911 / 62.817	9.376 / 34.960	0.872 / 47.965	1.191 / 44.812
	/	Win.	100	15.267 / 62.692	15.081 / 30.473	13.002 / 62.345	9.593 / 34.944	11.544 / 62.765	10.206 / 34.870	1.134 / 47.153	1.225 / 46.148
	E	Sum.	0	12.584 / 59.207	12.252 / 29.291	11.263 / 59.362	8.216 / 33.535	10.482 / 59.314	8.969 / 33.619	0.824 / 43.963	1.189 / 39.233
	(kWh)	Sum.	100	14.723 / 58.789	14.580 / 29.305	12.606 / 59.247	8.951 / 33.638	11.147 / 58.863	9.682 / 33.566	0.991 / 44.478	1.220 / 40.569
				(9)	(10)	(11)	(12)	(13)	(14)	(15)	(16)
		Win.	0	4.179 / 70.652	3.199 / 39.304	4.074 / 27.139	2.295 / 49.412	3.586 / 33.166	1.799 / 74.399	10.786 / 21.714	11.863 / 58.668
		Win.	100	4.685 / 70.635	3.777 / 39.433	4.351 / 27.402	2.488 / 50.630	3.696 / 34.750	2.253 / 70.706	11.870 / 21.722	12.971 / 58.643
		Sum.	0	3.857 / 66.472	2.860 / 37.865	4.065 / 22.983	2.286 / 43.471	3.323 / 31.558	1.408 / 72.065	10.011 / 20.898	11.230 / 55.833
		Sum.	100	4.404 / 66.322	3.380 / 37.915	4.340 / 24.980	2.478 / 44.660	3.674 / 30.027	1.637 / 71.673	11.186 / 20.991	12.448 / 55.778
				(17)	(18)	(19)	(20)	(21)	(22)	(23)	(24)
		Win.	0	8.622 / 67.478	7.544 / 39.308	10.092 / 26.112	10.708 / 39.308	8.562 / 21.758	9.210 / 39.306	4.011 / 17.508	6.884 / 61.304
		Win.	100	9.837 / 67.830	8.054 / 39.304	11.421 / 26.204	11.301 / 39.304	9.801 / 21.564	10.327 / 39.339	4.606 / 17.475	7.623 / 61.051
		Sum.	0	8.111 / 63.504	6.924 / 37.905	9.505 / 25.107	9.950 / 37.905	8.232 / 20.976	8.740 / 37.838	3.739 / 16.896	6.435 / 58.273
		Sum.	100	9.274 / 64.086	7.436 / 37.808	10.750 / 25.155	10.565 / 37.807	9.388 / 20.762	9.897 / 37.822	4.310 / 16.851	7.225 / 57.973
				(25)	(26)	(27)	(28)	(29)	(30)	(31)	(32)
		Win.	0	6.412 / 102.998	6.114 / 59.842	6.236 / 47.554	5.517 / 26.757	10.098 / 70.896	8.722 / 17.554	15.540 / 35.008	13.987 / 17.554
		Win.	100	7.222 / 102.806	7.420 / 59.809	6.446 / 49.440	5.864 / 26.581	10.685 / 70.621	10.197 / 17.476	16.855 / 34.964	16.034 / 17.476
		Sum.	0	5.976 / 94.643	5.570 / 57.423	6.228 / 39.420	5.499 / 26.105	9.554 / 66.288	8.142 / 16.865	14.863 / 33.689	13.140 / 16.865
		Sum.	100	6.777 / 94.640	6.921 / 57.398	6.438 / 41.324	5.849 / 25.910	10.072 / 66.721	9.631 / 16.695	16.171 / 33.642	15.253 / 16.695

FCHE	H2			(1)	(2)	(3)	(4)	(5)	(6)	(7)	(8)	(9)	(10)	(11)	(12)	(13)	(14)	(15)	(16)
	(kg)	Win.	0	15.097	14.914	13.408	10.643	13.024	11.382	3.590	3.823	7.561	6.544	4.904	5.516	4.877	7.033	12.015	12.361
		Win.	100	17.221	17.125	14.838	11.405	13.585	12.080	3.734	3.915	7.923	6.977	5.248	5.765	5.055	7.175	13.345	13.215
		Sum.	0	14.702	14.631	13.495	10.643	12.511	11.317	3.488	3.802	7.552	6.461	4.780	5.502	4.793	6.858	11.850	12.213
		Sum.	100	17.140	16.668	14.125	11.346	13.584	12.012	3.632	3.884	7.911	6.857	5.130	5.755	4.978	7.002	12.837	13.089
				(17)	(18)	(19)	(20)	(21)	(22)	(23)	(24)	(25)	(26)	(27)	(28)	(29)	(30)	(31)	(32)
		Win.	0	11.431	9.677	10.982	10.856	9.343	9.525	6.469	8.282	13.638	9.084	8.809	6.782	12.055	10.122	15.351	14.161
		Win.	100	12.354	10.180	11.974	11.618	10.672	10.681	7.051	8.876	14.300	10.297	9.087	7.255	13.095	11.522	16.590	15.815
		Sum.	0	11.216	9.422	10.765	10.614	9.158	9.463	6.428	8.193	13.209	9.001	8.584	6.649	12.008	10.005	15.179	13.637
		Sum.	100	12.180	9.959	11.797	11.426	10.227	10.597	7.008	8.781	14.162	10.099	8.868	7.115	12.943	11.254	16.433	15.289
BE	E			(1)	(2)	(3)	(4)	(5)	(6)	(7)	(8)	(9)	(10)	(11)	(12)	(13)	(14)	(15)	(16)
	(kWh)	Win.	0	196.672	190.991	181.394	147.995	171.446	155.809	111.826	0.000	0.000	178.428	0.000	142.441	0.000	163.549	62.646	261.892
		Win.	100	222.311	216.257	196.779	157.521	178.973	165.492	115.724	0.000	0.000	183.541	0.000	150.490	0.000	168.366	67.767	283.651
		Sum.	0	185.787	181.677	172.319	140.624	162.380	148.427	101.421	0.000	0.000	162.657	0.000	131.981	0.000	150.408	60.207	243.737
		Sum.	100	211.403	206.914	187.691	150.136	169.903	158.129	105.324	0.000	0.000	177.832	0.000	140.025	0.000	155.192	65.329	265.468
				(17)	(18)	(19)	(20)	(21)	(22)	(23)	(24)	(25)	(26)	(27)	(28)	(29)	(30)	(31)	(32)
		Win.	0	37.499	236.967	37.499	248.687	14.561	228.919	0.000	190.871	32.396	258.952	4.998	203.540	32.396	258.409	81.818	304.830
		Win.	100	43.622	252.608	43.622	263.138	16.063	260.398	0.000	206.528	35.461	281.623	5.189	202.479	35.461	279.637	91.043	319.052
		Sum.	0	36.117	217.615	36.117	229.309	14.022	213.752	0.000	177.208	30.718	237.749	4.518	194.426	30.718	239.805	78.699	287.305
		Sum.	100	42.255	233.245	42.255	244.341	15.521	245.195	0.000	192.870	33.796	260.913	4.712	202.361	33.796	260.571	87.928	314.596

Legend: DE = Diesel-electric, HE = Hybrid-electric, PIHE = Plug-in hybrid-electric, FCHE = Fuel cell hybrid-electric, BE = Battery-electric, ZESC = Zero-emission station control, FSMC = Finite state machine control, FAME = Fatty Acid Methyl Ester, HVO = Hydrotreated vegetable oil, LNG = Liquefied natural gas, H2 = Hydrogen, E = Electricity.

Table B.5: Estimated consumption of different energy carriers for WINK vehicle.

Propulsion system	Energy carrier	Season	Load (%)	Consumption per service															
HE	Diesel			(1)	(2)	(3)	(4)	(5)	(6)	(7)	(8)	(9)	(10)	(11)	(12)	(13)	(14)	(15)	(16)
(ZESC)	(l)	Win.	0	68.231	64.302	59.915	48.421	57.279	50.613	17.313	15.098	35.256	30.758	25.916	28.326	25.690	28.799	56.141	58.958
		Win.	100	73.632	72.094	63.609	50.561	59.085	53.487	17.716	15.269	36.750	31.114	27.081	27.576	26.469	27.577	59.849	60.941
		Sum.	0	73.410	68.548	63.038	51.527	60.378	53.528	17.954	15.659	37.283	33.931	27.468	30.847	27.934	29.958	59.838	63.912
		Sum.	100	78.788	75.497	66.816	53.641	62.237	56.365	18.357	15.820	38.755	34.379	28.608	29.874	28.688	28.846	63.517	65.592
				(17)	(18)	(19)	(20)	(21)	(22)	(23)	(24)	(25)	(26)	(27)	(28)	(29)	(30)	(31)	(32)
		Win.	0	53.362	45.330	52.081	51.639	43.391	43.983	29.244	39.816	48.532	43.858	41.272	34.087	53.863	47.666	67.749	65.334
		Win.	100	56.849	48.395	56.279	56.008	47.584	48.890	31.326	42.781	50.765	47.257	42.059	34.354	57.254	51.665	72.547	70.104
		Sum.	0	56.454	49.820	55.850	56.762	46.815	47.566	31.859	42.938	51.066	47.141	43.220	36.275	57.489	50.917	72.440	69.377
		Sum.	100	60.092	52.834	59.975	60.997	50.904	52.194	33.907	45.499	53.256	50.311	43.984	36.417	60.598	54.855	77.147	74.139
HE	FAME			(1)	(2)	(3)	(4)	(5)	(6)	(7)	(8)	(9)	(10)	(11)	(12)	(13)	(14)	(15)	(16)
(ZESC)	(l)	Win.	0	74.151	69.550	64.972	52.415	62.046	54.869	18.774	16.349	38.265	33.554	28.064	30.674	27.826	29.352	60.821	63.889
		Win.	100	79.777	78.085	67.941	54.711	63.949	57.902	19.191	16.539	39.828	34.812	29.318	29.890	28.664	31.727	64.789	65.938
		Sum.	0	79.701	74.150	68.347	55.776	65.399	58.028	19.469	16.957	40.460	37.679	29.745	33.388	30.256	30.717	64.824	69.249
		Sum.	100	85.377	81.770	71.246	58.042	67.363	61.015	19.885	17.142	41.999	38.202	30.969	32.379	31.070	33.004	68.762	70.970
				(17)	(18)	(19)	(20)	(21)	(22)	(23)	(24)	(25)	(26)	(27)	(28)	(29)	(30)	(31)	(32)
		Win.	0	58.062	50.775	56.838	57.240	46.685	48.962	31.752	43.169	52.584	47.550	44.748	36.917	58.388	51.674	73.982	70.687
		Win.	100	60.664	52.700	59.857	60.620	51.765	51.532	33.933	46.392	55.374	51.158	45.435	37.150	62.054	55.925	78.553	75.950
		Sum.	0	61.483	55.482	60.886	62.688	50.461	52.642	34.581	46.563	55.329	51.148	46.857	39.288	62.293	55.197	78.247	75.068
		Sum.	100	63.998	57.456	63.911	66.023	55.390	55.306	36.738	49.333	58.090	54.456	47.520	39.379	65.673	59.377	82.844	80.319
HE	HVO			(1)	(2)	(3)	(4)	(5)	(6)	(7)	(8)	(9)	(10)	(11)	(12)	(13)	(14)	(15)	(16)
(ZESC)	(l)	Win.	0	71.257	66.937	62.941	50.582	59.881	52.827	18.109	15.771	36.779	32.131	27.052	28.064	26.869	30.082	58.622	61.623
		Win.	100	76.826	75.326	65.456	52.817	61.706	55.840	18.510	15.976	38.344	32.544	28.262	28.784	27.589	30.607	62.529	63.912
		Sum.	0	76.669	71.371	66.502	53.830	63.122	55.873	18.779	16.356	38.898	35.448	28.668	30.481	29.215	31.292	62.481	66.813
		Sum.	100	82.213	78.881	68.643	56.033	64.999	58.844	19.180	16.552	40.441	35.975	29.853	31.184	29.910	31.837	66.360	68.737
				(17)	(18)	(19)	(20)	(21)	(22)	(23)	(24)	(25)	(26)	(27)	(28)	(29)	(30)	(31)	(32)
		Win.	0	55.659	47.959	54.310	55.252	44.802	46.726	30.582	41.598	50.288	45.871	43.132	35.576	57.791	50.288	70.736	67.757
		Win.	100	59.108	50.526	58.542	56.919	49.667	50.199	32.735	44.719	53.361	49.307	43.839	35.866	60.117	53.936	76.304	73.217
		Sum.	0	58.884	52.616	58.250	60.561	48.444	50.326	33.313	44.870	52.927	49.298	45.171	37.862	61.311	53.629	74.929	72.043
		Sum.	100	62.565	55.202	62.446	62.240	53.137	53.775	35.440	47.519	55.974	52.506	45.851	38.025	63.629	57.271	80.365	77.431
HE	LNG			(1)	(2)	(3)	(4)	(5)	(6)	(7)	(8)	(9)	(10)	(11)	(12)	(13)	(14)	(15)	(16)
(ZESC)	(kg)	Win.	0	49.732	46.844	43.802	35.300	41.807	36.851	12.643	10.982	25.706	22.401	18.877	19.632	18.770	21.026	40.896	42.760
		Win.	100	53.664	52.557	45.759	36.914	43.123	39.014	12.939	11.152	26.812	23.422	19.782	20.123	19.216	21.393	43.626	44.449
		Sum.	0	53.548	49.947	46.085	37.567	44.072	38.978	13.111	11.388	27.186	24.716	20.007	21.323	20.409	21.873	43.594	46.412
		Sum.	100	57.427	55.043	47.983	39.161	45.421	41.115	13.407	11.559	28.277	25.695	20.898	21.801	20.841	22.253	46.306	47.855
				(17)	(18)	(19)	(20)	(21)	(22)	(23)	(24)	(25)	(26)	(27)	(28)	(29)	(30)	(31)	(32)
		Win.	0	39.108	34.143	38.309	38.081	31.155	31.822	21.329	29.039	35.115	32.008	29.798	24.844	39.006	34.737	49.357	47.314
		Win.	100	41.292	35.691	40.863	40.368	34.713	35.695	22.877	31.245	37.304	34.439	30.868	25.004	41.786	37.685	52.904	51.137
		Sum.	0	41.379	37.370	41.037	41.800	33.702	34.432	23.241	31.316	36.960	34.438	31.215	26.441	41.635	37.111	52.289	50.308
		Sum.	100	43.694	38.904	43.596	44.039	37.154	38.108	24.763	33.214	39.134	36.679	32.286	26.508	44.227	40.016	55.801	54.084
HE	H2			(1)	(2)	(3)	(4)	(5)	(6)	(7)	(8)	(9)	(10)	(11)	(12)	(13)	(14)	(15)	(16)
(ZESC)	(kg)	Win.	0	20.385	19.202	17.995	14.462	17.123	15.116	5.174	4.511	10.519	9.191	7.741	8.464	7.680	8.607	16.778	17.630
		Win.	100	22.003	21.541	18.739	15.102	17.653	15.991	5.295	4.563	10.983	9.285	8.098	8.246	7.911	8.753	17.891	18.283
		Sum.	0	21.936	20.469	19.011	15.389	18.049	15.987	5.365	4.677	11.125	10.138	8.204	9.214	8.350	8.954	17.882	19.110
		Sum.	100	23.547	22.557	19.651	16.021	18.594	16.851	5.486	4.727	11.581	10.259	8.553	8.933	8.575	9.104	18.986	19.663
				(17)	(18)	(19)	(20)	(21)	(22)	(23)	(24)	(25)	(26)	(27)	(28)	(29)	(30)	(31)	(32)
		Win.	0	15.862	14.160	15.478	15.874	13.046	13.500	8.742	11.896	14.506	13.117	12.330	10.176	16.406	14.246	20.247	19.378
		Win.	100	16.858	14.709	16.644	16.394	14.283	14.630	9.360	12.787	15.170	14.117	12.659	10.262	17.250	15.431	21.841	20.956
		Sum.	0	16.796	15.462	16.617	17.375	14.069	14.510	9.523	12.827	15.262	14.095	12.913	10.830	17.410	15.218	21.447	20.604
		Sum.	100	17.756	16.009	17.768	17.909	15.280	15.616	10.131	13.597	15.914	15.026	13.239	10.878	18.255	16.384	23.002	22.161

(Table B.5 continued on the next page)

(Table B.5 continued from the previous page)

HE (FSMC)	Diesel (l)			(1)	(2)	(3)	(4)	(5)	(6)	(7)	(8)	(9)	(10)	(11)	(12)	(13)	(14)	(15)	(16)
		Win.	0	70.620	68.743	61.103	51.189	58.509	51.943	17.351	15.202	35.312	32.228	27.621	29.432	26.360	28.799	60.490	63.368
		Win.	100	75.907	75.349	64.431	53.093	60.317	54.709	17.757	15.373	36.802	33.521	28.611	28.437	27.126	27.581	63.970	64.860
		Sum.	0	73.740	71.552	63.067	53.879	60.410	55.139	17.989	15.759	37.337	35.414	28.413	31.357	28.674	29.959	64.421	67.474
		Sum.	100	79.144	78.441	66.845	55.595	62.270	57.538	18.394	15.921	38.806	35.867	29.411	30.692	29.036	28.850	67.703	68.697
				(17)	(18)	(19)	(20)	(21)	(22)	(23)	(24)	(25)	(26)	(27)	(28)	(29)	(30)	(31)	(32)
		Win.	0	54.035	49.231	55.184	56.245	45.897	46.627	31.862	41.277	48.670	46.264	41.423	36.091	55.039	51.226	72.221	69.042
		Win.	100	57.364	51.998	58.940	60.567	49.974	50.061	33.530	43.663	50.898	48.969	42.245	36.092	58.387	54.864	76.149	73.285
		Sum.	0	57.018	53.220	58.735	60.891	48.461	49.904	34.162	43.689	51.180	48.730	43.365	37.658	58.602	54.103	77.114	72.473
		Sum.	100	60.775	55.622	61.796	64.107	52.413	54.030	36.023	46.243	53.366	51.866	44.131	37.720	61.729	57.705	81.082	76.647
HE (FSMC)	FAME (l)			(1)	(2)	(3)	(4)	(5)	(6)	(7)	(8)	(9)	(10)	(11)	(12)	(13)	(14)	(15)	(16)
		Win.	0	76.705	74.280	66.231	55.411	63.381	56.313	18.815	16.462	38.327	34.989	29.912	31.823	28.550	29.355	65.537	68.722
		Win.	100	82.239	81.621	68.936	57.404	65.278	59.225	19.235	16.652	39.884	36.133	30.983	30.822	29.407	31.729	69.250	70.195
		Sum.	0	80.056	77.852	68.379	58.327	65.432	59.769	19.506	17.066	40.522	38.998	30.771	33.958	31.057	30.720	69.795	73.037
		Sum.	100	85.759	84.935	71.279	60.193	67.399	62.289	19.925	17.251	42.056	39.524	31.849	33.265	31.417	33.004	73.285	74.338
				(17)	(18)	(19)	(20)	(21)	(22)	(23)	(24)	(25)	(26)	(27)	(28)	(29)	(30)	(31)	(32)
		Win.	0	58.756	57.799	60.579	63.115	49.668	50.844	34.591	43.904	52.733	50.195	44.951	39.087	59.660	55.535	78.939	74.839
		Win.	100	61.305	56.638	62.519	65.552	53.999	53.426	36.322	47.353	55.520	53.008	45.637	38.959	63.283	59.375	82.433	79.454
		Sum.	0	62.005	61.418	63.217	67.004	52.868	54.999	37.098	47.410	55.452	52.861	47.014	40.782	63.490	58.939	83.896	78.572
		Sum.	100	64.670	60.517	66.587	69.384	56.718	57.601	39.025	50.128	58.210	56.142	47.679	40.943	66.897	62.455	87.770	83.075
HE (FSMC)	HVO (l)			(1)	(2)	(3)	(4)	(5)	(6)	(7)	(8)	(9)	(10)	(11)	(12)	(13)	(14)	(15)	(16)
		Win.	0	73.743	71.606	63.962	53.481	61.060	54.219	18.149	15.880	36.837	33.638	28.808	29.184	27.568	30.082	63.111	66.146
		Win.	100	79.197	78.743	66.413	55.471	62.991	57.119	18.553	16.085	38.398	35.026	29.874	29.678	28.268	30.607	66.826	68.005
		Sum.	0	77.014	74.533	66.532	56.292	63.156	57.556	18.815	16.460	38.956	36.969	29.632	31.017	29.988	31.292	67.229	70.528
		Sum.	100	82.581	81.952	68.675	58.080	65.032	60.077	19.219	16.658	40.494	37.537	30.709	32.071	30.277	31.838	70.720	72.028
				(17)	(18)	(19)	(20)	(21)	(22)	(23)	(24)	(25)	(26)	(27)	(28)	(29)	(30)	(31)	(32)
		Win.	0	56.373	51.923	57.571	60.715	47.947	48.909	33.344	42.302	50.433	48.403	43.329	37.671	59.010	53.982	75.399	71.735
		Win.	100	59.653	54.039	61.514	61.602	52.156	51.682	34.990	45.642	53.501	51.068	44.034	37.687	61.311	57.200	79.942	76.485
		Sum.	0	59.487	56.162	61.290	64.694	50.388	52.676	35.745	45.668	53.048	50.949	45.321	39.297	62.455	56.699	80.531	75.642
		Sum.	100	63.247	58.241	64.337	65.317	54.701	55.936	37.624	48.297	56.092	54.128	46.001	39.392	64.810	60.208	84.703	80.033
HE (FSMC)	LNG (kg)			(1)	(2)	(3)	(4)	(5)	(6)	(7)	(8)	(9)	(10)	(11)	(12)	(13)	(14)	(15)	(16)
		Win.	0	51.517	50.130	44.489	37.310	42.636	37.835	12.671	11.068	25.749	23.457	20.096	20.437	19.277	21.027	44.058	46.101
		Win.	100	55.317	54.966	46.429	38.759	44.018	39.910	12.969	11.228	26.849	24.302	20.901	20.750	19.752	21.393	46.657	47.319
		Sum.	0	53.789	52.173	46.108	39.278	44.097	40.145	13.136	11.471	27.228	25.787	20.672	21.674	20.969	21.873	46.931	49.162
		Sum.	100	57.664	57.210	48.006	40.587	45.444	41.977	13.434	11.633	28.314	26.585	21.485	22.407	21.043	22.252	49.384	50.109
				(17)	(18)	(19)	(20)	(21)	(22)	(23)	(24)	(25)	(26)	(27)	(28)	(29)	(30)	(31)	(32)
		Win.	0	39.542	38.861	40.418	41.927	33.376	33.743	23.260	29.543	35.216	33.792	29.935	26.330	39.860	37.319	52.642	50.107
		Win.	100	41.744	38.153	42.743	43.723	36.469	36.548	24.500	31.894	37.401	36.025	31.003	26.213	42.609	40.017	55.560	53.387
		Sum.	0	41.819	41.435	42.670	44.826	35.036	36.459	24.919	31.870	37.044	35.578	31.322	27.418	42.417	39.448	56.155	52.816
		Sum.	100	44.235	40.834	44.944	46.252	38.250	39.459	26.312	33.758	39.216	37.814	32.392	27.547	45.053	42.129	59.129	55.939
HE (FSMC)	H2 (kg)			(1)	(2)	(3)	(4)	(5)	(6)	(7)	(8)	(9)	(10)	(11)	(12)	(13)	(14)	(15)	(16)
		Win.	0	21.104	20.538	18.294	15.285	17.491	15.514	5.185	4.542	10.536	9.622	8.243	8.795	7.880	8.607	18.067	18.967
		Win.	100	22.684	22.486	19.012	15.859	18.020	16.357	5.307	4.594	10.998	10.018	8.555	8.503	8.107	8.753	19.124	19.463
		Sum.	0	22.034	21.371	19.020	16.092	18.058	16.468	5.376	4.707	11.141	10.573	8.479	9.366	8.571	8.954	19.245	20.160
		Sum.	100	23.652	23.432	19.660	16.606	18.604	17.203	5.497	4.757	11.596	10.703	8.794	9.177	8.679	9.105	20.239	20.607
				(17)	(18)	(19)	(20)	(21)	(22)	(23)	(24)	(25)	(26)	(27)	(28)	(29)	(30)	(31)	(32)
		Win.	0	16.065	16.062	16.443	17.344	13.744	13.981	9.528	12.330	14.547	13.839	12.386	10.775	16.758	15.313	21.594	20.509
		Win.	100	17.019	16.493	17.380	17.736	14.897	14.966	10.020	13.052	15.210	14.625	12.714	10.782	17.589	16.438	22.888	21.914
		Sum.	0	16.966	17.119	17.527	18.561	14.648	15.136	10.214	13.049	15.297	14.569	12.955	11.243	17.742	16.175	23.036	21.630
		Sum.	100	17.973	17.367	18.388	18.723	15.647	16.153	10.766	13.821	15.946	15.491	13.283	11.269	18.594	17.237	24.223	22.915

(Table B.5 continued on the next page)

(Table B.5 continued from the previous page)

PIHE	Diesel			(1)	(2)	(3)	(4)	(5)	(6)	(7)	(8)
	(l)	Win.	0	54.284 / 88.960	52.245 / 41.763	45.857 / 89.580	35.061 / 47.834	43.183 / 88.965	36.553 / 47.939	8.841 / 51.202	3.968 / 79.791
	/	Win.	100	59.529 / 88.414	59.085 / 41.788	49.471 / 88.992	36.959 / 47.887	44.933 / 88.507	39.277 / 47.887	9.448 / 50.753	3.956 / 81.036
	E	Sum.	0	57.556 / 94.679	55.362 / 43.873	48.429 / 94.047	37.488 / 50.093	45.337 / 94.755	39.143 / 50.217	9.345 / 56.644	3.981 / 89.256
	(kWh)	Sum.	100	62.228 / 94.382	62.305 / 43.762	51.928 / 94.099	39.394 / 49.883	47.042 / 94.551	41.529 / 49.883	9.550 / 55.917	3.974 / 90.492
				(9)	(10)	(11)	(12)	(13)	(14)	(15)	(16)
		Win.	0	19.529 / 104.284	17.246 / 53.936	14.401 / 36.592	16.562 / 66.749	12.670 / 60.159	17.051 / 74.800	46.248 / 29.876	52.867 / 66.777
		Win.	100	20.903 / 103.802	17.641 / 53.944	15.069 / 36.483	13.287 / 82.411	12.584 / 63.703	10.828 / 98.905	49.337 / 29.853	52.108 / 82.371
		Sum.	0	21.398 / 111.366	18.781 / 56.496	14.460 / 37.901	18.514 / 71.460	12.775 / 68.307	18.155 / 83.272	49.221 / 31.303	56.680 / 71.485
		Sum.	100	22.539 / 111.456	19.755 / 56.521	20.040 / 38.368	14.877 / 86.259	12.674 / 69.941	10.858 / 112.462	52.902 / 31.321	55.291 / 86.237
				(17)	(18)	(19)	(20)	(21)	(22)	(23)	(24)
		Win.	0	36.649 / 98.988	33.169 / 53.966	44.253 / 35.791	45.781 / 53.953	35.158 / 29.642	38.146 / 53.605	18.453 / 23.818	28.956 / 84.534
		Win.	100	40.106 / 98.547	35.518 / 53.963	47.983 / 35.630	49.672 / 53.710	39.257 / 29.582	41.404 / 53.572	20.102 / 23.896	31.436 / 84.780
		Sum.	0	39.528 / 105.662	36.206 / 56.491	47.717 / 37.569	49.751 / 56.475	37.506 / 31.043	40.780 / 56.217	20.565 / 25.132	31.387 / 88.852
		Sum.	100	42.551 / 105.208	38.634 / 56.516	51.430 / 37.535	53.150 / 56.236	41.442 / 30.988	44.993 / 56.532	22.159 / 25.205	33.802 / 88.882
				(25)	(26)	(27)	(28)	(29)	(30)	(31)	(32)
		Win.	0	28.083 / 160.902	26.078 / 84.720	26.750 / 93.041	20.518 / 35.526	43.811 / 102.973	37.171 / 23.772	63.800 / 47.966	57.981 / 23.772
		Win.	100	29.841 / 160.967	28.997 / 84.261	27.426 / 93.278	20.522 / 35.629	49.359 / 87.999	40.606 / 23.749	68.165 / 47.956	62.166 / 23.749
		Sum.	0	30.260 / 175.204	28.180 / 89.241	33.275 / 81.445	22.641 / 37.266	47.143 / 108.485	40.296 / 24.885	67.490 / 50.192	62.066 / 24.885
		Sum.	100	32.324 / 174.492	31.083 / 88.856	34.871 / 77.624	22.434 / 37.317	55.833 / 82.614	43.536 / 24.860	71.525 / 50.236	66.087 / 24.860
PIHE	FAME			(1)	(2)	(3)	(4)	(5)	(6)	(7)	(8)
	(l)	Win.	0	58.982 / 88.969	56.452 / 41.788	49.769 / 89.532	37.923 / 47.836	46.770 / 88.963	39.648 / 47.835	9.575 / 51.297	4.297 / 79.791
	/	Win.	100	64.481 / 88.506	63.993 / 41.789	52.829 / 88.971	39.941 / 47.879	48.597 / 88.632	42.493 / 47.880	10.234 / 50.768	4.285 / 81.004
	E	Sum.	0	62.516 / 94.759	59.836 / 43.765	52.547 / 94.043	40.590 / 50.108	49.103 / 94.752	42.428 / 50.105	10.123 / 56.743	4.312 / 89.257
	(kWh)	Sum.	100	67.407 / 94.435	67.476 / 43.762	55.464 / 94.061	42.587 / 49.904	50.897 / 94.609	44.942 / 49.913	10.357 / 55.858	4.304 / 90.455
				(9)	(10)	(11)	(12)	(13)	(14)	(15)	(16)
		Win.	0	21.247 / 104.136	17.898 / 54.041	15.597 / 36.593	17.886 / 66.778	13.723 / 60.142	11.414 / 98.902	50.111 / 29.876	57.299 / 66.783
		Win.	100	22.643 / 103.854	19.757 / 54.061	16.319 / 36.484	14.437 / 82.386	13.595 / 63.852	18.920 / 74.552	53.465 / 29.854	56.364 / 82.385
		Sum.	0	23.274 / 111.213	20.054 / 56.572	15.662 / 37.902	20.001 / 71.486	13.837 / 68.284	11.441 / 112.469	53.331 / 31.304	61.508 / 71.495
		Sum.	100	24.417 / 111.522	21.752 / 56.569	21.703 / 38.359	16.153 / 86.260	13.691 / 69.919	20.109 / 83.103	57.253 / 31.322	59.781 / 86.249
				(17)	(18)	(19)	(20)	(21)	(22)	(23)	(24)
		Win.	0	40.184 / 98.988	37.622 / 53.920	48.435 / 35.790	51.097 / 53.921	38.294 / 29.638	41.729 / 53.671	20.093 / 23.786	31.440 / 84.450
		Win.	100	42.239 / 98.546	38.704 / 53.962	50.781 / 35.615	53.777 / 53.663	42.759 / 29.646	44.090 / 53.597	21.790 / 23.783	34.092 / 84.804
		Sum.	0	42.839 / 105.663	40.553 / 56.189	51.708 / 37.563	54.987 / 56.180	41.239 / 31.090	45.121 / 56.468	22.372 / 25.133	34.064 / 88.819
		Sum.	100	45.280 / 105.207	42.005 / 56.515	54.993 / 37.533	57.579 / 56.198	45.265 / 31.054	47.263 / 56.219	24.012 / 25.102	36.665 / 88.886
				(25)	(26)	(27)	(28)	(29)	(30)	(31)	(32)
		Win.	0	30.478 / 160.918	28.319 / 84.643	29.022 / 92.996	22.224 / 35.527	47.540 / 102.946	40.336 / 23.798	69.653 / 47.974	62.742 / 23.798
		Win.	100	32.741 / 160.736	31.373 / 84.266	29.526 / 93.445	22.352 / 35.531	53.500 / 87.865	43.893 / 23.757	73.781 / 47.956	67.337 / 23.767
		Sum.	0	32.840 / 175.214	30.574 / 89.434	36.068 / 81.631	24.522 / 37.266	51.156 / 108.480	43.712 / 24.902	73.392 / 50.200	67.170 / 24.902
		Sum.	100	35.262 / 175.208	33.619 / 88.851	37.384 / 78.780	24.448 / 37.250	60.493 / 82.638	47.068 / 24.868	77.422 / 50.237	71.588 / 24.877
PIHE	HVO			(1)	(2)	(3)	(4)	(5)	(6)	(7)	(8)
	(l)	Win.	0	56.707 / 88.970	54.358 / 41.788	48.381 / 89.416	36.612 / 47.835	45.155 / 89.019	38.145 / 47.837	9.237 / 51.289	4.154 / 79.790
	/	Win.	100	61.922 / 88.496	61.727 / 41.789	50.872 / 88.960	38.574 / 47.882	46.925 / 88.382	40.932 / 47.882	9.716 / 50.821	4.116 / 81.173
	E	Sum.	0	60.112 / 94.759	57.613 / 43.765	50.999 / 94.090	39.172 / 50.105	47.424 / 94.733	40.880 / 50.120	9.769 / 56.720	4.160 / 89.256
	(kWh)	Sum.	100	64.907 / 94.439	65.098 / 43.763	53.411 / 94.069	41.147 / 49.866	49.146 / 94.343	43.344 / 49.866	9.964 / 55.981	4.135 / 90.633
				(9)	(10)	(11)	(12)	(13)	(14)	(15)	(16)
		Win.	0	20.331 / 104.322	17.990 / 54.040	15.044 / 36.700	13.103 / 82.370	13.239 / 60.369	17.814 / 74.817	48.220 / 29.874	55.294 / 66.748
		Win.	100	21.787 / 103.859	18.552 / 54.060	15.743 / 36.492	13.903 / 82.389	13.110 / 63.590	18.302 / 74.252	51.619 / 29.849	54.850 / 82.388
		Sum.	0	22.300 / 111.345	19.589 / 56.065	15.107 / 38.013	14.681 / 86.711	13.348 / 68.520	18.966 / 83.290	51.368 / 31.308	59.308 / 71.459
		Sum.	100	23.531 / 111.448	20.688 / 56.569	20.937 / 38.235	15.572 / 86.253	13.204 / 69.842	19.455 / 82.779	55.236 / 31.298	58.117 / 86.252
				(17)	(18)	(19)	(20)	(21)	(22)	(23)	(24)
		Win.	0	38.186 / 99.124	35.063 / 53.957	46.162 / 35.791	49.088 / 53.922	36.834 / 29.598	40.628 / 54.022	19.331 / 23.954	30.274 / 84.525
		Win.	100	41.765 / 98.327	37.289 / 53.968	49.968 / 35.588	50.319 / 53.954	40.973 / 29.582	42.782 / 53.555	21.042 / 23.762	32.827 / 84.929
		Sum.	0	41.186 / 105.815	38.313 / 56.480	49.765 / 37.568	53.102 / 56.160	39.195 / 30.999	43.518 / 56.424	21.506 / 25.129	32.817 / 88.843
		Sum.	100	44.411 / 104.730	40.471 / 56.521	53.563 / 37.535	54.114 / 56.506	43.260 / 30.987	45.854 / 56.137	23.167 / 25.102	35.333 / 88.867
				(25)	(26)	(27)	(28)	(29)	(30)	(31)	(32)
		Win.	0	29.020 / 160.931	27.279 / 84.742	27.928 / 93.101	21.419 / 35.495	48.836 / 91.748	38.969 / 23.794	66.681 / 47.974	60.109 / 23.810
		Win.	100	31.510 / 160.735	30.223 / 84.380	28.528 / 93.403	21.434 / 35.500	51.814 / 87.982	42.379 / 23.954	71.605 / 47.955	64.890 / 23.914
		Sum.	0	31.406 / 174.408	29.497 / 89.270	34.758 / 81.796	23.592 / 37.224	56.480 / 82.170	42.113 / 24.907	70.524 / 50.200	64.348 / 24.923
		Sum.	100	33.949 / 175.196	32.402 / 88.961	36.058 / 79.041	23.365 / 37.168	58.772 / 82.581	45.463 / 24.870	74.960 / 50.235	68.989 / 25.030

(Table B.5 continued on the next page)

(Table B.5 continued from the previous page)

PIHE	LNG (kg) / E (kWh)			(1)	(2)	(3)	(4)	(5)	(6)	(7)	(8)
		Win.	0	39.572 / 89.027	38.043 / 41.888	33.578 / 89.474	25.535 / 47.835	31.501 / 89.173	26.707 / 47.837	6.454 / 51.208	2.874 / 79.744
		Win.	100	43.251 / 88.542	43.065 / 41.790	35.553 / 88.993	26.961 / 47.883	32.775 / 88.491	28.592 / 47.883	6.787 / 50.857	2.890 / 81.004
		Sum.	0	41.945 / 94.824	40.299 / 43.871	35.417 / 94.085	27.328 / 50.108	33.075 / 94.972	28.509 / 50.125	6.826 / 56.634	2.883 / 89.213
		Sum.	100	45.329 / 94.557	45.312 / 43.763	37.325 / 94.098	28.757 / 49.874	34.330 / 94.434	30.267 / 49.914	6.979 / 55.891	2.902 / 90.456
				(9)	(10)	(11)	(12)	(13)	(14)	(15)	(16)
		Win.	0	14.202 / 104.335	12.539 / 53.955	10.492 / 36.603	9.168 / 82.542	9.277 / 60.024	12.456 / 74.799	33.648 / 29.974	38.267 / 66.606
		Win.	100	15.216 / 103.942	13.251 / 53.974	11.007 / 36.478	9.693 / 82.357	9.083 / 63.708	12.777 / 74.312	35.994 / 29.853	38.013 / 82.268
		Sum.	0	15.575 / 111.375	13.655 / 56.515	10.534 / 37.911	10.256 / 86.976	9.355 / 68.162	13.261 / 83.273	35.853 / 31.406	41.105 / 71.309
		Sum.	100	16.424 / 111.530	14.609 / 56.526	14.636 / 38.443	10.858 / 86.212	9.145 / 69.824	13.581 / 82.842	38.543 / 31.319	40.320 / 86.208
				(17)	(18)	(19)	(20)	(21)	(22)	(23)	(24)
		Win.	0	27.052 / 99.163	25.181 / 53.921	32.611 / 35.790	33.945 / 53.921	25.577 / 29.597	27.807 / 53.735	13.473 / 23.931	21.104 / 84.561
		Win.	100	29.176 / 98.321	26.274 / 53.953	34.887 / 35.744	35.557 / 53.711	28.629 / 29.615	30.223 / 53.710	14.684 / 23.791	22.946 / 84.929
		Sum.	0	28.725 / 105.862	27.244 / 56.210	34.870 / 37.567	36.660 / 56.209	27.249 / 30.997	29.599 / 56.464	15.011 / 25.236	22.882 / 88.898
		Sum.	100	31.019 / 104.784	28.396 / 56.512	37.419 / 37.640	38.455 / 56.235	30.227 / 31.021	32.858 / 56.636	16.182 / 25.101	24.698 / 88.862
				(25)	(26)	(27)	(28)	(29)	(30)	(31)	(32)
		Win.	0	20.261 / 160.947	19.068 / 84.604	19.169 / 93.649	14.960 / 35.491	31.732 / 102.974	27.103 / 23.780	46.534 / 47.974	42.020 / 23.780
		Win.	100	22.042 / 160.741	21.103 / 84.423	19.999 / 93.304	15.025 / 35.528	36.017 / 87.989	29.611 / 23.742	49.714 / 47.957	45.335 / 23.905
		Sum.	0	21.925 / 174.425	20.568 / 89.387	24.319 / 79.867	16.400 / 37.196	34.154 / 108.487	29.363 / 24.894	49.213 / 50.200	44.947 / 24.893
		Sum.	100	23.740 / 175.204	22.629 / 89.020	24.746 / 82.669	16.452 / 37.250	40.751 / 82.574	31.755 / 24.853	52.176 / 50.237	48.222 / 25.021
PIHE	H2 (kg) / E (kWh)			(1)	(2)	(3)	(4)	(5)	(6)	(7)	(8)
		Win.	0	16.216 / 88.970	15.592 / 41.788	13.826 / 89.466	10.461 / 47.834	12.913 / 89.020	10.918 / 47.834	2.642 / 51.202	1.186 / 79.791
		Win.	100	17.786 / 88.525	17.655 / 41.786	14.567 / 88.975	11.030 / 47.879	13.422 / 88.489	11.756 / 47.886	2.823 / 50.766	1.182 / 81.035
		Sum.	0	17.191 / 94.760	16.517 / 43.765	14.579 / 94.063	11.196 / 50.107	13.562 / 94.734	11.693 / 50.107	2.792 / 56.644	1.190 / 89.256
		Sum.	100	18.595 / 94.439	18.622 / 43.766	15.292 / 94.104	11.760 / 49.904	14.062 / 94.397	12.421 / 49.875	2.857 / 55.865	1.188 / 90.491
				(9)	(10)	(11)	(12)	(13)	(14)	(15)	(16)
		Win.	0	5.822 / 104.164	5.145 / 54.040	4.303 / 36.597	4.943 / 66.777	3.786 / 60.137	5.097 / 75.000	13.814 / 29.877	15.815 / 66.777
		Win.	100	6.244 / 103.851	5.265 / 53.953	4.503 / 36.481	3.989 / 82.274	3.761 / 63.733	5.220 / 74.393	14.755 / 29.849	15.700 / 82.274
		Sum.	0	6.384 / 111.212	5.603 / 56.605	4.321 / 37.907	5.525 / 71.485	3.818 / 68.280	5.427 / 83.474	14.709 / 31.304	16.974 / 71.485
		Sum.	100	6.733 / 111.503	5.897 / 56.531	5.989 / 38.399	4.461 / 86.194	3.787 / 69.937	5.549 / 82.927	15.812 / 31.298	16.634 / 86.195
				(17)	(18)	(19)	(20)	(21)	(22)	(23)	(24)
		Win.	0	10.930 / 98.452	10.477 / 53.919	13.177 / 35.792	14.109 / 53.919	10.558 / 29.637	11.567 / 54.022	5.522 / 23.818	8.647 / 84.534
		Win.	100	11.786 / 98.590	10.877 / 53.681	14.152 / 35.596	14.484 / 53.962	11.800 / 29.646	12.397 / 53.570	6.004 / 23.896	9.405 / 84.695
		Sum.	0	11.790 / 105.174	11.254 / 56.230	14.212 / 37.562	15.154 / 56.230	11.389 / 31.077	12.451 / 56.425	6.150 / 25.132	9.374 / 88.852
		Sum.	100	12.603 / 105.255	11.807 / 56.213	15.263 / 37.535	15.578 / 56.515	12.491 / 31.054	13.468 / 56.528	6.619 / 25.205	10.108 / 88.857
				(25)	(26)	(27)	(28)	(29)	(30)	(31)	(32)
		Win.	0	8.402 / 160.935	7.797 / 84.729	7.989 / 92.995	6.126 / 35.494	13.858 / 91.846	11.108 / 23.794	19.076 / 47.967	17.177 / 23.786
		Win.	100	9.126 / 160.958	8.659 / 84.260	8.199 / 93.415	6.129 / 35.627	14.883 / 87.819	12.113 / 23.749	20.498 / 47.956	18.584 / 23.757
		Sum.	0	9.054 / 175.233	8.428 / 89.255	9.946 / 81.532	6.750 / 37.225	16.061 / 82.171	12.042 / 24.907	20.177 / 50.195	18.380 / 24.899
		Sum.	100	9.779 / 175.224	9.280 / 88.845	10.274 / 80.839	6.680 / 37.300	16.814 / 82.642	12.989 / 24.860	21.459 / 50.236	19.759 / 24.868

FCHE	H2 (kg)			(1)	(2)	(3)	(4)	(5)	(6)	(7)	(8)	(9)	(10)	(11)	(12)	(13)	(14)	(15)	(16)
		Win.	0	16.710	15.597	16.161	12.248	14.602	12.754	5.150	5.585	10.324	8.783	6.347	7.409	6.544	10.122	14.839	15.812
		Win.	100	17.724	17.256	16.620	12.656	14.801	13.313	5.305	5.635	10.585	8.610	6.587	7.558	6.628	10.216	15.365	16.252
		Sum.	0	17.521	16.153	17.117	12.958	15.434	13.440	5.737	6.299	11.286	9.476	6.846	8.070	7.145	11.103	15.665	16.990
		Sum.	100	18.439	17.618	17.508	13.322	15.597	13.956	5.896	6.340	11.346	9.272	7.059	8.208	7.231	11.192	16.211	17.370
				(17)	(18)	(19)	(20)	(21)	(22)	(23)	(24)	(25)	(26)	(27)	(28)	(29)	(30)	(31)	(32)
		Win.	0	15.196	12.684	14.214	14.847	11.182	12.117	8.146	10.499	18.530	11.461	12.109	8.762	16.511	12.158	18.902	16.537
		Win.	100	15.715	13.114	14.784	15.042	12.081	13.385	8.552	11.120	19.007	12.141	11.942	8.465	17.035	12.932	19.513	17.501
		Sum.	0	16.433	13.711	15.259	16.052	11.760	12.979	8.712	11.355	20.151	12.364	13.078	9.447	17.902	12.945	19.664	17.203
		Sum.	100	16.749	14.116	15.623	16.125	12.708	14.239	9.098	11.955	20.496	12.658	12.888	9.127	18.400	13.641	20.328	18.122
BE	E (kWh)			(1)	(2)	(3)	(4)	(5)	(6)	(7)	(8)	(9)	(10)	(11)	(12)	(13)	(14)	(15)	(16)
		Win.	0	259.187	237.418	237.762	192.944	227.026	198.766	174.325	0.000	17.352	253.938	0.000	206.573	0.000	213.568	81.167	363.616
		Win.	100	274.709	261.467	245.058	198.638	231.985	207.286	176.863	0.000	18.517	258.614	0.000	208.896	0.000	247.320	85.706	378.998
		Sum.	0	277.494	253.067	253.015	205.340	242.263	211.170	191.879	0.000	18.539	279.131	0.000	224.198	0.000	232.358	85.249	394.240
		Sum.	100	293.027	277.140	260.315	211.043	247.228	219.697	194.373	0.000	19.693	283.837	0.000	226.522	0.000	269.481	89.782	409.586
				(17)	(18)	(19)	(20)	(21)	(22)	(23)	(24)	(25)	(26)	(27)	(28)	(29)	(30)	(31)	(32)
		Win.	0	47.809	340.100	47.809	349.614	18.850	309.085	0.000	263.120	43.979	379.900	8.083	287.652	43.979	361.794	106.259	405.970
		Win.	100	52.789	349.596	52.789	363.718	20.227	326.938	0.000	275.424	46.425	393.824	8.200	287.841	46.425	377.958	114.193	427.823
		Sum.	0	50.142	372.155	50.142	380.120	19.748	334.620	0.000	286.104	46.807	415.666	8.900	287.899	46.807	393.899	111.503	435.493
		Sum.	100	55.086	380.221	55.086	395.046	21.125	352.517	0.000	298.404	49.227	429.608	9.006	288.098	49.227	402.107	119.400	448.908

Legend: DE = Diesel-electric, HE = Hybrid-electric, PIHE = Plug-in hybrid-electric, FCHE = Fuel cell hybrid-electric, BE = Battery-electric, ZESC = Zero-emission station control, FSMC = Finite state machine control, FAME = Fatty Acid Methyl Ester, HVO = Hydrotreated vegetable oil, LNG = Liquefied natural gas, H2 = Hydrogen, E = Electricity.

Table B.6: Overall estimates of WTT energy use

Vehicle	Prop. system	Energy carrier	Overall estimates per distance (MJ/km)				Overall estimates per seat-distance (kJ/skm)				Rel. range (%)
			Mean	Max	Min	Range (Max-Min)	Mean	Max	Min	Range (Max-Min)	
GTW 2/6	DE	Diesel	9.221	14.872	6.745	8.127	86.993	140.300	63.631	76.669	88
	HE (ZESC)	Diesel	8.433	11.525	6.485	5.040	79.556	108.727	61.177	47.551	60
		FAME	35.961	49.008	27.674	21.334	339.251	462.344	261.078	201.266	59
		HVO (Rapeseed)	36.339	49.448	27.923	21.524	342.819	466.487	263.428	203.059	59
		HVO (Waste cooking oil)	5.191	7.064	3.989	3.075	48.973	66.639	37.632	29.008	59
		LNG	5.832	7.946	4.488	3.459	55.020	74.966	42.336	32.629	59
		H2 (SMR)	30.455	41.500	23.448	18.052	287.313	391.507	221.208	170.299	59
		H2 (Electrolysis - EU2030)	88.126	120.084	67.850	52.235	831.373	1132.87	640.092	492.781	59
		H2 (Electrolysis - Wind)	28.187	38.409	21.702	16.707	265.917	362.353	204.735	157.617	59
	HE (FSMC)	Diesel	8.392	11.525	6.515	5.010	79.170	108.727	61.464	47.264	60
		FAME	35.788	49.210	27.806	21.405	337.625	464.249	262.319	201.930	60
		HVO (Rapeseed)	36.174	49.649	28.056	21.593	341.268	468.386	264.678	203.708	60
		HVO (Waste cooking oil)	5.168	7.093	4.008	3.085	48.751	66.911	37.810	29.100	60
		LNG	5.795	7.979	4.509	3.470	54.668	75.274	42.542	32.732	60
		H2 (SMR)	30.255	41.674	23.561	18.113	285.427	393.152	222.274	170.878	60
		H2 (Electrolysis - EU2030)	87.547	120.589	68.177	52.412	825.917	1137.63	643.175	494.457	60
		H2 (Electrolysis - Wind)	28.002	38.571	21.806	16.764	264.172	363.875	205.721	158.153	60
	PIHE	Diesel / E (EU2030)	11.429	20.285	6.212	14.073	107.817	191.365	58.604	132.761	123
		Diesel / E (Wind))	5.570	7.820	2.503	5.316	52.545	73.772	23.617	50.155	95
		FAME / E (EU2030)	28.420	38.968	17.788	21.180	268.110	367.619	167.807	199.812	75
		FAME / E (Wind)	22.562	32.782	8.051	24.731	212.851	309.263	75.957	233.307	110
		HVO (Rapeseed) / E (EU2030)	28.691	39.080	17.934	21.145	270.674	368.676	169.190	199.486	74
		HVO (Rapeseed) / E (Wind)	22.883	33.168	8.806	24.362	215.881	312.902	83.071	229.830	106
		HVO (Waste cooking oil) / E (EU2030)	9.370	19.466	4.707	14.759	88.395	183.643	44.406	139.237	158
		HVO (Waste cooking oil) / E (Wind)	3.562	4.864	1.990	2.873	33.602	45.884	18.777	27.107	81
		LNG / E (EU2030)	9.824	19.633	4.884	14.749	92.683	185.217	46.080	139.137	150
		LNG / E (Wind)	3.949	5.430	1.994	3.436	37.252	51.227	18.808	32.419	87
		H2 (SMR) / E (EU2030)	25.027	34.402	15.484	18.918	236.107	324.544	146.072	178.472	76
		H2 (SMR) / E (Wind)	19.191	27.737	6.948	20.789	181.044	261.671	65.546	196.125	108
		H2 (Electrolysis - EU2030) / E (EU2030)	60.717	82.475	32.723	49.752	572.802	778.068	308.705	469.363	82
		H2 (Electrolysis - EU2030) / E (Wind)	54.880	79.983	18.523	61.460	517.740	754.558	174.743	579.815	112
		H2 (Electrolysis - Wind) / E (EU2030)	23.624	32.550	14.529	18.021	222.866	307.074	137.069	170.005	76
		H2 (Electrolysis - Wind) / E (Wind)	17.787	25.683	6.493	19.190	167.804	242.288	61.252	181.036	108
	FCHE	H2 (SMR)	27.429	44.103	21.068	23.035	258.767	416.063	198.754	217.309	84
		H2 (Electrolysis - EU2030)	79.370	127.616	60.962	66.654	748.771	1203.92	575.118	628.810	84
		H2 (Electrolysis - Wind)	25.387	40.818	19.499	21.319	239.497	385.080	183.953	201.127	84
	BE	E (EU2030)	13.938	41.581	0.000	41.581	131.489	392.275	0.000	392.275	298
		E (Wind)	0.774	2.310	0.000	2.310	7.305	21.793	0.000	21.793	298

(Table B.6 continued on the next page)

(Table B.6 continued from the previous page)

GTW 2/8	DE	Diesel	9.914	15.565	6.983	8.582	60.084	94.332	42.319	52.013	87
	HE (ZESC)	Diesel	9.273	12.158	6.843	5.316	56.198	73.685	41.470	32.215	57
		FAME	39.647	51.950	29.212	22.738	240.287	314.851	177.044	137.807	57
		HVO (Rapeseed)	39.949	52.330	29.478	22.852	242.114	317.153	178.658	138.496	57
		HVO (Waste cooking oil)	5.707	7.476	4.211	3.264	34.587	45.306	25.522	19.785	57
		LNG	6.442	8.411	4.738	3.672	39.043	50.973	28.718	22.256	57
		H2 (SMR)	33.588	43.956	24.739	19.218	203.563	266.403	149.930	116.472	57
		H2 (Electrolysis - EU2030)	97.190	127.193	71.584	55.609	589.032	770.867	433.841	337.026	57
		H2 (Electrolysis - Wind)	31.087	40.683	22.896	17.787	188.404	246.564	138.765	107.799	57
	HE (FSMC)	Diesel	9.274	12.135	6.924	5.211	56.207	73.546	41.964	31.581	56
		FAME	39.616	51.817	29.561	22.256	240.098	314.040	179.158	134.882	56
		HVO (Rapeseed)	39.874	52.279	29.833	22.446	241.661	316.844	180.809	136.035	56
		HVO (Waste cooking oil)	5.696	7.468	4.262	3.206	34.522	45.262	25.829	19.433	56
		LNG	6.431	8.420	4.795	3.625	38.979	51.030	29.061	21.968	56
		H2 (SMR)	33.568	43.873	25.038	18.835	203.441	265.894	151.743	114.151	56
		H2 (Electrolysis - EU2030)	97.132	126.950	72.449	54.501	588.679	769.397	439.087	330.310	56
		H2 (Electrolysis - Wind)	31.068	40.605	23.173	17.432	188.291	246.094	140.443	105.651	56
	PIHE	Diesel / E (EU2030)	12.384	21.401	6.703	14.699	75.054	129.705	40.622	89.083	119
		Diesel / E (Wind))	6.444	9.122	2.880	6.242	39.054	55.287	17.456	37.831	97
		FAME / E (EU2030)	32.264	44.814	19.964	24.851	195.542	271.601	120.991	150.609	77
		FAME / E (Wind)	26.325	38.044	9.508	28.536	159.544	230.569	57.625	172.945	108
		HVO (Rapeseed) / E (EU2030)	32.501	45.066	19.987	25.080	196.978	273.130	121.131	151.999	77
		HVO (Rapeseed) / E (Wind)	26.503	38.252	9.658	28.594	160.626	231.831	58.535	173.296	108
		HVO (Waste cooking oil) / E (EU2030)	10.086	20.234	5.045	15.188	61.130	122.628	30.577	92.051	151
		HVO (Waste cooking oil) / E (Wind)	4.089	5.715	2.105	3.611	24.779	34.639	12.757	21.882	88
		LNG / E (EU2030)	10.487	20.467	5.455	15.012	63.555	124.041	33.059	90.982	143
		LNG / E (Wind)	4.571	6.408	2.284	4.124	27.702	38.837	13.841	24.997	90
		H2 (SMR) / E (EU2030)	28.282	39.448	17.295	22.153	171.408	239.077	104.817	134.260	78
		H2 (SMR) / E (Wind)	22.309	32.249	8.225	24.024	135.206	195.450	49.850	145.600	108
		H2 (Electrolysis - EU2030) / E (EU2030)	69.862	97.746	36.551	61.195	423.405	592.399	221.518	370.880	88
		H2 (Electrolysis - EU2030) / E (Wind)	63.889	92.762	22.203	70.560	387.203	562.194	134.561	427.634	110
		H2 (Electrolysis - Wind) / E (EU2030)	26.647	37.226	16.205	21.021	161.498	225.610	98.211	127.399	79
		H2 (Electrolysis - Wind) / E (Wind)	20.674	29.870	7.676	22.194	125.296	181.028	46.519	134.509	107
	FCHE	H2 (SMR)	30.205	47.540	22.095	25.445	183.063	288.123	133.908	154.215	84
		H2 (Electrolysis - EU2030)	87.403	137.563	63.934	73.629	529.713	833.716	387.478	446.239	84
		H2 (Electrolysis - Wind)	27.956	44.000	20.449	23.551	169.430	266.667	123.936	142.731	84
	BE	E (EU2030)	15.718	45.069	0.000	45.069	95.263	273.148	0.000	273.148	287
		E (Wind)	0.873	2.504	0.000	2.504	5.292	15.175	0.000	15.175	287

(Table B.6 continued on the next page)

(Table B.6 continued from the previous page)

WINK	HE (ZESC)	Diesel	11.773	14.835	8.370	6.465	76.945	96.960	54.708	42.252	55
		FAME	50.322	62.918	35.716	27.202	328.904	411.229	233.440	177.789	54
		HVO (Rapeseed)	50.703	63.680	36.050	27.630	331.392	416.209	235.624	180.585	54
		HVO (Waste cooking oil)	7.243	9.097	5.150	3.947	47.341	59.457	33.660	25.797	54
		LNG	8.142	10.226	5.785	4.441	53.214	66.834	37.809	29.025	55
		H2 (SMR)	42.660	53.222	30.248	22.974	278.823	347.854	197.697	150.157	54
		H2 (Electrolysis - EU2030)	123.442	154.003	87.525	66.478	806.808	1006.55	572.059	434.497	54
		H2 (Electrolysis - Wind)	39.483	49.258	27.995	21.263	258.060	321.950	182.975	138.975	54
	HE (FSMC)	Diesel	12.165	15.003	8.849	6.155	79.507	98.062	57.835	40.226	51
		FAME	52.022	63.925	37.758	26.168	340.014	417.813	246.783	171.030	50
		HVO (Rapeseed)	52.389	64.419	38.117	26.303	342.409	421.042	249.128	171.914	50
		HVO (Waste cooking oil)	7.484	9.203	5.445	3.757	48.914	60.147	35.589	24.559	50
		LNG	8.419	10.353	6.114	4.239	55.024	67.667	39.961	27.705	50
		H2 (SMR)	44.132	54.098	31.969	22.130	288.441	353.585	208.947	144.637	50
		H2 (Electrolysis - EU2030)	127.700	156.540	92.506	64.034	834.638	1023.13	604.613	418.525	50
		H2 (Electrolysis - Wind)	40.845	50.070	29.588	20.482	266.962	327.254	193.387	133.866	50
	PIHE	Diesel / E (EU2030)	17.848	38.424	9.719	28.705	116.656	251.136	63.521	187.614	161
		Diesel / E (Wind))	8.755	11.726	4.903	6.824	57.223	76.642	32.043	44.598	78
		FAME / E (EU2030)	44.762	61.616	28.808	32.808	292.565	402.717	188.287	214.431	73
		FAME / E (Wind)	35.668	48.606	15.273	33.333	233.124	317.686	99.825	217.861	93
		HVO (Rapeseed) / E (EU2030)	45.113	61.881	28.997	32.884	294.859	404.451	189.524	214.927	73
		HVO (Rapeseed) / E (Wind)	36.080	49.385	15.340	34.044	235.815	322.775	100.262	222.513	94
		HVO (Waste cooking oil) / E (EU2030)	14.643	37.247	6.960	30.287	95.708	243.445	45.491	197.953	207
		HVO (Waste cooking oil) / E (Wind)	5.610	7.509	3.685	3.825	36.664	49.082	24.084	24.998	68
		LNG / E (EU2030)	15.291	37.431	7.511	29.919	99.943	244.646	49.094	195.551	196
		LNG / E (Wind)	6.229	8.352	3.906	4.445	40.715	54.585	25.531	29.054	71
		H2 (SMR) / E (EU2030)	39.511	55.935	25.100	30.836	258.245	365.591	164.051	201.540	78
		H2 (SMR) / E (Wind)	30.526	41.534	13.201	28.333	199.517	271.462	86.280	185.182	93
		H2 (Electrolysis - EU2030) / E (EU2030)	96.315	128.472	63.648	64.824	629.513	839.686	415.999	423.687	67
		H2 (Electrolysis - EU2030) / E (Wind)	87.330	119.328	34.878	84.450	570.785	779.924	227.962	551.963	97
		H2 (Electrolysis - Wind) / E (EU2030)	37.278	53.514	23.584	29.931	243.644	349.767	154.143	195.624	80
		H2 (Electrolysis - Wind) / E (Wind)	28.292	38.474	12.348	26.126	184.917	251.466	80.708	170.758	92
	FCHE	H2 (SMR)	39.663	68.139	25.617	42.522	259.236	445.352	167.431	277.920	107
		H2 (Electrolysis - EU2030)	114.770	197.168	74.126	123.042	750.130	1288.67	484.482	804.195	107
		H2 (Electrolysis - Wind)	36.709	63.065	23.709	39.355	239.931	412.187	154.963	257.224	107
	BE	E (EU2030)	23.231	75.700	0.000	75.700	151.835	494.770	0.000	494.770	326
		E (Wind)	1.291	4.206	0.000	4.206	8.435	27.487	0.000	27.487	326

Legend: DE = Diesel-electric, HE = Hybrid-electric, PIHE = Plug-in hybrid-electric, FCHE = Fuel cell hybrid-electric, BE = Battery-electric, ZESC = Zero-emission station control, FSMC = Finite state machine control, FAME = Fatty Acid Methyl Ester, HVO = Hydrotreated vegetable oil, LNG = Liquefied natural gas, H2 = Hydrogen, E = Electricity, SMR = steam methane reforming.

Table B.7: Overall estimates of TTW energy use

Vehicle	Prop. system	Energy carrier	Overall estimates per distance (MJ/km)				Overall estimates per seat-distance (kJ/skm)				Rel. range (%)
			Mean	Max	Min	Range (Max-Min)	Mean	Max	Min	Range (Max-Min)	
GTW 2/6	DE	Diesel	35.468	57.201	25.943	31.259	334.600	539.636	244.743	294.892	88
	HE (ZESC)	Diesel	32.435	44.329	24.942	19.387	305.994	418.197	235.303	182.893	60
		FAME	32.397	44.152	24.932	19.220	305.631	416.524	235.205	181.320	59
		HVO (any)	32.446	44.150	24.932	19.218	306.092	416.511	235.206	181.305	59
		LNG	32.401	44.147	24.931	19.215	305.667	416.477	235.202	181.275	59
		H2 (any)	32.399	44.149	24.945	19.204	305.652	416.497	235.328	181.169	59
	HE (FSMC)	Diesel	32.278	44.329	25.059	19.270	304.513	418.197	236.407	181.789	60
		FAME	32.242	44.334	25.050	19.283	304.166	418.241	236.322	181.918	60
		HVO (any)	32.299	44.330	25.050	19.280	304.707	418.206	236.323	181.884	60
		LNG	32.193	44.328	25.053	19.275	303.709	418.187	236.345	181.843	60
		H2 (any)	32.186	44.334	25.065	19.269	303.646	418.247	236.461	181.786	60
	PIHE	Diesel / E (any)	25.021	34.037	15.749	18.288	236.044	321.106	148.576	172.530	73
		FAME / E (any)	24.938	34.084	15.737	18.347	235.265	321.548	148.466	173.082	74
		HVO (any) / E (any)	25.007	33.948	15.748	18.200	235.920	320.260	148.566	171.694	73
		LNG / E (any)	24.955	33.990	15.751	18.239	235.423	320.658	148.595	172.063	73
		H2 (any) / E (any)	24.955	34.021	15.751	18.270	235.426	320.957	148.594	172.363	73
	FCHE	H2 (any)	29.180	46.918	22.413	24.505	275.284	442.620	211.440	231.180	84
	BE	E (any)	11.062	33.001	0.000	33.001	104.357	311.329	0.000	311.329	298
GTW 2/8	DE	Diesel	38.132	59.866	26.857	33.009	231.102	362.827	162.770	200.057	87
	HE (ZESC)	Diesel	35.665	46.764	26.318	20.445	216.154	283.416	159.506	123.910	57
		FAME	35.718	46.802	26.317	20.485	216.474	283.649	159.498	124.150	57
		HVO (any)	35.669	46.724	26.320	20.404	216.175	283.175	159.517	123.658	57
		LNG	35.789	46.725	26.324	20.401	216.906	283.184	159.542	123.642	57
		H2 (any)	35.732	46.762	26.318	20.445	216.556	283.407	159.501	123.906	57
	HE (FSMC)	Diesel	35.671	46.675	26.632	20.043	216.189	282.878	161.408	121.470	56
		FAME	35.690	46.682	26.632	20.050	216.304	282.918	161.403	121.515	56
		HVO (any)	35.602	46.678	26.637	20.041	215.771	282.899	161.438	121.461	56
		LNG	35.730	46.777	26.639	20.138	216.548	283.498	161.451	122.047	56
		H2 (any)	35.710	46.673	26.636	20.037	216.426	282.866	161.429	121.438	56
	PIHE	Diesel / E (any)	28.433	39.335	17.659	21.676	172.320	238.396	107.026	131.370	76
		FAME / E (any)	28.393	39.343	17.700	21.643	172.076	238.440	107.272	131.168	76
		HVO (any) / E (any)	28.389	39.284	17.581	21.703	172.056	238.086	106.554	131.532	76
		LNG / E (any)	28.432	39.363	17.660	21.703	172.314	238.563	107.031	131.532	76
		H2 (any) / E (any)	28.379	39.369	17.680	21.689	171.992	238.602	107.152	131.449	76
	FCHE	H2 (any)	32.133	50.575	23.505	27.070	194.748	306.513	142.455	164.058	84
	BE	E (any)	12.475	35.769	0.000	35.769	75.605	216.784	0.000	216.784	287

(Table B.7 continued on the next page)

(Table B.7 continued from the previous page)

WINK	HE	Diesel	45.281	57.059	32.195	24.864	295.955	372.936	210.423	162.512	55
	(ZESC)	FAME	45.335	56.683	32.177	24.506	296.309	370.475	210.305	160.170	54
		HVO (any)	45.271	56.858	32.188	24.669	295.889	371.619	210.380	161.238	54
		LNG	45.232	56.809	32.137	24.671	295.636	371.298	210.048	161.250	55
		H2 (any)	45.383	56.619	32.178	24.440	296.621	370.057	210.316	159.742	54
	HE	Diesel	46.789	57.708	34.035	23.672	305.808	377.174	222.452	154.722	51
	(FSMC)	FAME	46.867	57.590	34.016	23.574	306.318	376.407	222.326	154.081	50
		HVO (any)	46.776	57.518	34.033	23.485	305.725	375.934	222.438	153.497	50
		LNG	46.771	57.517	33.967	23.550	305.691	375.926	222.008	153.918	50
		H2 (any)	46.948	57.552	34.009	23.542	306.852	376.154	222.284	153.870	50
	PIHE	Diesel / E (any)	39.259	53.164	25.443	27.721	256.593	347.477	166.291	181.186	71
		FAME / E (any)	39.294	53.227	25.444	27.783	256.821	347.889	166.299	181.589	71
		HVO (any) / E (any)	39.331	53.180	25.420	27.760	257.067	347.584	166.144	181.440	71
		LNG / E (any)	39.262	53.181	25.403	27.778	256.612	347.589	166.032	181.557	71
		H2 (any) / E (any)	39.463	53.191	25.420	27.770	257.928	347.651	166.147	181.504	70
	FCHE	H2 (any)	42.195	72.488	27.252	45.236	275.783	473.778	178.118	295.660	107
	BE	E (any)	18.437	60.079	0.000	60.079	120.504	392.675	0.000	392.675	326

Legend: DE = Diesel-electric, HE = Hybrid-electric, PIHE = Plug-in hybrid-electric, FCHE = Fuel cell hybrid-electric, BE = Battery-electric, ZESC = Zero-emission station control, FSMC = Finite state machine control, FAME = Fatty Acid Methyl Ester, HVO = Hydrotreated vegetable oil, LNG = Liquefied natural gas, H2 = Hydrogen, E = Electricity.

Table B.8: Overall estimates of WTW energy use

Vehicle	Prop. system	Energy carrier	Overall estimates per distance (MJ/km)				Overall estimates per seat-distance (kJ/skm)				Rel. range (%)
			Mean	Max	Min	Range (Max-Min)	Mean	Max	Min	Range (Max-Min)	
GTW 2/6	DE	Diesel	44.689	72.073	32.688	39.386	421.592	679.936	308.374	371.561	88
	HE (ZESC)	Diesel	40.868	55.854	31.427	24.427	385.550	526.924	296.480	230.444	60
		FAME	68.358	93.160	52.606	40.554	644.882	878.868	496.282	382.586	59
		HVO (Rapeseed)	68.785	93.598	52.855	40.743	648.911	882.998	498.634	384.364	59
		HVO (Waste cooking oil)	37.637	51.214	28.921	22.293	355.065	483.150	272.837	210.312	59
		LNG	38.233	52.093	29.419	22.674	360.687	491.443	277.539	213.904	59
		H2 (SMR)	62.854	85.648	48.393	37.256	592.964	808.005	456.536	351.469	59
		H2 (Electrolysis - EU2030)	120.525	164.233	92.794	71.439	1137.02	1549.37	875.419	673.950	59
		H2 (Electrolysis - Wind)	60.586	82.558	46.647	35.911	571.569	778.850	440.063	338.787	59
	HE (FSMC)	Diesel	40.670	55.854	31.574	24.280	383.683	526.924	297.871	229.053	60
		FAME	68.030	93.544	52.856	40.688	641.791	882.489	498.641	383.849	60
		HVO (Rapeseed)	68.473	93.979	53.106	40.873	645.975	886.593	501.001	385.592	60
		HVO (Waste cooking oil)	37.467	51.422	29.058	22.364	353.458	485.117	274.133	210.984	60
		LNG	37.988	52.307	29.562	22.745	358.377	493.461	278.887	214.574	60
		H2 (SMR)	62.442	86.008	48.626	37.382	589.073	811.399	458.735	352.664	60
		H2 (Electrolysis - EU2030)	119.734	164.923	93.241	71.682	1129.56	1555.87	879.636	676.242	60
		H2 (Electrolysis - Wind)	60.189	82.905	46.871	36.034	567.818	782.122	442.183	339.939	60
	PIHE	Diesel / E (EU2030)	36.449	50.448	21.961	28.487	343.861	475.927	207.180	268.747	78
		Diesel / E (Wind))	30.590	41.450	19.441	22.009	288.588	391.037	183.409	207.628	72
		FAME / E (EU2030)	53.358	73.052	33.525	39.527	503.374	689.168	316.273	372.894	74
		FAME / E (Wind)	47.500	64.277	26.485	37.792	448.116	606.389	249.861	356.529	80
		HVO (Rapeseed) / E (EU2030)	53.699	73.027	33.682	39.345	506.594	688.936	317.756	371.180	73
		HVO (Rapeseed) / E (Wind)	47.891	64.745	28.068	36.677	451.800	610.803	264.797	346.006	77
		HVO (Waste cooking oil) / E (EU2030)	34.377	47.697	20.597	27.099	324.315	449.969	194.315	255.655	79
		HVO (Waste cooking oil) / E (Wind)	28.569	38.699	18.077	20.621	269.522	365.080	170.538	194.542	72
		LNG / E (EU2030)	34.779	48.264	20.873	27.391	328.106	455.320	196.915	258.405	79
		LNG / E (Wind)	28.904	39.277	18.353	20.924	272.675	370.539	173.145	197.394	72
		H2 (SMR) / E (EU2030)	49.983	68.423	31.235	37.189	471.533	645.501	294.665	350.835	74
		H2 (SMR) / E (Wind)	44.146	59.418	25.383	34.035	416.470	560.549	239.465	321.083	77
		H2 (Electrolysis - EU2030) / E (EU2030)	85.672	115.512	51.158	64.354	808.228	1089.73	482.624	607.109	75
		H2 (Electrolysis - EU2030) / E (Wind)	79.836	111.429	36.958	74.471	753.166	1051.21	348.663	702.554	93
		H2 (Electrolysis - Wind) / E (EU2030)	48.579	66.571	30.280	36.291	458.292	628.031	285.662	342.369	75
		H2 (Electrolysis - Wind) / E (Wind)	42.742	57.566	24.928	32.638	403.229	543.079	235.171	307.908	76
	FCHE	H2 (SMR)	56.609	91.020	43.481	47.540	534.050	858.684	410.194	448.490	84
		H2 (Electrolysis - EU2030)	108.550	174.534	83.375	91.159	1024.05	1646.54	786.558	859.990	84
		H2 (Electrolysis - Wind)	54.567	87.736	41.912	45.825	514.780	827.700	395.393	432.307	84
	BE	E (EU2030)	25.000	74.582	0.000	74.582	235.846	703.604	0.000	703.604	298
		E (Wind)	11.836	35.311	0.000	35.311	111.662	333.122	0.000	333.122	298

(Table B.8 continued on the next page)

(Table B.8 continued from the previous page)

GTW 2/8	DE	Diesel	48.046	75.431	33.840	41.592	291.187	457.159	205.088	252.070	87
	HE	Diesel	44.938	58.922	33.161	25.761	272.353	357.101	200.976	156.125	57
	(ZESC)	FAME	75.366	98.752	55.529	43.223	456.762	598.499	336.542	261.958	57
		HVO (Rapeseed)	75.618	99.054	55.799	43.255	458.289	600.329	338.175	262.154	57
		HVO (Waste cooking oil)	41.376	54.200	30.531	23.668	250.762	328.482	185.039	143.443	57
		LNG	42.232	55.136	31.063	24.073	255.949	334.157	188.259	145.898	57
		H2 (SMR)	69.320	90.719	51.056	39.662	420.119	549.810	309.431	240.379	57
		H2 (Electrolysis - EU2030)	132.922	173.955	97.901	76.054	805.588	1054.27	593.342	460.932	57
		H2 (Electrolysis - Wind)	66.818	87.445	49.214	38.231	404.960	529.971	298.266	231.705	57
	HE	Diesel	44.945	58.810	33.556	25.253	272.396	356.424	203.372	153.051	56
	(FSMC)	FAME	75.306	98.498	56.193	42.306	456.402	596.959	340.561	256.397	56
		HVO (Rapeseed)	75.476	98.958	56.471	42.487	457.432	599.743	342.247	257.497	56
		HVO (Waste cooking oil)	41.298	54.147	30.899	23.248	250.293	328.162	187.267	140.894	56
		LNG	42.162	55.197	31.434	23.763	255.527	334.528	190.512	144.016	56
		H2 (SMR)	69.278	90.546	51.673	38.872	419.867	548.761	313.172	235.589	56
		H2 (Electrolysis - EU2030)	132.842	173.623	99.085	74.538	805.105	1052.26	600.515	451.748	56
		H2 (Electrolysis - Wind)	66.778	87.278	49.809	37.470	404.717	528.960	301.872	227.088	56
	PIHE	Diesel / E (EU2030)	40.817	57.181	24.362	32.819	247.374	346.552	147.648	198.903	80
		Diesel / E (Wind))	34.877	48.115	21.849	26.265	211.374	291.604	132.421	159.184	75
		FAME / E (EU2030)	60.657	84.157	37.663	46.493	367.618	510.041	228.263	281.777	77
		FAME / E (Wind)	54.717	76.247	29.389	46.858	331.620	462.102	178.115	283.988	86
		HVO (Rapeseed) / E (EU2030)	60.891	84.351	37.568	46.783	369.033	511.216	227.684	283.531	77
		HVO (Rapeseed) / E (Wind)	54.893	76.328	29.612	46.716	332.682	462.591	179.466	283.125	85
		HVO (Waste cooking oil) / E (EU2030)	38.476	54.326	22.717	31.610	233.186	329.251	137.677	191.574	82
		HVO (Waste cooking oil) / E (Wind)	32.478	44.883	20.204	24.678	196.835	272.016	122.450	149.565	76
		LNG / E (EU2030)	38.918	54.856	23.119	31.737	235.869	332.463	140.116	192.347	82
		LNG / E (Wind)	33.003	45.609	20.607	25.002	200.016	276.416	124.889	151.527	76
		H2 (SMR) / E (EU2030)	56.661	78.817	34.975	43.842	343.400	477.678	211.969	265.709	77
		H2 (SMR) / E (Wind)	50.688	70.433	28.135	42.298	307.199	426.868	170.514	256.354	83
		H2 (Electrolysis - EU2030) / E (EU2030)	98.241	135.930	56.460	79.470	595.397	823.816	342.182	481.634	81
		H2 (Electrolysis - EU2030) / E (Wind)	92.267	130.946	42.112	88.834	559.196	793.612	255.225	538.387	96
		H2 (Electrolysis - Wind) / E (EU2030)	55.026	76.595	33.885	42.710	333.490	464.212	205.364	258.848	78
		H2 (Electrolysis - Wind) / E (Wind)	49.053	68.054	27.585	40.468	297.289	412.446	167.183	245.263	82
	FCHE	H2 (SMR)	62.339	98.115	45.600	52.515	377.810	594.636	276.363	318.273	84
		H2 (Electrolysis - EU2030)	119.536	188.138	87.439	100.699	724.461	1140.23	529.933	610.297	84
		H2 (Electrolysis - Wind)	60.089	94.575	43.955	50.620	364.178	573.180	266.391	306.789	84
	BE	E (EU2030)	28.193	80.839	0.000	80.839	170.868	489.933	0.000	489.933	287
		E (Wind)	13.348	38.273	0.000	38.273	80.898	231.959	0.000	231.959	287

(Table B.8 continued on the next page)

(Table B.8 continued from the previous page)

WINK	HE (ZESC)	Diesel	57.054	71.894	40.565	31.329	372.900	469.895	265.131	204.764	55
		FAME	95.658	119.601	67.893	51.708	625.214	781.704	443.745	337.959	54
		HVO (Rapeseed)	95.974	120.538	68.239	52.299	627.281	787.828	446.004	341.824	54
		HVO (Waste cooking oil)	52.514	65.955	37.338	28.616	343.230	431.076	244.040	187.036	54
		LNG	53.374	67.034	37.922	29.112	348.851	438.131	247.856	190.275	55
		H2 (SMR)	88.043	109.840	62.426	47.415	575.444	717.911	408.012	309.899	54
		H2 (Electrolysis - EU2030)	168.825	210.622	119.703	90.919	1103.42	1376.61	782.374	594.239	54
		H2 (Electrolysis - Wind)	84.866	105.877	60.173	45.704	554.681	692.007	393.290	298.717	54
	HE (FSMC)	Diesel	58.953	72.711	42.884	29.827	385.315	475.236	280.288	194.948	51
		FAME	98.889	121.516	71.774	49.742	646.332	794.221	469.109	325.111	50
		HVO (Rapeseed)	99.165	121.937	72.150	49.788	648.134	796.977	471.566	325.411	50
		HVO (Waste cooking oil)	54.260	66.721	39.478	27.242	354.640	436.082	258.027	178.055	50
		LNG	55.189	67.870	40.081	27.788	360.715	443.593	261.970	181.624	50
		H2 (SMR)	91.080	111.650	65.978	45.672	595.294	729.738	431.231	298.507	50
		H2 (Electrolysis - EU2030)	174.648	214.092	126.515	87.576	1141.49	1399.29	826.897	572.395	50
		H2 (Electrolysis - Wind)	87.794	107.621	63.598	44.024	573.814	703.408	415.672	287.736	50
	PIHE	Diesel / E (EU2030)	57.107	84.884	35.656	49.229	373.250	554.800	233.044	321.756	86
		Diesel / E (Wind))	48.014	64.877	31.342	33.535	313.816	424.030	204.847	219.183	70
		FAME / E (EU2030)	84.056	114.613	54.252	60.362	549.386	749.106	354.586	394.520	72
		FAME / E (Wind)	74.962	100.761	49.768	50.993	489.945	658.569	325.281	333.288	68
		HVO (Rapeseed) / E (EU2030)	84.445	114.809	54.417	60.391	551.927	750.383	355.668	394.715	72
		HVO (Rapeseed) / E (Wind)	75.411	101.085	49.938	51.148	492.883	660.688	326.389	334.299	68
		HVO (Waste cooking oil) / E (EU2030)	53.975	81.843	33.468	48.375	352.775	534.923	218.744	316.179	90
		HVO (Waste cooking oil) / E (Wind)	44.941	60.690	29.148	31.541	293.731	396.665	190.512	206.153	70
		LNG / E (EU2030)	54.553	82.550	33.843	48.706	356.555	539.540	221.199	318.341	89
		LNG / E (Wind)	45.491	61.533	29.561	31.971	297.327	402.174	193.212	208.962	70
		H2 (SMR) / E (EU2030)	78.975	109.112	50.520	58.592	516.173	713.151	330.198	382.953	74
		H2 (SMR) / E (Wind)	69.989	93.532	46.041	47.492	457.446	611.324	300.920	310.403	68
		H2 (Electrolysis - EU2030) / E (EU2030)	135.778	181.663	89.068	92.594	887.441	1187.33	582.146	605.191	68
		H2 (Electrolysis - EU2030) / E (Wind)	126.793	169.478	71.846	97.632	828.713	1107.69	469.579	638.118	77
		H2 (Electrolysis - Wind) / E (EU2030)	76.741	106.691	49.004	57.687	501.573	697.328	320.290	377.038	75
		H2 (Electrolysis - Wind) / E (Wind)	67.755	90.586	44.525	46.061	442.845	592.066	291.012	301.054	68
	FCHE	H2 (SMR)	81.858	140.627	52.869	87.758	535.019	919.130	345.549	573.580	107
		H2 (Electrolysis - EU2030)	156.965	269.656	101.378	168.278	1025.91	1762.45	662.600	1099.855	107
		H2 (Electrolysis - Wind)	78.904	135.553	50.961	84.591	515.714	885.965	333.081	552.884	107
	BE	E (EU2030)	41.668	135.779	0.000	135.779	272.340	887.445	0.000	887.445	326
		E (Wind)	19.728	64.285	0.000	64.285	128.940	420.162	0.000	420.162	326

Legend: DE = Diesel-electric, HE = Hybrid-electric, PIHE = Plug-in hybrid-electric, FCHE = Fuel cell hybrid-electric, BE = Battery-electric, ZESC = Zero-emission station control, FSMC = Finite state machine control, FAME = Fatty Acid Methyl Ester, HVO = Hydrotreated vegetable oil, LNG = Liquefied natural gas, H2 = Hydrogen, E = Electricity, SMR = steam methane reforming.

Table B.9: Overall estimates of WTT GHG emissions

Vehicle	Prop. system	Energy carrier	Overall estimates per distance (kgCO2e/km)				Overall estimates per seat-distance (gCO2e/skm)				Rel. range (%)
			Mean	Max	Min	Range (Max-Min)	Mean	Max	Min	Range (Max-Min)	
GTW 2/6	DE	Diesel	0.671	1.082	0.491	0.591	6.326	10.203	4.627	5.576	88
	HE (ZESC)	Diesel	0.613	0.838	0.472	0.367	5.786	7.907	4.449	3.458	60
		FAME	1.568	2.136	1.206	0.930	14.789	20.154	11.381	8.774	59
		HVO (Rapeseed)	1.684	2.291	1.294	0.997	15.884	21.614	12.206	9.409	59
		HVO (Waste cooking oil)	0.360	0.490	0.277	0.213	3.398	4.624	2.611	2.013	59
		LNG	0.538	0.733	0.414	0.319	5.074	6.913	3.904	3.009	59
		H2 (SMR)	3.544	4.830	2.729	2.101	33.438	45.565	25.745	19.820	59
		H2 (Electrolysis - EU2030)	3.843	5.236	2.958	2.278	36.250	49.397	27.910	21.487	59
		H2 (Electrolysis - Wind)	0.308	0.419	0.237	0.182	2.904	3.957	2.236	1.721	59
	HE (FSMC)	Diesel	0.610	0.838	0.474	0.364	5.758	7.907	4.470	3.437	60
		FAME	1.560	2.145	1.212	0.933	14.718	20.237	11.435	8.803	60
		HVO (Rapeseed)	1.676	2.300	1.300	1.000	15.812	21.702	12.264	9.439	60
		HVO (Waste cooking oil)	0.359	0.492	0.278	0.214	3.383	4.643	2.624	2.019	60
		LNG	0.534	0.736	0.416	0.320	5.041	6.941	3.923	3.018	60
		H2 (SMR)	3.521	4.850	2.742	2.108	33.219	45.756	25.869	19.887	60
		H2 (Electrolysis - EU2030)	3.817	5.258	2.973	2.285	36.012	49.604	28.044	21.560	60
		H2 (Electrolysis - Wind)	0.306	0.421	0.238	0.183	2.885	3.973	2.246	1.727	60
	PIHE	Diesel / E (EU2030)	0.734	1.191	0.410	0.781	6.926	11.239	3.869	7.371	106
		Diesel / E (Wind))	0.380	0.558	0.121	0.437	3.585	5.264	1.143	4.121	115
		FAME / E (EU2030)	1.323	1.827	0.812	1.016	12.478	17.239	7.656	9.583	77
		FAME / E (Wind)	0.969	1.423	0.315	1.108	9.137	13.421	2.968	10.454	114
		HVO (Rapeseed) / E (EU2030)	1.396	1.913	0.860	1.054	13.166	18.050	8.110	9.940	75
		HVO (Rapeseed) / E (Wind)	1.044	1.530	0.365	1.165	9.853	14.434	3.446	10.988	112
		HVO (Waste cooking oil) / E (EU2030)	0.575	1.128	0.304	0.824	5.421	10.637	2.865	7.772	143
		HVO (Waste cooking oil) / E (Wind)	0.223	0.327	0.078	0.249	2.108	3.088	0.737	2.351	112
		LNG / E (EU2030)	0.687	1.173	0.379	0.794	6.486	11.062	3.572	7.490	115
		LNG / E (Wind)	0.332	0.487	0.107	0.380	3.135	4.596	1.007	3.589	115
		H2 (SMR) / E (EU2030)	2.546	3.439	1.570	1.869	24.022	32.439	14.810	17.629	73
		H2 (SMR) / E (Wind)	2.194	3.211	0.711	2.500	20.694	30.293	6.711	23.582	114
		H2 (Electrolysis - EU2030) / E (EU2030)	2.731	3.682	1.630	2.052	25.763	34.735	15.375	19.360	75
		H2 (Electrolysis - EU2030) / E (Wind)	2.378	3.481	0.771	2.710	22.434	32.841	7.276	25.565	114
		H2 (Electrolysis - Wind) / E (EU2030)	0.543	1.115	0.276	0.839	5.126	10.516	2.603	7.913	154
		H2 (Electrolysis - Wind) / E (Wind)	0.190	0.279	0.062	0.217	1.797	2.631	0.583	2.048	114
	FCHE	H2 (SMR)	3.192	5.133	2.452	2.681	30.116	48.423	23.132	25.291	84
		H2 (Electrolysis - EU2030)	3.461	5.564	2.658	2.906	32.649	52.495	25.077	27.418	84
		H2 (Electrolysis - Wind)	0.277	0.446	0.213	0.233	2.615	4.205	2.009	2.196	84
	BE	E (EU2030)	0.796	2.374	0.000	2.374	7.508	22.398	0.000	22.398	298
		E (Wind)	0.000	0.000	0.000	0.000	0.000	0.000	0.000	0.000	0

(Table B.9 continued on the next page)

(Table B.9 continued from the previous page)

GTW 2/8	DE	Diesel	0.721	1.132	0.508	0.624	4.370	6.860	3.078	3.783	87
	HE (ZESC)	Diesel	0.674	0.884	0.498	0.387	4.087	5.359	3.016	2.343	57
		FAME	1.728	2.265	1.273	0.991	10.475	13.725	7.718	6.007	57
		HVO (Rapeseed)	1.851	2.425	1.366	1.059	11.218	14.695	8.278	6.417	57
		HVO (Waste cooking oil)	0.396	0.519	0.292	0.227	2.400	3.144	1.771	1.373	57
		LNG	0.594	0.776	0.437	0.339	3.600	4.701	2.648	2.052	57
		H2 (SMR)	3.909	5.116	2.879	2.237	23.691	31.005	17.449	13.555	57
		H2 (Electrolysis - EU2030)	4.238	5.546	3.121	2.425	25.684	33.612	18.917	14.695	57
		H2 (Electrolysis - Wind)	0.339	0.444	0.250	0.194	2.057	2.692	1.515	1.177	57
	HE (FSMC)	Diesel	0.674	0.883	0.504	0.379	4.088	5.348	3.052	2.297	56
		FAME	1.727	2.259	1.289	0.970	10.466	13.690	7.810	5.880	56
		HVO (Rapeseed)	1.848	2.422	1.382	1.040	11.197	14.681	8.378	6.303	56
		HVO (Waste cooking oil)	0.395	0.518	0.296	0.222	2.395	3.141	1.792	1.348	56
		LNG	0.593	0.776	0.442	0.334	3.594	4.706	2.680	2.026	56
		H2 (SMR)	3.907	5.106	2.914	2.192	23.677	30.946	17.660	13.285	56
		H2 (Electrolysis - EU2030)	4.235	5.535	3.159	2.376	25.668	33.548	19.145	14.402	56
		H2 (Electrolysis - Wind)	0.339	0.443	0.253	0.190	2.056	2.687	1.534	1.154	56
	PIHE	Diesel / E (EU2030)	0.802	1.269	0.446	0.824	4.863	7.694	2.702	4.991	103
		Diesel / E (Wind))	0.443	0.643	0.148	0.495	2.686	3.895	0.896	2.998	112
		FAME / E (EU2030)	1.491	2.083	0.906	1.177	9.039	12.626	5.492	7.134	79
		FAME / E (Wind)	1.132	1.646	0.378	1.268	6.863	9.973	2.289	7.685	112
		HVO (Rapeseed) / E (EU2030)	1.574	2.192	0.955	1.237	9.541	13.283	5.786	7.497	79
		HVO (Rapeseed) / E (Wind)	1.212	1.761	0.408	1.352	7.343	10.671	2.475	8.196	112
		HVO (Waste cooking oil) / E (EU2030)	0.622	1.178	0.324	0.855	3.769	7.141	1.961	5.180	137
		HVO (Waste cooking oil) / E (Wind)	0.259	0.377	0.087	0.289	1.571	2.283	0.529	1.753	112
		LNG / E (EU2030)	0.747	1.242	0.410	0.832	4.528	7.530	2.485	5.045	111
		LNG / E (Wind)	0.389	0.564	0.133	0.431	2.360	3.420	0.805	2.615	111
		H2 (SMR) / E (EU2030)	2.917	4.021	1.726	2.295	17.677	24.372	10.464	13.908	79
		H2 (SMR) / E (Wind)	2.556	3.719	0.859	2.860	15.488	22.540	5.206	17.334	112
		H2 (Electrolysis - EU2030) / E (EU2030)	3.132	4.333	1.799	2.534	18.979	26.262	10.901	15.360	81
		H2 (Electrolysis - EU2030) / E (Wind)	2.770	4.032	0.931	3.101	16.790	24.436	5.644	18.792	112
		H2 (Electrolysis - Wind) / E (EU2030)	0.583	1.160	0.295	0.864	3.534	7.028	1.789	5.239	148
		H2 (Electrolysis - Wind) / E (Wind)	0.222	0.323	0.075	0.248	1.345	1.957	0.452	1.505	112
	FCHE	H2 (SMR)	3.515	5.533	2.571	2.961	21.305	33.533	15.585	17.948	84
		H2 (Electrolysis - EU2030)	3.811	5.998	2.788	3.210	23.097	36.352	16.895	19.457	84
		H2 (Electrolysis - Wind)	0.305	0.480	0.223	0.257	1.850	2.912	1.353	1.559	84
	BE	E (EU2030)	0.897	2.573	0.000	2.573	5.439	15.596	0.000	15.596	287
		E (Wind)	0.000	0.000	0.000	0.000	0.000	0.000	0.000	0.000	0

(Table B.9 continued on the next page)

(Table B.9 continued from the previous page)

WINK	HE (ZESC)	Diesel	0.856	1.079	0.609	0.470	5.596	7.051	3.979	3.073	55
		FAME	2.194	2.743	1.557	1.186	14.338	17.926	10.176	7.750	54
		HVO (Rapeseed)	2.349	2.951	1.670	1.280	15.355	19.285	10.917	8.367	54
		HVO (Waste cooking oil)	0.503	0.631	0.357	0.274	3.285	4.125	2.336	1.790	54
		LNG	0.751	0.943	0.533	0.410	4.907	6.163	3.487	2.677	55
		H2 (SMR)	4.965	6.194	3.520	2.674	32.450	40.484	23.009	17.476	54
		H2 (Electrolysis - EU2030)	5.382	6.715	3.816	2.899	35.179	43.889	24.943	18.945	54
		H2 (Electrolysis - Wind)	0.431	0.538	0.306	0.232	2.818	3.516	1.998	1.518	54
	HE (FSMC)	Diesel	0.885	1.091	0.644	0.448	5.782	7.131	4.206	2.925	51
		FAME	2.268	2.787	1.646	1.141	14.822	18.213	10.758	7.456	50
		HVO (Rapeseed)	2.427	2.985	1.766	1.219	15.865	19.509	11.543	7.966	50
		HVO (Waste cooking oil)	0.519	0.639	0.378	0.261	3.394	4.173	2.469	1.704	50
		LNG	0.776	0.955	0.564	0.391	5.074	6.240	3.685	2.555	50
		H2 (SMR)	5.136	6.296	3.721	2.575	33.570	41.151	24.318	16.833	50
		H2 (Electrolysis - EU2030)	5.568	6.826	4.034	2.792	36.393	44.612	26.363	18.249	50
		H2 (Electrolysis - Wind)	0.446	0.547	0.323	0.224	2.915	3.573	2.112	1.462	50
	PIHE	Diesel / E (EU2030)	1.148	2.244	0.648	1.595	7.500	14.664	4.237	10.428	139
		Diesel / E (Wind))	0.598	0.820	0.230	0.590	3.907	5.359	1.505	3.854	99
		FAME / E (EU2030)	2.081	3.002	1.320	1.682	13.604	19.623	8.627	10.996	81
		FAME / E (Wind)	1.532	2.099	0.589	1.510	10.010	13.720	3.852	9.868	99
		HVO (Rapeseed) / E (EU2030)	2.193	3.119	1.395	1.725	14.335	20.388	9.115	11.273	79
		HVO (Rapeseed) / E (Wind)	1.647	2.267	0.629	1.638	10.765	14.819	4.114	10.705	99
		HVO (Waste cooking oil) / E (EU2030)	0.899	2.151	0.454	1.696	5.873	14.057	2.969	11.088	189
		HVO (Waste cooking oil) / E (Wind)	0.352	0.485	0.135	0.350	2.303	3.170	0.880	2.290	99
		LNG / E (EU2030)	1.073	2.215	0.596	1.618	7.014	14.474	3.896	10.578	151
		LNG / E (Wind)	0.525	0.719	0.201	0.518	3.433	4.702	1.314	3.388	99
		H2 (SMR) / E (EU2030)	4.034	5.403	2.640	2.763	26.369	35.316	17.255	18.061	68
		H2 (SMR) / E (Wind)	3.491	4.781	1.332	3.449	22.818	31.250	8.708	22.543	99
		H2 (Electrolysis - EU2030) / E (EU2030)	4.328	5.791	2.839	2.951	28.288	37.846	18.557	19.289	68
		H2 (Electrolysis - EU2030) / E (Wind)	3.785	5.183	1.444	3.739	24.737	33.878	9.440	24.438	99
		H2 (Electrolysis - Wind) / E (EU2030)	0.846	2.129	0.407	1.722	5.532	13.912	2.660	11.252	203
		H2 (Electrolysis - Wind) / E (Wind)	0.303	0.415	0.116	0.300	1.981	2.714	0.756	1.958	99
	FCHE	H2 (SMR)	4.616	7.930	2.981	4.949	30.171	51.831	19.486	32.345	107
		H2 (Electrolysis - EU2030)	5.004	8.597	3.232	5.365	32.708	56.190	21.125	35.065	107
		H2 (Electrolysis - Wind)	0.401	0.689	0.259	0.430	2.620	4.501	1.692	2.809	107
	BE	E (EU2030)	1.326	4.322	0.000	4.322	8.670	28.251	0.000	28.251	326
		E (Wind)	0.000	0.000	0.000	0.000	0.000	0.000	0.000	0.000	0

Legend: DE = Diesel-electric, HE = Hybrid-electric, PIHE = Plug-in hybrid-electric, FCHE = Fuel cell hybrid-electric, BE = Battery-electric, ZESC = Zero-emission station control, FSMC = Finite state machine control, FAME = Fatty Acid Methyl Ester, HVO = Hydrotreated vegetable oil, LNG = Liquefied natural gas, H2 = Hydrogen, E = Electricity, SMR = steam methane reforming.

Table B.10: Overall estimates of TTW GHG emissions

Vehicle	Prop. system	Energy carrier	Overall estimates per distance (kgCO2e/km)				Overall estimates per seat-distance (gCO2e/skm)				Rel. range (%)
			Mean	Max	Min	Range (Max-Min)	Mean	Max	Min	Range (Max-Min)	
GTW 2/6	DE	Diesel	2.596	4.187	1.899	2.288	24.494	39.503	17.916	21.587	88
	HE (ZESC)	Diesel	2.374	3.245	1.826	1.419	22.400	30.613	17.225	13.388	60
		FAME	0.000	0.000	0.000	0.000	0.000	0.000	0.000	0.000	0
		HVO (any)	0.000	0.000	0.000	0.000	0.000	0.000	0.000	0.000	0
		LNG	1.827	2.490	1.406	1.084	17.238	23.487	13.264	10.223	59
		H2 (any)	0.000	0.000	0.000	0.000	0.000	0.000	0.000	0.000	0
	HE (FSMC)	Diesel	2.363	3.245	1.834	1.411	22.291	30.613	17.306	13.308	60
		FAME	0.000	0.000	0.000	0.000	0.000	0.000	0.000	0.000	0
		HVO (any)	0.000	0.000	0.000	0.000	0.000	0.000	0.000	0.000	0
		LNG	1.816	2.500	1.413	1.087	17.128	23.584	13.329	10.255	60
		H2 (SMR)	0.000	0.000	0.000	0.000	0.000	0.000	0.000	0.000	0
	PIHE	Diesel / E (any)	1.471	2.160	0.469	1.691	13.879	20.382	4.425	15.957	115
		FAME / E (any)	0.000	0.000	0.000	0.000	0.000	0.000	0.000	0.000	0
		HVO (any) / E (any)	0.000	0.000	0.000	0.000	0.000	0.000	0.000	0.000	0
		LNG / E (any)	1.129	1.655	0.363	1.293	10.650	15.617	3.421	12.195	115
		H2 (any) / E (any)	0.000	0.000	0.000	0.000	0.000	0.000	0.000	0.000	0
	FCHE	H2 (any)	0.000	0.000	0.000	0.000	0.000	0.000	0.000	0.000	0
	BE	E (any)	0.000	0.000	0.000	0.000	0.000	0.000	0.000	0.000	0
GTW 2/8	DE	Diesel	2.791	4.382	1.966	2.416	16.917	26.560	11.915	14.645	87
	HE (ZESC)	Diesel	2.611	3.423	1.927	1.497	15.823	20.747	11.676	9.071	57
		FAME	0.000	0.000	0.000	0.000	0.000	0.000	0.000	0.000	0
		HVO (any)	0.000	0.000	0.000	0.000	0.000	0.000	0.000	0.000	0
		LNG	2.018	2.635	1.485	1.151	12.232	15.970	8.997	6.973	57
		H2 (any)	0.000	0.000	0.000	0.000	0.000	0.000	0.000	0.000	0
	HE (FSMC)	Diesel	2.611	3.417	1.950	1.467	15.826	20.708	11.816	8.892	56
		FAME	0.000	0.000	0.000	0.000	0.000	0.000	0.000	0.000	0
		HVO (any)	0.000	0.000	0.000	0.000	0.000	0.000	0.000	0.000	0
		LNG	2.015	2.638	1.502	1.136	12.212	15.988	9.105	6.883	56
		H2 (any)	0.000	0.000	0.000	0.000	0.000	0.000	0.000	0.000	0
	PIHE	Diesel / E (any)	1.716	2.488	0.573	1.915	10.400	15.079	3.471	11.608	112
		FAME / E (any)	0.000	0.000	0.000	0.000	0.000	0.000	0.000	0.000	0
		HVO (any) / E (any)	0.000	0.000	0.000	0.000	0.000	0.000	0.000	0.000	0
		LNG / E (any)	1.323	1.917	0.451	1.466	8.019	11.620	2.736	8.884	111
		H2 (any) / E (any)	0.000	0.000	0.000	0.000	0.000	0.000	0.000	0.000	0
	FCHE	H2 (any)	0.000	0.000	0.000	0.000	0.000	0.000	0.000	0.000	0
	BE	E (any)	0.000	0.000	0.000	0.000	0.000	0.000	0.000	0.000	0

(Table B.10 continued on the next page)

(Table B.10 continued from the previous page)

WINK	HE (ZESC)	Diesel	3.315	4.177	2.357	1.820	21.665	27.300	15.404	11.896	55
		FAME	0.000	0.000	0.000	0.000	0.000	0.000	0.000	0.000	0
		HVO (any)	0.000	0.000	0.000	0.000	0.000	0.000	0.000	0.000	0
		LNG	2.551	3.204	1.812	1.391	16.672	20.939	11.846	9.094	55
		H2 (any)	0.000	0.000	0.000	0.000	0.000	0.000	0.000	0.000	0
	HE (FSMC)	Diesel	3.425	4.224	2.491	1.733	22.386	27.610	16.284	11.326	51
		FAME	0.000	0.000	0.000	0.000	0.000	0.000	0.000	0.000	0
		HVO (any)	0.000	0.000	0.000	0.000	0.000	0.000	0.000	0.000	0
		LNG	2.638	3.244	1.916	1.328	17.239	21.200	12.520	8.680	50
		H2 (any)	0.000	0.000	0.000	0.000	0.000	0.000	0.000	0.000	0
	PIHE	Diesel / E (any)	2.314	3.175	0.892	2.283	15.127	20.749	5.827	14.922	99
		FAME / E (any)	0.000	0.000	0.000	0.000	0.000	0.000	0.000	0.000	0
		HVO (any) / E (any)	0.000	0.000	0.000	0.000	0.000	0.000	0.000	0.000	0
		LNG / E (any)	1.785	2.444	0.683	1.761	11.665	15.975	4.466	11.509	99
		H2 (any) / E (any)	0.000	0.000	0.000	0.000	0.000	0.000	0.000	0.000	0
	FCHE	H2 (any)	0.000	0.000	0.000	0.000	0.000	0.000	0.000	0.000	0
	BE	E (any)	0.000	0.000	0.000	0.000	0.000	0.000	0.000	0.000	0

Legend: DE = Diesel-electric, HE = Hybrid-electric, PIHE = Plug-in hybrid-electric, FCHE = Fuel cell hybrid-electric, BE = Battery-electric, ZESC = Zero-emission station control, FSMC = Finite state machine control, FAME = Fatty Acid Methyl Ester, HVO = Hydrotreated vegetable oil, LNG = Liquefied natural gas, H2 = Hydrogen, E = Electricity.

Table B.11: Overall estimates of WTW GHG emissions

Vehicle	Prop. system	Energy carrier	Overall estimates per distance (kgCO2e/km)				Overall estimates per seat-distance (gCO2e/skm)				Rel. range (%)
			Mean	Max	Min	Range (Max-Min)	Mean	Max	Min	Range (Max-Min)	
GTW 2/6	DE	Diesel	3.267	5.269	2.390	2.879	30.820	49.706	22.543	27.163	88
	HE (ZESC)	Diesel	2.988	4.083	2.297	1.786	28.185	38.520	21.674	16.846	60
		FAME	1.568	2.136	1.206	0.930	14.789	20.154	11.381	8.774	59
		HVO (Rapeseed)	1.684	2.291	1.294	0.997	15.884	21.614	12.206	9.409	59
		HVO (Waste cooking oil)	0.360	0.490	0.277	0.213	3.398	4.624	2.611	2.013	59
		LNG	2.365	3.222	1.820	1.403	22.312	30.400	17.168	13.232	59
		H2 (SMR)	3.544	4.830	2.729	2.101	33.438	45.565	25.745	19.820	59
		H2 (Electrolysis - EU2030)	3.843	5.236	2.958	2.278	36.250	49.397	27.910	21.487	59
		H2 (Electrolysis - Wind)	0.308	0.419	0.237	0.182	2.904	3.957	2.236	1.721	59
	HE (FSMC)	Diesel	2.973	4.083	2.308	1.775	28.049	38.520	21.776	16.745	60
		FAME	1.560	2.145	1.212	0.933	14.718	20.237	11.435	8.803	60
		HVO (Rapeseed)	1.676	2.300	1.300	1.000	15.812	21.702	12.264	9.439	60
		HVO (Waste cooking oil)	0.359	0.492	0.278	0.214	3.383	4.643	2.624	2.019	60
		LNG	2.350	3.236	1.829	1.407	22.169	30.525	17.252	13.273	60
		H2 (SMR)	3.521	4.850	2.742	2.108	33.219	45.756	25.869	19.887	60
		H2 (Electrolysis - EU2030)	3.817	5.258	2.973	2.285	36.012	49.604	28.044	21.560	60
		H2 (Electrolysis - Wind)	0.306	0.421	0.238	0.183	2.885	3.973	2.246	1.727	60
	PIHE	Diesel / E (EU2030)	2.205	2.983	1.408	1.575	20.805	28.139	13.283	14.856	71
		Diesel / E (Wind))	1.851	2.718	0.590	2.128	17.464	25.646	5.568	20.078	115
		FAME / E (EU2030)	1.323	1.827	0.812	1.016	12.478	17.239	7.656	9.583	77
		FAME / E (Wind)	0.969	1.423	0.315	1.108	9.137	13.421	2.968	10.454	114
		HVO (Rapeseed) / E (EU2030)	1.396	1.913	0.860	1.054	13.166	18.050	8.110	9.940	75
		HVO (Rapeseed) / E (Wind)	1.044	1.530	0.365	1.165	9.853	14.434	3.446	10.988	112
		HVO (Waste cooking oil) / E (EU2030)	0.575	1.128	0.304	0.824	5.421	10.637	2.865	7.772	143
		HVO (Waste cooking oil) / E (Wind)	0.223	0.327	0.078	0.249	2.108	3.088	0.737	2.351	112
		LNG / E (EU2030)	1.816	2.473	1.148	1.326	17.136	23.331	10.826	12.506	73
		LNG / E (Wind)	1.461	2.143	0.469	1.673	13.784	20.213	4.428	15.785	115
		H2 (SMR) / E (EU2030)	2.546	3.439	1.570	1.869	24.022	32.439	14.810	17.629	73
		H2 (SMR) / E (Wind)	2.194	3.211	0.711	2.500	20.694	30.293	6.711	23.582	114
		H2 (Electrolysis - EU2030) / E (EU2030)	2.731	3.682	1.630	2.052	25.763	34.735	15.375	19.360	75
		H2 (Electrolysis - EU2030) / E (Wind)	2.378	3.481	0.771	2.710	22.434	32.841	7.276	25.565	114
		H2 (Electrolysis - Wind) / E (EU2030)	0.543	1.115	0.276	0.839	5.126	10.516	2.603	7.913	154
		H2 (Electrolysis - Wind) / E (Wind)	0.190	0.279	0.062	0.217	1.797	2.631	0.583	2.048	114
	FCHE	H2 (SMR)	3.192	5.133	2.452	2.681	30.116	48.423	23.132	25.291	84
		H2 (Electrolysis - EU2030)	3.461	5.564	2.658	2.906	32.649	52.495	25.077	27.418	84
		H2 (Electrolysis - Wind)	0.277	0.446	0.213	0.233	2.615	4.205	2.009	2.196	84
	BE	E (EU2030)	0.796	2.374	0.000	2.374	7.508	22.398	0.000	22.398	298
		E (Wind)	0.000	0.000	0.000	0.000	0.000	0.000	0.000	0.000	0

(Table B.11 continued on the next page)

(Table B.11 continued from the previous page)

GTW 2/8	DE	Diesel	3.512	5.514	2.474	3.041	21.287	33.420	14.993	18.427	87
	HE	Diesel	3.285	4.307	2.424	1.883	19.910	26.106	14.692	11.413	57
	(ZESC)	FAME	1.728	2.265	1.273	0.991	10.475	13.725	7.718	6.007	57
		HVO (Rapeseed)	1.851	2.425	1.366	1.059	11.218	14.695	8.278	6.417	57
		HVO (Waste cooking oil)	0.396	0.519	0.292	0.227	2.400	3.144	1.771	1.373	57
		LNG	2.612	3.411	1.922	1.489	15.833	20.671	11.646	9.025	57
		H2 (SMR)	3.909	5.116	2.879	2.237	23.691	31.005	17.449	13.555	57
		H2 (Electrolysis - EU2030)	4.238	5.546	3.121	2.425	25.684	33.612	18.917	14.695	57
		H2 (Electrolysis - Wind)	0.339	0.444	0.250	0.194	2.057	2.692	1.515	1.177	57
	HE	Diesel	3.286	4.299	2.453	1.846	19.913	26.056	14.867	11.189	56
	(FSMC)	FAME	1.727	2.259	1.289	0.970	10.466	13.690	7.810	5.880	56
		HVO (Rapeseed)	1.848	2.422	1.382	1.040	11.197	14.681	8.378	6.303	56
		HVO (Waste cooking oil)	0.395	0.518	0.296	0.222	2.395	3.141	1.792	1.348	56
		LNG	2.608	3.414	1.945	1.470	15.807	20.694	11.785	8.909	56
		H2 (SMR)	3.907	5.106	2.914	2.192	23.677	30.946	17.660	13.285	56
		H2 (Electrolysis - EU2030)	4.235	5.535	3.159	2.376	25.668	33.548	19.145	14.402	56
		H2 (Electrolysis - Wind)	0.339	0.443	0.253	0.190	2.056	2.687	1.534	1.154	56
	PIHE	Diesel / E (EU2030)	2.518	3.470	1.583	1.886	15.262	21.028	9.595	11.433	75
		Diesel / E (Wind))	2.159	3.131	0.721	2.410	13.086	18.973	4.367	14.606	112
		FAME / E (EU2030)	1.491	2.083	0.906	1.177	9.039	12.626	5.492	7.134	79
		FAME / E (Wind)	1.132	1.646	0.378	1.268	6.863	9.973	2.289	7.685	112
		HVO (Rapeseed) / E (EU2030)	1.574	2.192	0.955	1.237	9.541	13.283	5.786	7.497	79
		HVO (Rapeseed) / E (Wind)	1.212	1.761	0.408	1.352	7.343	10.671	2.475	8.196	112
		HVO (Waste cooking oil) / E (EU2030)	0.622	1.178	0.324	0.855	3.769	7.141	1.961	5.180	137
		HVO (Waste cooking oil) / E (Wind)	0.259	0.377	0.087	0.289	1.571	2.283	0.529	1.753	112
		LNG / E (EU2030)	2.070	2.865	1.287	1.578	12.546	17.365	7.799	9.566	76
		LNG / E (Wind)	1.712	2.482	0.584	1.897	10.379	15.040	3.541	11.499	111
		H2 (SMR) / E (EU2030)	2.917	4.021	1.726	2.295	17.677	24.372	10.464	13.908	79
		H2 (SMR) / E (Wind)	2.556	3.719	0.859	2.860	15.488	22.540	5.206	17.334	112
		H2 (Electrolysis - EU2030) / E (EU2030)	3.132	4.333	1.799	2.534	18.979	26.262	10.901	15.360	81
		H2 (Electrolysis - EU2030) / E (Wind)	2.770	4.032	0.931	3.101	16.790	24.436	5.644	18.792	112
		H2 (Electrolysis - Wind) / E (EU2030)	0.583	1.160	0.295	0.864	3.534	7.028	1.789	5.239	148
		H2 (Electrolysis - Wind) / E (Wind)	0.222	0.323	0.075	0.248	1.345	1.957	0.452	1.505	112
	FCHE	H2 (SMR)	3.515	5.533	2.571	2.961	21.305	33.533	15.585	17.948	84
		H2 (Electrolysis - EU2030)	3.811	5.998	2.788	3.210	23.097	36.352	16.895	19.457	84
		H2 (Electrolysis - Wind)	0.305	0.480	0.223	0.257	1.850	2.912	1.353	1.559	84
	BE	E (EU2030)	0.897	2.573	0.000	2.573	5.439	15.596	0.000	15.596	287
		E (Wind)	0.000	0.000	0.000	0.000	0.000	0.000	0.000	0.000	0

(Table B.11 continued on the next page)

(Table B.11 continued from the previous page)

WINK	HE (ZESC)	Diesel	4.171	5.256	2.965	2.290	27.261	34.351	19.382	14.969	55
		FAME	2.194	2.743	1.557	1.186	14.338	17.926	10.176	7.750	54
		HVO (Rapeseed)	2.349	2.951	1.670	1.280	15.355	19.285	10.917	8.367	54
		HVO (Waste cooking oil)	0.503	0.631	0.357	0.274	3.285	4.125	2.336	1.790	54
		LNG	3.302	4.147	2.346	1.801	21.580	27.102	15.332	11.770	55
		H2 (SMR)	4.965	6.194	3.520	2.674	32.450	40.484	23.009	17.476	54
		H2 (Electrolysis - EU2030)	5.382	6.715	3.816	2.899	35.179	43.889	24.943	18.945	54
		H2 (Electrolysis - Wind)	0.431	0.538	0.306	0.232	2.818	3.516	1.998	1.518	54
	HE (FSMC)	Diesel	4.310	5.315	3.135	2.180	28.168	34.742	20.490	14.252	51
		FAME	2.268	2.787	1.646	1.141	14.822	18.213	10.758	7.456	50
		HVO (Rapeseed)	2.427	2.985	1.766	1.219	15.865	19.509	11.543	7.966	50
		HVO (Waste cooking oil)	0.519	0.639	0.378	0.261	3.394	4.173	2.469	1.704	50
		LNG	3.414	4.198	2.479	1.719	22.314	27.440	16.205	11.235	50
		H2 (SMR)	5.136	6.296	3.721	2.575	33.570	41.151	24.318	16.833	50
		H2 (Electrolysis - EU2030)	5.568	6.826	4.034	2.792	36.393	44.612	26.363	18.249	50
		H2 (Electrolysis - Wind)	0.446	0.547	0.323	0.224	2.915	3.573	2.112	1.462	50
	PIHE	Diesel / E (EU2030)	3.462	4.673	2.268	2.406	22.628	30.543	14.821	15.722	69
		Diesel / E (Wind))	2.912	3.995	1.122	2.873	19.035	26.109	7.333	18.776	99
		FAME / E (EU2030)	2.081	3.002	1.320	1.682	13.604	19.623	8.627	10.996	81
		FAME / E (Wind)	1.532	2.099	0.589	1.510	10.010	13.720	3.852	9.868	99
		HVO (Rapeseed) / E (EU2030)	2.193	3.119	1.395	1.725	14.335	20.388	9.115	11.273	79
		HVO (Rapeseed) / E (Wind)	1.647	2.267	0.629	1.638	10.765	14.819	4.114	10.705	99
		HVO (Waste cooking oil) / E (EU2030)	0.899	2.151	0.454	1.696	5.873	14.057	2.969	11.088	189
		HVO (Waste cooking oil) / E (Wind)	0.352	0.485	0.135	0.350	2.303	3.170	0.880	2.290	99
		LNG / E (EU2030)	2.858	3.870	1.850	2.020	18.679	25.296	12.094	13.202	71
		LNG / E (Wind)	2.310	3.164	0.884	2.279	15.098	20.677	5.780	14.897	99
		H2 (SMR) / E (EU2030)	4.034	5.403	2.640	2.763	26.369	35.316	17.255	18.061	68
		H2 (SMR) / E (Wind)	3.491	4.781	1.332	3.449	22.818	31.250	8.708	22.543	99
		H2 (Electrolysis - EU2030) / E (EU2030)	4.328	5.791	2.839	2.951	28.288	37.846	18.557	19.289	68
		H2 (Electrolysis - EU2030) / E (Wind)	3.785	5.183	1.444	3.739	24.737	33.878	9.440	24.438	99
		H2 (Electrolysis - Wind) / E (EU2030)	0.846	2.129	0.407	1.722	5.532	13.912	2.660	11.252	203
		H2 (Electrolysis - Wind) / E (Wind)	0.303	0.415	0.116	0.300	1.981	2.714	0.756	1.958	99
	FCHE	H2 (SMR)	4.616	7.930	2.981	4.949	30.171	51.831	19.486	32.345	107
		H2 (Electrolysis - EU2030)	5.004	8.597	3.232	5.365	32.708	56.190	21.125	35.065	107
		H2 (Electrolysis - Wind)	0.401	0.689	0.259	0.430	2.620	4.501	1.692	2.809	107
	BE	E (EU2030)	1.326	4.322	0.000	4.322	8.670	28.251	0.000	28.251	326
		E (Wind)	0.000	0.000	0.000	0.000	0.000	0.000	0.000	0.000	0

Legend: DE = Diesel-electric, HE = Hybrid-electric, PIHE = Plug-in hybrid-electric, FCHE = Fuel cell hybrid-electric, BE = Battery-electric, ZESC = Zero-emission station control, FSMC = Finite state machine control, FAME = Fatty Acid Methyl Ester, HVO = Hydrotreated vegetable oil, LNG = Liquefied natural gas, H2 = Hydrogen, E = Electricity, SMR = steam methane reforming.

Table B.12: Estimations of average relative change (%) of Well-to-Wheel (WTW) energy use and greenhouse gas (GHG) emissions per vehicle-distance and seat-distance compared to the baseline scenario (hybrid-electric vehicle with Zero-Emission Station Control (ZESC) running on diesel fuel).

Prop. system	Energy carrier	GTW 2/6		GTW 2/8		WINK	
		Energy use	GHG emissions	Energy use	GHG emissions	Energy use	GHG emissions
Diesel-Electric	Diesel	9.35	9.35	6.92	6.92	-	-_
Hybrid-Electric (ZESC)	Diesel	0.00	0.00	0.00	0.00	0.00	0.00
	FAME	67.26	-47.53	67.71	-47.39	67.66	-47.41
	HVO (rapeseed)	68.31	-43.64	68.27	-43.66	68.22	-43.67
	HVO (waste cooking oil)	-7.91	-87.94	-7.93	-87.95	-7.96	-87.95
	LNG	-6.45	-20.84	-6.02	-20.48	-6.45	-20.84
	Hydrogen (SMR)	53.80	18.64	54.26	18.99	54.32	19.04
	Hydrogen (elec. EU2030-mix)	194.91	28.61	195.79	29.00	195.90	29.05
	Hydrogen (elec. wind power)	48.25	-89.70	48.69	-89.67	48.75	-89.66
Hybrid-Electric (FSMC)	Diesel	-0.48	-0.48	0.02	0.02	3.33	3.33
	FAME	66.46	-47.78	67.58	-47.43	73.33	-45.63
	HVO (rapeseed)	67.55	-43.90	67.96	-43.76	73.81	-41.80
	HVO (waste cooking oil)	-8.32	-88.00	-8.10	-87.97	-4.90	-87.55
	LNG	-7.05	-21.35	-6.18	-20.61	-3.27	-18.15
	Hydrogen (SMR)	52.79	17.86	54.16	18.92	59.64	23.14
	Hydrogen (elec. EU2030-mix)	192.97	27.77	195.61	28.92	206.11	33.50
	Hydrogen (elec. wind power)	47.27	-89.77	48.60	-89.67	53.88	-89.31
Plug-In Hybrid-Electric	Diesel / Electricity (EU2030-mix)	-10.81	-26.18	-9.17	-23.34	0.09	-16.99
	Diesel / Electricity (wind power)	-25.15	-38.04	-22.39	-34.27	-15.84	-30.18
	FAME / Electricity (EU2030-mix)	30.56	-55.73	34.98	-54.60	47.33	-50.10
	FAME / Electricity (wind power)	16.23	-67.58	21.76	-65.53	31.39	-63.28
	HVO (rapeseed) / Electricity (EU2030-mix)	31.40	-53.29	35.50	-52.08	48.01	-47.41
	HVO (rapeseed) / Electricity (wind power)	17.18	-65.04	22.15	-63.12	32.18	-60.51
	HVO (waste cooking oil) / Electricity (EU2030-mix)	-15.88	-80.77	-14.38	-81.07	-5.40	-78.46
	HVO (waste cooking oil) / Electricity (wind power)	-30.09	-92.52	-27.73	-92.11	-21.23	-91.55
	LNG / Electricity (EU2030-mix)	-14.90	-39.20	-13.40	-36.99	-4.38	-31.48
	LNG / Electricity (wind power)	-29.28	-51.09	-26.56	-47.87	-20.27	-44.62
	Hydrogen (SMR) / Electricity (EU2030-mix)	22.30	-14.77	26.09	-11.22	38.42	-3.27
	Hydrogen (SMR) / Electricity (wind power)	8.02	-26.58	12.79	-22.21	22.67	-16.30
	Hydrogen (elec. EU2030-mix) / Electricity (EU2030-mix)	109.63	-8.60	118.61	-4.68	137.98	3.77
	Hydrogen (elec. EU2030-mix) / Electricity (wind power)	95.35	-20.41	105.32	-15.67	122.23	-9.26
	Hydrogen (elec. wind power) / Electricity (EU2030-mix)	18.87	-81.81	22.45	-82.25	34.51	-79.71
	Hydrogen (elec. wind power) / Electricity (wind power)	4.59	-93.62	9.16	-93.25	18.76	-92.73
Fuel Cell Hybrid-Electric	Hydrogen (SMR)	38.52	6.85	38.72	7.01	43.48	10.68
	Hydrogen (elec. EU2030-mix)	165.61	15.84	166.00	16.01	175.12	19.98
	Hydrogen (elec. wind power)	33.52	-90.72	33.72	-90.71	38.30	-90.39
Battery-Electric	Electricity (EU2030-mix)	-38.83	-73.36	-37.26	-72.68	-26.97	-68.20
	Electricity (wind power)	-71.04	-100.00	-70.30	-100.00	-65.42	-100.00

Legend: GHG = greenhouse gas, ZESC = Zero-emission station control, FSMC = Finite state machine control, FAME = Fatty Acid Methyl Ester, HVO = Hydrotreated vegetable oil, LNG = Liquefied natural gas, SMR = steam methane reforming.

Bibliography

Aatola, H., Larmi, M., Sarjovaara, T., Mikkonen, S., 2009. Hydrotreated vegetable Oil (HVO) as a renewable diesel fuel: Trade-off between NOx, particulate emission, and fuel consumption of a heavy duty engine. *SAE International Journal of Engines*, 1(1), 1251–1262.

ABB, 2018. BORDLINE® CC750 DE. For diesel-electric regional trains (DMU). URL: https://library.e.abb.com/public/1b988f5784ff4676b460b46553050347/BORDLINE CC750 DE M U RevC EN.pdf

Agbli, Krehi Serge, Devillers, N., Chauvet, F., Hissel, D., Sorrentino, M., 2016. Energetic Macroscopic Representation in Reverse Engineering Process: Railcar Hybridization. *2016 IEEE Vehicle Power and Propulsion Conference (VPPC)*, IEEE, 1–6.

Agbli, Kréhi Serge, Hissel, D., Sorrentino, M., Chauvet, F., Pouget, J., 2016. Reverse engineering of a railcar prototype via energetic macroscopic representation approach. *Energy Conversion and Management*, 112, 61–80.

Agora Verkehrswende, Agora Energiewende, Frontier Economics, 2018. The Future Cost of Electricity-Based Synthetic Fuels. URL: https://www.agora-energiewende.de/en/publications/the-future-cost-of-electricity-based-synthetic-fuels-1/

Akal, D., Öztuna, S., Büyükakın, M.K., 2020. A review of hydrogen usage in internal combustion engines (gasoline-Lpg-diesel) from combustion performance aspect. *International Journal of Hydrogen Energy*, 45, 35257–35268.

Al-Tony, F.E.-S., Lashine, A., 2000. Cost-benefit analysis of railway electrification: case study for Cairo-Alexandria railway line. *Impact Assessment and Project Appraisal*, 18, 323–333.

Alstom, 2020. Alstom's hydrogen train enters regular passenger service in Austria. URL: https://www.alstom.com/press-releases-news/2020/9/alstoms-hydrogen-train-enters-regular-passenger-service-austria

Alstom, 2016. Alstom to deliver two Prima H3 shunting locomotives to Metrans. URL: https://www.alstom.com/press-releases-news/2016/2/alstom-to-deliver-two-prima-h3-shunting-locomotives-to-metrans

Alstom, 2015. Alstom to supply two H3 hybrid shunting locomotives for Audi. URL: https://www.alstom.com/press-releases-news/2015/2/alstom-to-supply-two-h3-hybrid-shunting-locomotives-for-audi

Ambuhl, D., Guzzella, L., 2009. Predictive Reference Signal Generator for Hybrid Electric Vehicles. *IEEE Transactions on Vehicular Technology*, 58, 4730–4740.

Andersson, Ö., Börjesson, P., 2021. The greenhouse gas emissions of an electrified vehicle combined with renewable fuels: Life cycle assessment and policy implications. *Applied Energy*, 289, 116621.

Andrade, C.E.S. de, D'Agosto, M. de A., 2016. Energy use and carbon dioxide emissions assessment in the lifecycle of passenger rail systems: the case of the Rio de Janeiro Metro. *Journal of Cleaner Production*, 126, 526–536.

ANL, 2020. The Greenhouse gases, Regulated Emissions, and Energy use in Transportation (GREET) model.

Arriva, 2020. Voor jou, compleet vernieuwde GTW-trein. URL: https://www.arriva.nl/meer-arriva/nieuws-4/persberichten/voor-jou-compleet-vernieuwde-gtwtrein-.htm

Arriva, 2019. Arriva aan zet voor duurzamer regionaal treinverkeer. URL: https://www.arriva.nl/meer-arriva/nieuws-4/persberichten/arriva-aan-zet-voor-duurzamer-regionaal-treinverkeer.htm

Bagotsky, V.S., Skundin, A.M., Volfkovich, Y.M., 2015. *Electrochemical Power Sources: Batteries, Fuel Cells, and Supercapacitors*. John Wiley & Sons, Inc., Hoboken, New Jersey.

Bai, S., Liu, C., 2021. Overview of energy harvesting and emission reduction technologies in hybrid electric vehicles. *Renewable and Sustainable Energy Reviews*, 147, 111188.

Ballard, 2021. FCmove. URL: https://www.ballard.com/about-ballard/publication_library/product-specification-sheets/fcmovetm-spec-sheet

Banar, M., Özdemir, A., 2015. An evaluation of railway passenger transport in Turkey using life cycle assessment and life cycle cost methods. *Transportation Research Part D: Transport and Environment*, 41, 88–105.

Barbir, B., 2013. PEM Fuel Cells: *Theory and Practice*. Second Edition, Elsevier Inc.

Barbosa, F.C., 2019. Fuel Cell Rail Technology Review: A Tool for an Autonomous Rail Electrifying Strategy. *2019 Joint Rail Conference*, American Society of Mechanical Engineers.

Beatrice, C., Rispoli, N., Di Blasio, G., Konstandopoulos, A.G., Papaioannou, E., Imren, A., 2016. Impact of Emerging Engine and After-Treatment Technologies for Improved Fuel Efficiency and Emission Reduction for the Future Rail Diesel Engines. *Emission Control Science and Technology*, 2, 99–112.

Beatrice, C., Rispoli, N., Di Blasio, G., Patrianakos, G., Kostoglou, M., Konstandopoulos, A., Imren, A., Denbratt, I., Palacin, R., 2013. Emission Reduction Technologies for the Future Low Emission Rail Diesel Engines: EGR vs SCR. *SAE Technical Papers*, 6.

Bellman, R., 2003. *Dynamic Programming. Dover Publications*. Mineola, NY.

Bellman, R., 1952. On the theory of dynamic programming. *Proceedings of the National Academy of Sciences of the USA*, 38, 716–719.

Bomhauer-Beins, A., 2019. *Energy Saving Potentials in Railway Operations under Systemic Perspectives*, Doctoral thesis, ETH Zurich.

Boulter, P.G., McCrae, I.S., 2007. ARTEMIS: Assessment and Reliability of Transport Emission Models and Inventory Systems – Final Report.

Brünger, O., Dahlhaus, E., 2014. Running time estimation, in: Hansen, I.A., Pachl, J. (Eds.), *Railway Timetabling & Operations*. Eurailpress, Hamburg, 65–89.

Buzzoni, L., Pede, G., 2012. New prospects for public transport electrification. *Electrical Systems for Aircraft, Railway and Ship Propulsion (ESARS)*, 2–6.

Calvert, C., Allan, J., Amor, P., Hillmansen, S., Roberts, C., Weston, P., 2021. Concept development and testing of the UK's first hydrogen-hybrid train (HydroFLEX). *Railway Engineering Science*, 29, 248–257.

Cambridge Systematics Inc., 2012. Final technical memorandum, Task 8.3: Analysis of Freight Rail Electrification in the SCAG Region, prepared for Southern California association of governments.

Carrette, L., Friedrich, K.A., Stimming, U., 2001. Fuel Cells - Fundamentals and Applications. *Fuel Cells*, 1, 5–39.

CBS, 2021. Pump prices for motor fuels; location gas station, fuel type (in Dutch). URL: https://opendata.cbs.nl/statline/?ts=1585295852166#/CBS/nl/dataset/81567NED/table

CE Delft, 2020. Review of Dutch rail diesel emissions calculation methodology. Delft.

CEN, 2015. EN 15528: Railway applications - Line categories for managing the interface between load limits of vehicles and infrastructure.

CEN, 2012. Standard EN 16258: Methodology for calculation and declaration of energy consumption and GHG emissions of transport services (freight and passengers).

Chan, S., Miranda-Moreno, L., Patterson, Z., 2013. Analysis of GHG Emissions for City Passenger Trains: Is Electricity an Obvious Option for Montreal Commuter Trains? *Journal of Transportation Technologies*, 3, 17–29.

Chen, X., Wang, Y., Zhao, Y., Zhou, Y., 2016. A study of double functions and load matching of a phosphoric acid fuel cell/heat-driven refrigerator hybrid system. *Energy*, 101, 359–365.

Cipek, M., Pavković, D., Kljaić, Z., Mlinarić, T.J., 2019. Assessment of battery-hybrid diesel-electric locomotive fuel savings and emission reduction potentials based on a realistic mountainous rail route. *Energy*, 173, 1154–1171.

CleanER-D, 2020. Clean European Rail-Diesel. Seventh Framework Programme 7.2.1.1 Sustainable Surface Transport. Project deliverables. URL: http://www.cleaner-d.eu/deliverables.htm

CLECAT, 2012. Calculating GHG emissions for freight forwarding and logistics services in accordance with EN 16258: Terms , Methods , Examples.

CO2emissiefactoren, 2021. CO2emissiefactoren - Lijst emissiefactoren. URL: https://www.co2emissiefactoren.nl/lijst-emissiefactoren/

CORDIS, 2021. Final Report Summary - MERLIN (Sustainable and intelligent management of energy for smarter railway systems in Europe: an integrated optimisation approach).

Curran, M.A. (Ed.), 2012. *Life Cycle Assessment Handbook: A Guide for Environmentally Sustainable Products*. Wiley.

Davis, W.J., 1926. The tractive resistance of electric locomotives and cars. *General Electric Review*, 29, 685–707.

DEFRA, 2012. 2012 Guidelines to Defra / DECC's GHG Conversion Factors for Company Reporting: Methodology Paper for Emission Factors. London, UK.

Del Pero, F., Delogu, M., Pierini, M., Bonaffini, D., 2015. Life Cycle Assessment of a heavy metro train. *Journal of Cleaner Production*, 87, 787–799.

Deur, J., Škugor, B., Cipek, M., 2015. Integration of Electric Vehicles into Energy and Transport Systems. *Automatika*, 56, 395–410.

Deutz, 2021. DEUTZ hydrogen engine ready for the market. URL: https://www.deutz.com/en/media/press-releases/deutz-hydrogen-engine-ready-for-the-market

DiDomenico, G.C., Dick, C.T., 2015. Methods of Analyzing and Comparing Energy Efficiency of Passenger Rail Systems. *Transportation Research Record: Journal of the Transportation Research Board*, 2475, 54–62.

DieselNet, 2020. ISO 8178. URL: https://dieselnet.com/standards/cycles/iso8178.php

Din, T., Hillmansen, S., 2018. Energy consumption and carbon dioxide emissions analysis for a concept design of a hydrogen hybrid railway vehicle. *IET Electrical Systems in Transportation*, 8, 112–121.

Dincer, I., Hogerwaard, J., Zamfirescu, C., 2016. *Clean Rail Transportation Options, Green Energy and Technology*. Springer International Publishing, Cham.

Dincer, I., Zamfirescu, C., 2016. A review of novel energy options for clean rail applications. *Journal of Natural Gas Science and Engineering*, 28, 461–478.

Ding, X., Wang, Z., Zhang, L., 2021. Hybrid Control-Based Acceleration Slip Regulation for Four-Wheel-Independently-Actuated Electric Vehicles. *IEEE Transactions on Transportation Electrification*, 7, 1–14.

Ding, X., Wang, Z., Zhang, L., Wang, C., 2020. Longitudinal Vehicle Speed Estimation for Four-Wheel-Independently-Actuated Electric Vehicles Based on Multi-Sensor Fusion. *IEEE Transactions on Vehicular Technology*, 69, 12797–12806.

Dinić, D., 1986. *Railway traction* (in Serbian). Publishing Institute of Yugoslavian Railways, Belgrade.

Dittus, H., Hülsebusch, D., Ungethüm, J., 2011. Reducing DMU fuel consumption by means of hybrid energy storage. *European Transport Research Review*, 3, 149–159.

Doucette, R.T., McCulloch, M.D., 2011. Modeling the prospects of plug-in hybrid electric vehicles to reduce CO2 emissions. *Applied Energy*, 88, 2315–2323.

Dreier, D., Silveira, S., Khatiwada, D., Fonseca, K.V.O., Nieweglowski, R., Schepanski, R., 2018. Well-to-Wheel analysis of fossil energy use and greenhouse gas emissions for conventional, hybrid-electric and plug-in hybrid-electric city buses in the BRT system in Curitiba, Brazil. *Transportation Research Part D: Transport and Environment*, 58, 122–138.

Dunbar, R., Roberts, C., Zhao, N., 2017. A tool for the rapid selection of a railway signalling strategy to implement train control optimisation for energy saving. *Journal of Rail Transport Planning & Management*, 7, 224–244.

Ebbesen, S., Dönitz, C., Guzzella, L., 2012. Particle swarm optimisation for hybrid electric drive-train sizing. *International Journal of Vehicle Design*, 58, 181.

EC, 2019. Communication from the commission to the European Parliament, the European Council, the Council, the European Economic and Social Committee and the Committee of the Regions: The European Green Deal. COM (2019) 640. Brussels.

EC, 2018. Electrified railway lines. URL: https://ec.europa.eu/transport/facts-fundings/scoreboard/compare/energy-union-innovation/share-electrified-railway_en

EC, 2017. EU Transport in Figures: Statistical Pocketbook 2017.

EC, 2011. White paper on transport : roadmap to a single European transport area : towards a competitive and resource efficient transport system.

EC, 2005. Public Report: ultra low emission vehicle - transport using advanced propulsion 2 (ULEV-TAP II). Erlangen.

EcoWatch, 2017. Dutch Trains Are World's First to Run on 100% Wind Power. URL: https://www.ecowatch.com/dutch-trains-wind-energy-2187547588.html

Ellingsen, L.A.-W., Singh, B., Strømman, A.H., 2016. The size and range effect: lifecycle greenhouse gas emissions of electric vehicles. *Environmental Research Letters*, 11, 054010.

Engel, B., Soefker, C., 2001. The innovative traction system with the flywheel of the LIREX™. *World Congress on Railway Research 2001*.

Enric, 2021. LNG Vehicle Fuel Tank. URL: https://www.cimc-enric.com/lng-vehicle-fuel-tank-product/

Esters, T., Marinov, M., 2014. An analysis of the methods used to calculate the emissions of rolling stock in the UK. *Transportation Research Part D: Transport and Environment*, 33, 1–16.

Fathy, H.K., Reyer, J.A., Papalambros, P.Y., Ulsov, A.G., 2001. On the coupling between the plant and controller optimization problems, *Proceedings of the 2001 American Control Conference*, 1864–1869.

Fiori, C., Ahn, K., Rakha, H.A., 2016. Power-based electric vehicle energy consumption model: Model development and validation. *Applied Energy*, 168, 257–268.

Fotouhi, A., Auger, D.J., Propp, K., Longo, S., Wild, M., 2016. A review on electric vehicle battery modelling: From Lithium-ion toward Lithium–Sulphur. *Renewable and Sustainable Energy Reviews*, 56, 1008–1021.

Fragiacomo, P., Piraino, F., 2021. Vehicle-to-grid application with hydrogen-based tram. *Energy Conversion and Management*, 250, 114915.

Fragiacomo, P., Piraino, F., 2019. Fuel cell hybrid powertrains for use in Southern Italian railways. *International Journal of Hydrogen Energy*, 44, 27930–27946.

FuelCellWorks, 2020. Siemens Mireo Plus H Fuel Cell Hydrogen Train - The Middle Distance Champion. URL: https://fuelcellsworks.com/news/siemens-mireo-plus-h-fuel-cell-hydrogen-train-the-middle-distance-champion/

FuelCellWorks, 2022. World's First Hydrogen Train With a Speed of 160 Kilometers Per Hour Rolled Out in China. URL: https://fuelcellsworks.com/news/worlds-first-hydrogen-train-with-a-speed-of-160-kilometers-per-hour-rolled-out-in-china/

Fuhs, A., 2008. *Hybrid Vehicles*. CRC Press.

Fujii, T., Teraya, N., Osawa, M., 2004. Special edition paper Development of an NE train. *JR EAST Technical Review*, 62–70.

Gallucci, M., 2019. Hydrogen trains roll into service: A new hybrid locomotive signals a growing push for zero-emission rail technologies - [News]. *IEEE Spectrum*, 56, 6–7.

Gangwar, M., Sharma, S.M., 2014. Evaluating choice of traction option for a sustainable Indian Railways. *Transportation Research Part D: Transport and Environment*, 33, 135–145.

Gao, D.W., Mi, C., Emadi, A., 2007. Modeling and Simulation of Electric and Hybrid Vehicles. *Proceedings of the IEEE*, 95, 729–745.

García-Garre, A., Gabaldón, A., 2019. Analysis, Evaluation and Simulation of Railway Diesel-Electric and Hybrid Units as Distributed Energy Resources. *Applied Sciences*, 9, 3605.

García Márquez, F.P., Lewis, R.W., Tobias, A.M., Roberts, C., 2008. Life cycle costs for railway condition monitoring. *Transportation Research Part E: Logistics and Transportation Review*, 44, 1175–1187.

Garcia, P., Fernandez, L.M., Garcia, C.A., Jurado, F., 2010. Energy Management System of Fuel-Cell-Battery Hybrid Tramway. *IEEE Transactions on Industrial Electronics*, 57, 4013–4023.

Ghaviha, N., Bohlin, M., Holmberg, C., Dahlquist, E., 2019. Speed profile optimization of catenary-free electric trains with lithium-ion batteries. *Journal of Modern Transportation*, 27, 153–168.

Ghaviha, N., Bohlin, M., Holmberg, C., Dahlquist, E., Skoglund, R., Jonasson, D., 2017a. A driver advisory system with dynamic losses for passenger electric multiple units. *Transportation Research Part C: Emerging Technologies*, 85, 111–130.

Ghaviha, N., Campillo, J., Bohlin, M., Dahlquist, E., 2017b. Review of Application of Energy Storage Devices in Railway Transportation. *Energy Procedia*, 105, 4561–4568.

Giro Batalla, R., Feenstra, M., 2012. Energy consumption in GTW DMU trains - ECO Driving. Project statement, Arriva Nederland.

González-Gil, A., Palacin, R., Batty, P., 2013. Sustainable urban rail systems: Strategies and technologies for optimal management of regenerative braking energy. *Energy Conversion and Management*, 75, 374–388.

González-Gil, A., Palacin, R., Batty, P., Powell, J.P., 2014. A systems approach to reduce urban rail energy consumption. *Energy Conversion and Management*, 80, 509–524.

Guo, Y., Dai, X., Jermsittiparsert, K., Razmjooy, N., 2020. An optimal configuration for a battery and PEM fuel cell-based hybrid energy system using developed Krill herd optimization algorithm for locomotive application. *Energy Reports*, 6, 885–894.

Gustafsson, M., Svensson, N., Eklund, M., Dahl Öberg, J., Vehabovic, A., 2021. Well-to-wheel greenhouse gas emissions of heavy-duty transports: Influence of electricity carbon intensity. *Transportation Research Part D: Transport and Environment*, 93, 102757.

Guzzella, L., Sciarretta, A., 2013. *Vehicle propulsion systems: Introduction to modeling and optimization*, Third Edition. Springer, Berlin.

Han, Y., Cao, N., Hong, Z., Li, Q., Chen, W., 2016. Experimental Study on Energy Management Strategy for Fuel Cell Hybrid Tramway. *2016 IEEE Vehicle Power and Propulsion Conference (VPPC)*, 1–6.

Han, Y., Li, Q., Wang, T., Chen, W., Ma, L., 2018. Multisource Coordination Energy Management Strategy Based on SOC Consensus for a PEMFC–Battery–Supercapacitor Hybrid Tramway. *IEEE Transactions on Vehicular Technology*, 67, 296–305.

Han, Y., Meng, X., Zhang, G., Li, Q., Chen, W., 2017. An energy management system based on hierarchical control and state machine for the PEMFC-battery hybrid tramway. *2017 IEEE Transportation Electrification Conference and Expo, Asia-Pacific (ITEC Asia-Pacific)*, 1–5.

Hillmansen, S., Roberts, C., Mcgordon, A., Jennings, P., 2009. DMU hybrid concept evaluation. Final Report DfTRG/0078/2007. Birmingham.

Hillmansen, S., Roberts, C., Mcgordon, A., Jennings, P., 2008. Concept Validation for Hybrid Trains. Final Report DfTRG/0078/2007. Birmingham.

Hirose, H., Yoshida, K., Shibanuma, K., 2012. Development of catenary and storage battery hybrid train system. *Electrical Systems for Aircraft, Railway and Ship Propulsion*, 1–4.

Hoffrichter, A., Hillmansen, S., Roberts, C., 2016. Conceptual propulsion system design for a hydrogen-powered regional train. *IET Electrical Systems in Transportation*, 6, 56–66.

Hoffrichter, A., Miller, A.R., Hillmansen, S., Roberts, C., 2012. Well-to-wheel analysis for electric, diesel and hydrogen traction for railways. *Transportation Research Part D: Transport and Environment*, 17, 28–34.

Hong, Z., Li, Q., Han, Y., Shang, W., Zhu, Y., Chen, W., 2018. An energy management strategy based on dynamic power factor for fuel cell/battery hybrid locomotive. *International Journal of Hydrogen Energy*, 43, 3261–3272.

Horrein, L., Bouscayrol, A., Delarue, P., Verhille, J.N., Mayet, C., 2012. Forward and backward simulations of a power propulsion system, *IFAC Proceedings Volumes*, (IFAC-PapersOnline).

Huerlimann, D., Nash, A., 2003. Opentrack-simulation of railway networks, user manual version 1.3.

IEA, 2020. The Netherlands 2020: Energy Policy Review. Paris.

IEA, UIC, 2017. Railway Handbook 2017. Energy Consumption and CO2 Emissions. Focus on Passenger Rail Services.

INSIDEEVs, 2015. Meet Audi’s Plug-In Hybrid Locomotive. URL: https://insideevs.com/news/328130/meet-audis-plug-in-hybrid-locomotive/

IPCC, 2021. Climate Change 2021: The Physical Science Basis.

IPCC, 2007. Climate Change 2007: The Physical Science Basis.

IRJ, 2019. Zillertalbahn hydrogen train design revealed. URL: https://www.railjournal.com/fleet/zillertalbahn-hydrogen-train-design-revealed/

Jones, H., Moura, F., Domingos, T., 2017. Life cycle assessment of high-speed rail: a case study in Portugal. *The International Journal of Life Cycle Assessment*, 22, 410–422.

Joud, L., Da Silva, R., Chrenko, D., Kéromnès, A., Le Moyne, L., 2020. Smart Energy Management for Series Hybrid Electric Vehicles Based on Driver Habits Recognition and Prediction. *Energies*, 13, 2954.

JRC, 2020a. JEC Well-To-Wheels report v5. Well-to-Wheels analysis of future automotive fuels and powertrains in the European context. Luxembourg.

JRC, 2020b. JEC Well-to-Tank report v5. Well-to-Wheels analysis of future automotive fuels and powertrains in the European context. Luxembourg.

Kapetanović, M., Núñez, A., van Oort, N., Goverde, R.M.P., 2022. Analysis of hydrogen-powered propulsion system alternatives for diesel-electric regional trains. *Journal of Rail Transport Planning & Management*, 23, 100338.

Kapetanović, M., Núñez, A., van Oort, N., Goverde, R.M.P., 2021a. Reducing fuel consumption and related emissions through optimal sizing of energy storage systems for diesel-electric trains. Applied Energy, 294, 117018.

Kapetanović, M., Vajihi, M., Goverde, R.M.P., 2021b. Analysis of Hybrid and Plug-In Hybrid Alternative Propulsion Systems for Regional Diesel-Electric Multiple Unit Trains. Energies, 14, 5920.

Kapetanović, M., van Oort, N., Nunez, A., Goverde, R., 2019. Sustainability of Railway Passenger Services: A Review of Aspects, Issues, Contributions and Challenges of Life Cycle Emissions, in: Peterson, A., Joborn, M., Bohlin, M. (Eds.), *RailNorrköping 2019: 8th International Conference on Railway Operations Modelling and Analysis (ICROMA)*, Norrköping, Sweden, Linköping University Electronic Press, 528–547.

Kirschstein, T., Meisel, F., 2015. GHG-emission models for assessing the eco-friendliness of road and rail freight transports. *Transportation Research Part B: Methodological*, 73, 13–33.

Klebsch, W., Guckes, N., Heininger, P., 2020. Evaluation of climate-neutral alternatives to diesel multiple units: Economic viability assessment based on the example of the ›Düren network‹. VDE, Frankfurt am Main.

Klebsch, W., Heininger, P., Geder, J., Hauser, A., 2018. Battery Systems for Multiple Units: Emission-free drives powered by lithium-ion cells. VDE, Frankfurt am Main.

Klebsch, W., Heininger, P., Martin, J., 2019. Alternatives to diesel multiple units in regional passenger rail transport: Assessment of systemic potential. VDE, Frankfurt am Main.

Knorr, H., Held, W., Prumm, W., Rudiger, H., 1998. The MAN hydrogen propulsion system for city buses. *International Journal of Hydrogen Energy*, 23, 201–208.

Knörr, W., Heidt, C., Notter, B., Läderach, A., Biemann, K., Antes, R., 2018. Ecological Transport Information Tool for Worldwide Transports. Methodology and Data, Update 2018.

Knörr, W., Hüttermann, R., 2016. EcoPassenger: Environmental Methodology and Data. Heidelberg/Hannover.

Kono, Y., Shiraki, N., Yokoyama, H., Furuta, R., 2014. Catenary and storage battery hybrid system for electric railcar series EV-E301. *2014 International Power Electronics Conference (IPEC-Hiroshima 2014 - ECCE ASIA)*, 2120–2125.

Konstandopoulos, A.G., Kostoglou, M., Beatrice, C., Di Blasio, G., Imren, A., Denbratt, I., 2015. Impact of Combination of EGR, SCR, and DPF Technologies for the Low-Emission Rail Diesel Engines. *Emission Control Science and Technology*, 1, 213–225.

Kordesch, K., Hacker, V., Gsellmann, J., Cifrain, M., Faleschini, G., Enzinger, P., Fankhauser, R., Ortner, M., Muhr, M., Aronson, R.R., 2000. Alkaline fuel cells applications. *Journal of Power Sources*, 86, 162–165.

Krastev, I., Tricoli, P., 2022. Boost Multilevel Cascade Inverter for Hydrogen Fuel Cell Light Railway Vehicles. *IEEE Transactions on Industrial Electronics*, 69, 7837–7847.

Küng, L., Bütler, T., Georges, G., Boulouchos, K., 2018. Decarbonizing passenger cars using different powertrain technologies: Optimal fleet composition under evolving electricity supply. *Transportation Research Part C: Emerging Technologies*, 95, 785–801.

Kuttler, M., Pichlmaier, S., 2021. Analysis of Fuel and Powertrain Combinations for Heavy-Duty Vehicles from a Well-to-Wheels Perspective: Model Development and Sample Application. *Progress in Life Cycle Assessment*, 25–40.

Lanneluc, C., Pouget, J., Poline, M., Chauvet, F., Gerbaud, L., 2017. Optimal Energy Management of a Hybrid Train: Focus on Saving Braking Energy. *2017 IEEE Vehicle Power and Propulsion Conference (VPPC)*, 1–6.

Leska, M., Aschemann, H., 2015. Fuel-optimal combined driving strategy and energy management for a parallel hybrid electric railway vehicle. *20th International Conference on Methods and Models in Automation and Robotics (MMAR)*, 1127–1132.

Leska, M., Aschemann, H., Melzer, M., Meinert, M., 2017. Comparative Calculation of the Fuel-Optimal Operating Strategy for Diesel Hybrid Railway Vehicles. *International Journal of Applied Mathematics and Computer Science*, 27, 323–336.

Leska, M., Gruning, T., Aschemann, H., Rauh, A., 2013. Optimal trajectory planning for standard and hybrid railway vehicles with a hydro-mechanic transmission. *2013 European Control Conference (ECC 2013)*, 4550–4555.

Leska, M., Gruning, T., Aschemann, H., Rauh, A., 2012. Optimization of the longitudinal dynamics of parallel hybrid railway vehicles. *Proceedings of the IEEE International Conference on Control Applications*, 202–207.

Leska, M., Prabel, R., Aschemann, H., Rauh, A., 2014. Optimal Operating Strategy for Hybrid Railway Vehicles based on a Sensitivity Analysis. *IFAC Proceedings*, 47, 942–947.

Li, H., Ravey, A., N'Diaye, A., Djerdir, A., 2019. Online adaptive equivalent consumption minimization strategy for fuel cell hybrid electric vehicle considering power sources degradation. *Energy Conversion and Management*, 192, 133–149.

Li, Minggao, Li, Ming, Han, G., Liu, N., Zhang, Q., Wang, Y., 2018. Optimization Analysis of the Energy Management Strategy of the New Energy Hybrid 100% Low-Floor Tramcar Using a Genetic Algorithm. *Applied Sciences*, 8, 1144.

Li, Q., Yang, H., Han, Y., Li, M., Chen, W., 2016. A state machine strategy based on droop control for an energy management system of PEMFC-battery-supercapacitor hybrid tramway. *International Journal of Hydrogen Energy*, 41, 16148–16159.

Lipman, T.E., 2020. Chapter 12 - Vehicle technologies for achieving near and longer term fuel economy and climate goals, in: Deakin, E. (Ed.), *Transportation, Land Use, and Environmental Planning*. Elsevier, 217-236.

Liu, J., Wu, X., Li, H., Qi, L., 2020. An optimal method of the energy consumption for fuel cell hybrid tram. *International Journal of Hydrogen Energy*, 45, 20304–20311.

Logan, K.G., Nelson, J.D., McLellan, B.C., Hastings, A., 2020. Electric and hydrogen rail: Potential contribution to net zero in the UK. *Transportation Research Part D: Transport and Environment*, 87, 102523.

Lu, S., Hillmansen, S., Roberts, C., 2011. A Power-Management Strategy for Multiple-Unit Railroad Vehicles. *IEEE Transactions on Vehicular Technology*, 60, 406–420.

Lu, S., Hillmansen, S., Roberts, C., 2010. Power management strategy study for a multiple unit train. *IET Conference on Railway Traction Systems (RTS 2010)*, 29–29.

Luan, X., Wang, Y., De Schutter, B., Meng, L., Lodewijks, G., Corman, F., 2018. Integration of real-time traffic management and train control for rail networks - Part 2: Extensions towards energy-efficient train operations. *Transportation Research Part B: Methodological*, 115, 72–94.

Luxfer, 2020a. Hydrogen Cylinders for Alternative Fuel Trains. URL: https://www.luxfercylinders.com/support/hydrogen-cylinders-for-alternative-fuel-trains/alternative-fuel

Luxfer, 2020b. Specification Data: G-Stor H2 Alternative Fuel Cylinders. URL: https://www.luxfercylinders.com/support/luxfer-g-stor-h2-spec-sheet

Madovi, O., Hoffrichter, A., Little, N., Foster, S.N., Isaac, R., 2021. Feasibility of hydrogen fuel cell technology for railway intercity services: a case study for the Piedmont in North Carolina. *Railway Engineering Science*, 29, 258–270.

Maleki, A., Rosen, M.A., 2017. Design of a cost-effective on-grid hybrid wind–hydrogen based CHP system using a modified heuristic approach. *International Journal of Hydrogen Energy*, 42, 15973–15989.

MAN, 2020. MAN presents Zero-Emission Roadmap. Press Release. MAN Truck & Bus. URL: https://press.mantruckandbus.com/man-presents-zero-emission-roadmap/

Mao, F., Li, Z., Zhang, K., 2020. Carbon dioxide emissions estimation of conventional diesel buses electrification: A well-to-well analysis in Shenzhen, China. *Journal of Cleaner Production*, 277, 123048.

Marin, G.D., Naterer, G.F., Gabriel, K., 2010. Rail transportation by hydrogen vs. electrification – Case study for Ontario, Canada, II: Energy supply and distribution. *International Journal of Hydrogen Energy*, 35, 6097–6107.

Marsilla, M., 2013. CleanER-D Deliverable 7.5.4: Future scenarios and recommendations for implementation of hybrid solutions.

Masatsuki, I., 2011. Development of Catenary and Battery powered hybrid railcar system. *9th World Congress on Railwau Reearch*, Lille, France.

Masatsuki, I., 2010. Development of the battery charging system for the new hybrid train that combines feeder line and the storage battery. *The 2010 International Power Electronics Conference - ECCE ASIA*, 3128–3135.

Maxwell, 2021. 125 Volt Transportation Module. URL: https://www.maxwell.com/products/ultracapacitors/125v-tran-modules#

Mayet, C., Mejri, M., Bouscayrol, A., Pouget, J., Riffonneau, Y., 2012. Energetic Macroscopic Representation and inversion-based control of the traction system of a hybrid locomotive. *2012 IEEE Vehicle Power and Propulsion Conference*, 491–496.

Meinert, M., Melzer, M., Kamburow, C., Palacin, R., Leska, M., Aschemann, H., 2015a. Benefits of hybridisation of diesel driven rail vehicles: Energy management strategies and life-cycle costs appraisal. *Applied Energy*, 157, 897–904.

Meinert, M., Prenleloup, P., Schmid, S., Palacin, R., 2015b. Energy storage technologies and hybrid architectures for specific diesel-driven rail duty cycles: Design and system integration aspects. *Applied Energy*, 157, 619–629.

Meynerts, L., Brito, J., Ribeiro, I., Peças, P., Claus, S., Götze, U., 2018. Life Cycle Assessment of a Hybrid Train – Comparison of Different Propulsion Systems. *Procedia CIRP*, 69, 511–516.

Miller, A.R., Hess, K.S., Barnes, D.L., Erickson, T.L., 2007. System design of a large fuel cell hybrid locomotive. *Journal of Power Sources*, 173, 935–942.

Mojtaba Lajevardi, S., Axsen, J., Crawford, C., 2019. Comparing alternative heavy-duty drivetrains based on GHG emissions, ownership and abatement costs: Simulations of freight routes in British Columbia. *Transportation Research Part D: Transport and*

Environment, 76, 19–55.

Mueller, F., Guerster, M., Obrenovic, N., Bierlaire, M., 2020. Can regional railway become emission-free with recently announced vehicles? - A case study of Bavaria. *European Journal of Transport and Infrastructure Research*, 20, 286–305.

Mwambeleko, J.J., Kulworawanichpong, T., 2017. Battery electric multiple units to replace diesel commuter trains serving short and idle routes. *Journal of Energy Storage*, 11, 7–15.

Nazari, S., Middleton, R., Siegel, J., Stefanopoulou, A., 2019. Equivalent Consumption Minimization Strategy for a Power Split Supercharger. *WCX SAE World Congress Experience*.

Neste, 2016. Neste Renewable Diesel Handbook. URL: https://www.neste.com/sites/default/files/attachments/neste_renewable_diesel_handbook.pdf

Nocera, S., Cavallaro, F., 2016. Economic valuation of Well-To-Wheel CO2 emissions from freight transport along the main transalpine corridors. *Transportation Research Part D: Transport and Environment*, 47, 222–236.

Ogawa, T., Yoshihara, H., Wakao, S., Kondo, K., Kondo, M., 2007. Energy consumption analysis of FC-EDLC hybrid railway vehicle by dynamic programming. *2007 European Conference on Power Electronics and Applications*, 1–8.

Orecchini, F., Santiangeli, A., 2010. Automakers’ Powertrain Options for Hybrid and Electric Vehicles. *Electric and Hybrid Vehicles*, 579–636.

Orecchini, F., Santiangeli, A., Dell’Era, A., 2014. EVs and HEVs Using Lithium-Ion Batteries. *Lithium-Ion Batteries*, 205–248.

Paukert, H., 2011. CleanER-D Deliverable 7.2.1: Detailed Specification: Parameters definition.

Peng, F., Chen, W., Liu, Z., Li, Q., Dai, C., 2014. System integration of China’s first proton exchange membrane fuel cell locomotive. *International Journal of Hydrogen Energy*, 39, 13886–13893.

Peng, F., Zhao, Y., Chen, T., Zhang, X., Chen, W., Zhou, D., Li, Q., 2018. Development of robust suboptimal real-time power sharing strategy for modern fuel cell based hybrid tramways considering operational uncertainties and performance degradation. *Applied Energy*, 226, 503–521.

Peng, H., Li, J., Löwenstein, L., Hameyer, K., 2020a. A scalable, causal, adaptive energy management strategy based on optimal control theory for a fuel cell hybrid railway vehicle. *Applied Energy*, 267, 114987.

Peng, H., Li, J., Thul, A., Deng, K., Ünlübayir, C., Löwenstein, L., Hameyer, K., 2020b. A scalable, causal, adaptive rule-based energy management for fuel cell hybrid railway vehicles learned from results of dynamic programming. *eTransportation*, 4, 100057.

Peredel’skii, V.A., Lastovskii, Y. V., Darbinyan, R. V., Savitskii, A.I., Savitskii, A.A., 2005. Analysis of the desirability of replacing petroleum-based vehicle fuel with liquefied natural gas. *Chemical and Petroleum Engineering*, 41, 590–595.

Pesaran, A., Kim, G.-H., Gonder, J., 2005. PEM Fuel Cell Freeze and Rapid Startup Investigation, Milestone Report NREL/MP-540-38760. Golden, Colorado.

Piraino, F., Fragiacomo, P., 2020. A multi-method control strategy for numerically testing a fuel cell-battery-supercapacitor tramway. *Energy Conversion and Management*, 225, 113481.

Pisu, P., Rizzoni, G., 2007. A Comparative Study Of Supervisory Control Strategies for Hybrid Electric Vehicles. *IEEE Transactions on Control Systems Technology*, 15, 506–518.

Poline, M., Gerbaud, L., Pouget, J., Chauvet, F., 2019. Simultaneous optimization of sizing and energy management — Application to hybrid train. *Mathematics and Computers in Simulation*, 158, 355–374.

Pourabdollah, M., 2012. On Optimization of Plug-in Hybrid Electric Vehicles. Thesis for the degree of licentiate of engineering. Chalmers University of Technology, Göteborg, Sweden.

Pourabdollah, M., Murgovski, N., Grauers, A., Egardt, B., 2014. An iterative dynamic programming/convex optimization procedure for optimal sizing and energy management of PHEVs. *IFAC Proceedings*, 47, 6606–6611.

Pourabdollah, M., Murgovski, N., Grauers, A., Egardt, B., 2013. Optimal Sizing of a Parallel PHEV Powertrain. *IEEE Transactions on Vehicular Technology*, 62, 2469–2480.

Pourahmadiyan, A., Ahmadi, P., Kjeang, E., 2021. Dynamic simulation and life cycle greenhouse gas impact assessment of CNG, LNG, and diesel-powered transit buses in British Columbia, Canada. *Transportation Research Part D: Transport and Environment*, 92, 102724.

Profillidis, V.A., 2000. *Railway Engineering*. Second Edition, Ashgate Publishing Company, Burlington, USA.

Pröhl, L., 2017a. OPEUS Deliverable DO2.2 - OPEUS simulation tool, EU-project OPEUS (S2R-OC-CCA-02-2015).

Pröhl, L., 2017b. OPEUS Deliverable DO2.1 - OPEUS simulation methodology, EU-project OPEUS (S2R-OC-CCA-02-2015).

Pröhl, L., 2017c. OPEUS Deliverable DO2.3 - OPEUS simulation tool manual, EU-project OPEUS (S2R-OC-CCA-02-2015).

Prohl, L., Aschemann, H., 2019. Grey Wolf optimisation of an operating strategy for energy storage systems in electrically driven railway vehicles.*18th European Control Conference - ECC 2019*, 1908–1913.

ProRail, 2020. Network Statement 2020.

Railcolor News, 2018. Romania's first hybrid locomotive design plugs-in to sustainability. URL: https://railcolornews.com/2018/02/28/ro-romanias-first-hybrid-locomotive-design-plugs-in-to-sustainability/

RailTech, 2020. Report from a night-time trial on a hydrogen train. URL: https://railcolornews.com/2018/02/28/ro-romanias-first-hybrid-locomotive-design-plugs-in-to-sustainability/

RailTech, 2019. Stadler gets first order for Akku battery-powered trains. URL: https://www.railtech.com/rolling-stock/2019/06/20/stadler-gets-first-order-for-akku-battery-powered-trains/?gdpr=accept

Railway Gazette International, 2015. Hybrid drive demonstrates 15% fuel saving. URL: https://www.railwaygazette.com/news/traction-rolling-stock/single-view/view/hybrid-drive-demonstrates-15-fuel-saving.html

Railway Gazette International, 2022. Prototype battery multiple-units ordered as suburban EMUs unveiled. URL: https://www.railwaygazette.com/passenger/prototype-battery-multiple-units-ordered-as-suburban-emus-unveiled/63239.article

RailwayTechnology, 2020. Bombardier Talent 3 Battery Train. URL: https://www.railway-technology.com/projects/bombardier-talent-3-battery-train/

Requia, W.J., Adams, M.D., Arain, A., Koutrakis, P., Ferguson, M., 2017. Carbon dioxide emissions of plug-in hybrid electric vehicles: A life-cycle analysis in eight Canadian cities. *Renewable and Sustainable Energy Reviews*, 78, 1390-1396.

Research and Technology Centre of Deutsche Bahn AG, 2001. Applications for energy storage flywheels in vehicles of Deutsche Bahn AG. *World Congress on Railway Research*.

Romare, M., Dahllöf, L., 2017. The Life Cycle Energy Consumption and Greenhouse Gas Emissions from Lithium-Ion Batteries. Report C 243, IVL Swedish Environmental Research Institute.

S&T, 2020. GHGenius. URL: https://www.ghgenius.ca/

SAFT, n.d. Ion-OnBoard® Regen, the Li-ion regenerative hybrid traction battery system. URL: https://www.saftbatteries.com/products-solutions/products/ion-onboard®-regen-li-ion-regenerative-hybrid-traction-battery-system?page=1

SAFT, UNEW, 2017. OPEUS Deliverable D6.1 - Innovative technologies outlook update. EUproject OPEUS (S2R-OC-CCA-02-2015).

Sarma, U., Ganguly, S., 2020. Design optimisation for component sizing using multi-objective particle swarm optimisation and control of PEM fuel cell-battery hybrid energy system for locomotive application. *IET Electrical Systems in Transportation*, 10, 52–61.

Sarma, U., Ganguly, S., 2018. Determination of the component sizing for the PEM fuel cell-battery hybrid energy system for locomotive application using particle swarm optimization. *Journal of Energy Storage*, 19, 247–259.

Scheepmaker, G.M., Goverde, R.M.P., Kroon, L.G., 2017. Review of energy-efficient train control and timetabling. *European Journal of Operational Research*, 257, 355–376.

Schmid, S., Ebrahimi, K., Pezouvanis, A., Commerell, W., 2017. Model-based comparison of hybrid propulsion systems for railway diesel multiple units. *International Journal of Rail Transportation*, 6, 16–37.

Shakya, S.R., Shrestha, R.M., 2011. Transport sector electrification in a hydropower resource rich developing country: Energy security, environmental and climate change co-benefits. *Energy for Sustainable Development*, 15, 147–159.

Shift2Rail, 2021. OPEUS - Modelling and strategies for the assessment and OPtimisation of Energy USage aspects of rail innovation. URL: https://projects.shift2rail.org/s2r_ipcc_n.aspx?p=OPEUS

Shinde, A.M., Dikshit, A.K., Singh, R.K., Campana, P.E., 2018. Life cycle analysis based comprehensive environmental performance evaluation of Mumbai Suburban Railway, India. *Journal of Cleaner Production*, 188, 989–1003.

Shiraki, N., Satou, H., Arai, S., 2010. A hybrid system for diesel railcar series Ki-Ha E200. *The 2010 International Power Electronics Conference - ECCE ASIA*, 2853–2858.

Shiraki, N., Tokito, K., Yokozutsumi, R., 2015. Propulsion system for catenary and storage battery hybrid electric railcar series EV-E301. *2015 International Conference on Electrical Systems for Aircraft, Railway, Ship Propulsion and Road Vehicles (ESARS)*, 1–7.

Siddiqui, O., Dincer, I., 2019. A Review on Fuel Cell-Based Locomotive Powering Options for

Sustainable Transportation. *Arabian Journal for Science and Engineering*, 44, 677–693.

Siemens, n.d. Desiro ML ÖBB Cityjet eco for ÖBB Personenverkehr AG. URL: https://assets.new.siemens.com/siemens/assets/api/uuid:b26911b1-2b0e-48b4-b593-81adbf032d75/db-desiro-ml-oebb-cityjet-eco-e.pdf

Siemens, n.d. Mireo Plus B Ortenau for SFBW, Baden-Württemberg, Germany. URL: https://assets.new.siemens.com/siemens/assets/api/uuid:636c61e0-bd2d-4f97-a2c7-78e690792a44/mors-b10022-00dbmireoplusortenauenus-72_original.pdf

Silvas, E., Hofman, T., Murgovski, N., Etman, P., Steinbuch, M., 2016. Review of Optimization Strategies for System-Level Design in Hybrid Electric Vehicles. *IEEE Transactions on Vehicular Technology*, 66, 1–1.

Sopian, K., Wan Daud, W.R., 2006. Challenges and future developments in proton exchange membrane fuel cells. *Renewable Energy*, 31, 719–727.

Sorrentino, M., Cirillo, V., Nappi, L., 2019. Development of flexible procedures for co-optimizing design and control of fuel cell hybrid vehicles. *Energy Conversion and Management*, 185, 537–551.

Sorrentino, M., Serge Agbli, K., Hissel, D., Chauvet, F., Letrouve, T., 2020. Application of dynamic programming to optimal energy management of grid-independent hybrid railcars. *Proceedings of the Institution of Mechanical Engineers, Part F: Journal of Rail and Rapid Transit*, 235, 236-247.

Soukhov, A., Mohamed, M., 2022. Occupancy and GHG emissions: thresholds for disruptive transportation modes and emerging technologies. *Transportation Research Part D: Transport and Environment*, 102, 103127.

Spiryagin, M., Cole, C., Sun, Y.Q., McClanachan, M., Spiryagin, V., McSweeney, T., 2014. *Design and Simulation of Rail Vehicles*. First Edition, Taylor & Francis Group, LLC.

Stadler, 2021. Overview of references. URL: https://www.stadlerrail.com/en/references/overview-references/

Stadler, 2020. WINK BMU / WINK ZERO EMISSION: Arriva Netherlands, Noordelijke Lijnen franchise - Preliminary datasheet. URL: https://www.stadlerrail.com/media/pdf/warr0420e.pdf

Stadler, 2005. GTW DMU-2 2/6 and GTW 2/8 low-floor for Arriva, Netherlands. URL: https://www.stadlerrail.com/media/pdf/garr1008e.pdf

Stripple, H., Uppenberg, S., 2010. Life cycle assessment of railways and rail transports - Application in environmental product declarations (EPDs) for the Bothnia Line. Goteborg, Sweden.

Sun, Y., Anwar, M., Hassan, N.M.S., Spiryagin, M., Cole, C., 2021. A review of hydrogen technologies and engineering solutions for railway vehicle design and operations. *Railway Engineering Science*, 29, 212–232.

Sun, Y., Cole, C., Spiryagin, M., Godber, T., Hames, S., Rasul, M., 2013. Conceptual designs of hybrid locomotives for application as heavy haul trains on typical track lines. *Proceedings of the Institution of Mechanical Engineers, Part F: Journal of Rail and Rapid Transit*, 227, 439–452.

Sundström, O., Ambühl, D., Guzzella, L., 2010. On Implementation of Dynamic Programming for Optimal Control Problems with Final State Constraints. *Oil & Gas Science and Technology - Revue d'IFP Energies nouvelles*, 65, 91–102.

Sundstrom, O., Guzzella, L., 2009. A generic dynamic programming Matlab function. *2009 IEEE International Conference on Control Applications*, 1625–1630.

Takami, N., Inagaki, H., Tatebayashi, Y., Saruwatari, H., Honda, K., Egusa, S., 2013. High-power and long-life lithium-ion batteries using lithium titanium oxide anode for automotive and stationary power applications. *Journal of Power Sources*, 244, 469–475.

Tao, S., Chen, W., Gan, R., Li, L., Zhang, G., Han, Y., Li, Q., 2021. Energy management strategy based on dynamic programming with durability extension for fuel cell hybrid tramway. *Railway Engineering Science*, 29, 299–313.

The MathWorks Inc., 2021. MATLAB and Simulink. URL: https://mathworks.com/products.html?s_tid=gn_ps

Torreglosa, J.P., Jurado, F., García, P., Fernández, L.M., 2011a. Hybrid fuel cell and battery tramway control based on an equivalent consumption minimization strategy. *Control Engineering Practice*, 19, 1182–1194.

Torreglosa, J.P., Jurado, F., García, P., Fernández, L.M., 2011b. Application of cascade and fuzzy logic based control in a model of a fuel-cell hybrid tramway. *Engineering Applications of Artificial Intelligence*, 24, 1–11.

Toshiba, 2021. SCiB™ Rechargeable battery. URL: https://www.global.toshiba/ww/products-solutions/battery/scib.html

Tran, D.-D., Vafaeipour, M., El Baghdadi, M., Barrero, R., Van Mierlo, J., Hegazy, O., 2020. Thorough state-of-the-art analysis of electric and hybrid vehicle powertrains: Topologies and integrated energy management strategies. *Renewable and Sustainable Energy Reviews*, 119, 109596.

UIC, CER, 2012. Moving towards sustainable mobility: A Strategy for 2030 and Beyond for the European Railway Sector. Paris.

UN, 2015. Paris Agreement. Paris.

UN, 1998. Kyoto Protocol to the United Nations Framework Convention on Climate Change. Kyoto.

United Nations. Economic Commission for Europe, 2011. ECE/TRANS/WP.6/2011/5: Definitions of vehicle energy types. Geneva.

US Department of Energy, 2021. Comparison of Fuel Cell Technologies. URL: https://www.energy.gov/eere/fuelcells/comparison-fuel-cell-technologies

Vazquez, S., Lukic, S.M., Galvan, E., Franquelo, L.G., Carrasco, J.M., 2010. Energy storage systems for transport and grid applications. *IEEE Transactions on Industrial Electronics*, 57, 3881–3895.

Vučić, V., 1987. *Public transport* (in Serbian). Scientific Book, Belgrade.

Wang, J., Rakha, H.A., 2017. Electric train energy consumption modeling. *Applied Energy*, 193, 346–355.

Wang, Y., Chen, K.S., Mishler, J., Cho, S.C., Adroher, X.C., 2011. A review of polymer electrolyte membrane fuel cells: Technology, applications, and needs on fundamental research. *Applied Energy*, 88, 981–1007.

Washing, E., Pulugurtha, S., 2015. Well-to-Wheel Analysis of Electric and Hydrogen Light Rail. *Journal of Public Transportation*, 18, 74–88.

Washing, E.M., Pulugurtha, S.S., 2016. Energy demand and emission production comparison of electric, hydrogen and hydrogen-hybrid light rail trains. *International Journal of Rail Transportation*, 4, 55–70.

Williamson, S.S., 2013. *Energy Management Strategies for Electric and Plug-in Hybrid Electric Vehicles*. Springer, New York.

Xu, L., Li, J., Ouyang, M., 2015a. Energy flow modeling and real-time control design basing on mean values for maximizing driving mileage of a fuel cell bus. *International Journal of Hydrogen Energy*, 40, 15052–15066.

Xu, L., Mueller, C.D., Li, J., Ouyang, M., Hu, Z., 2015b. Multi-objective component sizing based on optimal energy management strategy of fuel cell electric vehicles. Applied Energy, 157, 664–674.

Yan, Y., Huang, W., Liu, J., Li, Q., Chen, W., 2019. The Control Strategy of Fuel Cell Hybrid Tram Based on State Machine Control. *2019 IEEE Sustainable Power and Energy Conference (ISPEC)*, 699–703.

Yazdanie, M., Noembrini, F., Dossetto, L., Boulouchos, K., 2014. A comparative analysis of well-to-wheel primary energy demand and greenhouse gas emissions for the operation of alternative and conventional vehicles in Switzerland, considering various energy carrier production pathways. *Journal of Power Sources*, 249, 333–348.

Yazdanie, M., Noembrini, F., Heinen, S., Espinel, A., Boulouchos, K., 2016. Well-to-wheel costs, primary energy demand, and greenhouse gas emissions for the production and operation of conventional and alternative vehicles. *Transportation Research Part D: Transport and Environment*, 48, 63–84.

Zhang, G., Li, Q., Chen, W., Meng, X., Deng, H., 2019. A coupled power-voltage equilibrium strategy based on droop control for fuel cell/battery/supercapacitor hybrid tramway. *International Journal of Hydrogen Energy*, 44, 19370–19383.

Zhang, H., Yang, J., Zhang, J., Song, P., Li, M., 2020. Optimal energy management of a fuel cell-battery-supercapacitor-powered hybrid tramway using a multi-objective approach. *Proceedings of the Institution of Mechanical Engineers, Part F: Journal of Rail and Rapid Transit*, 234, 511–523.

Zhang, H., Yang, J., Zhang, J., Song, P., Xu, X., 2019. A Firefly Algorithm Optimization-Based Equivalent Consumption Minimization Strategy for Fuel Cell Hybrid Light Rail Vehicle. *Energies*, 12, 2665.

Zhang, W., Li, J., Xu, L., Ouyang, M., 2017. Optimization for a fuel cell/battery/capacity tram with equivalent consumption minimization strategy. *Energy Conversion and Management*, 134, 59–69.

Zhang, W., Li, J., Xu, L., Ouyang, M., Liu, Y., Han, Q., Li, K., 2016. Comparison study on life-cycle costs of different trams powered by fuel cell systems and others. *International Journal of Hydrogen Energy*, 41, 16577–16591.

Summary

Regional non-electrified railways in Europe are facing significant challenges to improve energy efficiency and reduce greenhouse gas (GHG) emissions. In addition to GHG emission regulations, companies are also imposing voluntary emission reduction targets, not only because of corporate responsibility, but also in an attempt to improve their market share, company image, and value. Featured with low transport demand compared to the main corridors, complete electrification of regional lines is often not economically viable. The solutions are being sought in alternative energy carriers and catenary-free propulsion systems. The transition from conventional diesel traction is a complex and context-specific dynamic decision-making process that requires involvement of multiple stakeholders and consideration of numerous aspects. It requires in-depth analyses that include identification of available technology, design, modelling, and assessment of potential alternatives, with respect to the particular case-related constraints imposed by infrastructure, technical and operational characteristics (e.g., track geometry, speed, and axle load limitations, maintaining existing timetables, noise-free and emission-free operation in stations, etc.). Hence, the overarching aim of this thesis is to identify and assess potential solutions in reducing overall (Well-to-Wheel) energy use and GHG emissions from the operation of regional trains, focussing primarily on synergetic adoption of alternative propulsion systems and energy carriers. We use the case study of the Dutch Northern lines with rolling stock and train services of Arriva to undertake this research, providing several scientific and practical contributions, which are summarized as follows.

First, we gradually develop a backward-looking quasi-static simulation model to encompass various alternative (hybrid) propulsion systems for the conventional diesel-electric topology. We start with the model of a hybrid-electric system with an internal combustion engine (ICE) as the prime mover coupled with a lithium-ion battery (LB). The model is subsequently extended with a double-layer capacitor (DLC) as an alternative energy storage system (ESS) technology, together with a plug-in hybrid-electric concept. Finally, we introduce a fuel cell hybrid-electric system, with an additional hybrid ESS configuration that combines both LB and DLC technologies. Low-order models of individual main components (modules)

along the traction chain are coupled with a suitable energy management and control strategy (EMCS) to address the high complexity of hybrid systems reflected in simultaneous operation of multiple power sources. The requirement of emission-free and noise-free operation in terminal stations with longer stabling periods is incorporated in the design of both propulsion systems and the EMCS. The backward-looking approach enables estimation and comparative assessment of powertrain dynamics for a range of propulsion systems by capturing main, typically available vehicle, infrastructure and operation parameters influencing energy performance of a train. An energy-optimized velocity profile is used as the main input for the simulation, which offers a phased-out influence of the driver's behaviour, lower complexity, and a faster execution time compared to the forward-looking approach. Finally, in contrast to the energetic macroscopic representation approach it does not require field test data, which are often unavailable.

Second, we develop a bi-level multi-objective optimization approach for determining the optimal size of the LB-based ESS in a hybrid-electric vehicle, by integrating the ESS sizing and control optimization levels. The proposed framework includes most relevant design aspects, such as the requirement of achieving emissions-free and noise-free operation in stations, the trade-off (preference) between lower fuel consumption and hybridization cost, technical constraints related to battery voltage and maximum allowed mass, and the influence of the EMCS. Using derived LB parameters at the cell level, we employ a nested coordination framework, where a brute force search finds the optimal battery size using dynamic programming for full EMCS optimization for each feasible solution. In this way, the global minimum for fuel consumption for each battery configuration is achieved. Overall, the results indicated significant potential benefits of hybridization in terms of fuel savings and related GHG emissions reduction compared to the conventional diesel-electric vehicle, while stipulating the need for the integration of different design and optimization levels and further performance improvement of real-time controllers towards the global optimum. The presented methodology allows for fair generalization and relatively easy adaptation to other railway networks and vehicles, regardless of the geographical context, vehicle and/or services type, ESS technology, etc.

Third, we present a simulation-based analysis of hybrid-electric and plug-in hybrid-electric propulsion system concepts for diesel-electric multiple unit vehicles, with encompassed LBs or DLCs as alternative ESS technologies, and newly developed causal and easy-to-implement real-time power control for each concept. The proposed ECMSs are based on a finite state machine control (FSMC), with different states and corresponding transition triggers defined to satisfy the requirements of removing emissions and noise in terminal stops by switching off the ICE and supplying auxiliary systems from an ESS or electric power grid, and improving fuel economy by maximizing the use of regenerative braking energy, avoiding low load ICE operation, and supporting ICE by an ESS during high power demand phases (acceleration). The results indicated positive effects from further conversion of a hybrid-electric to a plug-in hybrid-electric system reflected in additional fuel savings, GHG emissions and direct energy costs reduction compared to the conventional diesel-electric vehicle, with identified significant influence of the type of service (express or stopping), energy storage technology selection (LB or DLC), electricity production (green or grey electricity), and charging facilities configuration (charging in terminal stations with or without additional charging possibility during short intermediate stops).

Fourth, we propose a conceptual design of hydrogen-powered propulsion systems for the conversion of diesel-electric trains. The analysis encompasses technology identification, system design, modelling and assessment of alternative powertrains in terms of feasibility, fuel economy and produced emissions. We consider an ICE and a fuel cell system as the alternative prime mover configurations, coupled with LB, DLC or a hybrid ESS that combines both technologies. We upgrade the simulation model and previously developed FSMC to the new system layouts. The slow dynamic response feature of a fuel cell system is coupled with estimated power and energy demand in sizing the ESS, with fuel cell system size derived from the gradeability power. The hydrogen storage system size is determined according to the requirement of a daily operation without refuelling. The feasibility of the obtained propulsion systems is investigated by considering available weight and volumetric space constraints. According to the comparative assessment results, the highest fuel-efficiency is obtained for the fuel cell-based hybrid propulsion systems with LB or a hybrid ESS. The remaining configurations are featured with higher hydrogen consumption, while at the same time reduced fuel storage is available due to the weight and volumetric space constraints, resulting in reduced vehicle range. This brings the challenge of implementing efficient refuelling system comparable to that for diesel vehicles, which would prevent compromising timetable fulfilment and daily operation. Furthermore, a transition to a non-hybrid powertrain powered solely by hydrogen ICE demonstrated a significant increase of GHG emissions compared to the diesel baseline, confirming the necessity for a hybrid systems implementation.

Fifth, we present a framework for the estimation of Well-to-Wheel (WTW) energy use and GHG emissions attributed to the implementation of alternative propulsion systems in conjunction with a range of energy carriers. The considered alternative propulsion systems are conventional diesel-electric, hybrid-electric, plug-in hybrid-electric, fuel cell hybrid-electric and battery-electric. Fatty acid methyl esters (FAME) as the first generation biofuel, hydrotreated vegetable oil (HVO) as the second generation biofuel, liquefied natural gas (LNG), hydrogen, and electricity are considered as alternative energy carriers to diesel. We employ a bottom-up consumption-based approach, with direct fuel and/or electricity consumption assessed in the Tank-to-Wheel (TTW) stage using the developed backward-looking quasi-static simulation model, further extended with a battery-electric system and a new simplified FSMC for hybrid-electric configurations to reflect the current system. The obtained estimations are then combined with various energy carriers' production pathways linked to the Well-to-Tank (WTT) stage in the overall comparative assessment using energy and GHG emission factors relevant for the Dutch and European context. The case study encompassed different multiple units and passenger services currently operated by Arriva in the Northern lines, with commercially available technologies considered in the vehicles' conceptual retrofit to alternative propulsion systems, while maintaining the overall weight and tractive characteristics. The battery-electric system running on wind-power based electricity provides the lowest energy use and zero-emission trains operation from the WTW perspective. Hydrogen offers a significant reduction of GHG emissions compared to the current system only if produced from electrolysis using green electricity, with negative effects in both energy use and emissions if produced from non-renewable sources. Overall, the production pathway of the energy carrier is identified as the most significant contributor to the total energy use and produced emissions. Thus, focusing on fuels such as HVO and systems with infrastructure already in place could be an instantly implementable and cost-effective approach in reaching significant energy and GHG emissions savings in the short-term. This approach would facilitate a smooth transition toward more energy efficient and environment friendly solutions, while providing the time for novel technologies to mature and reach the economy of scale required for their wider adoption, as well as the time required for the development of the supporting infrastructure.

In summary, this thesis provides methods and models for assessing the overall energy use and GHG emissions linked to the implementation of various advanced propulsion systems and energy carriers in non-electrified regional railway networks. The outcomes of this thesis will be leveraged by the railway undertaking and decision-makers in the complex transition process towards energy-efficient and low or zero-emission trains operation.

Samenvatting

Regionale ongeëlektrificeerde spoorwegen in Europa staan voor een grote uitdaging om de energie efficiëntie te verbeteren en de uitstoot van broeikasgassen te verminderen. Naast regelgeving omtrent de uitstoot van broeikasgassen, leggen bedrijven zichzelf ook vrijwillige emissiereductiedoelstellingen op, niet alleen vanwege de verantwoordelijkheid van het bedrijf, maar ook om hun marktaandeel, bedrijfsimago en waarde te verbeteren. Gekenmerkt door een lage transportvraag in vergelijking met de hoofdspoorlijnen, waardoor volledige elektrificatie van regionale lijnen vaak niet economisch haalbaar is, worden de oplossingen gezocht in alternatieve energiedragers en aandrijfsystemen zonder bovenleiding. De overgang van conventionele dieseltractie is een complex en context specifiek dynamisch besluitvormingsproces dat de betrokkenheid van meerdere belanghebbenden vereist met aandacht voor diverse aspecten. Dit vereist diepgaande analyses, waaronder identificatie van beschikbare technologie, ontwerp, modellering en beoordeling van mogelijke alternatieven, met betrekking tot de voor een specifieke casus gerelateerde infrastructurele, technische en operationele beperkingen (bijv. belastingbeperkingen, aanhouden van bestaande dienstregelingen, geluids- en emissievrije operaties in stations, etc.). Daarom is het overkoepelende doel van dit proefschrift het identificeren en beoordelen van mogelijke oplossingen voor het verminderen van het algehele (“Well-to-Wheel”) energieverbruik en de uitstoot van broeikasgassen door exploitatie van regionale treinen, waarbij de nadruk vooral ligt op de synergetische acceptatie van alternatieve voortstuwingssystemen en energiedragers. We gebruiken de casestudy van de Nederlandse Noordelijke lijnen met rollend materieel en treindiensten van Arriva om dit onderzoek uit te voeren, waarbij we verschillende wetenschappelijke en praktische bijdragen leveren, die als volgt worden samengevat.

Eerst ontwikkelen we een terugwaarts quasi-statisch simulatiemodel dat verschillende alternatieve (hybride) voortstuwingssystemen omvat voor de conventionele dieselelektrische topologie. We beginnen met het model van een hybride-elektrisch systeem met een verbrandingsmotor (ICE) als drijvende kracht in combinatie met een lithium-ion batterij (LB). Het model wordt vervolgens uitgebreid met een dubbellaagse condensator (DLC) als alternatieve energieopslagsysteemtechnologie (ESS), samen met een plug-in hybride-elektrisch concept. Ten slotte introduceren we een hybride-elektrisch brandstofcelsysteem, met een aanvullende hybride ESS-configuratie die zowel LB- als DLC-technologieën combineert. Lage-orde modellen van individuele hoofdcomponenten (modules) langs de tractieketen worden gekoppeld aan een geschikte energiebeheer- en regelstrategie (EMCS) om de hoge complexiteit van hybride systemen aan te pakken weerspiegeld in de gelijktijdige werking van meerdere stroombronnen. De eis van emissie- en geluidsarme processen in eindstations met lange opsteltijden is meegenomen in het ontwerp van zowel voortstuwingssystemen als het EMCS. De terugwaartse benadering maakt schatting en vergelijkende beoordeling mogelijk van de dynamiek van de aandrijflijn voor een reeks voortstuwingssystemen door de belangrijkste, typisch beschikbare voertuig-, infrastructuur- en bedrijfsparameters vast te leggen die de energieprestaties van een trein beïnvloeden. Het energie-optimale snelheidsprofiel dat als belangrijkste input voor de simulatie wordt gebruikt, biedt een geleidelijke vermindering van variërend rijgedrag van de bestuurder, een lagere complexiteit, en een snellere uitvoeringstijd in vergelijking met de voorwaarts gerichte aanpak. Ten slotte zijn er, in tegenstelling tot de energetische macroscopische representatieaanpak, geen veldtestgegevens vereist, die vaak niet beschikbaar zijn.

Ten tweede ontwikkelen we een bi-level multi-doelen optimalisatiebenadering voor het bepalen van de optimale grootte van de LB-gebaseerde ESS in een hybride-elektrisch voertuig, door de optimalisatie van de ESS-dimensionering en regeling te integreren. Het voorgestelde kader omvat de meest relevante ontwerpaspecten, zoals de vereiste van emissievrije en geluidsvrije operatie in stations, de afweging (voorkeur) tussen lager brandstofverbruik en hybridisatiekosten, technische beperkingen met betrekking tot batterijspanning en maximaal toegestane massa, en de invloed van het EMCS. Met behulp van afgeleide LB-parameters op celniveau gebruiken we een genest coördinatieraamwerk, waar een brute force-zoekalgoritme de optimale batterijgrootte vindt met behulp van dynamische programmering voor volledige EMCS-optimalisatie voor elke haalbare oplossing. Op deze manier wordt het globale minimum voor brandstofverbruik voor elke batterijconfiguratie bereikt. Over het algemeen wijzen de resultaten op significante potentiële voordelen van hybridisatie in termen van brandstofbesparing en gerelateerde reductie van de uitstoot van broeikasgassen in vergelijking met een conventioneel dieselelektrische voertuig, terwijl de noodzaak wordt benadrukt van de integratie van verschillende ontwerp- en optimalisatieniveaus, en verdere prestatieverbetering van real-time controllers naar het globale optimum. De gepresenteerde methodologie maakt een eerlijke generalisatie en relatief gemakkelijke aanpassing aan andere spoorwegnetwerken en voertuigen mogelijk, ongeacht de geografische context, het type voertuig en/of diensten, ESS-technologie, enz.

Ten derde presenteren we een op simulatie gebaseerde analyse van hybride-elektrische en plug-in hybride-elektrische voortstuwingssysteemconcepten voor dieselelektrische treinstellen inclusief LB's of DLC's als alternatieve ESS-technologieën, en nieuw ontwikkelde causale en gemakkelijk te implementerem real-time vermogensregeling voor elk concept. De voorgestelde ECMS-en zijn gebaseerd op finite state machine control (FSMC), met verschillende toestanden en overeenkomstige conditionele overgangen die zijn gedefinieerd om te voldoen aan de vereisten voor het verwijderen van emissies en geluidsoverlast op eindstations door de ICE uit te schakelen en hulpsystemen te voeden vanaf een ESS of elektrische voedingsnet, en het brandstofverbruik te verbeteren door het maximaliseren van het gebruik van regeneratieve remenergie, het vermijden van ICE-bedrijf met lage belasting en het ondersteunen van ICE door een ESS tijdens fases met veel vraag naar vermogen (optrekken). De resultaten wijzen op positieve effecten van de verdere conversie van een hybride-elektrisch naar een plug-in hybride-elektrisch systeem, weerspiegeld in extra besparingen op brandstof, broeikasgasemissies, en directe energiekosten in vergelijking met een conventioneel dieselelektrische voertuig, waarbij een significante invloed van het type treindienst (intercity of stoptrein), de geselecteerde energieopslagtechnologie (LB of DLC), de elektriciteitsproductie (groene of grijze stroom) en de configuratie van oplaadvoorzieningen (opladen in eindstations met of zonder extra oplaadmogelijkheid tijdens korte tussenstops).

Verder stellen we een conceptueel ontwerp voor van voortstuwingssystemen op waterstof voor de ombouw van dieselelektrische treinen. De analyse omvat technologie-identificatie, systeemontwerp, modellering en beoordeling van alternatieve aandrijflijnen in termen van haalbaarheid, brandstofverbruik en geproduceerde emissies. We beschouwen een ICE en een brandstofcelsysteem als de alternatieve prime mover-configuraties, gekoppeld aan LB, DLC of een hybride ESS die beide technologieën combineert. We upgraden het simulatiemodel en de eerder ontwikkelde FSMC naar de nieuwe systeemlay-outs. De trage dynamische respons van een brandstofcelsysteem is gekoppeld aan een geschat vermogen en energievraag bij het dimensioneren van de ESS, waarbij de grootte van het brandstofcelsysteem is afgeleid van het klimvermogen. De grootte van het waterstofopslagsysteem wordt bepaald op basis van de behoefte aan dagelijks gebruik zonder tanken. De haalbaarheid van de verkregen voortstuwingssystemen wordt onderzocht door rekening te houden met het beschikbare gewicht en de ruimtebeperkingen. Volgens de resultaten van de vergelijkende beoordeling wordt het hoogste brandstofrendement behaald voor de op brandstofcellen gebaseerde hybride aandrijfsystemen met LB of een hybride ESS. De overige configuraties hebben een hoger waterstofverbruik, terwijl tegelijkertijd minder brandstofopslag beschikbaar is vanwege het gewicht en de beperkte ruimte, zodat deze een kleinere actieradius hebben. Dit brengt de uitdaging met zich mee om een efficiënt tanksysteem te implementeren dat vergelijkbaar is met dat voor dieselvoertuigen, waardoor de uitvoering van de dienstregeling en de dagelijkse operaties niet in het gedrang komen. Bovendien toonde de overgang naar een niet-hybride aandrijflijn die uitsluitend wordt aangedreven door ICE op waterstof een significante toename van de uitstoot van broeikasgassen in vergelijking met de referentie van diesel, wat de noodzaak voor de implementatie van hybride systemen bevestigt.

Ten vijfde presenteren we een raamwerk voor de schatting van het energieverbruik van Well-to-Wheel (WTW) en de uitstoot van broeikasgassen (BKG) die worden toegeschreven aan de implementatie van alternatieve voortstuwingssystemen in combinatie met een reeks energiedragers. De overwogen alternatieve voortstuwingssystemen zijn conventioneel dieselelektrisch, hybride-elektrisch, plug-in hybride-elektrisch, brandstofcelhybride-elektrisch en batterij-elektrisch. Vetzuurmethylesters (FAME) als biobrandstof van de eerste generatie, met waterstof behandelde plantaardige olie (HVO) als biobrandstof van de tweede generatie, vloeibaar aardgas (LNG), waterstof en elektriciteit worden beschouwd als alternatieve energiedragers voor diesel. We hanteren een bottom-up verbruiksbenadering, waarbij het directe brandstof- en/of elektriciteitsverbruik wordt beoordeeld in de Tank-to-Wheel (TTW)-fase met behulp het ontwikkelde terugwaartse quasi-statisch simulatiemodel, verder uitgebreid met een batterij-elektrische systeem en een nieuwe vereenvoudigde FSMC voor hybride-elektrische configuraties om het huidige systeem weer te geven. De verkregen schattingen worden vervolgens gecombineerd met de productieroutes van verschillende energiedragers gekoppeld aan de Well-to-Tank (WTT)-fase in de algehele vergelijkende beoordeling met behulp van energie- en BKG-emissiefactoren die relevant zijn voor de Nederlandse en Europese context. De casestudy omvatte verschillende treinstellen en reizigersdiensten die momenteel worden geëxploiteerd door Arriva op de Noordelijke lijnen, waarbij commercieel beschikbare technologieën werden overwogen bij de conceptuele aanpassing van de voertuigen aan alternatieve voortstuwingssystemen, met behoud van het totale gewicht en de trekeigenschappen. Een batterij-elektrisch systeem met elektriciteit opgewekt uit windenergie, zorgt voor het laagste energieverbruik en emissievrije treinen vanuit het WTW-perspectief. Waterstof biedt alleen een aanzienlijke vermindering van de uitstoot van broeikasgassen in vergelijking met het huidige systeem als het wordt geproduceerd door elektrolyse met behulp van groene stroom, met negatieve effecten op zowel het energieverbruik als de emissies als het wordt geproduceerd uit niet-hernieuwbare bronnen. Over het algemeen wordt het productietraject van de energiedrager geïdentificeerd als de belangrijkste bijdrage aan het totale energieverbruik en de geproduceerde emissies. Het richten op brandstoffen zoals HVO en systemen met reeds bestaande infrastructuur zou dus een onmiddellijk implementeerbare en kosteneffectieve aanpak kunnen zijn om op korte termijn aanzienlijke besparingen op energie en broeikasgasemissies te bereiken. Deze benadering zou een soepele overgang naar meer energie-efficiënte en milieuvriendelijke oplossingen vergemakkelijken, en tegelijkertijd de tijd geven aan nieuwe technologieën om volwassen te worden en de schaalvoordelen te bereiken die nodig zijn voor een bredere acceptatie ervan, evenals de tijd die nodig is voor de ontwikkeling van de ondersteunende infrastructuur.

Samenvattend biedt dit proefschrift methoden en modellen voor het beoordelen van het totale energieverbruik en de uitstoot van broeikasgassen gekoppeld aan de implementatie van verschillende geavanceerde voortstuwingssystemen en energiedragers in niet-geëlektrificeerde regionale spoorwegnetwerken. De resultaten van dit proefschrift zullen door de spoorwegonderneming en besluitvormers worden gebruikt in het complexe overgangsproces naar energie-efficiënte en emissiearme of emissievrije treinen.

About the author

Marko Kapetanović was born in Loznica, Serbia in 1989. He received both his BSc degree in 2013 and MSc degree in 2014 in Railway Transport and Traffic Engineering from the University of Belgrade. After graduation, Marko worked as a Junior Researcher and a Teaching Assistant at the Faculty of Transport and Traffic Engineering, University of Belgrade, and as a Short Term Consultant at the World Bank.

In July 2018, Marko joined the Department of Transport and Planning at Delft University of Technology to conduct his PhD research in the project “Improving sustainability of regional railway services”, supported by Arriva, the largest regional railway undertaking in the Netherlands. His research focused on modelling and assessment of potential energy efficiency improvement and emissions reduction linked to the implementation of alternative propulsion systems and fuels in regional non-electrified railway networks.

He assisted in teaching activities of the Master course “Railway Traffic Management” at the Department of Transport and Planning, and the Bachelor course “Introduction to Operations Research” at Beijng Jiaotong University. During his PhD research, he presented his research at a number of national and international scientific and professional conferences. He served as a reviewer at various international journals and as a student liaison at the Institute for Operations Research and the Management Sciences (INFORMS).

Marko is an avid learner with a wide range of interests spanning from academic ones, focusing on operations research, simulation, transport systems and environmental science, to keen non-academic interests in psychology, philosophy, economics and politics. He is a member of various associations and societies, including INFORMS, the International Association of Railway Operations Research (IAROR), and MENSA Serbia.

Publications

Journal articles

1. **Kapetanović, M.**, Núñez, A., van Oort, N., Goverde, R.M.P. (2023). Energy use and greenhouse gas emissions of traction alternatives for regional railways. (*Under review*).

2. **Kapetanović, M.**, Núñez, A., van Oort, N., Goverde, R.M.P. (2022). Analysis of hydrogen-powered propulsion system alternatives for diesel-electric regional trains. *Journal of Rail Transport Planning & Management*, 23, 100338.

3. **Kapetanović, M.**, Vajihi, M., Goverde, R.M.P. (2021). Analysis of Hybrid and Plug-In Hybrid Alternative Propulsion Systems for Regional Diesel-Electric Multiple Unit Trains. *Energies*, 14, 5920.

4. **Kapetanović, M.**, Núñez, A., van Oort, N., Goverde, R.M.P. (2021). Reducing fuel consumption and related emissions through optimal sizing of energy storage systems for diesel-electric trains. *Applied Energy*, 294, 117018.

5. Macura, D., **Kapetanović, M.**, Knežević, N., Bojović, N. (2019). Rail Projects Ranking under Fuzzy Environment. Serbian Rail Projects Case Study. *International Journal of Transport Economics*, 46(4), 91-112.

6. **Kapetanović, M.**, Bojović, N., Milenković, M. (2018). Booking limits and bid price based revenue management policies in rail freight transportation. *European Journal of Transport and Infrastructure Research*, 18(1), 60-75.

7. Bojović, N., Milenković, M., **Kapetanović, M.**, Knežević, N. (2016). Innovations Impact on Efficiency of European Railway Companies. *Management: Journal for Theory and Practice Management*, 21(79), 13-25.

Peer-reviewed conference contributions

1. **Kapetanović, M.**, Núñez, A., van Oort, N., Goverde, R.M.P. (2023). Vehicle-to-Grid Concept for Hydrogen Fuel Cell Hybrid-Electric Regional Trains. *10th International Conference on Railway Operations Modelling and Analysis (RailBelgrade)*, Belgrade, Serbia.
   (Elected in the top 10 best papers of RailBelgrade conference).

2. **Kapetanović, M.**, Bešinović, N., Núñez, A., van Oort, N., Goverde, R.M.P. (2022). Optimal network electrification plan for operation of battery-electric multiple unit regional trains. *11th Triennial Symposium on Transportation Analysis (TRISTAN)*, Mauritius Island, Mauritius.

3. **Kapetanović, M.**, Núñez, A., van Oort, N., Goverde, R.M.P. (2022). Life Cycle Assessment of Alternative Traction Options for Non-Electrified Regional Railway Lines. *13th World Congress on Railway Research (WCRR)*, Birmingham, United Kingdom.

4. **Kapetanović, M.**, Núñez, A., van Oort, N., Goverde, R.M.P. (2021). Analysis of Hydrogen-Powered Propulsion System Alternatives for Diesel-Electric Multiple Unit Regional Trains. *9th International Conference on Railway Operations Modelling and Analysis (RailBeijing)*, Beijing, China.
(Elected in the top 10 best papers of RailBeijing conference).

5. **Kapetanović, M.**, van Oort, N., Núñez, A., Goverde, R.M.P. (2019). Sustainability of Railway Passenger Services: A Review of Aspects, Issues, Contributions and Challenges of Life Cycle Emissions. *8th International Conference on Railway Operations Modelling and Analysis (RailNorrköping)*, Norrköping, Sweden.

6. **Kapetanović, M.**, Bojović, N., Milenković, M. (2017). Discriminatory revenue management policies in rail freight transportation. *6th Symposium of the European Association for Research in Transportation (hEART)*, Haifa, Israel.

7. **Kapetanović, M.**, Bojović, N., Milenković, M. (2016). Revenue management policies in railway freight transportation: A case study of Serbian Railways. *5th Symposium of the European Association for Research in Transportation (hEART)*, Delft, the Netherlands.

8. Macura D., **Kapetanović, M.**, Bojović, N., Milošević, M. (2016). One Model for Rail Projects Evaluation with Interval-Valued Fuzzy Numbers. *4th International Conference On Road and Rail Infrastructure (CETRA)*, Šibenik, Croatia.

Professional contributions

1. **Kapetanović, M.** (2023). Alternative Traction Options for Regional Trains in the Northern Netherlands. *RailTech Rail Infra Forum 2023: Infrastructure for Sustainable Rolling Stock,* Rotterdam, the Netherlands. [Presentation]

2. **Kapetanović, M.** (2022). How can railways phase out diesel from their operations? Sustainability of Fuel Production. *The Digital Magazine: Sustainable Rolling Stock,* RailTech.com. [Interview]

3. **Kapetanović, M.** (2022). Improving Environmental Sustainability of Regional Railway Services in the Netherlands. *Reducing rail emissions: Shifting to diesel alternatives,* RailTech.com. [Webinar]

4. Hettinga, A., van Oort, N., **Kapetanović, M.** (2019). CO2 Barometer. *Klimaattop Noord-Nederland,* Groningen, the Netherlands. [Presentation]

TRAIL Thesis Series

The following list contains the most recent dissertations in the TRAIL Thesis Series. For a complete overview of more than 275 titles see the TRAIL website: www.rsTRAIL.nl.

The TRAIL Thesis Series is a series of the Netherlands TRAIL Research School on transport, infrastructure and logistics.

Kapetanović, M., *Improving Environmental Sustainability of Regional Railway Services,* T2023/6, June 2023, TRAIL Thesis Series, the Netherlands

Li, G., *Uncertainty Quantification and Predictability Analysis for Traffic Forecasting at Multiple Scales,* T2023/5, April 2023, TRAIL Thesis Series, the Netherlands

Harter, C., *Vulnerability through Vertical Collaboration in Transportation: A complex networks approach,* T2023/4, March 2023, TRAIL Thesis Series, the Netherlands

Razmi Rad, S., *Design and Evaluation of Dedicated Lanes for Connected and Automated Vehicles,* T2023/3, March 2023, TRAIL Thesis Series, the Netherlands

Eikenbroek, O., *Variations in Urban Traffic,* T2023/2, February 2023, TRAIL Thesis Series, the Netherlands

Wang, S., *Modeling Urban Automated Mobility on-Demand Systems: an Agent-Based Approach,* T2023/1, January 2023, TRAIL Thesis Series, the Netherlands

Szép, T., *Identifying Moral Antecedents of Decision-Making in Discrete Choice Models,* T2022/18, December 2022, TRAIL Thesis Series, the Netherlands

Zhou, Y., *Ship Behavior in Ports and Waterways: An empirical perspective,* T2022/17, December 2022, TRAIL Thesis Series, the Netherlands

Yan, Y., *Wear Behaviour of A Convex Pattern Surface for Bulk Handling Equipment,* T2022/16, December 2022, TRAIL Thesis Series, the Netherlands

Giudici, A., *Cooperation, Reliability, and Matching in Inland Freight Transport,* T2022/15, December 2022, TRAIL Thesis Series, the Netherlands

Nadi Najafabadi, A., *Data-Driven Modelling of Routing and Scheduling in Freight Transport,* T2022/14, October 2022, TRAIL Thesis Series, the Netherlands

Heuvel, J. van den, *Mind Your Passenger! The passenger capacity of platforms at railway stations in the Netherlands,* T2022/13, October 2022, TRAIL Thesis Series, the Netherlands

Haas, M. de, *Longitudinal Studies in Travel Behaviour Research,* T2022/12, October 2022, TRAIL Thesis Series, the Netherlands

Dixit, M., *Transit Performance Assessment and Route Choice Modelling Using Smart Card Data,* T2022/11, October 2022, TRAIL Thesis Series, the Netherlands

Du, Z., *Cooperative Control of Autonomous Multi-Vessel Systems for Floating Object Manipulation,* T2022/10, September 2022, TRAIL Thesis Series, the Netherlands

Larsen, R.B., *Real-time Co-planning in Synchromodal Transport Networks using Model Predictive Control,* T2022/9, September 2022, TRAIL Thesis Series, the Netherlands

Zeinaly, Y., *Model-based Control of Large-scale Baggage Handling Systems: Leveraging the theory of linear positive systems for robust scalable control design,* T2022/8, June 2022, TRAIL Thesis Series, the Netherlands

Fahim, P.B.M., *The Future of Ports in the Physical Internet,* T2022/7, May 2022, TRAIL Thesis Series, the Netherlands

Huang, B., *Assessing Reference Dependence in Travel Choice Behaviour,* T2022/6, May 2022, TRAIL Thesis Series, the Netherlands

Reggiani, G., *A Multiscale View on Bikeability of Urban Networks*, T2022/5, May 2022, TRAIL Thesis Series, the Netherlands

Paul, J., *Online Grocery Operations in Omni-channel Retailing: opportunities and challenges,* T2022/4, March 2022, TRAIL Thesis Series, the Netherlands

Liu, M., *Cooperative Urban Driving Strategies at Signalized Intersections,* T2022/3, January 2022, TRAIL Thesis Series, the Netherlands

Feng, Y., *Pedestrian Wayfinding and Evacuation in Virtual Reality*, T2022/2, January 2022, TRAIL Thesis Series, the Netherlands

Scheepmaker, G.M., *Energy-efficient Train Timetabling,* T2022/1, January 2022, TRAIL Thesis Series, the Netherlands

Bhoopalam, A., *Truck Platooning: planning and behaviour,* T2021/32, December 2021, TRAIL Thesis Series, the Netherlands

Hartleb, J., *Public Transport and Passengers: optimization models that consider travel demand,* T2021/31, TRAIL Thesis Series, the Netherlands

Azadeh, K., *Robotized Warehouses: design and performance analysis,* T2021/30, TRAIL Thesis Series, the Netherlands

Chen, N., *Coordination Strategies of Connected and Automated Vehicles near On-ramp Bottlenecks on Motorways,* T2021/29, December 2021, TRAIL Thesis Series, the Netherlands

Onstein, A.T.C., *Factors influencing Physical Distribution Structure Design*, T2021/28, December 2021, TRAIL Thesis Series, the Netherlands

Olde Kalter, M.-J. T., *Dynamics in Mode Choice Behaviour,* T2021/27, November 2021, TRAIL Thesis Series, the Netherlands